UNIVERSITÄT ZU LÜBECK

From the Lübeck Institute of Experimental Dermatology
of the University of Lübeck
Director: Prof. Dr. Saleh M. Ibrahim

"Host genome – microbiome interaction and its influence on chronic inflammation in the skin in the mouse"

Dissertation
for Fulfillment of
Requirements
for the Doctoral Degree
of the University of Lübeck

from the Department of Natural Sciences

Submitted by

Adina-Malin Hartmann
From Schleswig

Lübeck, 2023

First referee: Prof. Dr. Saleh Ibrahim

Second referee: Prof. Dr. Christian Sina

Date of oral examination: 30.10.2023

Approved for printing: Lübeck, 10.11.2023

Eigenständigkeitserklärung

Hiermit versichere ich, dass ich die hier vorliegende Dissertation eigenständig und ohne fremde Hilfe angefertigt habe. Alle verwendeten Hilfsmittel und Quellen wurden angegeben. Zudem bestätige ich, dass ich weder vorher noch gleichzeitig woanders einen Zulassungsantrag gestellt noch diese Dissertation vorgelegt habe.

Summary

Autoimmune diseases of the skin become more and more prevalent, as the incidence is rising all over the world and the etiology is not completely understood. Two factors that might play a role in disease susceptibility and development are the mitochondrial genome and the microbiome. Mitochondria are essential for the organism in terms of energy metabolism, cell signaling and oxidative stress. The immune system is directly influenced by the mitochondrial function. The microbiome on the other hand populates all surfaces of the body, especially the intestine, and interacts directly with immune system through microbial metabolites. Shifts in the composition and diversity of the microbiome are an indicator for several autoimmune diseases.

This study aims to investigate the role of the mitochondrial genome and the microbiome in terms of the autoimmune skin blistering disease Epidermolysis bullosa acquisita (EBA). Therefore, the conplastic mouse strain B6-mt^{FVB} is used as model organism. This strain is of interest because 1) it carries a non-synonymous substitution in the *mt-Atp8* gene, which was already identified to play a role in Bullous pemphigoid patients. 2)Its gut and skin microbiome differ from the common lab strain B6. 3) The strain seems to be protected to some extend in the experimental induced EBA model.

First, does the mitochondrial mutation influence the immune system in terms of immune cell subpopulations and the integrity of the gut? Therefore, expression levels of tight junction proteins and cytokines in the gut were analyzed, immune cell subpopulations in skin and spleen were quantified via flowcytometry and immune cells in the skin were counted using immunohistochemistry. The amount of γδ T cells is significantly less in the back skin of B6-mt^{FVB} mice, whereas there is no difference in the other parameters. Next, to what extend does the microbiome influence EBA disease development and what parameters are different in the microbiome of B6-mt^{FVB} mice? EBA experiments in germ-free mice revealed that the disease progression is significantly milder than in conventional housed mice. Furthermore, in the analysis of shotgun metagenomics data of cecum content significantly different indicator species, abundant pathways and gene families were identified. After checking the relationship of the indicator species to significantly different abundant metabolites found in metabolomic analysis from liver samples, the next question was whether the here identified metabolites Spermidine, D-Ribose, D-Glucosamine, N-acetyl-D-Glucosamine and Oxalate could directly influence the disease outcome in EBA. The identified metabolites showed their anti-inflammatory potential *in vitro* as they reduced ATP, nitric oxide and TNFα production in RAW 264.7 cell macrophages after LPS exposure. The most promising metabolites Spermidine and N-acetyl-D-Glucosamine were tested in the EBA mouse model and N-acetyl-D-Glucosamine showed an alleviating trend in male B6 mice.

In conclusion, this study indicates a correlation between the mitochondrial genome and the amount of γδ T cells in the skin. It also highlights the importance of the microbiome in terms of EBA disease development and identified promising metabolites such as N-acetyl-D-Glucosamine, which can be used in therapy approaches for EBA.

Zusammenfassung

Autoimmunerkrankungen der Haut sind von immer größerem Interesse, da die weltweite Inzidenzrate steigt und die Ursachen noch nicht völlig bekannt sind. Zwei wichtige Ursachen in Bezug auf Krankheitsanfälligkeit und -entwicklung könnten das mitochondriale Genom und das Mikrobiom sein. Mitochondrien sind essentiell für den Organismus, da sie an Energiestoffwechsel, Zellsignalen und oxidativem Stress maßgeblich beteiligt sind. Daher beeinflusst ihre Funktion direkt das Immunsystem. Dahingegen bevölkert das Mikrobiom alle Körperoberflächen, insbesondere den Darm, und interagiert direkt mit dem Immunsystem via mikrobiellen Metaboliten. Veränderungen des Mikrobioms in der Komposition und Diversität sind Indikatoren für mehrere Autoimmunerkrankungen.

Diese Studie untersucht die Rolle des mitochondrialen Genoms und des Mikrobioms in Bezug auf die blasenbildende Autoimmundermatose Epidermolysis bullosa acquisita (EBA). Als Modellorganismus dient dafür der konplastische Mausstamm B6-mt^{FVB}. Dieser Mausstamm ist von Interesse, da er 1) eine nichtsynonyme Substitution im *mt-Atp8* Gen trägt, dessen Rolle schon in Patienten mit bullösem Pemphigoid erkannt wurde; 2) sein Haut- und Darmmikrobiom sich vom Laborstamm B6 unterscheidet, und 3) der Stamm im experimentell induzierten EBA-Modell milder betroffen ist als B6.

Die erste Frage, die zu beantworten wäre, beschäftigt sich mit Einfluss des mitochondrialen Genoms auf das Immunsystem in Bezug auf Immunzellteilpopulation und Darmintegrität. Dafür wurden wurden Expressionslevel von Zytokinen sowie Proteinen der Tight Junctions analysiert, Immunzellteilpopulationen in Haut und Milz mittels Durchflusszytometrie analysiert und Immunzellen in der Haut mittels Immunhistochemie gezählt. Es konnte gezeigt werden, dass B6-mt^{FVB} Mäuse signifikant weniger γδ T-Zellen in der Rückenepidermis aufweisen, während es bei den anderen Parametern keinen Unterschied gibt. Als nächstes wurde untersucht, in wie weit das Mikrobiom die Krankheitsentwicklung von EBA beeinflusst und welche mikrobiellen Parameter im Mikrobiom von B6-mt^{FVB} Mäusen anders sind. EBA Experimente in keimfreien Mäusen offenbarten, dass der Krankheitsverlauf signifikant milder verläuft als in konventionell gehaltenen Tieren. Des Weiteren konnten in metagenomischen Datensätzen aus Proben des Ceacuminhalts signifikant unterschiedliche Indikatorspezies, genutzte Stoffwechselwege und Genfamilien identifiziert werden. Als nächstes wurden die Verbindungen der Indikatorspezies mit den aus metabolomischen Analysen identifizierten, signifikant unterschiedlich vorhandenen Lebermetaboliten untersucht. Daraus entstand die Frage ob die identifizierten Metabolite Spermidin, D-Ribose, D-Glucosamin, N-acetyl-D-Glucosamin und Oxalat die Krankheitsentwicklung in EBA direkt beeinflussen können. *In vitro* konnte das entzündungshemmende Potential aller Metabolite festgestellt werden, da sie die ATP-, Stickoxid-

und TNFα Produktion in LPS-stimulierten RAW 264.7 Makrophagen reduzieren. Die vielversprechendsten Metabolite Spermidin und N-acetyl-D-Glucosamin wurden im EBA Mausmodell getestet und letzteres zeigte einen mildernden Trend in männlichen B6 Mäusen.

Zusammenfassend zeigen diese Ergebnisse eine Korrelation zwischen dem mitochondrialen Genom und der Anzahl von γδ T-Zellen in der Haut. Außerdem heben sie die Bedeutung des Mikrobioms in Bezug auf den Krankheitsverlauf in EBA hervor und identifizierten vielversprechende Metabolite wie N-acetyl-D-Glucosamin, die als neue Therapieansätze für EBA dienen.

Table of contents

List of figures

List of tables

Abbreviations

Abbreviation	Complete word	Meaning
AIBDs	Autoimmune blistering diseases	Chronic inflammatory diseases of the skin
ATP	Adenosine triphosphate	Energy provider for many processes in the cell
B6	C57BL/6, “Black 6”	Common lab mouse strain
BCA assay	Bicinchoninic acid assay	Method to determine total protein concentration
BSA	Bovine Serum Albumin	Proteins from bovine blood, used e.g., as protein standard or as blocker in immunohistochemistry
cDNA	complementary DNA	DNA without introns, reversed transcribed from RNA
DAPI	4’,6-diamidino-2-phenylindole	A fluorescent stain which binds DNA
DMEM	Dulbecco’s Modified Eagle’s Medium	Standardized growth medium for cell culture
DNA	Deoxyribonucleic acid	A two chained molecule carrying genetic information
EBA	Epidermolysis bullosa acquisita	Autoimmune skin blistering disease
ELISA	Enzyme-linked immunosorbent assay	Biochemical assay to detect and quantify target molecules
ELPHO buffer	Electrophoresis buffer	Buffer to reduce electric resistance during the electrophoresis
FITC	Fluorescein isothiocyanate	Green fluorochrome with emission spectrum between 495 – 519 nm
FMT	Fecal microbiota transplantation	Therapy approach to overcome dysfunctional gut microbiome
HRP	Horseradish peroxidase	Enzyme used to detect target molecules
IBD	Inflammatory bowel disease	Autoimmune disease of the gut. Two types: Crohn’s disease and Ulcerative colitis

IFNγ	Interferon gamma	Important cytokine in innate and adaptive immunity
IgG	Immunoglobulin G	antibody
KEGG	Kyoto Encyclopedia of Genes and Genomes	Collection of molecular databases
LC-MS	Liquid chromatography – mass spectrometry	Analytical chemistry technique
LDH	Lactate dehydrogenase	enzyme that is released during tissue damage
LPS	Lipopolysaccharides	Component of the outer membrane of gram-negative bacteria, promotes pro-inflammatory immune response
MELUND	Ministerium für Energiewende, Landwirtschaft, Umwelt, Natur und Digitalisierung	Ministry, responsible for permissions of animal experiments
MOPS buffer	(3-(N-morpholino) propane sulfonic acid buffer	Buffer used e.g., for protein purification
MT-ATP8	mitochondrially encoded ATP synthase membrane subunit 8	Complex V enzyme, which is responsible for the last step of oxidative phosphorylation in the electron transport chain
mtDNA	Mitochondrial DNA	DNA of the mitochondrial genome
NaCl	Sodium chloride	Salt used for isotonic solutions
PBS	Phosphate-buffered saline	Isotonic buffer to maintain the pH
PCR	Polymerase chain reaction	Method to amplify genomic material
RIPA buffer	Radioimmunoprecipitation Assay buffer	A lysis buffer for cells and tissue for fast solubilization of proteins
RNA	Ribonucleic acid	Needed for translation from genetic information into proteins
rpm	Rounds per minute	Unit for centrifugation speed
ROS	Reactive oxygen species	Highly reactive chemicals with roles in cell signaling
SDS-PAGE	sodium dodecyl sulphate–	A method to separate proteins

	polyacrylamide gel electrophoresis	according to their molecular mass
TBS	Tris-Buffered Saline	Isotonic buffer to maintain the pH
TBST	Tris-Buffered Saline plus Tween20	Isotonic buffer to maintain the pH and solve antibodies
TMB	3,3’,5,5’-Tetramethylbenzidine	A chromogenic substrate used to visualize e.g., HRP labeled molecules
TNFα	Tumor necrosis factor alpha	Cytokine which is used as an inflammatory response

1 Introduction

1.1 Mitochondria - Genome and function

Mitochondria are important organelles of the animal cell. They are thought to originate from bacteria and therefore keep a bit of independence[1]. Mitochondria are called the powerhouse of the cell[2], which describes their dominant role. They produce energy in form of ATP in dependence of oxygen, the so called aerobic respiration[3].

For the electron transport chain NADH and $FADH_2$ are required, which are produced via the citric acid cycle or by glycolysis[4]. The electrons from the NADH and $FADH_2$ are transferred to energy rich oxygen and protonic hydrogen (H+)[3]. This process is performed by NADH dehydrogenase, cytochrome c reductase and cytochrome c oxidase. The accumulated protons in the mitochondrial intermembrane space are utilized by the ATP synthase to phosphorylate ADP to ATP, fueled by the energy of the strong electrochemical gradient[4]. ATP/ADP translocase helps the ATP to leave the inner membrane, which then exits the outer membrane via porins[5] Imbalance in the electron transport chain can cause in the formation of reactive oxygen species (ROS) such as superoxide which lead to oxidative stress and a decline in mitochondrial function[6].

Besides the energy supply mitochondria also possess other important functions such as signaling through reactive oxygen species[7], calcium[8] and hormones[9–11]. Additionally, they regulate the cellular metabolism, cellular differentiation, the cell cycle, cell growth and membrane potential[4,12]. Another important task is the programmed cell death including calcium-evoked apoptosis[8,13,14]. Moreover, mitochondria also function in heme synthesis reactions[15], steroid synthesis[16] and reporting the neuronal status towards the microglia in terms of cellular quality control[17]. And last but not least, mitochondria are essential for the function of the immune system[18,19]. For example in terms of T cell activation and differentiation, memory T cell formation, macrophage polarization and innate immune signaling response[19–21].

Mitochondria possess their own genome in form of a circular double-stranded DNA, which is in parts similar to bacterial genomes[22]. For humans the mitochondrial genome contains about 16 kilobases and encodes 37 genes[23]. Among these are 13 protein coding genes for the subunits of the respiratory complexes I, III, IV and V, 2 genes for 12S and 16S rRNA and 22 genes for tRNAs for each amino acid plus an extra gene for serine and leucine[23–25]. The mtDNA lacks introns[24] and can be present in up to ten copies per mitochondrion[26]. Nevertheless, most proteins required for the mitochondrial function are encoded in the nuclear DNA of the cell and transported into the mitochondrion[24].

Replication of the mitochondria occurs through mitochondrial fission. The host cell tightly regulates this process which is mainly a response to the energy needs of the cell. Therefore, mitochondria

numbers differ between different cell types and are also randomly distributed during host cell division. The balance between mitochondrial fusion and fission dynamics is an important factor in several disease pathologies[27–30].

The mitochondrial genome was thought to be exclusively inherited by the mother as paternal mitochondria are ubiquitinylated for later destruction in the embryo[31]. Nevertheless, Luo *et al*. showed recently that biparental inheritance of mitochondria indeed occurs in humans in rare exceptions[32,33].

1.2 Role of mitochondria in diseases

Playing a critical role in cell metabolism, mitochondrial dysfunction can cause diseases in every organ of the body[34]. Among these diseases are e.g., mitochondrial diseases[35], cardiac dysfunction up to heart failure[36,37], the onset of Alzheimer's disease[38], Parkinson's disease[39] and other neurodegenerative diseases[40]. But also mental health is affected by dysfunctional mitochondria as shown in attention-deficit/hyperactivity disorder[41], autism[42,43], bipolar disorder[44], depression and schizophrenia[45,46].

In general, damaged mitochondria have the ability to be repaired[47]. Therefore, fusion of two malfunctioning mitochondria is required, then they reform and split again resulting in one functional mitochondrion and one that is damaged[48]. Dysfunctional mitochondria can also be transported away or accumulate and introduce programmed cell death[34]. Failures in repair, transport or destruction lead e.g. to the above-mentioned diseases.

Another important factor for dysfunctional mitochondria is the production of reactive oxygen species (ROS). High levels of ROS can lead to oxidative stress which in turn damages cell structures and genetic information[49]. It was observed that an imbalance between antioxidant defenses and ROS production can interfere with cellular function e.g., in aging[50]. Additionally, mtDNA fragments that arise during mtDNA degradation by ROS damage can enter the cytosol of the cell and induce effective type I IFN production[51–53].

As mitochondria affect every cell of the human body their influence in complex diseases, especially in autoimmunity is critical. Further research to disentangle the influence of every single mitochondrial compartment is needed.

1.3 Microbiome – general Overview

The microbiome is a complex community of thousands of microorganisms such as bacteria, fungi and viruses that colonize different habitats such as skin, vagina, oral cavity and the gut[54,55]. The habitats are colonized after birth and differ in composition and abundance between location and

individuals[54,55]. The biggest community is the gut microbiome, consisting of over 1500 species and more than 50 phyla[56,57]. The most dominant phyla are Bacteroidetes and Firmicutes followed by Proteobacteria, Fusobacteria, Tenericutes, Actinobacteria and Verrucomicrobia[58,59].

The microbiome diversity and composition depend on several factors. Starting from the mode of delivery where infants harbor either vaginal or skin microbial communities[60–62], breast feeding[63] and aging[64–70]. But also other environmental factors such as the geographic location impacts the microbiome, probably because of different atmosphere, host genetics and lifestyles[71–74]. Lifestyle impacts can be e.g. smoking[75,76] or how much exercise the individuum gets[77]. Another factor is usage of antibiotics, which will not only kill the harmful bacteria but also the commensals and therefore lead to dysbiosis[78–80]. Concentration and intake duration are a critical point to adjust antibiotic treatment[81].

One of the biggest impacts on the microbiome has diet. It can modulate the microbiota and their produced metabolites in a harmful or a useful direction[82].The diet consumed mainly in Western society is rich on fats and proteins. This type of diet increases susceptibility to infection by reducing immunity and also increases the risk to develop metabolic diseases[58]. Correlating with a high fat and high protein diet is a suppression of Firmicutes and the abundance of bile tolerant species e.g. Bacteroides, Alistipes and Bilophila[83,84]. An essential food source on the other hand is dietary fiber consumption. It improves the intestinal barrier integrity[85] and controls glucose levels to promote a healthier metabolic profile[86]. One additional sign of gut health is the fermentation of dietary fiber to short chain fatty acids (SCFAs).

SCFAs such as acetate, propionate and butyrate are bioactive food components which can enter the colon and serve as an energy supply for intestinal epithelial cells as well as supporting the mucosal barrier integrity[87–90]. They are produced mainly by Firmicutes, Bacteroidetes and other anaerobic species, which increase in response to exercise[91,92]. SCFAs impact human health in different ways: Propionate and butyrate have anti-inflammatory properties as they prevent e.g. from allergic airway diseases[93] or stimulate immune cells to produce cytokines[94]. Additionally, SCFAs have chemo-preventive potential and can act as tumor suppressors[95,96]. Next, SCFAs also strengthen the blood brain barrier by increasing the production tight junction proteins[97]. All these effects are probably due to the fact that SCFAs are able to reduce the activity of histone deacetylase in several cells[98]. Consequently, disturbance of the microbiome especially when antagonistic to SCFA producing species will have pathogenic effects on the host[99].

Beside SCFAs the microbiome also produces other important metabolites. It produces e.g. vitamin B and K as well as biotin, cobalamin, nicotine, thiamine, riboflavin and therefore is essential in the

vitamin synthesis[100]. Additionally, the bacteria are able to produce bile acids as well as conjugated fatty acids and cholesterol for lipid digestion and cell signaling[101]. It was also shown that the gut microbiome can synthesize neurochemicals that lead to a crosstalk between gut, brain and central nervous system and therefore influences the mood and behavior of the host[102–105]. The microbial products influence the whole system of the host and is therefore an important factor for its health.

Talking about health, the microbiome exhibits crucial functions for the host by counteracting pathogens through antimicrobial peptide production and immune system activation[106,107]. The immune system and the microbiome interact closely as it impacts the development and function of the immune system[63,108–112]. The immune system recognizes the microbiome through pattern recognition receptors such like Toll-like receptors or nucleotide-binding oligomerization domains[113,114]. These receptors can distinguish between microbe-associated molecular patterns (MAMPs) and pathogen-associated molecular patterns (PAMPs)[115,116]. Therefore, the microbiome is a critical factor in the balance of health and disease.

1.4 Role of microbiome in diseases

Lately, the importance of commensals in several disease pathologies including autoimmune diseases, has come into focus. The microbiome and the host form a complex symbiosis. Changes in this concept leading to dysbiosis have detrimental effects on both parts as dysbiosis is associated with several diseases such as gastrointestinal, metabolic, oncologic, neurologic, psychologic and immune related diseases[59,117].

The microbiome can contribute to disease development in different ways. Examples for diseases associated with microbial dysbiosis are Irritable bowel disease[118], Inflammatory bowel diseases[119,120], obesity and type 2 diabetes[121–123], cardiovascular diseases[124], asthma and allergic diseases[125–127], psoriasis and atopic dermatitis[128], and autistic spectrum disorders[129]. Additionally, changes in the metabolism and function of the microbiota can promote diseases as shown in liver disease[130], obesity[131], cardiovascular diseases[123,132] or in the case of *Staphylococcus epidermidis*, which can switch its metabolism from a friendly to an inflammation promoting state[133–136]. Furthermore, the microbiome is able to regulate aspects of the immune system e.g., through high amounts of LPS that trigger cytokine expression, promoting antimicrobial peptide production or decreasing the barrier integrity of the respective surface[117,137–139]. This interference can be seen in type 1 diabetes[140], psoriasis[141–143], anxiety[144], depression[145] and Alzheimer's disease[59,146]. And last but not least also single bacteria strains can have detrimental effects as seen in the carcinogenic properties of *Helicobacter pylori* or *Fusobacterium nucleatum*[147,148]. They produce compounds that are either harmful to host DNA or create a pro-inflammatory environment which enhances tumor development[149]. So the capacity of disease promotion depends on the host's genetic predisposition,

the state of activation of the immune system, the localization of the microbe an the presence of other commensal and/or pathogenic microbes[150].

The microbiome can also be used as a therapeutic target. There are three different possibilities yet: Probiotics and prebiotics, fecal microbiota transplantations (FMTs) and phage therapy[59].

Probiotics are living bacteria such as *Lactobacillus* or *Bifidobacteria* that were shown to improve health in individuals when taken[151,152]. These bacteria produce SCFAs which lower the pH, can synthesize B and K vitamins, show antimicrobial activity against pathogens and stimulate the immune system of the host[153,154]. Diseases treated with probiotics are obesity, urinary tract infections, diarrhea, irritable bowel syndrome, cardiovascular diseases, diabetes, depression and anxiety[155–158]. Probiotics can also be given as prevention for dysbiosis e.g., in antibiotic therapy or long stress situations[59,159]. Prebiotics are microbial products or other selected metabolites that modulate the function and organization of the gut microbiome to improve health[160]. They can strengthen the mucosal barrier, increase the host immunity or act as growth inhibitor for pathogens[161].

The principle of FMTs is to restore the dysfunctional and disturbed gut microbiome of patients by transplanting the fecal bacterial communities of healthy donors[162]. This therapy approach was already tested in diseases such as diarrhea, IBD, obesity, insulin resistance, metabolic syndrome, colon cancer, neuropsychiatric conditions, autism and Parkinson's disease[59,163–167]. One big disadvantage of this method is the hard to predict safety of the transferred microbiome due to its complexity[168,169]. Furthermore, it was shown in several studies that phenotypes can be transplanted with the microbiome e.g., insulin resistance, obesity, cardiovascular diseases, metabolic syndromes and depression[108,170–174].

For phage therapy small viruses, bacteriophages, are used that attach to bacterial cells and infect them[175]. The infected cells are unable to reproduce and instead help to increase the amount of phages[175]. Phages have a big therapeutic potential as they are very specific in their target bacteria and therefore, can be used not only as antimicrobial agent but also for modulation purposes of the microbiome[176]. Nevertheless, the dose and timing of the phage treatment is still under investigation as the amplification rate of the phages is not constant and the hosts immune response also interferes with the treatment outcome[177].

1.5 Autoimmune skin blistering diseases

As for other autoimmune diseases the etiology for autoimmune blistering diseases (AIBSs) is multifactorial. Trigger factors are the environment as well as age, gender, ethnicity and genetics of the patients[178]. Yet, compared to other autoimmune diseases like rheumatoid arthritis AIBDs incidence is still rare but nevertheless potentially fatal[178]. AIBD patients produce autoantibodies

targeting molecules in the dermal-epidermal junctions or the epidermis itself. Antibody binding leads to subsequent loss of cell-matrix and cell-cell contact and the inflammation develops in form of erosion and blister formation[179,180]. According to their antigen location AIBDs can be divided into pemphigus and pemphigoid diseases.

Pemphigus diseases are described by targeting intraepidermal molecules. Those molecules are most of the time desmogleins 1 or 3, which are respectively expressed in the upper or lower layer of the epidermis[178,181,182]. Degradation of these structures leads to intraepidermal blister formation[178]. Most prominent pemphigus diseases accounting for nearly 90% of all cases are pemphigus vulgaris (PV) and pemphigus foliaceus(PF)[178]. Interestingly, the incidence of pemphigus diseases differs between populations with PV being more prevalent in Western populations and PF in South America and Northern Africa[183].

Pemphigoid diseases are described by antibodies targeting molecules in the dermal epidermal junctions. The subsequent inflammation in the dermal epidermal junctions results in the degradation of anchoring fibrils and filaments and next to subepidermal blister formation[178]. The most common pemphigoid disease in Central Europe is bullous pemphigoid (BP). Inflammatory cell infiltration as well as subepidermal blistering is characteristic for this disease[178,180]. The target proteins of BP are bullous pemphigoid antigen (BPAG) 1 and BPAG 2 (type XVII collagen), which are mostly bound by IgG and IgA[184–186].

Different treatment strategies exist for AIBDs. Starting from corticosteroids, both topical and systemic supplied[187,188], immunosuppressant drugs such as azathioprine, dapsone, doxycycline, methotrexate, or mycophenolate mofetil[189], anti-inflammatory drugs like tetracycline antibiotics and niacinamide[190,191] up to biologic therapy approaches with intravenous immunoglobulins or the adjuvant rituximab[192,193]. Nevertheless, treatment of AIBD patients is challenging not only because of severe side effects of the drugs but also because only a minority achieve clinical remission[189].

1.6 Epidermolysis bullosa acquisita

Epidermolysis bullosa acquisita (EBA) belongs to the pemphigoid diseases and is characterized by autoantibodies against the anchoring fibril type VII collagen[194]. The incidence of EBA is comparably rare with 0.2-0.5 cases per million/year and usually develops in adulthood[194,195]. EBA can be divided into two subtypes: the mechanobullous EBA characterized by skin fragility, scarring, noninflammatory tense bullae and the formation of milia, and the inflammatory EBA which is reminiscent of BP or other subepithelial AIBDs[179,195].

EBA is characterized by autoantibodies against type VII collagen a major component of anchoring fibrils[196,197]. These antibodies can be detected in serum of EBA patients[198], with direct

immunofluorescence microscopy of perilesional skin[199–202] and ELISA[203]. Type VII collagen has major antigenic epitopes, which are located in the noncollagenous (NC)1 domain, responsible for maintaining the structural integrity of the dermal epidermal junctions[195,204]. In EBA patients the number of these anchoring fibrils is reduced, explaining the skin fragility and bullous formation[205,206]. In theory, autoimmunity against type VII collagen could be influenced by the MHC locus HLA-DR2 which is associated genetic factor in the disease onset[179,207].

EBA often co-occurs together with other diseases such as systemic lupus erythematosus, rheumatoid arthritis, diabetes, amyloidosis, multiple endocrinopathy syndrome, pulmonary fibrosis, thyroiditis, chronic lymphocytic leukemia and thymoma[208]. Most common is the association with inflammatory bowel disease (IBD)[204]. A potential link between these disease is the presence of type VII collagen in the colon and the presence of antibodies against type VII collagen in some IBD patients[195,209–211]. More studies are needed to elucidate the relationship between IBD and EBA.

Optimal treatment approaches for EBA are lacking as the disease is difficult to treat and so rare that it is hard to get enough patients for randomized therapeutic trials[212]. So, to examine the pathogenicity of type VII collagen antibodies as well es the route of inflammation and possible therapy approaches passive transfer studies in animals were developed[213–215]. Briefly, rabbits were injected with murine type VII collagen and produce antibodies (IgG) against it. These antibodies were extracted from the serum and injected subcutaneously in the mice, which subsequently develop skin lesions comparable to EBA in humans[214]. Thus, this animal model is perfectly suited to examine the disease and try out new therapy approaches.

1.7 B6-mt^{FVB} mouse strain in EBA

Genetic predisposition of the host is an important factor in the development of AIBDs. To investigate the influence of specific genes, especially in the mtDNA, Yu *et al*. generated conplastic mouse strains[216]. One of these strains is the B6-mt^{FVB} mouse strain, which harbors the nuclear genome of the common lab strain B6 and the mitochondrial genome of FVB mice (Figure 1). This mitochondrial genome has three polymorphisms compared to wild type B6 mice (Table 1): An insertion in the *mt-Tr* repeat, a non-synonymous substitution in the *mt-Nd3* gene, and a synonymous substitution in the *mt-Atp8* gene from Aspartate to Tyrosine.

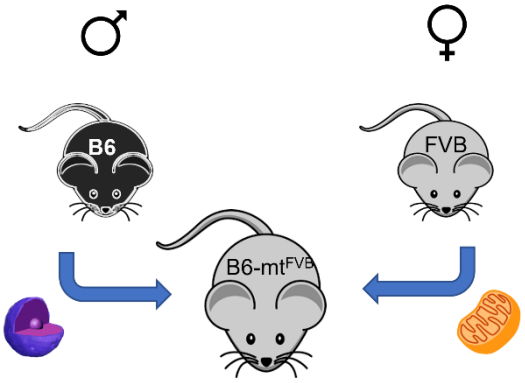

Figure 1: Schematic description of conplastic mouse line B6-mt^{FVB}. The conplastic mouse line B6-mt^{FVB} carries the nuclear genome of the B6 mice and the mitochondrial genome of the FVB mouse strain.

Table 1: mtDNA polymorphisms in B6 and B6-mt^{FVB} mice. Substitutions occur non-synonymously in the mt-Atp8 gene, synonymously in the mt-Nd3 gene; and in the mitochondrial arginine-tRNA. Asp: Aspartate; Met: Methionine; Tyr: Tyrosine; mtXXXX: position of the nucleotides in the mtDNA.

Gene	Nucleotide differences			Consequence
	Position of the mutation	C57BL/6J (B6)	C57BL/6J-mt$^{FVB/NJ}$ (B6-mt^{FVB})	
mt-Atp8	**mt7778**	**G**	**T**	**Asp → Tyr**
mt-Nd3	mt9461	C	T	Met → Met
mt-Tr	mt9821	8A	9A	-

The polymorphism in the mitochondrial encoded ATP synthase 8 gene is of special interest as it was shown to play a role in endotoxic liver failure[217], aggravate diet-induced non-alcoholic steatohepatitis (NASH)[218], diabetes[219], anxiety[220] and Alzheimer's disease[221]. Additionally, it was shown that susceptibility to bullous pemphigoid in a German cohort is associated with *mt-Atp8* gene[222]. Following these results, Schilf *et al*. performed the experimental induced EBA mouse model in wild type B6 and B6-mt^{FVB} mice and could show that the conplastic mice develop significantly less disease. (Figure 2)[223].

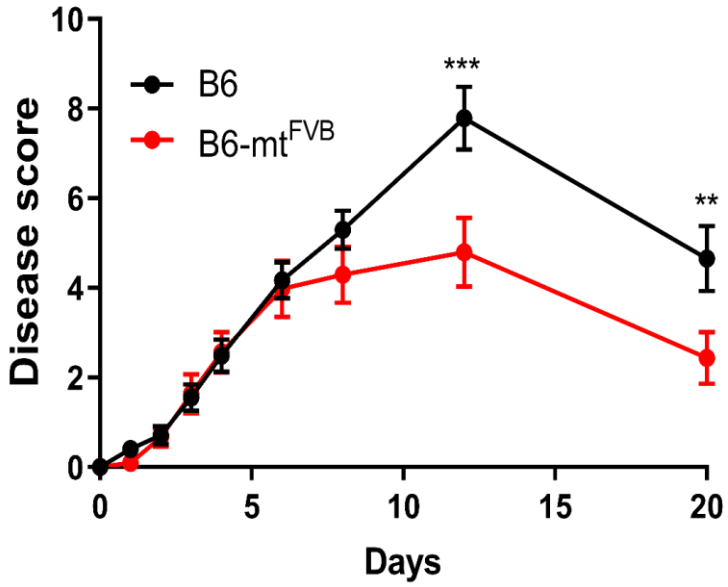

*Figure 2: Disease development of passive induced Epidermolysis bullosa acquisita in B6 and B6-mt^{FVB} mice. B6-mt^{FVB} mice (red) develop significantly less disease compared to wild type B6 mice (black). (Two Way ANOVA*** p<0.001, ** p<0.01. n = 17 males (B6), 20 males (B6-mt^{FVB})). Schilf et al. 2021[223]*

1.8 Microbiome of B6-mt^{FVB} mice

Besides the interesting disease results the skin and gut microbiome of B6 and B6-mt^{FVB} mice was analyzed using 16S rRNA sequencing[224]. It could be shown that both the skin and the gut microbiome have a significant different beta diversity compared to wild type mice (Figure 3)[224].

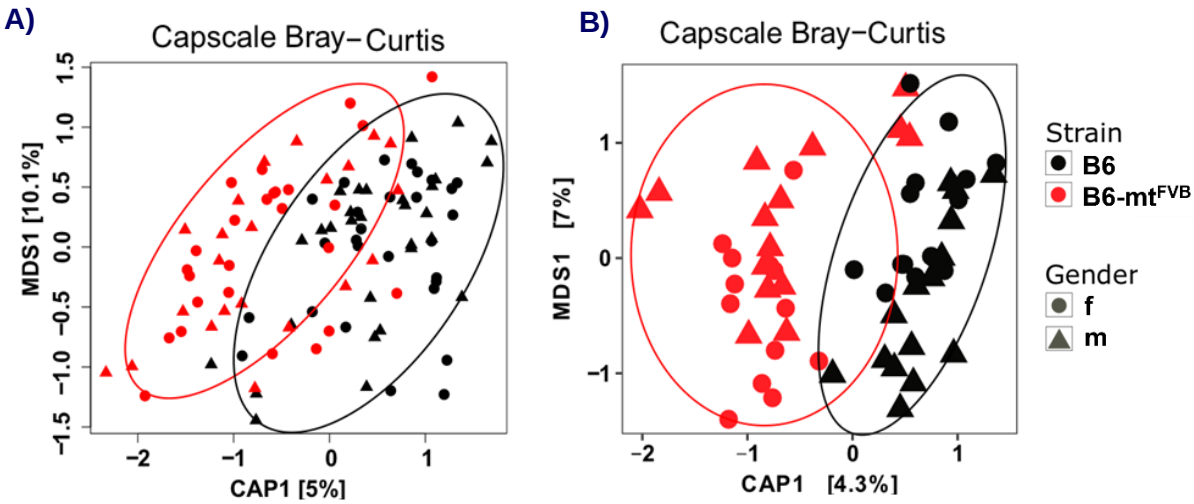

Figure 3: Beta diversities of microbial communities from A) gut and B) skin microbiome. Bacterial DNA was extracted for 16SrRNA amplicon next generation sequencing. Hirose et al. 2017.[224]

Following these results, the microbiome went in focus of interest. Therefore, a targeted metabolomic analysis of bacterial produced SCFAs in liver, skin lymph nodes and thymus was performed. It was shown, that levels of Propionyl-L-carnitine are increased in tissues of B6-mt^{FVB} mice compared to B6 mice, whereas levels for butyrate and acetate are similar or decreased in tissues of conplastic mice

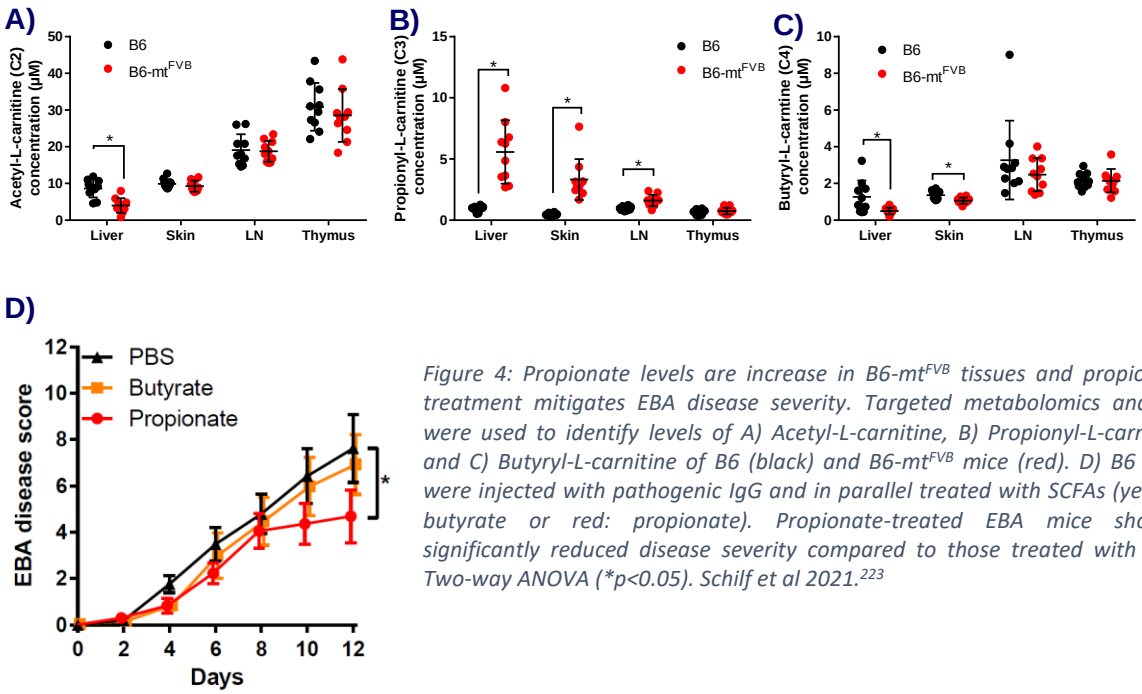

*Figure 4: Propionate levels are increase in B6-mt^{FVB} tissues and propionate treatment mitigates EBA disease severity. Targeted metabolomics analysis were used to identify levels of A) Acetyl-L-carnitine, B) Propionyl-L-carnitine and C) Butyryl-L-carnitine of B6 (black) and B6-mt^{FVB} mice (red). D) B6 mice were injected with pathogenic IgG and in parallel treated with SCFAs (yellow: butyrate or red: propionate). Propionate-treated EBA mice showed significantly reduced disease severity compared to those treated with PBS. Two-way ANOVA (*p<0.05). Schilf et al 2021.[223]*

(Figure 4 A-C)[223]. Propionate was already shown to have anti-inflammatory properties as it suppresses colonic inflammation[225], decreases immune response to microbial stimulation[226], protects from allergic airway inflammation[93] and improves insulin sensitivity in obese mice[227]. Treating wild type mice with propionate during the passive EBA model lead to a milder disease development, whereas butyrate had no effect (Figure 4 D)[223].

1.9 Objective

This study aims to investigate three objectives: First, whether the mitochondrial mutation alone influences the disease outcome. Therefore, the influence of the mitochondrial mutation on skin, gut and immune tissues in terms of immune cell composition, cytokine expression and gut permeability changes is analyzed.

Second aim is to what extend the microbiome alone influences the disease outcome by comparing the EBA development of germ-free and conventional housed B6 mice. Furthermore, to identify potential microbial species and/or metabolites that drive the disease outcome with the help of metabolomics from liver and shotgun metagenomics of cecum content.

Third, examining the anti-inflammatory potential of the identified metabolites *in vitro* with assays in RAW 264.7 cell macrophages and in the disease setting.

2 Methods

2.1 Mouse strains and growth conditions

Two mouse strains were used for the experiments: The C57BL/6J (B6) strain from Jackson laboratory (Bar Harbor, ME, USA) and the conplastic mouse strain C57BL/6J-mt$^{FVB/NJ}$ (B6-mt^{FVB}) from Yu *et al*. (2009)[216]. Both mouse strains were bred and housed in the animal facility of the University of Lübeck. They have food and water available *ad libitum* and live in a stable light-dark cycle as well as controlled temperature and humidity. All mice are checked daily by the animal care takers.

All performed experiments were permitted by the ethical committee of the ministry of energy transition, agriculture, environment, nature and digitalization (MELUND) of Schleswig-Holstein and follow the guidelines of animal welfare.

2.1.1 Germ-free mice

Some experiments were performed in the germ-free mouse facility of the Max Planck Institute of Evolutionary Biology in Plön. B6 and B6-mt^{FVB} mice lived under germ-free conditions in isolators. Lines were introduced via hysterectomy and raised by germ-free foster mothers. Everything entering the isolator was autoclaved and or incubated for 1 hour in 3% peracetic acid for decontamination.

2.2 Cryotome sections of skin tissue

Hair was shaved from the backs of the mice and the naked dorsal skin was taken for further analysis. The tissue was snap frozen in liquid nitrogen and stored at -80° C until further procedure. Then the tissue was positioned in a Tissue-Tek Cryomold Intermediate plastic using forceps and Tissue-Tek O.C.T. Compound was added to the tissue inside the –20° C cold cryotome chamber. After the compound was frozen, 6 µm thick sections were performed with the cryotome. The sections were directly put on microscopy slides and quality checked under the microscope. Then the microscopy slides were stored at -20° C.

2.3 Immunohistochemistry of skin sections

The prepared microscopy slides with cryo sections from 2.2 were incubated for 10 min at room temperature. Afterwards the sections were fixed on the slides due to 10 min incubation in cold Acetone at 4° C. To get rid of the remaining Tissue Tek residues and Acetone the slides were washed three times for 5 min in TBST (50 mM Tris, 150 mM NaCl, 0.05 % Tween 20, pH 7.6) and then circled with a hydrophobic Dako pen. At next the samples were blocked for 45 min at room temperature with TBS (50 mM Tris, 150 mM NaCl) with 3 % Biotin free BSA. Then the primary Biotin anti mouse CD3ε antibody (BioLegend, #100304, 1:100 in TBS) or the isotype control Biotin Armenian Hamster IgG (BioLegend, #400904, 1:100 in TBS) was applied and incubated for 1 h at room temperature, followed by 3 washing steps in TBST buffer for 5 min each. Then the fluorophore Streptavidin Dylight

594 (Thermo Scientific, #21842, 1:200 in TBS) was coupled for 30 min at room temperature in darkness, followed by 3 washing steps in TBST buffer for 10 min each. At a next step the Biotin anti-mouse TCR γ/δ antibody (BioLegend, #118103, 1:100 in TBS) or its isotype control Armenian Hamster IgG was applied and incubated for 1 h at room temperature, followed by 3 washing steps with TBST buffer for 5 min each. Afterwards the second fluorophore Streptavidin Dylight 488 (Thermo Scientific, #21842, 1:200 in TBS) was coupled for 30 min at room temperature, followed by 3 washing steps with TBST buffer for 10 min each. At last step the cover slip was mounted with DAPI and slides should be stored at 4° C in the dark. Analysis was done with Keyence BZ-9000E fluorescence microscope (Keyence Deutschland GmbH, Germany) and ImageJ software.

2.4 Generation and isolation of pathogenic IgG

2.4.1 Isolation of total IgG via affinity purification

To generate antibodies against murine collagen VII, rabbits were injected with murine collagen VII. Rabbit serum was collected and purified with protein G resin affinity chromatography. Briefly, 5 ml of protein G resin was incubated with 100 ml rabbit serum for 1 hour at 4°C to bind the Fc region of the IgG. PBS was used to wash out the free proteins followed by the elution of the IgG fraction with 0.1 M glycine buffer (pH 2.8). At a next step, 1 M Tris-base (pH > 9) was used to neutralize the fraction. The solution was exchanged with PBS over night at 4°C and concentrated with 30.000 Da filter pore sized Amicon centrifugation tubes (Merck Millipore, Germany). The final concentration was adjusted to 25 mg/ml IgG.

2.4.2 Titer determination of isolated total IgG

To determine the titer of the isolated total IgG serial dilutions were prepared (1:5.000; 1:10.000; 1:20.000; 1:30.000; 1:40.000; 1:50.000). These dilutions were tested on their binding efficiency on cryo-embedded mouse tail sections. The sections were thawed and washed with PBS. Then each section was circled with a wax pen and 50-100 µl of the antibody dilutions were added on top. Next, the slides were incubated for 1 hour in a wet box at 4°C. After washing the sections twice with PBS for 10 minutes 50 µl of 1:100 diluted swine anti-rabbit – FITC conjugated IgG/F(ab)2 antibody (Southern Biotech, # 6311-02, USA) were added to each section and incubated again at 4°C for 1 hour in a wet box. The slides were washed again 2 times with PBS for 10 minutes in the dark followed by liquid removal and mounting with 50% glycerol/PBS. The IgG titer was determined by using a Keyence BZ-9000E fluorescence microscope (Keyence Deutschland GmbH, Germany) to detect the green fluorescence limit at the dermal-epidermal junctions. Experience wise, a titer of 1:30.000 is wanted.

2.5 Antibody-transfer induced EBA

Mice were injected subcutaneously in the neck with 3 mg total IgG on day 0 and 2. On day 2, 4, 7, 10 and 14 mice are scored under anesthesia (10 mg/ml Ketamine and 1.5 mg/ml Xylazine). Therefore, the mice were weighed, and the affected body surface area was evaluated according to the formation of erythema, crusts, alopecia and erosion. Animals were sacrificed on day 14 by cervical dislocation to sample organs for further analysis.

2.6 Flow Cytometry

Single cell suspensions of different tissues such as blood, spleen or skin can be used for flow cytometric analysis. Cells are filtered with a 70 µm strainer and washed in PBS with 10 mM EDTA. Next, the cells are stained with Zombie Violet Dye (1:1000) for Live/Dead staining (BioLegend, #423113, USA) and incubate 30 minutes at room temperature. Afterwards 1:10 FcR Blocking Reagent (MACS Miltenyi, #130-092-575, Germany) was added and the cells incubate again for 10 min at 4°C. At a last step the antibodies of interest were added (Table 2) and incubated on ice for 20 minutes in the dark. Next all samples were washed with FACS buffer (2% FCS in PBS) and checked with Life technology Attune Nxt acoustic focusing cytometer (Thermo Fisher Scientific, USA). Data was analyzed using the FlowJo software.

Table 2: Flow cytometry antibodies

Target	**Clone**	**Tag**
B220 (CD45R)	RA3-6B2	APC
CD3	17A2	APC-Cy7
CD3	17A2	FITC
CD4	RM4-5	APC
CD8a	53-6.7	FITC
CD11b	M1/70	FITC
CD11c	N418	BV605
CD45	30-F11	PE
F4/80	BM8	APC-Cy7
γδTCR	GL3	APC
Langerin (CD207)	4C7	APC
Ly-6C	HK1.4	BV605
Ly-6G	1A8	FITC
Zombie Violet Dye	Life/dead staining	Pacific Blue

2.7 Cell viability Assay

The procedure follows the protocol of the CellTiter-Glo® Luminescent Cell Viability Assay (Promega, #G7571, USA). Briefly, cells were stimulated and incubated over night at 37°C (20.000 cells per well in 100 µl media) in an opaque-walled 96-well plate. After incubation equilibrate the plate to room temperature and add an equal volume of CellTiter-Glo® Reagent to the cells and mix. After 10

minutes incubation at room temperature for luminescent signal stabilization luminescence can be recorded with a TECAN infinite M200 Pro plate reader (Tecan Group, Switzerland). It is recommended to use a standard curve of known ATP concentrations to evaluate the viability in the tested wells.

2.8 Nitric Oxide Production Assay

The Griess assay by Koo *et al.*[228] was used to detect the nitric oxide levels in culture supernatants. Briefly, cells were cultured over night with the respective treatment at 37°C (20.000 cells per well in 100 µl media). Next, 50 µl of culture supernatants were transferred to flat bottomed 96-well plate and incubated with 50 µl 1% sulfanilamide in 5% phosphoric acid for 5 minutes room temperature. Afterwards 50 µl 0.1% N-(1-napthyl) ethylenediamine dihydrochloride (Sigma Aldrich, USA) were added and incubated again for 5 minutes at room temperature. The absorbance was measured using a TECAN infinite M200 Pro plate reader (Tecan Group, Switzerland) at wavelength 550 nm and subtracting the reference wavelength at 650 nm. To determine the nitric oxide values a standard curve ranging from 0 to 50 µM sodium nitrite is recommended.

2.9 Cytotoxicity Assay

The experiment follows the protocol of the Pierce LDH Cytotoxicity Assay Kit (Thermo Scientific, #13464269, USA). To perform the cytotoxicity assay, 50 µl of cell culture supernatant will be transferred to a fresh flat bottomed 96-well plate. Optimum cell number for RAW 264.7 macrophages is 20.000 cells per well. As a control, untreated cells of the same experiment will be incubated with Lysis Buffer for 45 minutes at 37°C and then 50 µl supernatant were taken as well. Then 50 µl Substrate mix is added to the supernatants and the plate is incubated for 30 min at room temperature in the dark. Afterwards 50 µl Stop solution is added and to the supernatants and absorbance is measured in a TECAN infinite M200 Pro plate reader (Tecan Group, Switzerland) at 490 nm and 680 nm. The percentage of cytotoxicity will be calculated first by subtracting the background 680 nm absorbance value from the 490 nm absorbance value and second by the following formula: (Compound-treated LDH activity – Spontaneous LDH activity)/(Maximum LDH activity – Spontaneous LDH activity) *100.

2.10 Isolation of intestinal crypts for organoid culture

The protocol follows the procedure by Sato *et al.*[229] . Briefly, mice were sacrificed and cut open. The whole gut was removed from the body and the first 20 cm small intestine proximal from the stomach were taken into cold PBS. Next, the fat tissue and the stool were removed, the gut was opened longitudinally and flushed three times with cold PBS. Cut the small intestine into small pieces and wash it 15-20 times with 15 ml cold PBS until the buffer appears clear. The supernatant was removed

and the tissue was incubated in 25 ml Gentle Cell Dissociation reagent (Stemcell™ Technologies, #100-0485, Canada) for 15 minutes on a rocking platform at room temperature. After discarding the supernatant tissue was suspended in 10 ml PBS + 0.1% BSA. After tissue has settled down the supernatant was taken and filtered through a 70 µm strainer. The filtrate is labeled "Fraction 1". This step is repeated to create fractions 2-4. Next, all fractions were centrifuged for 5 min at 290 x*g* at 4°C and the supernatant discarded. The pellet was resuspended in 10 ml cold PBS + 0.1% BSA and transferred into a 15 ml tube followed by a second centrifugation step for 5 minutes at 200 x*g* at 4°C. After discarding the supernatant, the crypts were resuspended in 10 ml cold DMEM/F-12 (with 15 mM HEPES) media (Stemcell™ Technologies, #36254, Canada). 1 ml of each fraction was used in a 6-well plate and checked under the microscope for the amount of crypts. The fraction with the most crypts was chosen and 10 µl were counted in a Neubauer counting chamber (Note: the complete area was counted) to determine the amount of crypts per ml. Next, the amount for 1500 and 3000 crypts were calculated, transferred to fresh tubes and centrifuged again for 5 minutes at 200 x*g* at 4°C. As much supernatant as possible is discarded and resuspended in 100 µl fully prepared IntestiCult™ Organoid Growth Medium (Mouse) (Stemcell™ Technologies, #06005, Canada). Also 100 µl thawed Corning®Matrigel®Matrix (Corning, #356231, USA) were added and mixed carefully to avoid bubble formation. 50 µl of the mix were pipetted in the middle of a 24-well plate well to create a dome, 4 wells per concentration. The plate was incubated for 10 minutes at 37°C to set the Matrigel and then carefully 750 µl of fully prepared organoid growth media (Stemcell™ Technologies, #06005, Canada) were added around the dome. Empty wells were filled with PBS to avoid dehydration and the plate was incubated at 37°C and 5% CO_2. Media was changed twice per week and after 7-10 days the organoids are mature enough for further applications.

2.11 qPCR of tight junction proteins and cytokines

2.11.1 RNA isolation

For RNA isolation the innuPREP RNA MiniKit 2.0 (Analytik Jena, #845-KS-2040050, Germany) was used. To isolate RNA from tissue, samples were frozen in liquid nitrogen and mashed with a spatula. This procedure is repeated 2-3 times. Next, 450 µl Lysis Buffer were added and the samples were frozen and mashed again several times until the solution appears vicious. 200 µl Lysis Buffer were added and the samples were centrifuged for 1 minute at high speed. The supernatant was transferred to blue Spin Filter D column. Next, the samples were centrifuged again for 2 min at 12.000 rpm. An equal amount of 70 % Ethanol was added to the flow through and pipetted up and down until the RNA is visible. The solution was transferred onto a purple Spin Filter R column and centrifuged again for 2 min at 12.000 rpm. The flow through was discarded and 75 µl DNase I Mix (ThermoScientific, #10649890, USA) was added to the membrane of the column and incubated at

room temperature for 15 min. Then, 500 µl Wash buffer HS was added to the column membrane and centrifuged for 2 min at 12.000 rpm. The flow through was discarded, 700 µl Wash buffer LS and centrifuged again for 2 min at 12.000 rpm. The flow through was discarded and the empty column was centrifuged again for 2 min at 12.000 rpm to dry the membrane. Next, 60 µl of DNase and RNase free water were added on the membrane and incubated for 5 min at room temperature. Last, the samples were centrifuged again for 1 min at 8.000 rpm and the purity and concentration of the flow through was measured with a NanoDrop 2000c (ThermoScientific, USA).

2.11.2 cDNA synthesis

For cDNA synthesis the First strand cDNA Synthesis kit (Thermo Scientific, #K1612, USA) was used. Briefly, 2 µg RNA in 10 µl volume were used. 1 µl Oligo Prime T18 was added and the mixture was incubated for 5 min at 65°C. Then, the Mastermix (4 µl 5x Buffer, 0.5 µl Ribolock (40 U/µl), 2 µl dNTP-mix (10 mM), 2 µl M-Mulu-RT (20 U/µl), 0.5 µl H_2O) was added to the RNA up to total volume of 20 µl and incubated for 1 hour at 37°C and afterwards for inactivation 5 min at 70°C. 80 µl H_2O was added to the samples and stored at -20°C.

2.11.3 quantitative real time PCR

The quantitative real time PCR was performed as follows: Maxima Sybr Green qPCR Master (ThermoFisher, #K0221, USA) was used as a standardized master mix. The primer (Table 3) were diluted 1:10 with H_2O (10 µl primer for + 10 µl primer rev + 80 µl H_2O). 2 µl cDNA were used per well in triplicates. Then, 5 µl Sybr Green, 0.4 µl Primer mix (10 µM) and 2.6 µl H2O were mixed and added to each well. Next, the 96-well plate was sealed with a clear foil and quickly centrifuged to make sure all ingredients are at the bottom of the well. Then the 96-well plate was placed into the Mastercycler ep realplex 2 qPCR machine (Eppendorf, Germany) and the following program was turned on: 10 min at 95°C; then 40 cycles of 15 sec at 95°C, 30 sec at 60°C and 30 sec at 72°C; then for the melting curve 15 sec at 95°C, 15 sec at 60°C and 15 sec at 95°C. The data was analyzed using the $2^{\Delta CT}$ method.

Table 3: qPCR primer. Each sequence is written from 5'to 3'.

Primer name	**Primer sequence**
β-Actin for	CACTGTCGAGTCGCGTCC
β-Actin rev	CGCAGCGATATCGTCATCCA
Claudin-1 for	TCCTTGCTGAACTTGAACA
Claudin-1 rev	AGCCATCCACTACTTCTG
Claudin-2 for	TATGTTGGTGCCAGCATTGT
Claudin-2 rev	TCATGCCCACCACAGAGATA
Claudin-4 for	TCGTGGGTGCTCTGGGGATGCTTC
Claudin-4 rev	GCGGATGACGTTGTGAGCGGTC
Claudin-15 for	GCTTCTTCATGTCAGCCCTG
Claudin-15 rev	TTCTTGGAGAGATCCATGTTGC
Occludin for	CCTCCAATGGCAAAGTGAAT

Occludin rev	CTCCCCACCTGTCGTGTAGT
ZO-1 for	CCACCTCTGTCCAGCTCTTC
ZO-1 rev	CACCGGAGTGATGGTTTTCT
Defα-22-for	AGCAGCCAGGGGAAGAG
Defα-22-rev	CCTCTATTGCAGCGACGT
IL-1β for	CTTCCAGGATGAGGACATGA
IL-1β rev	CACACCAGCAGGTTATCATCATC
IL-6 for	CTCCCAACAGACCTGTCTATAC
IL-6 rev	GTGCATCATCGTTGTTCATAC
IL-8/KC for	TGAGAGTGATTGAGAGTGGACCA
IL-8/KC rev	TCAGCCCTCTTCAAAAACTTCTCC
IL-10 for	TCCCTGGGTGAGAAGCTGAAG
IL-10 rev	CACCTGCTCCACTGCCTTG
TNFα for	CTGTAGCCCACGTCGTAGC
TNFα rev	TTGAGATCCATGCCGTTG
GLP1 for	GGCACATTCACCAGCGACTACA
GLP1 rev	GCCCTCCAAGTAAGAACTCACATC
GLP1R for	TCAGAGACGGTGCAGAAATG
GLP1R rev	CAGCTGACATTCACGAAGGA
B2M for	GCTATCCAGAAAACCCCTCAA
B2M rev	CATGTCTCGATCCCAGTAGACGGT
Beclin for	AATCTAAGGAGTTGCCGTTATAC
Beclin rev	CCAGTGTCTTCAATCTTGCC
Lysozym-1 for	GCCAAGGTCTACAATCGTTGTGAGTTG
Lysozym-1 rev	CAGTCAGCCAGCTTGACACCACG

2.12 Protein Immunoblot analysis

2.12.1 Stimulation of organoids

Crypts from small intestines of B6 and B6-mt^{FVB} mice were harvested according to 2.10 and let develop into mature organoids within 7 days. Then the organoids were counted and stimulated for 48 h with or without 10 ng/ml IFNγ in organoid growth medium.

2.12.2 Protein isolation

To isolate proteins from organoids the crypts were harvested by pipetting up and down the media in the well to destroy the Matrigel dome. Then rinse the well with 500 µl PBS. Centrifuge the tubes and discard the supernatant. Mix 100 µl RIPA buffer (150 mM NaCl, 50 mM Tris-HCl (pH 7.4), 1mM EDTA, 1% Na-deoxycholate, 1% NP-40. 0.1% SDS, sterile-filtered) and 1 µl Protease Inhibitor Cocktail Set III (Merck Millipore, #535140, USA) and add 30 µl to each crypt pellet and resuspend. Incubate 30 min on ice. Centrifuge 15 min at 12.000 *xg* at 4°C.

To determine the protein concentration a BCA assay (Pierce BCA Protein Assay kit, Thermo Scientific, #23227, USA) was performed. All samples were measured in duplicates and with 1:10 dilution in a 96-well plate. Briefly, 25 µl protein standard or 2.5 µl sample plus 22.5 µl H_2O were added to a 96-

well plate. Add 200 µl WR Solution to each well and pipette up and down. Incubate 30 min at 37°C and measure absorbance at 592 nm with a TECAN infinite M200 Pro plate reader (Tecan Group, Switzerland).

2.12.3 SDS-PAGE

To purify the wanted proteins an SDS-PAGE was performed. Therefore, a MOPS running buffer was prepared basically by mixing one bag of TRIS-MOPS-SDS Running Buffer Powder (GenScript, #M00138, USA) with 1 L Aqua dest.. 20 – 40 µg protein were used per sample and run in a final volume of 20 µl. SDS is added in 1:5 ratio. The mix was incubated for 5 min at 95°C. Ready-to-use ExpressPlus™PAGE gels (GenScript, #M41212, USA) were used, which were fixed in the BIO-RAD Mini-PROTEAN Tetra System electrophorese chamber (BIO-RAD Laboratories, USA) and filled with MOPS-buffer. 7 µl Spectra™ Multicolor Broad Range Protein Ladder (Thermo Scientific, #26634, USA) was used as well as 20 µl sample mix. The electrophoresis was started with 120 V and 84 mA for 60-90 min.

2.12.4 Western Blot

To plot the SDS-PAGE gel an Amersham™ Protran® Premium Western-Blotting-Membrane, Nitrocellulose (Amersham GE Healthcare Life Science, #10600006, United Kingdom) was used and cut in the size of the gel and put in box with a filter paper underneath and on top. Then 50 µl ELPHO-buffer (5 ml ELPHO Buffer 10x (15.3 g Tris, 72 g Glycine, 5 g SDS in 500 ml, pH 8.4), 10 ml Methanol, 35 ml H_2O) were added on top to soak the membrane and everything was incubated at 4°C until use. To plot the gel a Trans-Blot Turbo Transfer System (BIO-RAD Laboratories, USA) was used. The cassette was filled as follows: filter paper, membrane, SDS-gel, filter paper. Air bubbles were carefully removed with a roller and the cassette was put in the machine. The standard program with 25 V for 30 min was used.

Next, 4 % milk (nonfat dried milk powder, AppliChem, #A0830.1000, Germany) in TBST buffer was prepared. The membrane was put into a 50 ml Falcon tube, 3 ml milk were added and the whole mix was incubated for 1 h on a rocking platform at room temperature. Then the milk was discarded and the 1st antibody (Table 4) in 1:1000 dilution in TBST with 4% BSA was added to the membrane and incubated overnight on a rocking platform at 4°C.

Next, the membrane was washed 3 times in TBST for 15 min each on a rocking platform at room temperature. Then, the 2nd antibody Polyclonal Goat Anti-Rabbit Immunoglobulins HRP (Agilent, USA) was added in a 1:4000 dilution in milk and incubated for 1 h on a rocking platform at room temperature. The membrane was washed 3 times with TBST for 15 min each on a rocking platform at room temperature. Next, the blot was developed by mixing 1:1 Peroxide Solution with Luminol

Reagent from the Immobilon Western Chemiluminescent HRP Substrate (Merck Millipore, #WBKLS0500, USA) and adding 1 ml of this mix to the membrane in a flat orientation. Pictures of the blot were taken with a Chemidoc (Bio-Rad, USA).

Table 4: Westernblot antibodies

Antibody name	**Company**
Beta Actin (13E5) Rabbit mAb	Cell signaling technology, #4970S
Claudin-2 (E1H90) Rabbit mAb	Cell signaling technology, #48120S

2.13 TNFα ELISA of RAW 264.7 cell macrophage supernatants

2.13.1 Stimulation of RAW 264.7 cell macrophages

RAW 264.7 cell macrophages were seeded with 20.000 cells per well in a 96-well plate and incubated in 100 µl DMEM high glucose media (Sigma Aldrich, #D6429, USA) at 37°C and 5% CO_2. Stimulate the cells with 2 µl metabolites in the respective concentrations and 2 µl LPS (1 ng/ml, 5 ng/ml) and incubate the cells overnight. On the next day the supernatants can be harvested and stored at -80°C until use.

2.13.2 TNFα ELISA

The TNFα ELISA was performed using the Mouse TNF-α ELISA MAX™ Deluxe Set (BioLegend, #430204, USA). Briefly, one day prior to experiment a Mikrotest plate 96-well, F (Sarstedt, #82.1581.001, Germany) is coated with 100 µl Capture antibody in Coating buffer, sealed and incubated overnight at 4°C. On the next day, when all reagents are at room temperature, the plate is washed 4 times with 300 µl Wash buffer (0.05% Tween-20 in PBS). Then, 200 µl Assay Diluent A is added to the wells, the plate is sealed and incubated for 1 h on a rocking platform at room temperature to block non-specific binding. Afterwards, the plate is washed again for 4 times with 300 µl Wash buffer and then the standard and the samples were added in 100 µl volume. The RAW 264.7 cell supernatants were diluted 1:4 to achieve values in a good range according to the standard. The plate was sealed and incubated for 2 h on a rocking platform at room temperature, followed by an additional 4 times washing step. 100 µl Detection antibody were added next and the plate was sealed again and incubated for 1 h on a rocking platform at room temperature. After another washing step 100 µl diluted Avidin-HRP solution was added and the sealed plate was incubated for 30 min on a rocking platform at room temperature. The plate was washed 5 times with 300 µl Wash buffer and to reduce background the wells were soaked for 1 min. Next, 100 µl TMB Substrate Solution was added, and the plate was incubated for 15 min in the dark. To stop the reaction 100 µl Stop solution (1 M H_3PO_4) was added. The color of the wells turned from blue to yellow and

absorbance as detected at 450 nm and 570 nm using a TECAN infinite M200 Pro plate reader (Tecan Group, Switzerland).

2.14 Shotgun metagenomics of cecum content

2.14.1 DNA isolation

Cecum content from 10 B6 and 10 B6-mt^{FVB} mice was taken and stored at -80°C. For DNA isolation the Qiagen AllPrep DNA/RNA/Protein kit (Qiagen, #80004, Netherlands) was used. First, the samples were placed in lysis buffer and homogenized in a Bead Ruptor 3 times for 45 sec, followed by a 2 h incubation at room temperature. After centrifuging for 30 sec and 13.000 rpm the supernatant was pipetted in a QIAshredder column (Qiagen, #79656, Netherlands) for further homogenization and centrifuged again. The flow through was used for further DNA isolation by adding it to an Allprep DNA spin column and centrifuge 30 sec at 10.000 rpm. The Flow through can be used for further RNA isolation. The membrane of the column is washed 2 times and then placed into a fresh 1.5 ml tube. 50 µl preheated Elution buffer were added, 2 min at room temperature incubated and then centrifuged. The concentration of the eluted DNA was measured using a Nanodrop. The samples were stored at -20°C.

2.14.2 Library preparation

The library was prepared by Dr. Sven Künzel (Department of Evolutionary Genetics, Max Planck Institute for Evolutionary Biology, Plön) using the NextSeq 500/550 High Output Kit v2.5 (300 cycles) (Illumina, #20024908, USA) and the NextSeq 500 sequencing machine (Illumina, USA). Briefly, 50 ng of genomic DNA in 20 µl were used per sample. Add 25 µl TD Buffer and 5 µl TDE1 Buffer and mix. Afterwards, centrifuge samples at 280 x*g* at 20°C for 1 minute. Next, place the samples on a thermal cycler and incubate for 5 minutes at 55°C. Transfer 50 µl of the genomic DNA mix to a new plate and mix with 180 µl Zymo DNA binding buffer. Then, transfer the samples to the Zymo-Spin I-96 well plate and centrifuge for 2 minutes at 1300 x*g* at 20°C. Discard flow through and wash 2 times with 300 µl Zymo wash buffer. Centrifuge for 2 minutes at 1300 x*g* at 20°C and place the Zymo-Spin I-96 well plate on a fresh 96 well plate. Next, add 25 µl RSB and incubate 2 minutes at room temperature before centrifuging again. For DNA amplification add 5 µl of each index adapter to the samples. Next, add 15 µl NPM and 5 µl PPC. Transfer 20 µl of the mix to fresh plate and centrifuge for 1 minute at 280 x*g*. For the amplification step, place the plate on a thermos cycler and run the following program: 72°C for 3 minutes, 98°C for 30 seconds followed by 5 cycles of 98°C for 10 seconds, 63°C for 30 seconds and 72°C for 3 minutes. To clean up the library, centrifuge the plate for 1 minute at 280 x*g* and transfer the contents to a fresh plate. Add 30 µl thoroughly vortexed AMPure XP beads to the samples and pipette up and down 10 times to mix. Incubate 5 minutes at room temperature and place on a magnetic stand until the solution is clear. Remove the supernatant and wash 2 times with

200 µl of 80% Ethanol. Remove ethanol residuals and let the beads air dry for 15 minutes. For the next step, remove the plate from the magnetic stand, add 32.5 µl RSB to the beads and pipette up and down to mix. Incubate 2 minutes at room temperature and place the plate back on the magnetic stand to clear the solution. Transfer 30 µl of the supernatant to a fresh plate. Check the concentration of the libraries, normalize them to 2 nM and pool them. The pooled libraries are mixed with 0.2 N NaOH and afterwards with 200 mM Tris-HCL, pH 7, for denaturing and diluted to 20 pM. Same happens to PhiX Control, which is combined with the denatured and diluted library afterwards. The library is now ready to be loaded on the cartridge for sequencing.

2.14.3 Analysis of the sequencing data

The analysis was performed by Dr. Axel Künstner and Michael Olbrich (both Department of Systems Biology, University of Lübeck). To assess the quality of the sequencing data fastp was used. At a next step BBDuk and KneadData (https://github.com/biobakery/**kneaddata**) were used to remove host contamination sequences. For species profiling as well as checking alpha and beta diversity the MetaWRAP pipeline[230] as well as the mOTU_v2 profiler in combination with Utility commands were utilized[231]. With Kaiju[232] as well as the Kraken2 Bracken pipeline[233,234] indicator species were identified and visualized using the CRAN package corrr 0.4.3 and the Krona visualization tool [235]. Next, pathway abundances were analyzed, using the HUMAnN2 pipeline followed by analysis with MaAsLin2 (Microbiome Multivariable Associations with Linear Models) [236,237]. For this analysis data was grouped to UniRef90 gene families and mapped to Pfam (Protein Families), GO (Gene Ontology), KO (KEGG Orthology), eggNOG, Level-4 enzyme commission (EC) and MetaCyc databases. Only Features with minimum 10% non-zero values were analyzed.

2.15 Metabolomics of liver tissue

For metabolomics analysis approximately 100 mg liver tissue was freshly sampled. All samples were immediately frozen at -80°C. Next, all samples were sent on dry ice to “Leibniz-Institut für Nutztierbiologie” in Dummerstorf for Liquid chromatography – mass spectrometry (LC-MS). Samples were prepared for analysis as followed: All solvents should be prechilled before start of the procedure and everything is handled on ice. 75 mg of tissue was accurately weighed and added to a Precellys tube followed by the addition of 4 µl/mg methanol and 0.85 µl/mg water. At a next step, the tubes were placed in the Precellys 24 homogenizer and burst for 2 times 10 seconds at 6400 rpm. After transfering the mixture into a glass vial tube the Precellys tube was flushed with 1 µl/mg methanol/water mix (1:0.9), vortexed and transfered as well to the glass vial tube. Next, 5 µl/mg chloroform and 2 µl/mg water were added to the mix and vortexed for 30 seconds. After chilling the tube on ice for 30 seconds they were centrifuged at 1800 x*g* for 10 minutes at 4°C. The tube were left on room temperature for 5 minutes and then the upper (polar) and lower (non-polar) layer were

separated into fresh tubes. The polar samples were lyophilized for 3-4 hours with no heat in a centrifuge evaporator and reconstituted in acetonitrile/water mix (3:1). The non-polar samples were lyophilized under a nitrogen steam and reconstituted in methanol/water mix (3:1). A pooled quality control was created for both polar and non-polar samples and all were centrifuged at 15.800 x*g* for 15 minutes at 4°C. Then, all samples were transferred to UPLC vials. Now, LC-MS was performed.

The obtained data was analyzed by Dr. Axel Künstner (Department of Systems Biology, University of Lübeck). The metabolites were mapped to KEGGCompoundIDs using Bioconductor package KEGGrest[238]. Then the data was log2 transformed to perform linear modeling using LIMMA[239]. The significantly different metabolites were plotted in a principal component analysis (PCA) and volcano plots. Moreover, an enrichment analysis was performed using metabolites with compound IDs and a *p*-value<0.1. The metabolites were enriched and analyzed using the Bioconductor package FELLA 1.16.0 [240,241] by running against KEGG database and the results could be visualized as pathway maps. Additionally, GO annotations from GO:0005739, which is the mitochondrial cellular function gene ontology were added to the identified pathway maps.

2.16 Statistics

For statistical analysis as well as for graph creation the GraphPad Prism8.0.2 software was used. The statistical tests are mentioned in the figure and/or table descriptions. All data with *p*-values < 0.05 were stated as significant.

Metagenomics and metabolomics data was further analyzed using respective packages of the R software environment v3.4.2 (R Core Team, 2017).

3 Results

3.1 Does the mutation in the *mt-Atp8* gene influences the immune system and the barrier integrity of the gut?

3.1.1 Less γδ T cells in back skin sections of healthy B6-mt^{FVB} mice

First, the side of infection, the skin, was taken under closer inspection. Mice contain skin resident γδ T cells in the epidermis, which play a role and wound healing, immune barrier maintenance and immune response regulation upon injury[245]. To investigate whether the immune potential of the skin is different between B6 and B6-mt^{FVB} mice the abundance of skin resident γδ T cells was checked via immunohistochemistry in back skin sections of healthy mice. γδ T cells were identified by double positive staining for γδ T cell receptor (green) and CD3+ (red) (Figure 5 A+B). 5 mice per strain, 3 different sections per mouse and 3 different areas per section were used for analysis. B6-mt^{FVB} mice showed significantly less γδ T cells in the epidermis of the back skin (p = 0.005, Welch two sample test) (Figure 5C)).

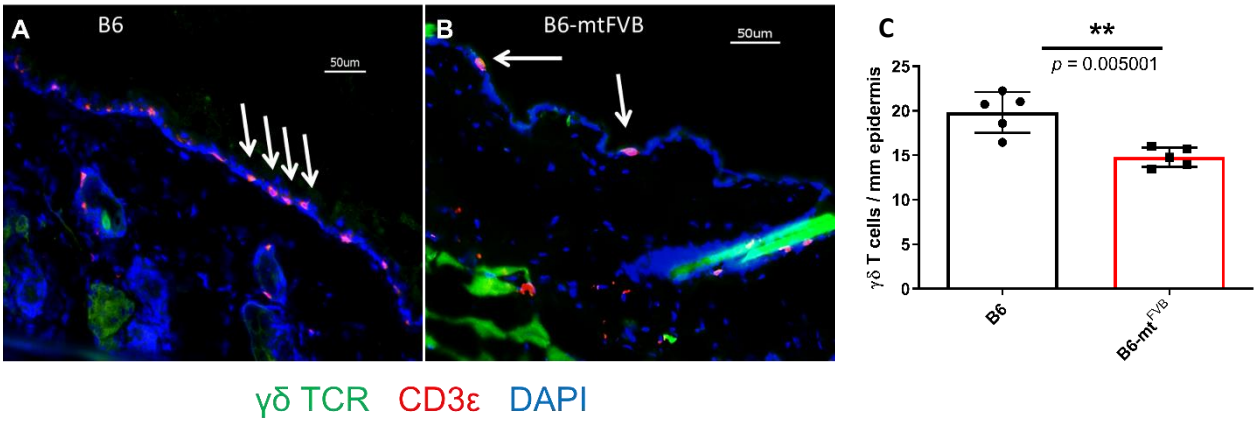

*Figure 5: Immunohistochemistry staining of γδ T cells in murine dorsal skin of B6 mice (A) and B6-mt^{FVB} mice (B). γδ T cell receptor (TCR; clone GL3): green, CD3ε cells (clone 145-2C11): red, nuclei (DAPI): blue. Arrows indicate exemplarily γδ T cells. C) shows γδ T cell counts as mean of 10 sections per mouse. Error bars indicate the standard deviation to the mean. (Welch two sample test *p<0.05, **p<0.01), n = 5/group).*

To validate the immunohistochemistry findings of γδ T cell abundance in the skin of B6 and B6-mt^{FVB} mice the immune cells were isolated out of skin layers from ears, stained and counted the living cells with a flow cytometer. Cells were stained for CD45 and γδ TCR as well as life dead staining. In Figure 6 you can see the real counts (A) as well as the percentage of viable single CD45+ γδ TCR + cells (B). No difference could be detected in the amount of γδ T cells in ears of B6 and B6-mt^{FVB} mice.

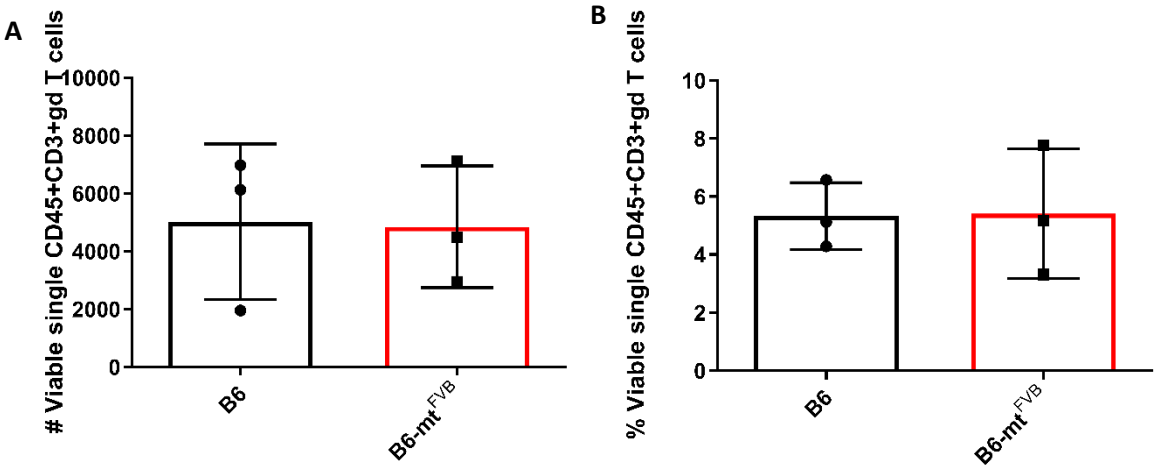

Figure 6: Isolated γd T cells in epidermis of murine ears. A) shows total counts of single, viable CD45+ and γd TCR + cells, B) shows the percentage of single, viable CD45+ and γd TCR + cells. The error bars indicate the standard deviation to the mean. (n = 3)

3.1.2 Amount of γδ T cells correlates with EBA disease severity in different body sites

After the contradictory results of γδ T cell numbers in ears and back skin the disease severity in different areas of the body in the EBA data was analyzed (Figure 7). It is visible that there is no significant difference in the EBA severity in ears between B6 and B6-mt^{FVB} mice (Figure 7A). But looking at the disease severity in the back area (Figure 7B) the difference is significant (Welch's T-test: *p*-value = 0.05), especially when comparing the area under the curve of the disease score of the back (Welch's T-test: *p*-value = 0.0464) (Figure 7C). Thus the EBA disease severity in ears and back skin correlates with the numbers of γδ T cells found in the epidermis. The more γδ T cells present in the epidermis, the more severe is the disease.

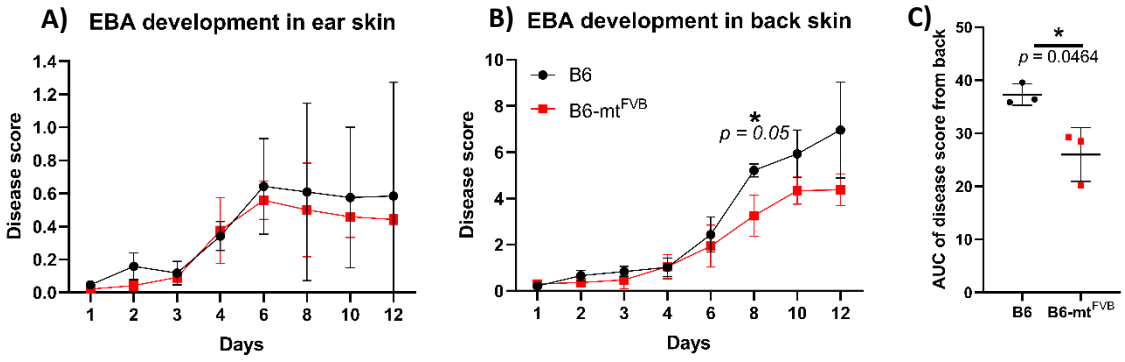

*Figure 7: EBA severity in ears and back skin of B6 and B6-mt^{FVB} mice. A) shows the scoring results (percentage of affected skin surface area) for both ears combined. B) shows the scoring results (percentage of affected skin surface area) for trunk and head-neck area combined as a representative for back. C) shows the area under the curve (AUC) for disease score of the back skin. EBA was induced as described in 2.5. (Welchs's T test, * p-value ≤ 0.05, n = 3/group).*

3.1.3 No difference in immune cell subpopulations over EBA disease progression

To investigate whether the immune cell subpopulation composition changes over disease progression of EBA and if the most involved cell populations differ between B6 and B6-mt^{FVB} mice spleen and skin samples were taken on day 2, 4, 6, 12 and 16 of an EBA experiment, processed them into single cell solutions, stained them and analyzed via flow cytometry. All samples were gated for immune cells, followed by single cells, living cells and CD45+ cells (Figure 8) followed by the individual panels (Table 5).

Table 5: Immune panel for flow cytometry analysis.

Panel	1	2	3	4
Cells	Ear/spleen/blood	Ear/spleen/blood	Ear/spleen/blood	Ear/spleen/blood
FITC	Ly-6G	CD8a	CD11b	CD3
PE	CD45	CD45	CD45	CD45
APC	B220	CD4	Langerin	gdTCR (GL3)
APC-Cy7	CD3	CD3	F4/80	
Pacific Blue	Zombie	Zombie	Zombie	Zombie
BV605	Ly-6C		CD11c	

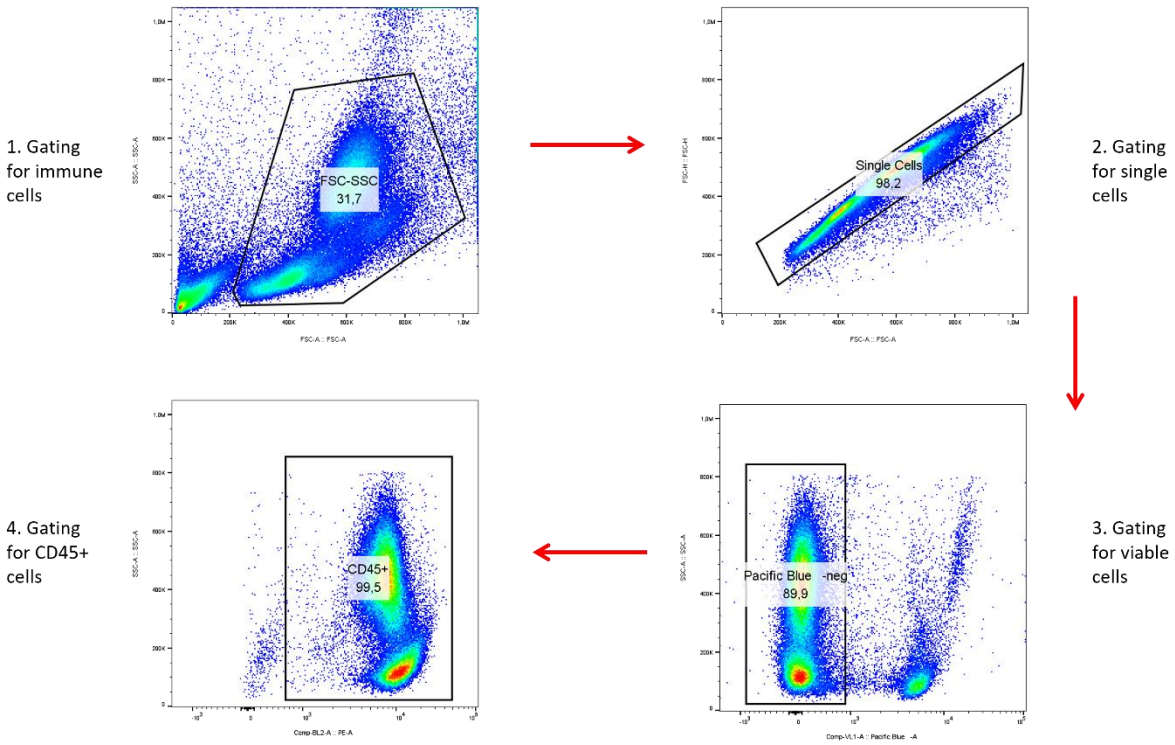

Figure 8: Gating strategy for Flow cytometry analysis. First were gated for lymphocytes, then among these for single cells using FSC.A vs FSC.H. Next, pacific blue negative cells which reflect viable cells were gated and afterwards CD45+ cells were selected.

In Figure 9 the results of immune cell subpopulations in the spleen are shown. In A) you can see CD45+GR1+ Monocytes, which are up in the early phase of the EBA disease, then decrease until day 6 and rise again to a peak on day 12. B6 and B6-mt^{FVB} mice differ only in day 2 and 16, with more monocytes present in B6 mice at day 2 and less at day 16 compared to B6-mt^{FVB} mice. The amount of CD4 T cells (B) is very high at the onset of disease (~20% of viable single cells) and slightly decrease over disease progression with no difference between strains. CD8 T cells (C) are present in high amounts at the beginning and decrease over the disease progression, in B6 faster than in B6-mt^{FVB}, with a strong increase in the last days. B cells (D) rise at first days of EBA disease until Day 6 and decrease until the end of disease development, with B cells in B6-mt^{FVB} mice starting at higher levels and decrease to lower levels at the end. In E) the progression of 11b+ myeloid lineage cells high amounts could be seen at the disease onset with steady decrease in cell numbers until Day 16 with no difference in mouse strains. γδT cells (F) show a decrease in cell numbers in the first days, then increase towards Day 12 and slightly decrease again with no difference between strains.

In comparison Figure 10 shows the results of immune cell subpopulations in the skin during EBA disease development. Percentage of CD45+GR1+ Monocytes shown in A) does not differ between the two mouse strains and is extremely increased on day 12. CD4 T cells show a small increase on Day 4 and then a steady increase until the end of disease development (B) with CD4 T cells in skin of B6-mt^{FVB} mice rising even more. CD8 T cells show a peak at Day 4 and Day 12 with no difference in mouse strains (C). B cells (D) show the same pattern as CD45+GR1+ Monocytes (A) but are present in extremely low percentage (peak on day 12 at 0.6% of viable single cells). The percentage of CD11b+ myeloid lineage cells increase in the first days of disease development (E) and decreases towards the end with CD11b+ myeloid lineage cells decreasing faster in skin of B6 mice. γδ T cells are increasing until Day 12 and then slightly decrease again (F) with cells in B6-mt^{FVB} mice already reaching a first peak on Day 4 and showing a milder decrease until Day 16 compared to B6 mice.

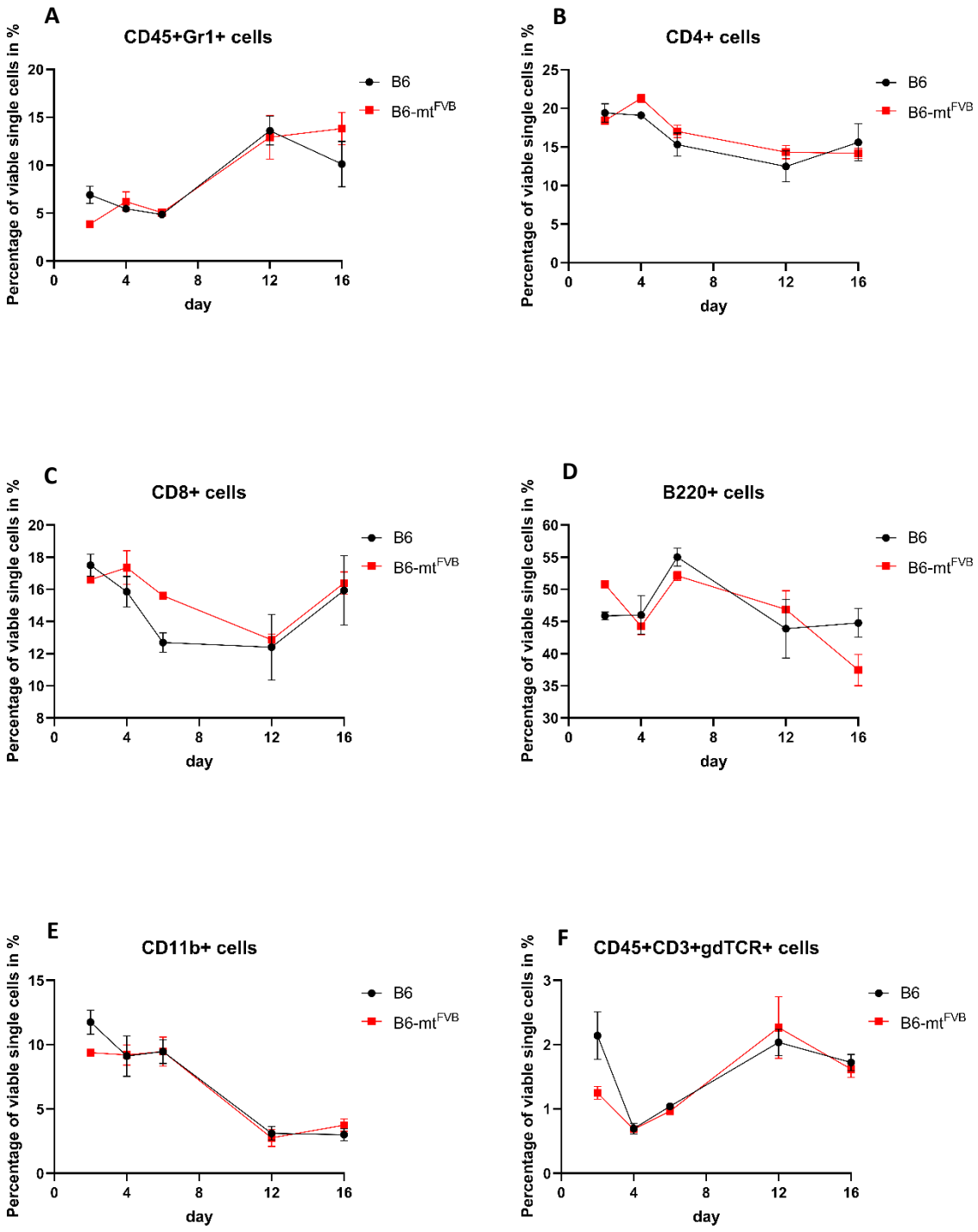

Figure 9: Immune cell subpopulation analysis during EBA development in spleen of B6 and B6-mt^{FVB} mice. Shown are the timely changes for A) CD45+ Gr1+ cells, B) CD4+ T cells, C) CD8+ T cells, D) B220+ B cells, E) CD11b+ cells and F) γd T cells. B6 mice are shown in black, B6-mt^{FVB} mice are shown in red. Error bars indicate the standard deviation to the mean. (n = 3).

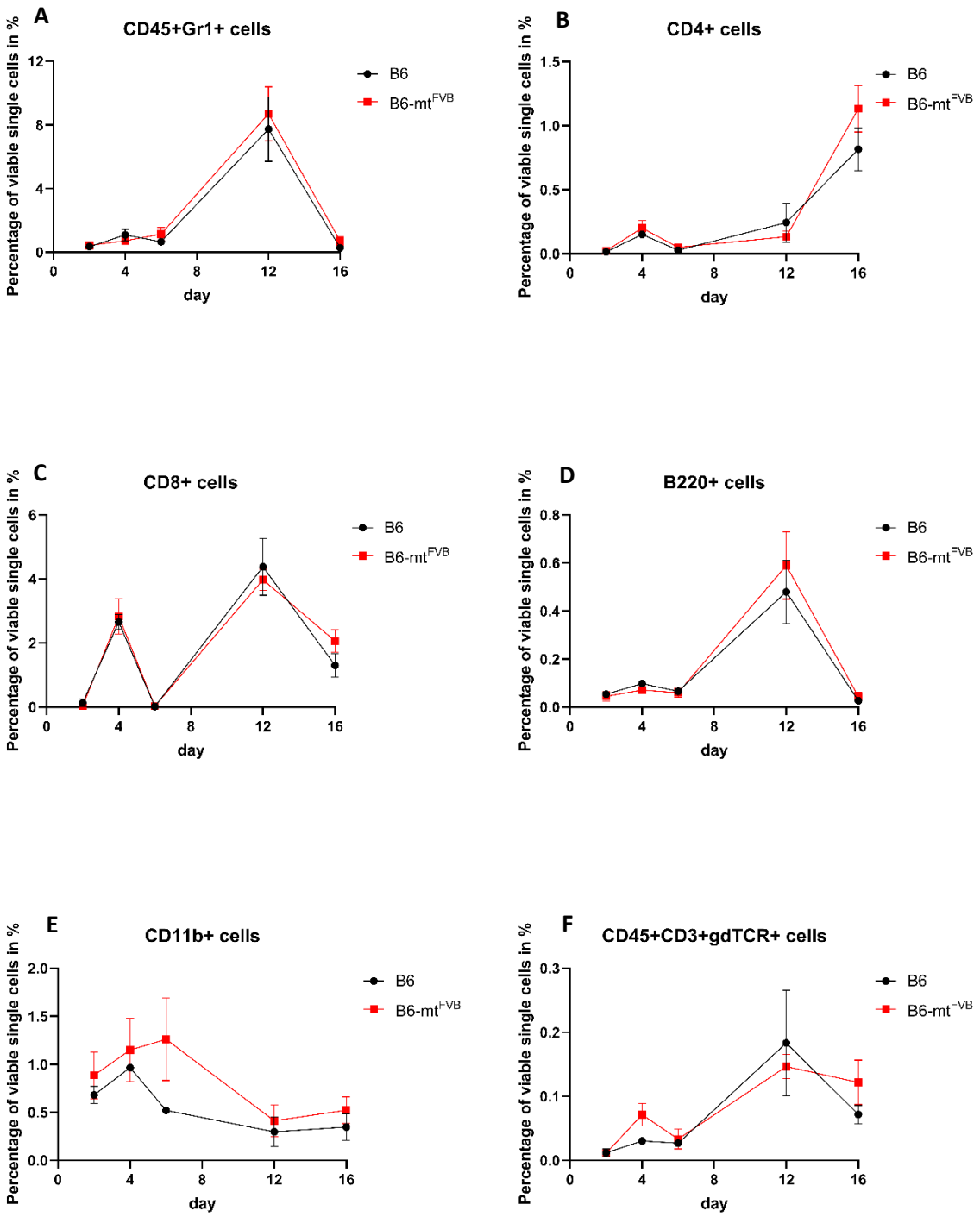

Figure 10: Immune cell subpopulation analysis during EBA development in skin of B6 and B6-mt^{FVB} mice. Shown are the timely changes for A) CD45+ Gr1+ cells, B) CD4+ T cells, C) CD8+ T cells, D) B220+ B cells, E) CD11b+ cells and F) γd T cells. B6 mice are shown in black, B6-mt^{FVB} mice are shown in red. Error bars indicate the standard deviation to the mean. (n = 3)

3.1.4 IFNγ treated organoids show Cld2 degradation in B6 mice

On the other hand, the gut as first site of immunity was checked. It was already reported for other autoimmune diseases that gut permeability plays a role in disease onset and development[242]. Since Hirose *et al*. already show that the gut microbiome differs in beta diversity[224] this study aims to identify whether the mutations in the *mt-Atp8* gene influence the gut permeability. Therefore, focus was set on tight junction proteins, which have major roles in the integrity of epithelial barriers as well as trans-cellular transport functions[243].

Bardenbacher *et al*. showed that INFγ stimulation leads to increased permeability in intestinal organoids [244], therefore leading to the question whether there are differences between organoids generated from B6 mice compared to those generated from B6-mt^{FVB} mice. 350 organoids per group were stimulated with and without IFNγ (10 ng/ml) for 48 h. Afterwards proteins were harvested and 60 µg per group were used to detect Claudin 2 (Cld2) and as reference β-Actin (Actβ) in a Western blot (Figure 11). According to Bardenbacher *et al*. treatment with INFγ results in Cld2 fragmentation with a size of 15 kDa[244]. This finding could be proofed for organoids generated from B6 mice whereas the result for B6-mt^{FVB} generated organoids is unclear.

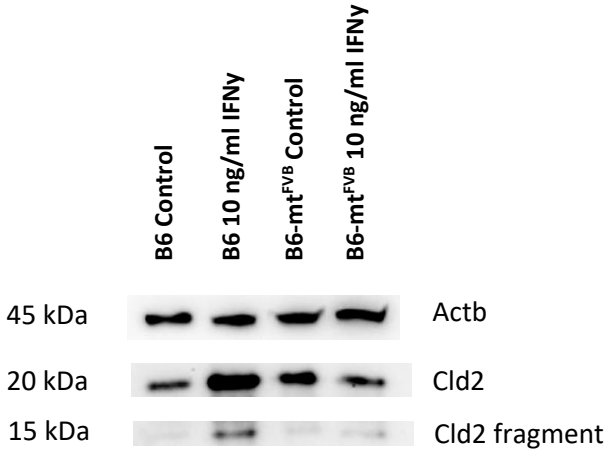

Figure 11: Effect of IFNγ stimulation on Claudin 2 in organoids from B6 and B6-mt^{FVB} mice. Western blot results of organoids treated with and without 10 ng/ml IFNγ of B6 and B6-mtFVB mice. B-Actin as reference at 45 kDa, Claudin 2 with mature size at 20 kDa and denatured at 15 kDa. (n = 350 organoids/group).

3.1.5 No difference in tight junction protein expression in colon, small intestine and cecum tissue of healthy and EBA mice

Additionally, the expression of more tight junction proteins (Claudin-2, Claudin-15, Occludin and Zonulin-1) was checked in three different gut parts (small intestine, cecum and colon) of healthy mice as well as mice at the peak of EBA disease severity (day 12) to see whether the gut permeability is different between B6 and B6-mt^{FVB} mice and if the gut permeability changes with disease progression. In Figure 12 the result for healthy mice is shown. In the small intestine the expression of all tight junction proteins is slightly decreased in B6-mt^{FVB} mice compared to wildtype B6. Whereas Claudin-2 is increased in the cecum and ZO-1 is increased in cecum and colon compared to healthy wildtype mice.

The results for mice at the peak of EBA on day 12 is shown in Figure 13. For the small intestine Claudin-2 and Claudin-15 are slightly increased in B6-mt^{FVB} mice. The other relation of the expression of the other tight junction proteins remains the same as in healthy mice. The expression pattern in Colon shows a change. Except for Claudin-2 all tight junction proteins are slightly more expressed in B6-mt^{FVB} mice compared to B6 mice.

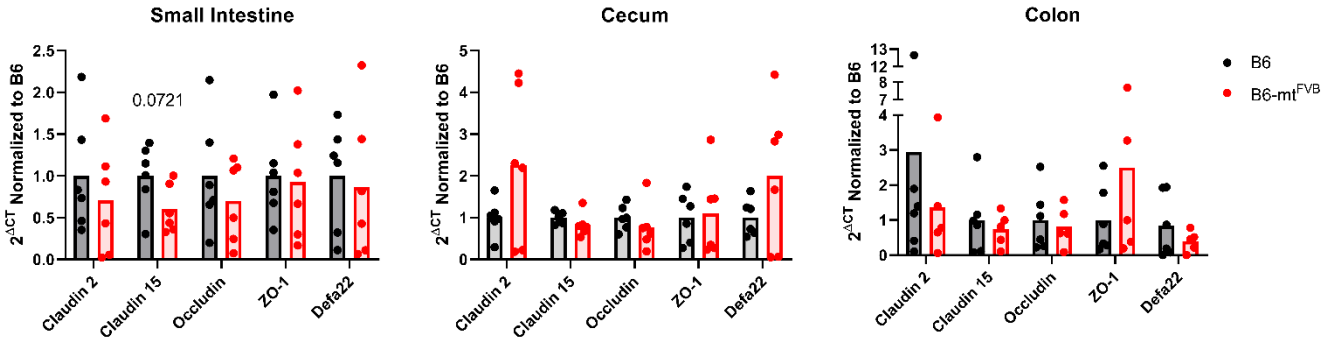

Figure 12: Expression of tight junction proteins in the gut of healthy B6 and B6-mt^{FVB} mice. Shown are the expression patterns in small intestine, cecum and colon. Values for B6 are shown in black and for B6-mt^{FVB} in red. The expression was calculated using the $2^{\Delta CT}$ method with normalization to B6 mean value. (T-test, n = 6)

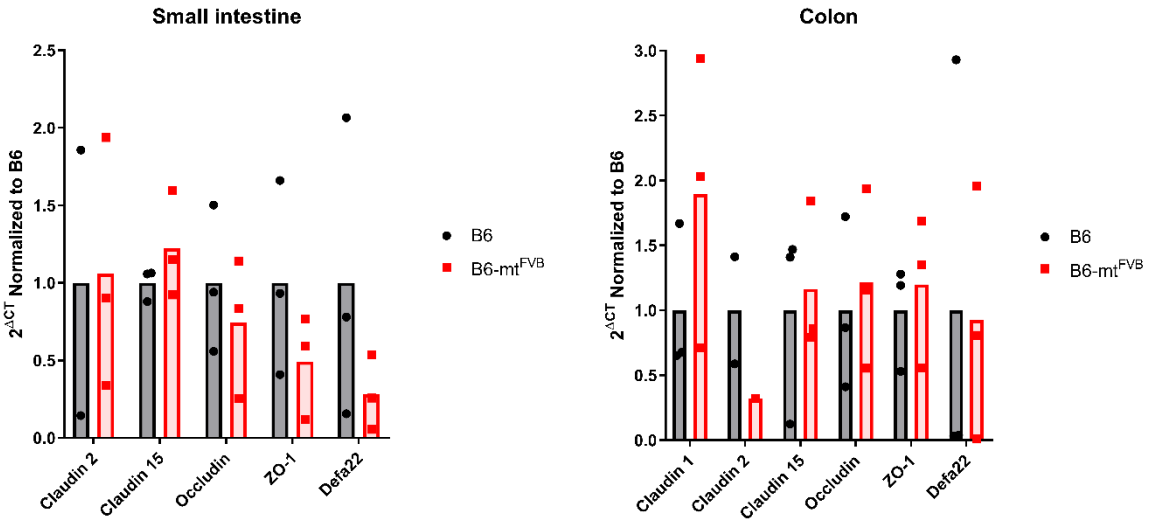

Figure 13: Expression of tight junction proteins in the gut of B6 and B6-mt^{FVB} mice on EBA day 12. Shown are the expression patterns in small intestine and colon. Values for B6 are shown in black and for B6-mt^{FVB} in red. The expression was calculated using the $2^{\Delta CT}$ method with normalization to B6 mean value. (T-test, n = 3)

3.1.6 Cytokine expression is increased in small intestine of mice suffering from EBA

Many molecules such as cytokines or hormones are known to enhance or counteract inflammation. Schilf *et al*. already showed that the mutation in the *mt-Atp8* gene leads to reduced number of T cells, that produce the cytokine IL-17[223]. To investigate to what extend the mutation in the *mt-Atp8* gene also influences the gut epithelial cells this study asked if the hormone and cytokine expression in the small intestine as indicator of inflammation also differs between the two strains in healthy and diseased state. The expression patterns of glucagon like peptide 1 (GLP1) and its receptor as well as the cytokines IL-1β, IL-6, IL-8(KC), IL-10 and TNFα were checked.

In Figure 14 it is shown that expression of GLP1 significantly decreases in the small intestine of EBA mice compared to healthy mice in both strains (B6: p = 0.0023, B6-mt^{FVB}: p = 0.05). For the GLP1 receptor expression only increases in EBA B6 mice whereas for B6-mt^{FVB} mice the expression level stayed the same in healthy and disease state and are in general a bit lower than in B6 mice.

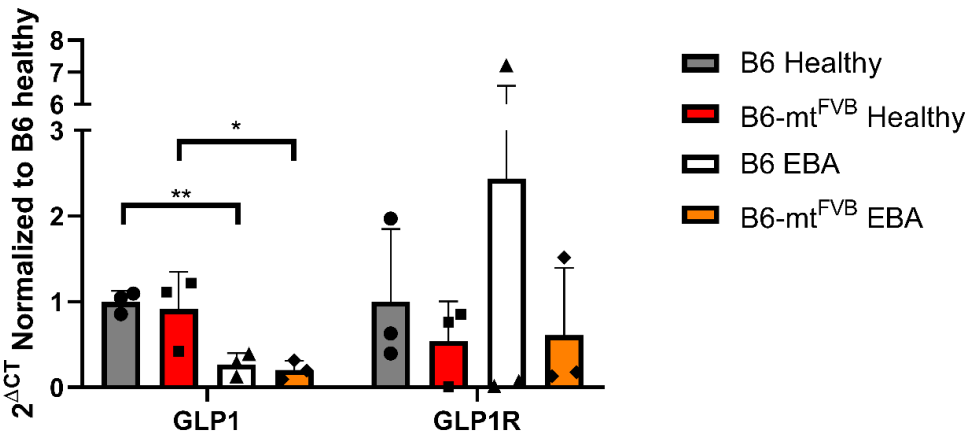

*Figure 14: Expression of glucagon like peptide 1 (GLP1) and its receptor in small intestine of healthy and diseased mice. Healthy B6 mice are shown in grey and diseased B6 mice in white. Healthy B6-mt^{FVB} mice are shown in red and diseased B6-mt^{FVB} mice are shown in orange. Error bars indicate the standard deviation to the mean. (Unpaired t-test, * p = 0.05, ** p = 0.0023, n = 3)*

In Figure 15 the cytokine expression levels are shown. The levels of TNFα are increased in disease state for both mouse strains whereas expression levels of IL-1β are only increased in diseased B6 mice. For IL-10 there is no difference between healthy and disease state for B6 mice, but the levels of IL-10 are increased in diseased B6-mt^{FVB} mice. Next, the expression levels of IL-6 and IL-8 (KC for mice respectively) were checked (Supplemental Figure 1) but due to extremely low values (IL-6) or extreme outliers (IL-8) these results are hard to interpret. At least IL-8 showed high expression levels in disease state.

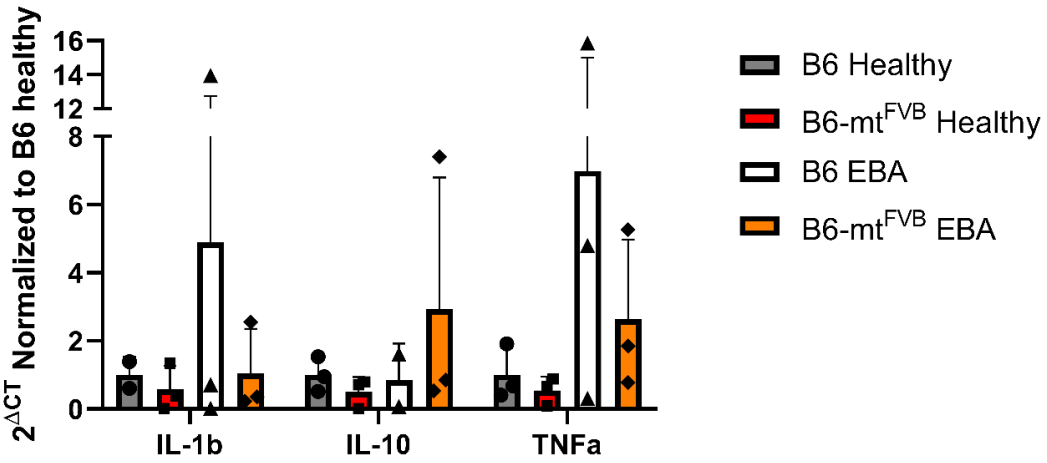

Figure 15: Cytokine expression in small intestine of healthy and diseased B6 and B6-mt^{FVB} mice. Healthy B6 mice are shown in grey, mice suffering from EBA in white. Healthy B6-mt^{FVB} mice are shown in red, mice suffering from EBA in orange. Error bars indicate the standard deviation to the mean. (Unpaired t-test, n = 3)

Additionally, to further test the potential anti-inflammatory effect of propionate as shown by Schilf *et al.*[223], intestinal organoids were stimulated over night with different Propionate concentrations and checked the expression levels of GLP1, TNFα and IL-8 (KC) (Supplemental Figure 2). It seems like cytokine expression of IL-8 and TNFα as well as GLP1 is increasing with Propionate concentrations.

3.2 To what extent does the microbiome play a role in EBA disease development and is it and its metabolome impacted by the mutation in the *mt-Atp8* gene?

3.2.1 Germ-free mice are lesser affected by EBA disease than conventional housed mice

The EBA experiment in 8 germ-free B6-Tac and 8 conventional B6-Tac mice was performed to check to what extend the microbiome is responsible for disease outcome. The mice were injected with 5 mg pathogenic IgG on day 0, 2 and 4 of the experiment. On day 4, 7, 10 and 14 the mice were weighed and scored for disease symptoms. As shown in Figure 16 germ-free housed mice possess significantly milder disease than conventional housed mice (Day 7: *p*-value: 0.0031; Day 10: *p*-value < 0.0001; Day 14: *p*-value < 0.0001). Nevertheless, the result seems to be antibody dose dependent, as 3 doses of 3 mg total IgG did not show any difference between B6J germ-free and conventional mice (See Supplemental Figure 3).

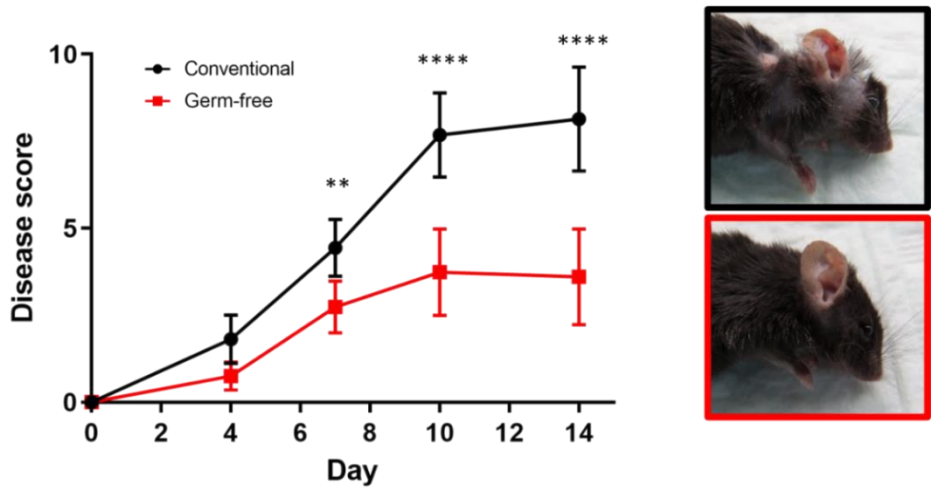

*Figure 16: EBA disease development in germ-free versus conventional housed mice. On the left the disease score is portrayed with germ-free mice in red and conventional mice in black. Mice were injected on Day 0, 2 and 4 with 5 mg total IgG each. On the right are example pictures of the mice on day 14. Error bars indicate standard deviation to the mean. (n = 8, Sidak's multiple comparison test, **: p-value = 0.0031; ****: p-value < 0.0001).*

3.2.2 No difference in immune cell subpopulations in germ-free versus conventional housed mice

To investigate to what extend the composition of immune cells differ between germ-free and conventional housed B6Tac mice an immune cell subpopulation analysis was performed. Therefore, single cells were isolated out of blood, skin and spleen tissue, stained them with antibodies of an immune panel (Table 5) and analyzed the composition with flow cytometry (Figure 17). All samples were gated for immune cells, followed by single cells, living cells and CD45+ cells. In blood samples (A), germ-free mice showed increased B- cells (B220+), slightly decreased CD3+ T cells and decreased monocytes (Ly6C+ Ly6G+). In samples from spleen (B), the same pattern can be seen for B cells, whereas CD3+ T cells are slightly increased, especially the CD8a+ cell subset. In skin samples (C) the CD3+ T cells are increased in germ-free mice, especially the γδ T cell subset, whereas monocytes are slightly decreased.

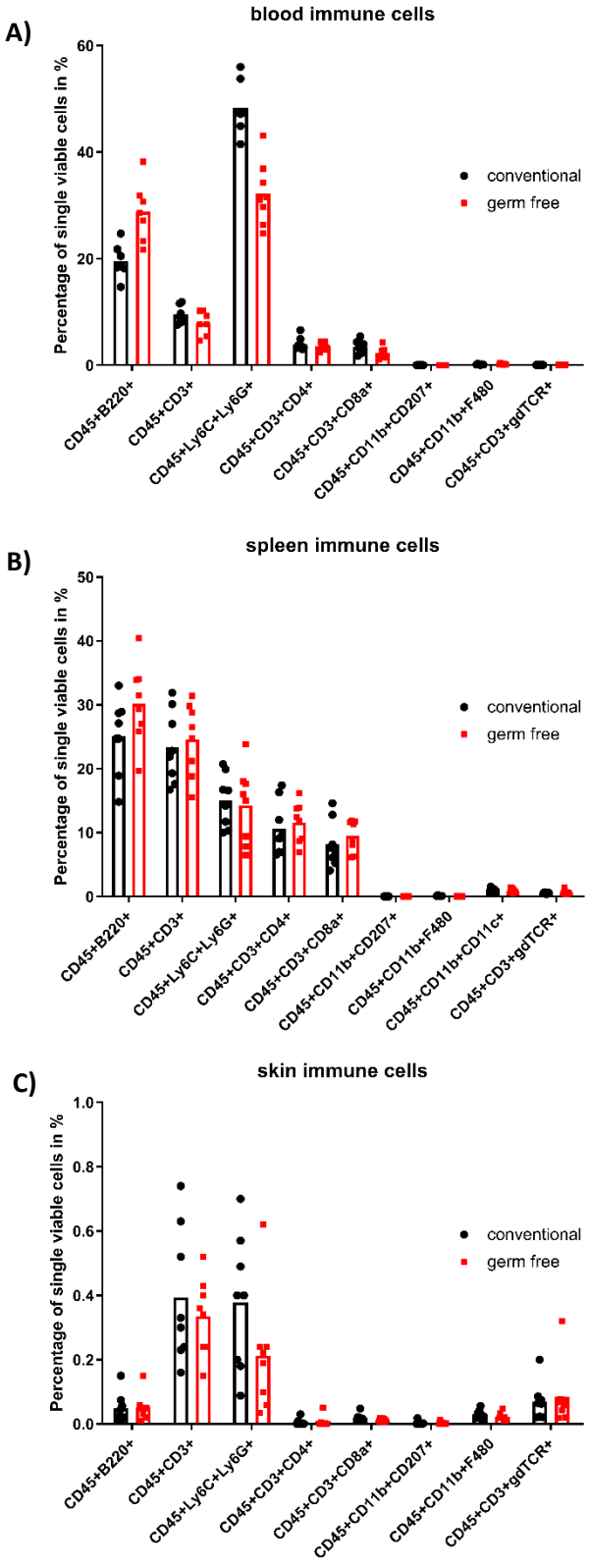

Figure 17: Immune cell subset analysis from germ-free and conventional housed mice. Immune cells derived from blood (A), spleen (B) and skin (C) were analysed. (n = 8 mice per housing condition).

3.2.3 Metabolomic analysis reveals a significant different metabolome between mice strains as well as candidate metabolites

As it is already known that bacteria influence the metabolome in the gut through their metabolism and their own microbial metabolites towards a healthy or more inflamed state. Schilf *et al*.[223] showed that microbial metabolites differ in their abundance in liver tissue of B6 and B6-mt^{FVB} mice. A metabolomics analysis of liver tissue was performed to get an even closer look on the liver metabolome and to identify metabolites that differ in their abundance between the mouse strains and might play a role in disease development of EBA.

The metabolomic analysis revealed that B6 and B6-mt^{FVB} mice have different metabolites in their liver tissue. In Figure 18 is clearly shown that the significantly different abundant metabolites (limma, $p < 0.05$) cluster apart from each other in a principal component analysis with a difference in axis 1 from 75.1%. Same could also be visualized in a volcano plot (Figure 19) with significantly different abundant metabolites (p-value [-log10] > 1) being mapped to KEGGCompoundIDs.

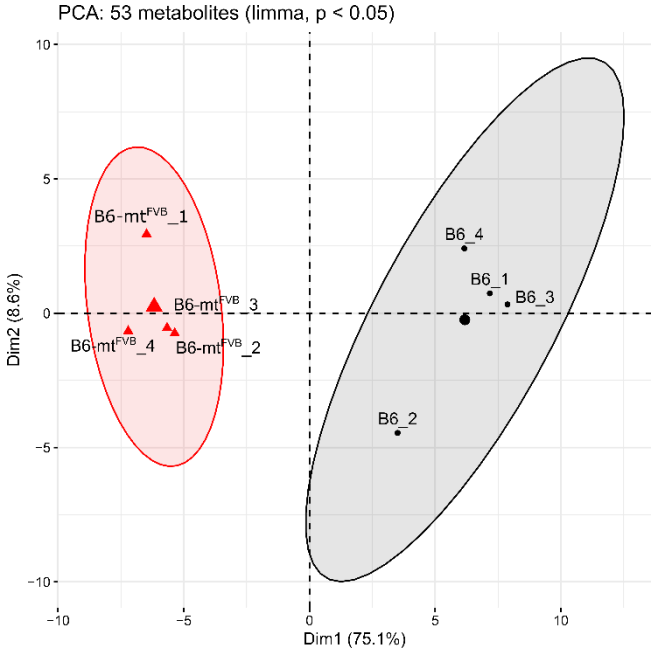

Figure 18: Principal component analysis of significantly different abundant metabolites in liver tissue of B6 (black) and B6-mt^{FVB} mice (red). (n = 4).

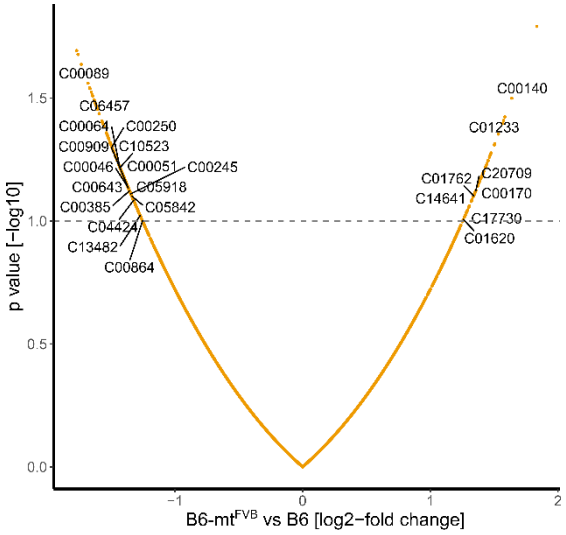

Figure 19: Volcano plot of significantly different abundant metabolites in liver tissue of B6 and B6-mt^{FVB} mice. All metabolites with a p- value [-log10] higher than 1 are mapped to KEGGCompoundIDs. (n = 4)

Furthermore, to identify metabolites of interest and extend the knowledge of Schilf *et al.*[223] the enrichment analysis for metabolites from liver tissue with *p*-values <0.1 and Compound IDs was performed by running against KEGG database, and the results for liver are shown in Table 6. For B6 mice 60 compounds are significantly enriched in liver tissue, for B6-mt^{FVB} 50 enriched metabolites could be identified. Further results containing enzymes, reactions and pathways can be found in (Supplemental Table 1). The results could be visualized as pathway maps (B6: Figure 20; B6-mt^{FVB}: Figure 21). Additionally, GO annotations from the mitochondrial cellular function gene ontology (GO:0005739) were added to the identified pathway maps (B6: Figure 22; B6-mt^{FVB}: Figure 23).

Table 6: Significantly enriched metabolites of liver tissue of B6 and B6-mt^{FVB} mice. (Limma, n = 4)

KEGG ID	**KEGG name**	***p*-value (Limma)**	**Enriched in**
C00071	Aldehyde	0.006889	B6-mt^{FVB}
C00093	sn-Glycerol 3-phosphate	0.006589	B6-mt^{FVB}
C00121	D-Ribose	0.008889	B6-mt^{FVB}
C00140	N-Acetyl-D-Glucosamine	0.00049	B6-mt^{FVB}
C00162	Fatty acid	0.006489	B6-mt^{FVB}
C00170	5'-Methylthioadenosine	0.00029	B6-mt^{FVB}
C00209	Oxalate	0.00439	B6-mt^{FVB}
C00315	Spermidine	0.00798929	B6-mt^{FVB}
C00329	D-Glucosamine	0.004789578	B6-mt^{FVB}
C00357	N-Acetyl-D-Glucosamine 6-phosphate	0.006189452	B6-mt^{FVB}
C00385	Xanthine	0.004089641	B6-mt^{FVB}

C00461	Chitin	0.005289533	B6-mt^{FVB}
C00645	N-Acetyl-D-mannosamine	0.005089551	B6-mt^{FVB}
C00655	Xanthosine 5'-phosphate	0.004289623	B6-mt^{FVB}
C00670	sn-Glycero-3-phosphocholine	0.006489425	B6-mt^{FVB}
C00700	XTP	0.006789398	B6-mt^{FVB}
C00734	Chitosan	0.008889209	B6-mt^{FVB}
C00750	Spermine	0.00698938	B6-mt^{FVB}
C00927	Isonocardicin A	0.006389434	B6-mt^{FVB}
C01137	S-Adenosylmethioninamine	0.00498956	B6-mt^{FVB}
C01233	sn-Glycero-3-phosphoethanolamine	0.000789938	B6-mt^{FVB}
C01234	1-Aminocyclopropane-1-carboxylate	0.004089641	B6-mt^{FVB}
C01620	Threonate	0.001489875	B6-mt^{FVB}
C01672	Cadaverine	0.00798929	B6-mt^{FVB}
C01674	Chitobiose	0.003589686	B6-mt^{FVB}
C01739	Nocardicin E	0.007189362	B6-mt^{FVB}
C01762	Xanthosine	0.000689947	B6-mt^{FVB}
C01941	Nocardicin A	0.008589236	B6-mt^{FVB}
C03064	3-Dehydro-L-threonate	0.003689677	B6-mt^{FVB}
C03089	5-Methylthio-D-ribose	0.003489695	B6-mt^{FVB}
C04132	N-Acetyl-D-Glucosamine 6-sulfate	0.002589776	B6-mt^{FVB}
C04188	S-Methyl-5-thio-D-ribose 1-phosphate	0.006689407	B6-mt^{FVB}
C04438	1-Acyl-sn-glycero-3-phosphoethanolamine	0.001489875	B6-mt^{FVB}
C04501	N-Acetyl-alpha-D-Glucosamine 1-phosphate	0.005389524	B6-mt^{FVB}
C04517	1-(1-Alkenyl)-sn-glycero-3-phosphocholine	0.006889389	B6-mt^{FVB}
C04582	S-Methyl-5-thio-D-ribulose 1-phosphate	0.008689227	B6-mt^{FVB}
C04635	1-Alkenylglycerophosphoethanolamine	0.005789488	B6-mt^{FVB}
C05515	5-Ureido-4-imidazole carboxylate	0.008389254	B6-mt^{FVB}
C05973	2-Acyl-sn-glycero-3-phosphoethanolamine	0.001489875	B6-mt^{FVB}
C06023	D-Glucosaminide	0.007889299	B6-mt^{FVB}
C06156	alpha-D-Glucosamine 1-phosphate	0.007889299	B6-mt^{FVB}
C16352	7-Methylxanthosine	0.001789848	B6-mt^{FVB}
C16565	Aminopropylcadaverine	0.007789308	B6-mt^{FVB}
C17351	Nocardicin C	0.008589236	B6-mt^{FVB}
C17352	Isonocardicin C	0.007089371	B6-mt^{FVB}

C17355	Nocardicin G	0.008289263	B6-mt^{FVB}
C18049	N-Acyl-L-homoserine lactone	0.002489785	B6-mt^{FVB}
C18168	Diacylglycerylhomoserine	0.00198983	B6-mt^{FVB}
C18169	Diacylglyceryl-N,N,N-trimethylhomoserine	0.003289713	B6-mt^{FVB}
C19787	5'-S-Methyl-5'-thioinosine	0.003089731	B6-mt^{FVB}
C00018	Pyridoxal phosphate	0.012088921	B6
C00051	Glutathione	0.001289893	B6
C00064	L-Glutamine	0.003089731	B6
C00089	Sucrose	0.003189722	B6
C00245	Taurine	0.002089821	B6
C00250	Pyridoxal	0.000689947	B6
C00268	Dihydrobiopterin	0.012888849	B6
C00372	Dextran	0.009289173	B6
C00385	Xanthine	0.002889749	B6
C00519	Hypotaurine	0.008689227	B6
C00534	Pyridoxamine	0.00498956	B6
C00588	Choline phosphate	0.007289353	B6
C00643	5-Hydroxy-L-tryptophan	0.002689767	B6
C00647	Pyridoxamine phosphate	0.010089101	B6
C00831	Pantetheine	0.011688957	B6
C00847	4-Pyridoxate	0.008389254	B6
C00864	Pantothenate	0.002389794	B6
C00909	Leukotriene A4	0.000189992	B6
C00971	4-Pyridoxolactone	0.00698938	B6
C01210	N-Methylethanolamine phosphate	0.007389344	B6
C01678	Cysteamine	0.008889209	B6
C01725	Levanbiose	0.009289173	B6
C01762	Xanthosine	0.010889029	B6
C01959	Taurocyamine	0.01098902	B6
C02165	Leukotriene B4	0.006489425	B6
C02166	Leukotriene C4	0.002889749	B6
C02282	Glutaminyl-tRNA	0.01298884	B6
C02591	Sucrose 6'-phosphate	0.007089371	B6
C02918	1-Methylnicotinamide	0.005589506	B6

C03149	N-Phosphotaurocyamine	0.009089191	B6
C03193	(5-L-Glutamyl)-peptide	0.010189092	B6
C03323	(2,1-beta-D-Fructosyl)n	0.005589506	B6
C03451	(R)-S-Lactoylglutathione	0.011588966	B6
C03492	D-4'-Phosphopantothenate	0.012488885	B6
C04148	Phenylacetylglutamine	0.012188912	B6
C04650	L-Phosphinothricin	0.006289443	B6
C04805	5(S)-HETE	0.007189362	B6
C04853	20-OH-Leukotriene B4	0.007889299	B6
C05122	Taurocholate	0.01198893	B6
C05356	5(S)-HPETE	0.006589416	B6
C05465	Taurochenodeoxycholate	0.011888939	B6
C05515	5-Ureido-4-imidazole carboxylate	0.012588876	B6
C05646	5-Hydroxyindolepyruvate	0.005689497	B6
C05648	5-Hydroxy-N-formylkynurenine	0.008289263	B6
C05731	3-Ketosucrose	0.006489425	B6
C05842	N1-Methyl-2-pyridone-5-carboxamide	0.002089821	B6
C05843	N1-Methyl-4-pyridone-5-carboxamide	0.007489335	B6
C05844	5-L-Glutamyl-taurine	0.010189092	B6
C05939	Linatine	0.009089191	B6
C05944	Pantothenol	0.006389434	B6
C06215	Levan	0.009189182	B6
C06457	Bialaphos	0.00298974	B6
C06735	Aminoacetaldehyde	0.006089461	B6
C13482	Phosphodimethylethanolamine	0.004189632	B6
C14180	S-(Hydroxymethyl)glutathione	0.012788858	B6
C15522	4a-Hydroxytetrahydrobiopterin	0.010389074	B6
C16566	Glutathionylaminopropylcadaverine	0.013688777	B6
C16688	Sucrose 6-phosphate	0.007689317	B6
C17951	N-Acetylbialaphos	0.004889569	B6
C17952	N-Acetylphosphinothricin	0.008689227	B6

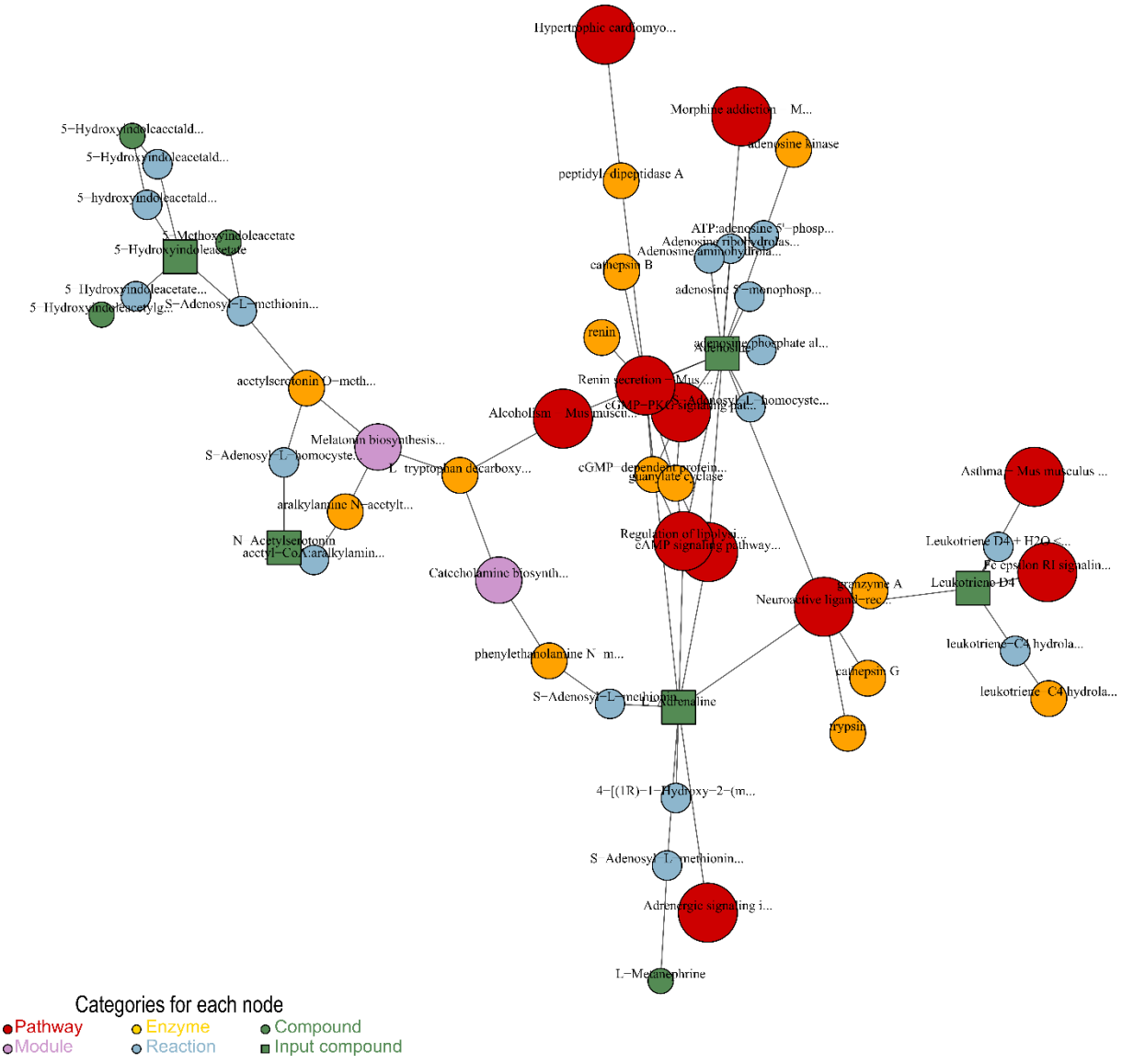

Figure 20: Enriched metabolites and corresponding pathways in liver tissue of B6 mice. All shown metabolites were analyzed against the KEGG database and show a Limma p-value < 0.05. (n = 4)

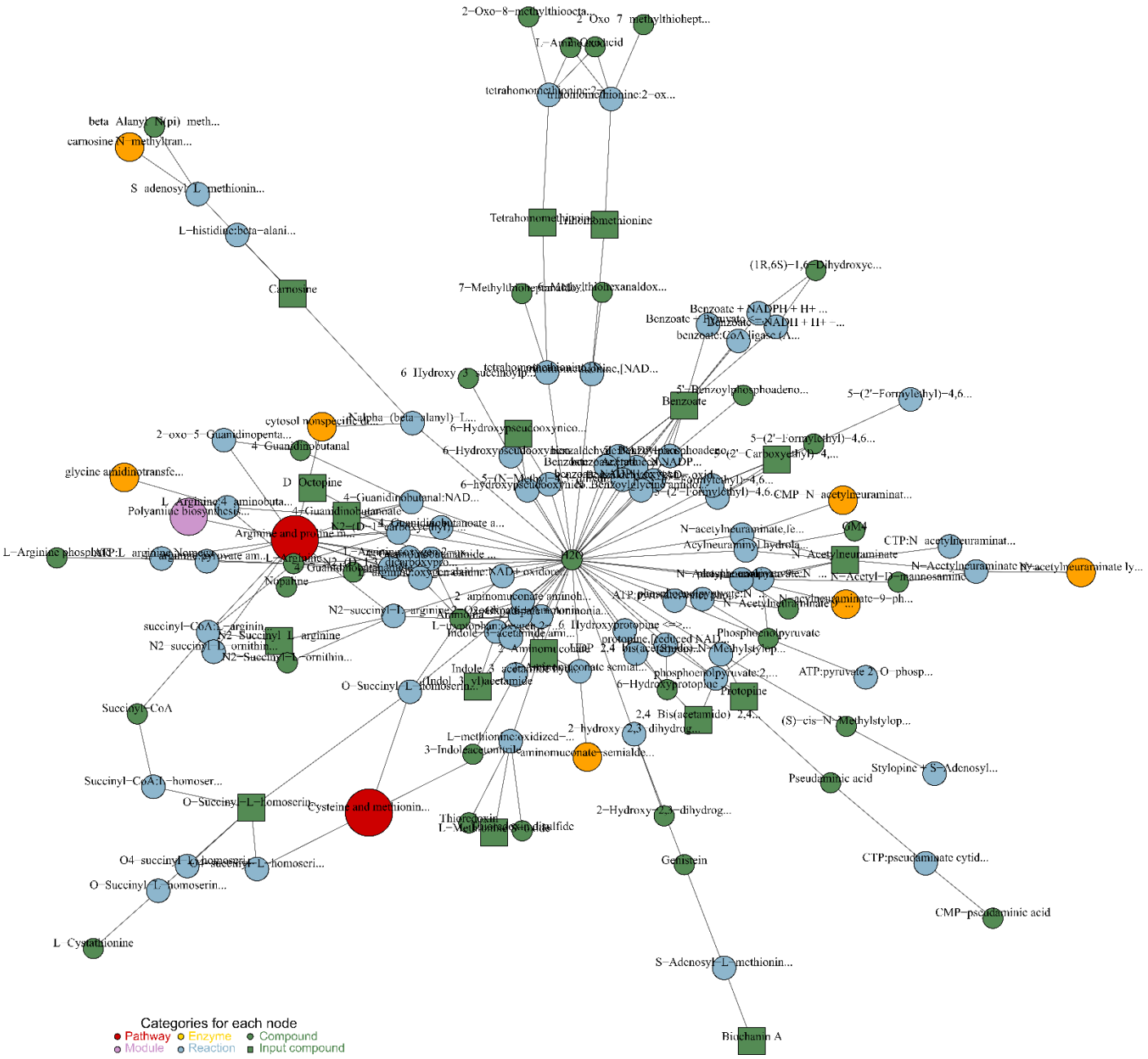

Figure 21: Enriched metabolites and pathways in liver tissue of B6-mt^{FVB} mice. All shown metabolites were analyzed against the KEGG database and show a Limma p-value < 0.05. (n = 4)

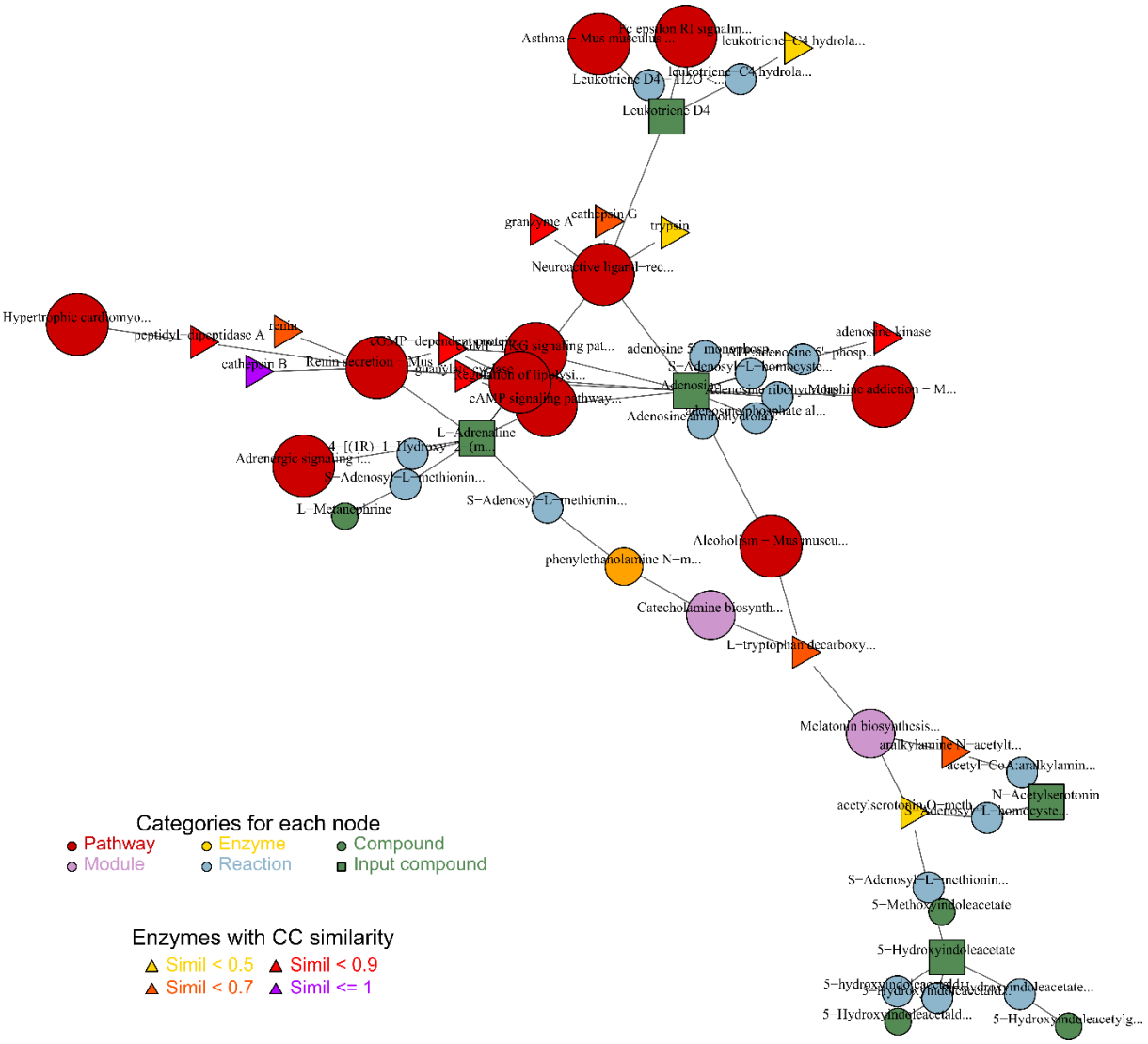

Figure 22: Enriched metabolite pathways with GO annotations from the mitochondrial cellular function gene ontology (GO:0005739) of liver tissue from B6 mice. (Limma, n = 4)

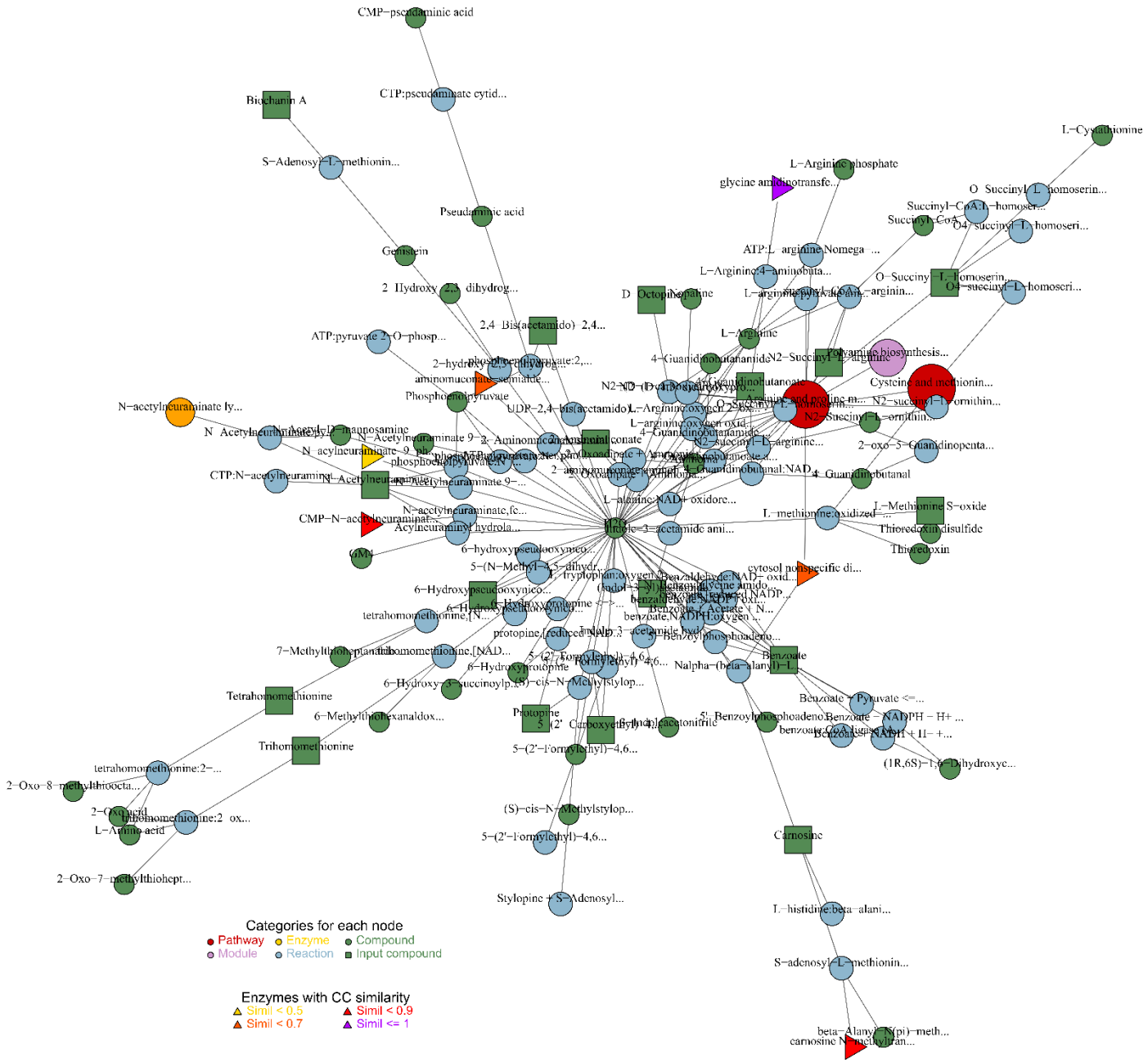

Figure 23:Enriched metabolite pathways with GO annotations from the mitochondrial cellular function gene ontology (GO:0005739) of liver tissue from B6-mt^{FVB} mice. (Limma, n = 4)

3.2.4 Shotgun metagenomic analysis of cecum content reveals indicator species, different abundant pathways and gene families

Additionally, to get a more detailed look into the microbiome of the mice and because the data of the 16S-rRNA sequencing analysis is limited, shotgun metagenomics sequencing was performed on cecum content of both mouse strains. Metagenomics analysis not only gives insight into the phylogeny of the samples but also into the pathway usage of the single species and significant activated gene families.

Shotgun metagenomic sequencing was performed in Max Planck Institute for Evolutionary Biology in Plön, Germany on 10 samples per mouse strain. Sequencing quality was assessed using fastp program. Over 20 million read pairs per sample passed. 2 samples had host contamination over 70% and where therefore removed from further analysis.

As a first step, the data was analyzed for phylogenetic properties such as most abundant phyla, families, genera and species (Figure 24) using mOTUs_v2. There is no significant difference in the abundance of phyla between the two mouse strains although B6-mt^{FVB} mice have more *Bacteroidetes* and less *Actinobacteria, Proteobacteria* and *Verrucomicrobia* compared to B6 mice. Two significantly different abundant families could be found: *Bifidobacteriaceae* (more abundant in B6) and *Bacteroidacea* (more abundant in B6-mt^{FVB} mice). Both families have a *p*-value lower than 0.05. Comparing the abundant genera in cecum content of B6 and B6-mt^{FVB} mice there is a significant difference in the abundance of *Bifidobacteria* and *Bacteroides*, with first one being more present in B6 mice and the latter in B6-mt^{FVB} mice (both $p<0.05$). Additionally, two significantly different abundant species could be identified, which are both more abundant in B6 mice: *Lactobacillus hominis* and *Bifidobacterium animalis* (both $p<0.05$) (Supplemental Figure 4).

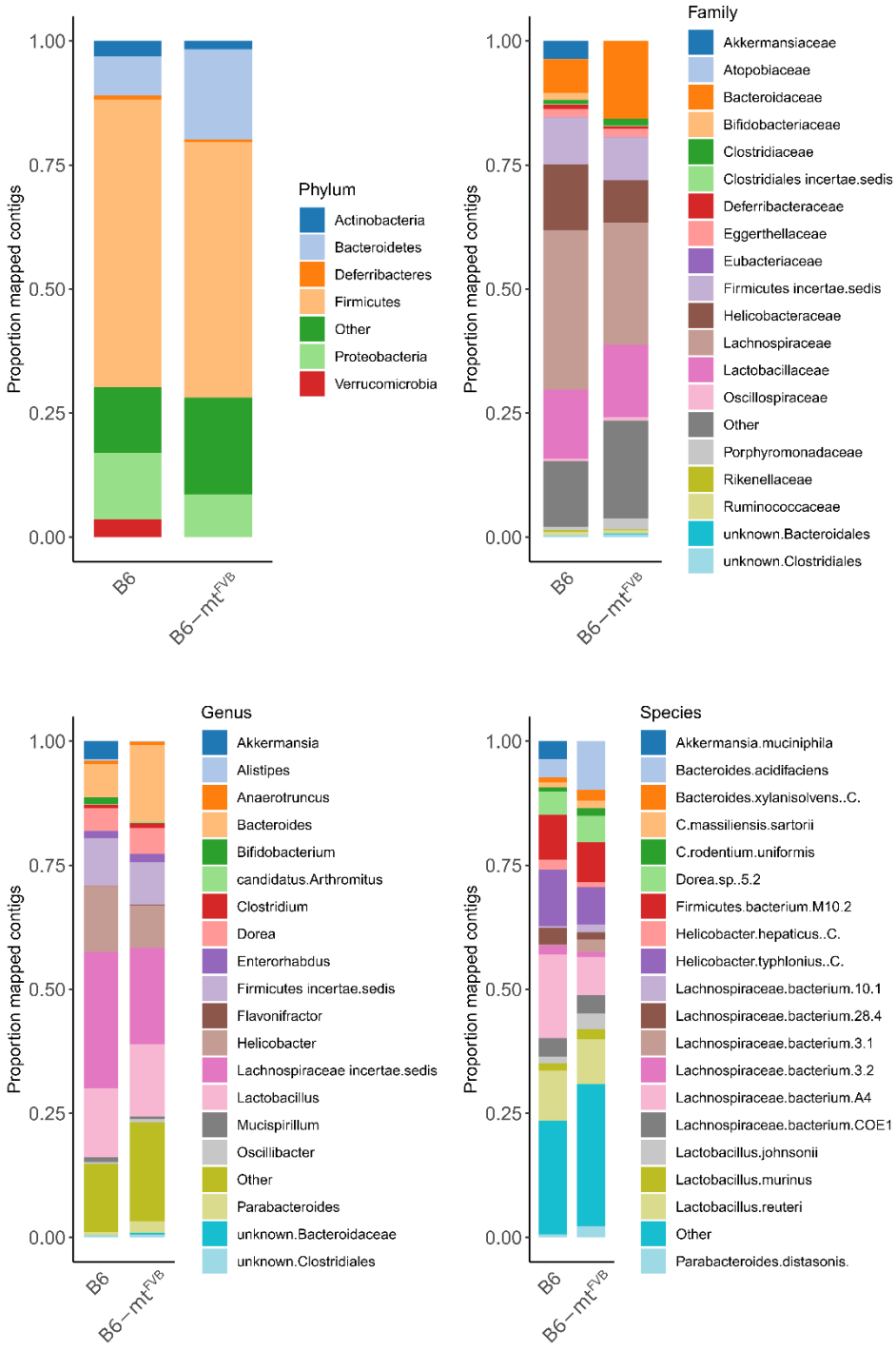

Figure 24: Most abundant phyla, genera, families, and species in shotgun metagenomic data of cecum content from B6 and B6-mt^{FVB} mice. (n = 10)

Afterwards, the alpha and beta diversity were assessed (Figure 25). Shotgun metagenomics data of B6 and B6-mt^{FVB} mice shows no difference neither in alpha diversity (p = 0.1850) nor in beta diversity (Adonis test (9.999 permutations), p = 0.2023, R^2 = 0.07099). Additionally, the Bacteroidetes/Firmicutes ratio was analyzed (Figure 26), which also shows no difference between strains (p = 0.1051).

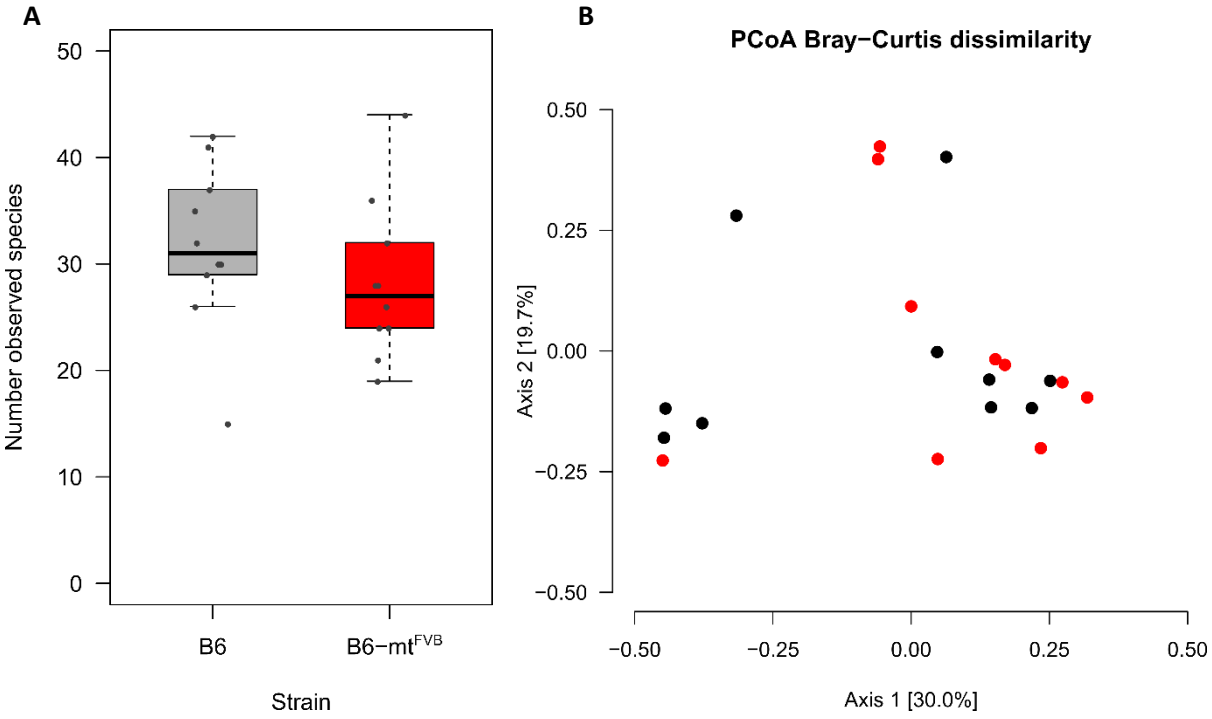

Figure 25: Alpha and Beta diversity of shotgun metagenomics data. A) shows the number of observed species as proxy for alpha diversity, B) shows the beta diversity (PCoA Bray-Curtis, n = 10).

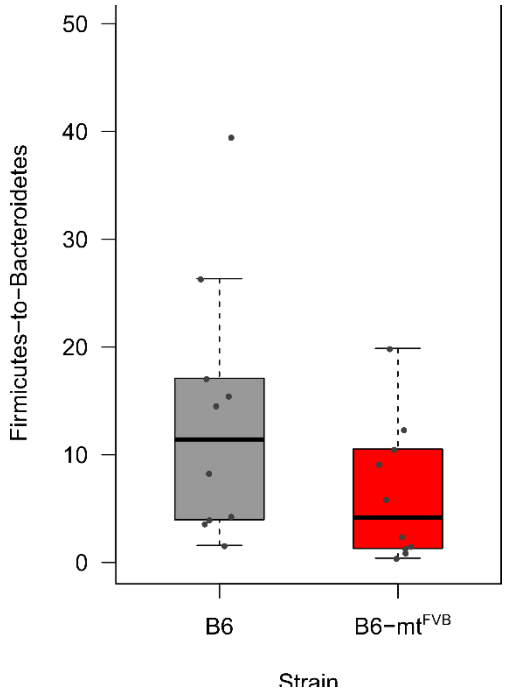

Figure 26: Bacteroidetes / Firmicutes ratio in shotgun metagenomics data of cecum content.

Furthermore, the shotgun metagenomics data was analyzed in more ways. First, functional profiling was performed by checking the differentially abundant pathways using the HUMAnN2 pipeline[236] (Table 7) and visualized them overall (Figure 27A) and for pathways correlated to short chain fatty acids (Figure 27B). The PCoA by Bray-Curtis does not show significant difference neither for all, not for SCFA related pathways. All different abundant pathways (*p*-value < 0.1) are listed in Table 7. There are 45 pathways more present in cecum content of B6 mice and 15 pathways are more present in B6-mt^{FVB} mice.

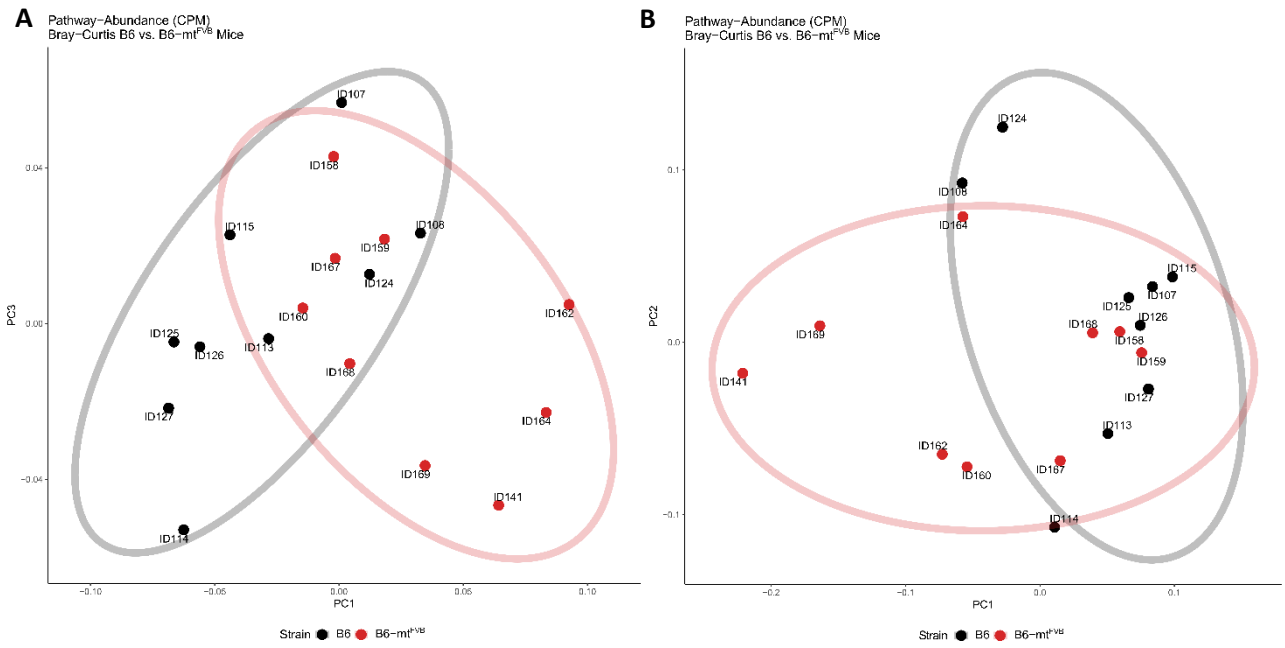

Figure 27: Principal Coordinate Analysis of bacterial pathway abundance in B6 and B6-mt^{FVB} mice. A) All bacterial pathways present in the gut cluster apart between B6 (black) and B6-mtFVB mice (red), whereas the effect is not as clear for short chain fatty acid related pathways (B). (Bray Curtis analysis. n = 9 mice per strain)

Table 7: Different abundant pathways in shotgun metagenomics data. Data was analyzed using the HUMAnN2 pipeline. All pathways with a p-value < 0.1 for differential abundance are shown and matched to the corresponding BioCyc database ID.

BioCyc ID	**Pathway task**	***p*-value**	**Up in**
ARGININE-SYN4-PWY	L-ornithine de novo biosynthesis	0.03998	B6-mt^{FVB}
ASPASN-PWY	superpathway of L-aspartate and L-asparagine biosynthesis	0.09391	B6-mt^{FVB}
BIOTIN-BIOSYNTHESIS-PWY	biotin biosynthesis I	0.00532	B6
CENTFERM-PWY	pyruvate fermentation to butanoate	0.03386	B6
FASYN-ELONG-PWY	fatty acid elongation -- saturated	0.02089	B6
FASYN-INITIAL-PWY	superpathway of fatty acid biosynthesis initiation (E. coli)	0.02089	B6
GLCMANNANAUT-PWY	superpathway of N-acetylglucosamine, N-acetylmannosamine and N-acetylneuraminate degradation	0.05031	B6-mt^{FVB}
GOLPDLCAT-PWY	superpathway of glycerol degradation to 1,3-propanediol	0.08493	B6

HEME-BIOSYNTHESIS-II	heme biosynthesis I (aerobic)	0.03386	B6
HEMESYN2-PWY	heme biosynthesis II (anaerobic)	0.08980	B6
HISDEG-PWY	L-histidine degradation I	0.01061	B6-mt^{FVB}
HOMOSER-METSYN-PWY	L-methionine biosynthesis I	0.01876	B6
HSERMETANA-PWY	L-methionine biosynthesis III	0.0337	B6
MET-SAM-PWY	superpathway of S-adenosyl-L-methionine biosynthesis	0.01876	B6
METSYN-PWY	L-homoserine and L-methionine biosynthesis	0.01876	B6
P108-PWY	pyruvate fermentation to propanoate I	0.07724	B6
P4-PWY	superpathway of L-lysine, L-threonine and L-methionine biosynthesis I	0.07946	B6
P42-PWY	incomplete reductive TCA cycle	0.05031	B6
POLYAMSYN-PWY	superpathway of polyamine biosynthesis I	0.03542	B6
PWY-241	C4 photosynthetic carbon assimilation cycle, NADP-ME type	0.08774	B6
PWY-4702	phytate degradation I	0.07724	B6
PWY-5030	L-histidine degradation III	0.07701	B6-mt^{FVB}
PWY-5101	L-isoleucine biosynthesis II	0.06253	B6-mt^{FVB}
PWY-5104	L-isoleucine biosynthesis IV	0.06253	B6
PWY-5347	superpathway of L-methionine biosynthesis (transsulfuration)	0.03147	B6
PWY-5384	sucrose degradation IV (sucrose phosphorylase)	0.09001	B6
PWY-5676	acetyl-CoA fermentation to butanoate II	0.09613	B6
PWY-5690	TCA cycle II (plants and fungi)	0.03386	B6
PWY-5913	TCA cycle VI (obligate autotrophs)	0.03542	B6
PWY-5941	glycogen degradation II (eukaryotic)	0.06253	B6-mt^{FVB}
PWY-5973	cis-vaccenate biosynthesis	0.09391	B6-mt^{FVB}
PWY-5989	stearate biosynthesis II (bacteria and plants)	0.01835	B6
PWY-6151	S-adenosyl-L-methionine cycle I	0.06253	B6-mt^{FVB}
PWY-6168	flavin biosynthesis III (fungi)	0.01876	B6-mt^{FVB}
PWY-6282	palmitoleate biosynthesis I (from (5Z)-dodec-5-enoate)	0.02089	B6
PWY-6519	8-amino-7-oxononanoate biosynthesis I	0.00532	B6
PWY-6545	pyrimidine deoxyribonucleotides de novo biosynthesis III	0.02443	B6
PWY-6588	pyruvate fermentation to acetone	0.07724	B6
PWY-6590	superpathway of Clostridium acetobutylicum acidogenic fermentation	0.03386	B6
PWY-6609	adenine and adenosine salvage III	0.07701	B6-mt^{FVB}
PWY-6628	superpathway of L-phenylalanine biosynthesis	0.09272	B6

PWY-7115	C4 photosynthetic carbon assimilation cycle, NAD-ME type	0.07724	B6
PWY-7117	C4 photosynthetic carbon assimilation cycle, PEPCK type	0.08774	B6
PWY-7219	adenosine ribonucleotides de novo biosynthesis	0.03998	B6-mt^{FVB}
PWY-7234	inosine-5'-phosphate biosynthesis III	0.09391	B6
PWY-7282	4-amino-2-methyl-5-phosphomethylpyrimidine biosynthesis (yeast)	0.01204	B6
PWY-7388	octanoyl-[acyl-carrier protein] biosynthesis (mitochondria, yeast)	0.02089	B6
PWY-7456	mannan degradation	0.01395	B6
PWY-7664	oleate biosynthesis IV (anaerobic)	0.02089	B6
PWY-821	superpathway of sulfur amino acid biosynthesis (Saccharomyces cerevisiae)	0.03386	B6
PWY0-1479	tRNA processing	0.03386	B6
PWY0-781	aspartate superpathway	0.04208	B6
PWY0-845	superpathway of pyridoxal 5'-phosphate biosynthesis and salvage	0.01204	B6
PWY0-862	(5Z)-dodec-5-enoate biosynthesis	0.02089	B6
PWY66-373	sucrose degradation V (sucrose α-glucosidase)	0.03386	B6
PWYG-321	mycolate biosynthesis	0.02089	B6
PYRIDOXSYN-PWY	pyridoxal 5'-phosphate biosynthesis I	0.01204	B6
RIBOSYN2-PWY	flavin biosynthesis I (bacteria and plants)	0.01876	B6-mt^{FVB}
THRESYN-PWY	superpathway of L-threonine biosynthesis	0.03147	B6-mt^{FVB}
TRNA-CHARGING-PWY	tRNA charging	0.02443	B6-mt^{FVB}

Beside the pathway analysis indicator species for both strains were also analyzed using the Kraken2Bracken pipeline. Therefore, all identified 5718 species were checked and filtered for their abundance of > 0.01% in at least two samples. The remaining 922 species were analyzed for their indicator species potential and effect size (Cohens D). All species with a corrected p-value < 0.05 are displayed in Table 8. There are 39 indicator species for the microbiome of B6 mice and 18 indicator species for the microbiome of B6-mt^{FVB} mice. The most prominent species for B6 mice are *Ochrobactrum anthropic, Bacillus sonorensis, Desulfovibrio desulfuricans, Escherichia coli* and *Pseudoalteromonas sp. Scap06.* The bacteria species *D. desulfuricans* also appeared in the random forest analysis and random core bacteria list of the 16SrRNA sequencing data set of Hirose *et al*. [224]. The most prominent indicator species for B6-mt^{FVB} mice are *Dokdonia sp. MED134, Alistipes sp. Dk3624, Duncaniella sp. C9, Bradyrhizobium lablabi* and *Halomonas sp. JS92-SW72.* The genus *Alistipes* already appeared in the indicator species analysis of the 16SrRNA sequencing analysis of cecum content [224].

Table 8: Indicator species identified for the microbiome of B6 and B6-mt^{FVB} mice. Shown are all species that have a minimum abundance of 0.01 % in at least two samples and after the indicator species analysis and Šidák correction a p-value < 0.5. The Cohens D effect size for each identified indicator species is shown.

Genus	**Species**	***p*-value** (Šidák correction)	**Effect size** (Cohens D)	**Indicator for**
Ochrobactrum	*Ochrobactrum anthropi*	0.000119996	2.288466864	B6
Bacillus	*Bacillus sonorensis*	0.000559922	1.563185519	B6
Desulfovibrio	*Desulfovibrio desulfuricans*	0.003776428	1.409319749	B6
Escherichia	*Escherichia coli*	0.013196176	1.204798488	B6
Pseudoalteromonas	*Pseudoalteromonas sp. Scap06*	0.013653078	1.164110287	B6
Brevibacterium	*Brevibacterium aurantiacum*	0.014109874	1.162680755	B6
Enterococcus	*Enterococcus saigonensis*	0.015499472	1.157953194	B6
Akkermansia	*Akkermansia glycaniphila*	0.006569176	1.157412302	B6
Desulfovibrio	*Desulfovibrio sp. DSM 107105*	0.013951	1.139531783	B6
Dehalococcoides	*Dehalococcoides mccartyi*	0.014129732	1.127902209	B6
Citrobacter	*Citrobacter sp. RHBSTW-00229*	0.000899797	1.082788285	B6
Megasphaera	*Megasphaera stantonii*	0.012083276	1.062905569	B6
Desulfovibrio	*Desulfovibrio sp. 86*	0.024428956	1.055201445	B6
Pectobacterium	*Pectobacterium carotovorum*	0.027587068	1.028849739	B6
	Victivallales bacterium CCUG 44730	0.02877004	1.020183381	B6
Desulfovibrio	*Desulfovibrio piger*	0.033887932	0.989888538	B6
Collinsella	*Collinsella aerofaciens*	0.032944108	0.986935108	B6
Hydrogenophaga	*Hydrogenophaga sp. PBC*	0.011387396	0.965049684	B6
Candidatus Solibacter	*Candidatus Solibacter usitatus*	0.038090207	0.96485271	B6
Paenibacillus	*Paenibacillus alvei*	0.041226111	0.949529696	B6
Slackia	*Slackia heliotrinireducens*	0.042009287	0.941229705	B6
Desulfovibrio	*Desulfovibrio alaskensis*	0.042381184	0.940839544	B6
Staphylospora	*Staphylospora marina*	0.04353556	0.935216174	B6
Bifidobacterium	*Bifidobacterium animalis*	0.005991	0.932922299	B6
Trueperella	*Trueperella pyogenes*	0.023737436	0.926025897	B6
Unclassified Tenericutes	*Tenericutes bacterium MZ-XQ*	0.043437758	0.924144146	B6
Pseudomonas	*Pseudomonas mendocina*	0.036225842	0.924091539	B6
Arabia	*Arabia massiliensis*	0.038364803	0.910983447	B6

Desulfobulbus	*Desulfobulbus oralis*	0.048887438	0.910477147	B6
Olsenella	*Olsenella sp. oral taxon 807*	0.020652256	0.898875467	B6
Desulfovibrio	*Desulfovibrio sulfodismutans*	0.049803952	0.892016581	B6
unclassified Eggerthellaceae	*Eggerthellaceae bacterium zg-1050*	0.041206528	0.874737781	B6
Gordonibacter	*Gordonibacter pamelaeae*	0.048867932	0.874362796	B6
Olsenella	*Olsenella umbonata*	0.003057659	0.849513918	B6
Rickettsia	*Rickettsia canadensis*	0.017661323	0.75528192	B6
Psychrobacillus	*Psychrobacillus sp. AK 1817*	0.022215231	0.748191152	B6
Parolsenella	*Parolsenella catena*	0.015757432	0.70902723	B6
Libanicoccus	*Libanicoccus massiliensis*	0.012659678	0.666765947	B6
Olsenella	*Olsenella sp. GAM18*	0.031015703	0.629366431	B6
Dokdonia	*Dokdonia sp. MED134*	0.001519422	-1.6420428	B6-FVB
Alistipes	*Alistipes sp. Dk3624*	0.001859135	-1.49754607	B6-FVB
Duncaniella	*Duncaniella sp. C9*	0.006768508	-1.33445537	B6-FVB
Bradyrhizobium	*Bradyrhizobium lablabi*	0.007426162	-1.30387798	B6-FVB
Halomonas	*Halomonas sp. JS92-SW72*	0.008402276	-1.25375795	B6-FVB
Hydrogenophaga	*Hydrogenophaga sp. NH-16*	0.011089086	-1.22834841	B6-FVB
Tannerella	*Tannerella forsythia*	0.013136572	-1.14813071	B6-FVB
Bacillus	*Bacillus vietnamensis*	0.013255778	-1.10733277	B6-FVB
Parabacteroides	*Parabacteroides distasonis*	0.021879	-1.07124303	B6-FVB
Hymenobacter	*Hymenobacter sp. HDW8*	0.02957799	-1.02114996	B6-FVB
Alistipes	*Alistipes indistinctus*	0.030247742	-1.01700864	B6-FVB
Dysgonomonas	*Dysgonomonas sp. HDW5B*	0.040246691	-0.95072585	B6-FVB
Mucilaginibacter	*Mucilaginibacter paludis*	0.034359671	-0.88648532	B6-FVB
Flavobacterium	*Flavobacterium sp. I3-2*	0.011606128	-0.88350231	B6-FVB
Bacillus	*Bacillus horikoshii*	0.013275644	-0.87684029	B6-FVB
Runella	*Runella sp. HYN0085*	0.028888297	-0.84992952	B6-FVB
Myroides	*Myroides odoratimimus*	0.046662568	-0.83620335	B6-FVB
Bacillus	*Bacillus sp. JAS24-2*	0.030523456	-0.82451591	B6-FVB

Additionally, I've also analyzed the significant different gene families using the microbiome multivariable association tool MaAsLin2[237]. The results are shown in Table 9. The data was analyzed by mapping against 6 databases (Pfam, GO, KO, eggNOG, Level-4 EC, MetaCyc). The found gene families belong to different fields, like phage DNA antirepressors, phage integrase proteins, transmembrane domains (2TM domain), ABC1 family, DNA binding domains, peptide transporters, replication, recombination and repair (ATP-dependent DNA helicase RecG, Transposase). The found significant gene families are all up in B6 and are associated with 3 *Lactobacillus* strains: *Lactobacillus johnsonii*, *Lactobacillus murinus* and *Lactobacillus reuteri*.

Table 9: Significant different gene families in shotgun metagenomics data of cecum content of B6 and B6-mt^{FVB} mice. The data was analyzed using the biobakery tool MaAsLin2 [237]. Data was mapped against Pfam, eggNOG, KO, GO, level-4 EC and MetaCyc databases. The data was log transformed. Analysis method was fitting linear models (LM). Method for correction of multiple testing is Benjamini Hochberg (BH).

Data-base	**Database ID**	**Gene family**	**Associated bacteria strain**	***p*-value (LM)**	***q*-value (BH)**
pfam	PF03374	Phage antirepressor protein KilAC domain	*Lactobacillus johnsonii*	8.19E+06	0.00118
pfam	PF08346	AntA/AntB antirepressor	*Lactobacillus johnsonii*	9.18E+06	0.00118
pfam	PF14659	Phage integrase, N-terminal SAM-like domain	*Lactobacillus johnsonii*	1.09E+07	0.00118
pfam	PF03382	Mycoplasma protein of unknown function, DUF285	*Lactobacillus murinus*	1.61E+07	0.00131
pfam	PF03382	Mycoplasma protein of unknown function, DUF285		3.54E+08	0.02303
pfam	PF13239	2TM domain		3.13E+09	0.16980
pfam	PF03109	ABC1 family	*Lactobacillus murinus*	7.72E+09	0.22810
pfam	PF04326	Putative DNA binding domain	*Lactobacillus murinus*	7.27E+09	0.22810
pfam	PF06152	Phage minor capsid protein 2	*Lactobacillus murinus*	5.53E+08	0.22810
pfam	PF08352	Oligopeptide dipeptide transporter C terminal region	*Lactobacillus reuteri*	7.54E+09	0.22810
pfam	PF13749	Putative ATP dependent DNA helicase recG C terminal	*Lactobacillus murinus*	7.27E+09	0.22810
eggNOG	COG3666	Transposase	*Lactobacillus reuteri*	1.23E+09	0.23556
eggNOG	ENOG4105EUN	Transposase	*Lactobacillus reuteri*	1.23E+09	0.23556

3.2.5 Integrated analysis of metabolomics and shotgun metagenomics data lead to 3 indicator species and 5 metabolite candidates for further tests

At a next step, the indicator species list as well as the enriched metabolite data were manually checked if there is a correlation between the abundance of the metabolites as well as the species. First, all indicator species were filtered for their environment to select only the bacteria assciated with the gut. To control this manual selection a correlation analysis of the remaining species was performed using Spearman correlation to check whether the species abundance correlates (Figure 28A). It shows that most species are positively correlated or do not have a correlation at all. Only the abundance of *Bacillus sonorensis* and *Bacillus species JAS24.2* is negatively correlated. This result underlines the shared habitat for the selected bacteria. Additionally, a network correlation analysis was performed using the CRAN package corrr 0.4.3. The results are shown in (Figure 28B). The closer the species cluster together the higher is the correlation in abundance. Figure 28B shows that the species cluster together according to mouse strains (Indicator species for B6-mt^{FVB} mice are on the left and for B6 mice on the right) and to the analysis methods used (top: indicator species analysis according to Kraken2Bracken pipeline; Bottom: functional pathway analysis with HUMAnN2 and significantly abundant gene families with MaAsLin2).

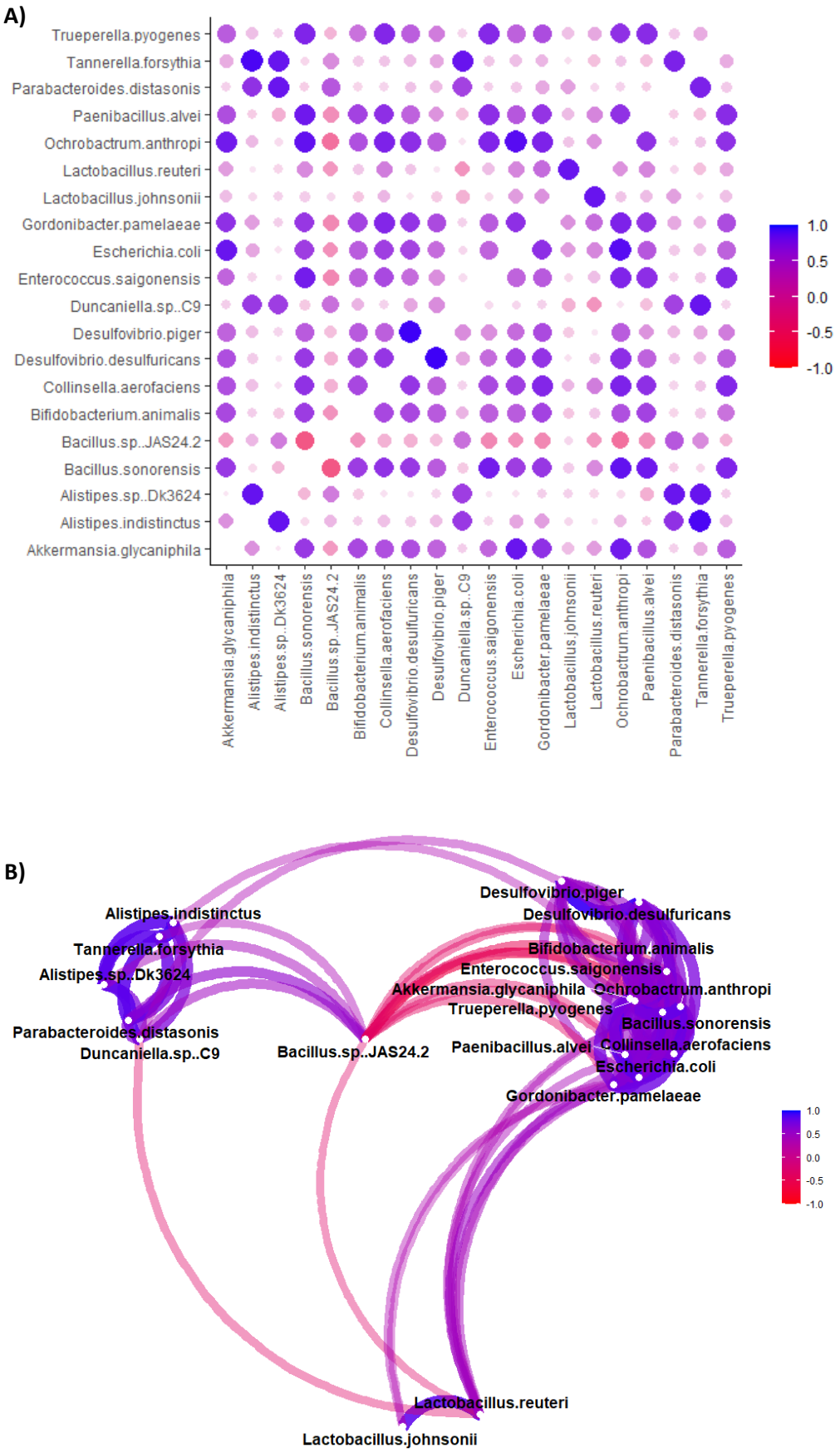

Figure 28: Abundance of bacteria species of mouse gut correlates to mouse strains. A) Correlation analysis of indicator species. B) Network correlation analysis. Positive correlation is depicted in blue and negative correlation in red. Analysis was performed using CRAN package corrr 0.4.3 (Spearman correlation).

To identify the association of the bacteria and the significantly different metabolites the webpage "Virtual Metabolic Human" (https://www.vmh.life/#home) was used. On this database one could search for the single strains and get a list of their associated metabolites. This way a manual heatmap of strains and metabolites was created (figure 29). At a next step, this data was compared to the 16SrRNA data from Hirose *et al.*[224] and further literature to decide for candidate species and metabolites according to these results. These are for the bacteria: *Duncaniella sp. C9 (muris)*[246], *Alistipes indistinctus*[224] and *Lactobacillus reuteri*[247]; and for the metabolites: Spermidine, D-Glucosamine, N-acetyl-D-Glucosamine, D-Ribose and Oxalate.

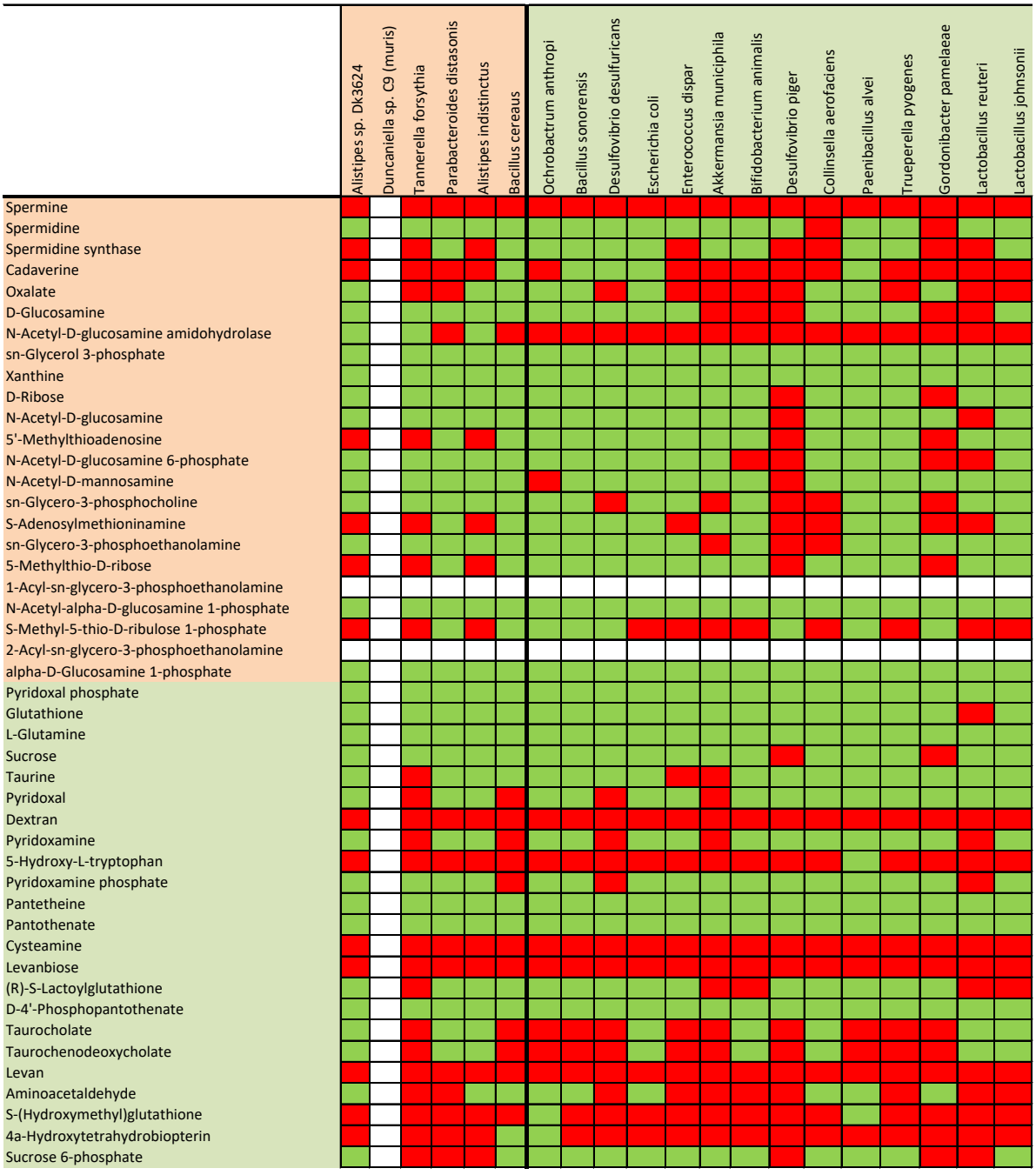

Figure 29: Integrative analysis of identified metabolites from liver tissue and indicator species in the microbiome of B6 and B6-mt^{FVB} mice. The bacteria are present on the top and the metabolites are listed on the left side. Orange background refers to B6-mt^{FVB} mice and green background to B6 mice. In the heat map green color means that the metabolite is considered with the bacterium and red color means it is not. Analysis was performed manually using the "Virtual Metabolic Human" webpage (https://www.vmh.life/#home).

3.3 Are the identified microbial metabolites good candidates for EBA therapy approaches?

3.3.1 D-Ribose enhances tight junction protein expression of IFNγ stimulated organoids

To check the effect of the identified metabolites on the permeability of the intestinal barrier, intestinal organoids with and without 2.5 ng IFNγ stimulation were treated with the metabolites (0.5 mM N-acetyl-D-Glucosamine, 25 mM D-Ribose, 8 µM Spermidine). Next, RNA was isolated and transcribed so the expression of the tight junction proteins Occludin and ZO-1 in the different groups could be tested. As seen in Figure 30 treatment with IFNγ leads to a decrease in the expression of both tight junction proteins. Treatment with D-Ribose leads to an increase in expression for both tight junction proteins, but especially for ZO-1. Spermidine treatment has no effect on Occludin expression but keeps the expression level of ZO-1 comparable to the level of untreated organoids. N-acetyl-D-Glucosamine has no effect on the expression of both tight junction proteins.

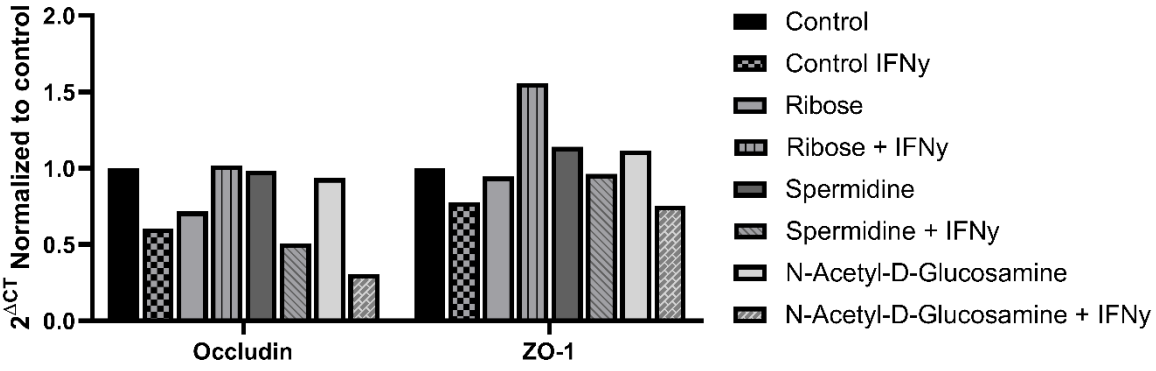

Figure 30: Expression of tight junction proteins in intestinal organoids during IFNγ treatment with and without metabolites. Intestinal organoids were treated with or without 2.5 ng IFNγ and the metabolites D-Ribose (25 mM), Spermidine (8 µM) and N-acetyl-D-Glucosamine (0.5 mM). (n = 170 organoids per treatment group)

3.3.2 Metabolites cannot counteract INFγ induced cytokine expression in organoids

To check the potential anti-inflammatory effect of the candidate metabolites, the organoid cultures were treated as described in the section before but this time the expression of pro-inflammatory cytokines interleukin 8 (IL-8) and TNFα was tested via qPCR (Figure 31). N-acetyl-D-Glucosamine reduces the expression of IL-8 both in IFNγ stimulated and unstimulated intestinal organoids. Especially for the IFNγ treated organoids, the expression of IL-8 is on the same level as for the untreated control. The other two metabolites have no anti-inflammatory effect on IL-8 and Spermidine even enhances the expression in combination with IFNγ. None of the metabolites influences TNFα expression in IFNγ treated and untreated intestinal organoids.

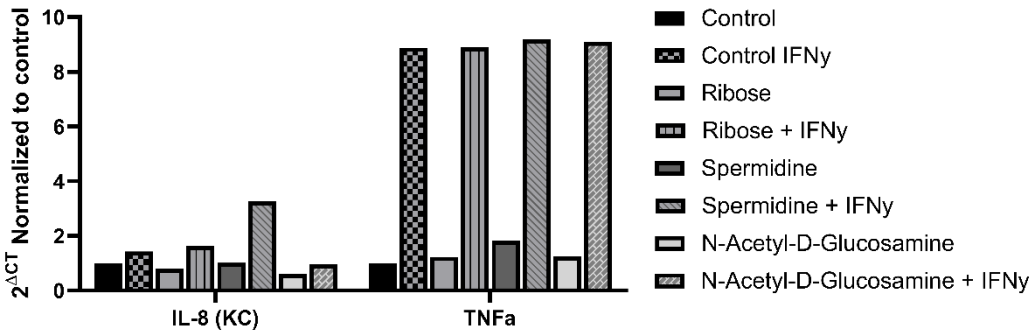

Figure 31: Cytokine expression in IFNγ stimulated organoids under metabolite treatment. Intestinal organoids were treated with or without 2.5 ng IFNγ and the metabolites D-Ribose (25 mM), Spermidine (8 µM) and N-acetyl-D-Glucosamine (0.5 mM). (n = 170 organoids per treatment group)

3.3.3 Metabolites alleviate ATP and nitric oxide production in LPS stimulated RAW 264.7 cell macrophages

Moreover, the anti-inflammatory potential of all five identified metabolites was further investigated in three assays: 1) Cell viability assay (Figure 32), 2) Cytotoxicity assay (Figure 33) and 3) Nitric oxide production assay (Figure 34). The cell viability assay measures the release of ATP which is a sign for inflammatory cell activation[248]. The cytotoxicity assay measures the LDH production which is a proof for cell damage[249]. The nitric oxide assay measures the nitric oxide production which is produced as a defense product in macrophages[250]. RAW 264.7 cell macrophages were stimulated over night with 10 ng/ml LPS and the respective metabolite concentrations (10 nM, 100 nM, 1 µM, 3 µM, 5 µM, 10 µM).

Treatment with Spermidine leads to a decrease in ATP release when simultaneously treated with LPS. Additionally, it also decreases the nitric oxide production, the higher the Spermidine concentration the lower the nitric oxide production. But higher concentrations of Spermidine show cytotoxic potential (10 µM Spermidine ~ 15% cytotoxicity), which might cause the results for NO production.

D-Ribose treatment decreases the ATP release and nitric oxide production on LPS treated RAW 264.7 cell macrophages on the same level for all five concentrations. D-Ribose does not show cytotoxic potential.

Treatment with D-Glucosamine leads to decrease ATP release and nitric oxide production in LPS treated RAW 264.7 cell macrophages. The last one even slightly correlated with the metabolite concentration. D-Glucosamine does not show cytotoxic potential.

N-acetyl-D-Glucosamine treatment shows a decrease in ATP release of LPS treated RAW 264.7 cell macrophages with a slight correlation in metabolite concentration. Nitric oxide production is also decreased, and no cytotoxic potential is indicated.

RAW 264.7 cell macrophages treated with Oxalate and LPS also show decreased ATP release levels and nitric oxide production and no cytotoxic potential.

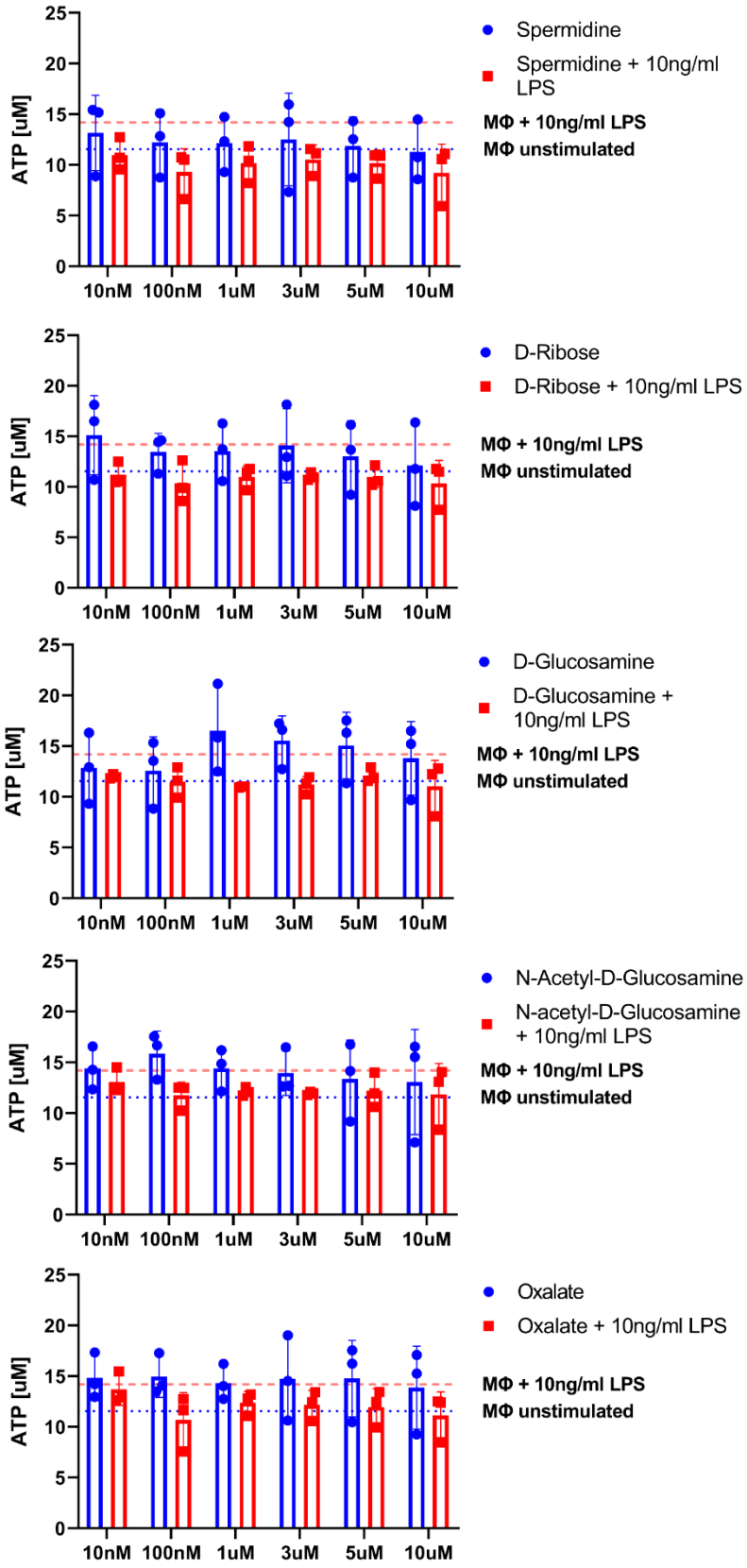

Figure 32: Cell viability assay results of LPS stimulated RAW 264.7 cell macrophages with metabolites. A) Spermidine, B) D-Ribose, C) D-Glucosamine, D) N-acetyl-D-Glucosamine and E) Oxalate. (n = 20,000 cells per well in triplicates and 3 experiments). Error bars indicate the standard deviation to the mean.

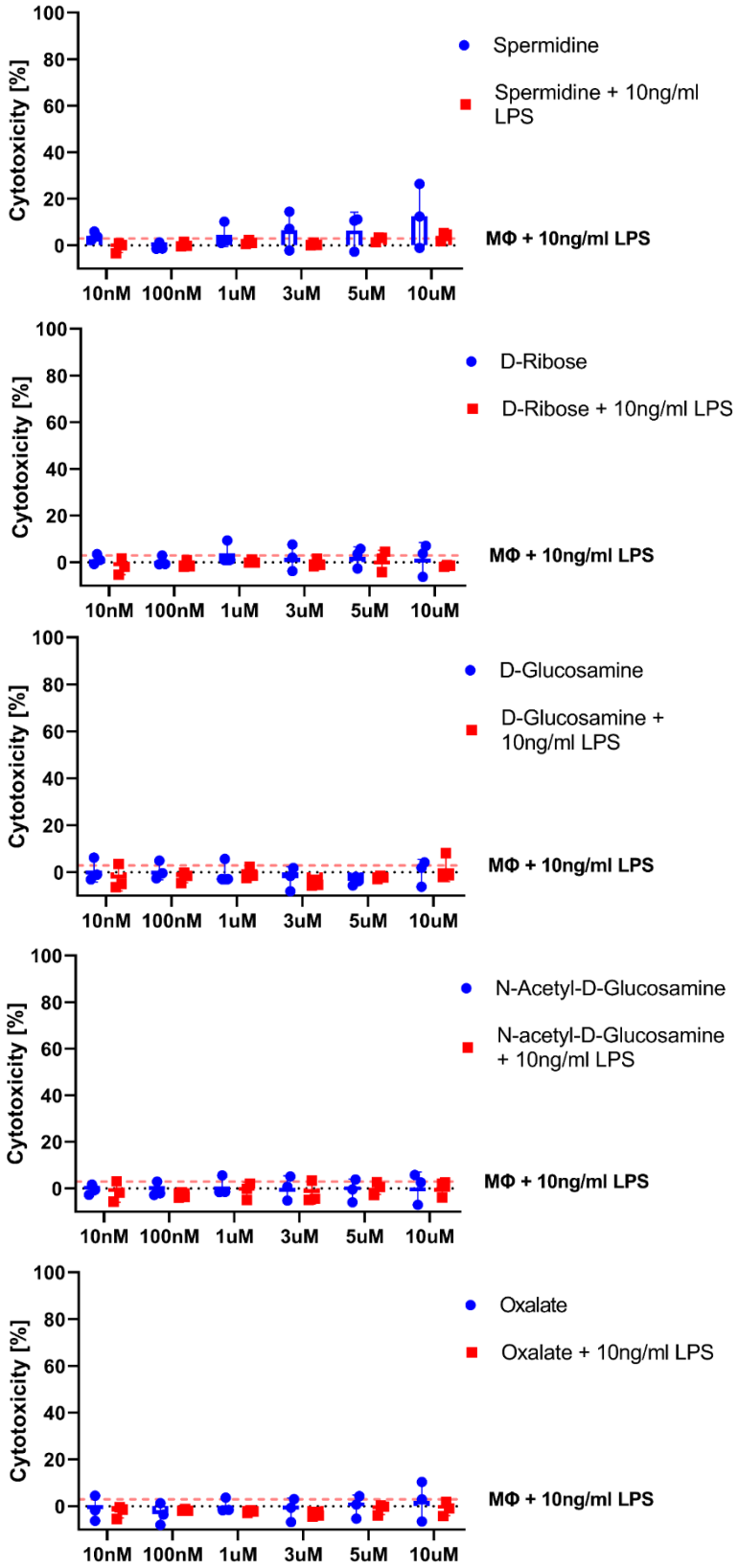

Figure 33: Cytotoxicity assay of LPS and metabolite treated RAW 264.7 cell macrophages. A) Spermidine, B) D-Ribose, C) D-Glucosamine, D) N-acetyl-D-Glucosamine and E) Oxalate. (n = 20,000 cells per well in triplicates and 3 experiments). Error bars indicate the standard deviation to the mean.

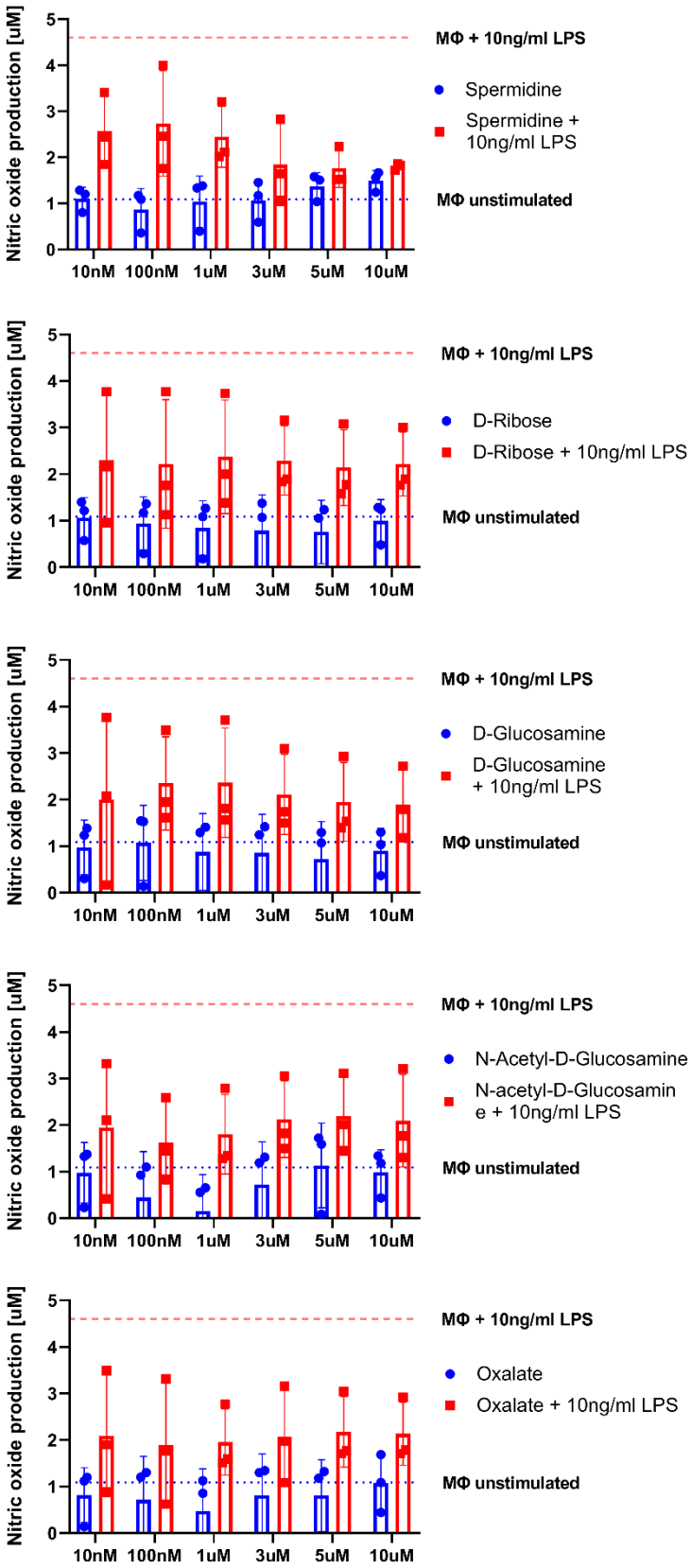

Figure 34: Nitric oxide production of LPS and metabolite treated RAW 264.7 cell macrophages. A) Spermidine, B) D-Ribose, C) D-Glucosamine, D) N-acetyl-D-Glucosamine and E) Oxalate. (n = 20,000 cells per well in triplicates and 3 experiments). Error bars indicate the standard deviation to the mean.

3.3.4 TNFα production of RAW 264.7 cell macrophages stimulated with LPS is influenced by Spermidine, D-Ribose and N-acetyl-D-Glucosamine

After the results of the three assays above another anti-inflammatory signal was checked via TNFα production in a TNFα ELISA. RAW 264.7 cell macrophages were stimulated for 48 h with 10 ng/ml LPS and 1 µM of the respective metabolites and then the culture supernatant was used for the assay. As shown in Supplemental Figure 5A none of the metabolites alone is increasing the TNFα production. In combination with LPS (Supplemental Figure 5B) D-Ribose and N-acetyl-D-Glucosamine are decreasing the TNFα production whereas Spermidine and especially Oxalate increase the amount of cytokine.

To take a deeper look in the effects of the metabolites on TNFα production the three most promising metabolites according to the literature Spermidine, D-Ribose and N-acetyl-D-Glucosamine were tested in different concentrations on 1 ng/ml, 5 ng/ml and no LPS (Figure 35). Spermidine shows high TNFα production decreasing potential especially for 100 µM on all LPS concentrations (Figure 35). Although showing a significant decrease in TNFα production in smaller metabolite and higher LPS concentration before, D-Ribose doesn't show any effect on TNFα production in none of the combinations anymore (Supplemental Figure 6A). N-acetyl-D-Glucosamine shows a slight dose dependent decrease in TNFα production in combination with 5 ng/ml LPS (Supplemental Figure 6B) whereas there is no effect in combination with 1 ng/ml LPS.

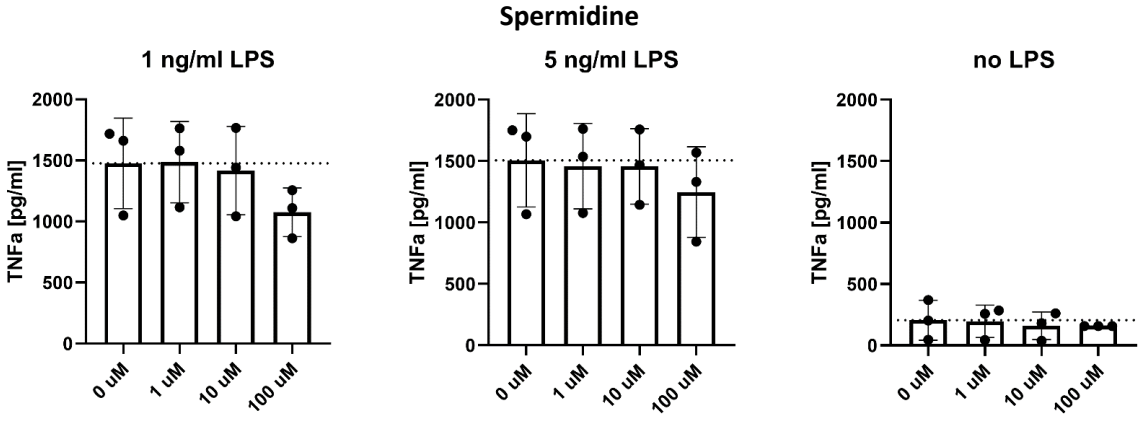

Figure 35: TNFa production upon stimulation with Spermidine and LPS concentrations. The macrophages were treated with different Spermidine concentrations ranging from 0 µM, 1 µM, 10 µM and 100 µM and with 0 ng/ml, 1 ng/ml or 5 ng/ml LPS overnight. The supernatants were used for the TNFα ELISA. Error bars indicate standard deviation to the mean. (Paired T-test, n = 3)

3.3.5 Spermidine treatment has no effect on EBA development and severity

After elucidating the anti-inflammatory potential of spermidine *in vitro* an experiment in animals was conducted. 20 mice were injected with either 5 mg/kg spermidine or PBS as a control on day 0, 2 and 4 of the experiment. Higher concentration and more injections of spermidine had lethal effects on the mice. The mice were weighed daily and scored for disease signs on day 2, 4, 8 and 12. As seen in Figure 36A, Spermidine treatment does not impact disease severity in B6 mice, neither for males (Figure 36B) nor for females (Figure 36C). The same results apply for B6-mt^{FVB} mice (Supplemental Figure 7), whereas the disease score for females treated with Spermidine is even higher than for the control group treated with PBS.

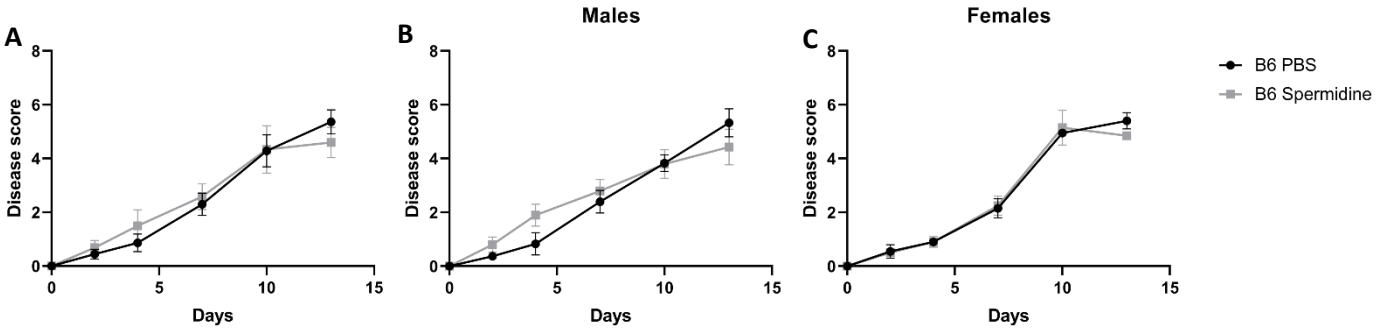

Figure 36: EBA development in B6 mice under Spermidine treatment. Mice treated with 5 mg/kg body weight Spermidine are displayed in grey, control mice treated with PBS are displayed in black. A) shows all sexes combined (3 males + 2 females per group), B) shows only male mice (3 per group), and C) shows only female mice (2 per group). Error bars indicate standard deviation to the mean.

3.3.6 N-Acetyl-D-Glucosamine treatment alleviates EBA disease severity in male B6 mice

At a next step another metabolite, N-acetyl-D-Glucosamine was tested and its anti-inflammatory potential *in vivo*. Therefore, mice were substituted with 200 mg/kg body weight N-acetyl-D-Glucosamine (NAG) or PBS. The experiment started with daily injections one week before applying the IgG to induce the disease and continue throughout disease development. The mice were weighed daily and scored for disease signs on day 2, 4, 8 and 12. As you can see in Figure 37 male B6 mice treated with NAG develop a milder disease compared to the PBS treated mice (Day 12 *p*-value=0.09). Female B6 mice treated with NAG only show a slight decrease in disease severity (Supplemental Figure 8A) and B6-mt^{FVB} mice treated with NAG show absolutely no difference in disease severity compared to control mice (Supplemental Figure 8B).

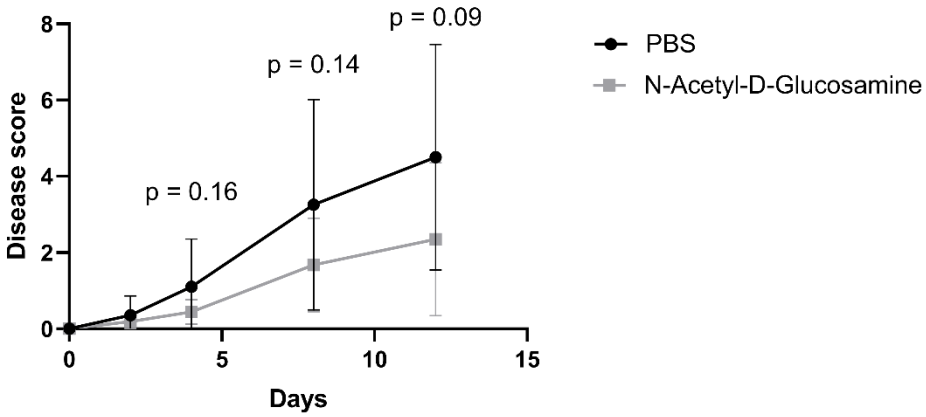

Figure 37: EBA disease development in N-acetyl-D-Glucosamine treated male B6 mice. Mice treated with N-acetyl-D-Glucosamine (NAG) are shown in grey, the control group treated with PBS is shown in black. Mice were injected daily with NAG or PBS starting 1 week before onset of disease. Error bars indicate standard deviation to the mean. (Welch's T-test, n = 10).

4 Discussion

4.1 Mutation in the *mt-Atp8* gene impacts the abundance of immune cells

The skin is the main site of inflammation in Epidermolysis bullosa acquisita. Therefore, I checked the immune potential at the site of disease, specifically γδ T cells. γδ T cells represent only a small amount in circulating CD3+ lymphocytes, but play a vital role when it comes to murine skin immunity[267,268]. Skin resident γδ T cells have several functions such as wound healing, maintaining the skin homeostasis and protecting the barrier of the epithelial microenvironment of the skin in a physical and immune way[245,267,269,270]. In Figure 5 it is clearly shown that B6-mt^{FVB} mice have less γδ T cells than B6 mice in sections of back skin. Isolating and counting these cells from ears using flow cytometry the difference is not visible anymore. This difference can be explained by the sampling site, as Marshall *et al*. showed the density of γδ T cells differs between skin from ears, back and footpads[245]. Additionally, when comparing the disease severity in ears and back of the mice (Figure 7) the results fit to the presence of the γδ T cells. Ears have no difference in γδ T cells present in the skin and no difference in disease severity, whereas in back skin B6-mt^{FVB} mice have less γδ T cells and less severe disease. In conclusion, it was proven that γδ T cells play a role in disease severity in mice.

Why the number of γδ T cell is lower in the back of B6-mt^{FVB} mice remains unknown. Probably, the generation or the maturation of these cells is affected by the mutation in the *mt-Atp8* gene. A specific microenvironment is needed for the negative selection in the fetal thymus as well as for the maturation in the skin[271,272]. On the other hand it is known that γδ T cells can be activated by mitochondrial damage-associated molecular patterns[273]. So maybe an overactivation might lead to a decrease in number which was also proposed by Marshall *et al*. in terms of site specificity [245]. Further experiments are needed to disentangle the role of the mitochondria.

Beside the γδ T cells also further immune cell populations were checked in the spleen and the skin over the disease development of EBA in both mouse strains (Figure 9 + 10). The induction with the pathogenic IgG against type VII collagen leads to activation of the complement system and cytokines which then attracts macrophages and neutrophils to join the site of inflammation[214,274–278]. Due to a migratory feedback loop T cells migrate towards neutrophils activated by immune complex and attract further neutrophils to the site of inflammation[277,279]. For EBA disease progression γδ T cells are more important than CD4+ and CD8+ cells as shown by Bieber *et al*.[279] My data shows a peak in the induction phase of EBA for 11b+ myeloid cells in spleen and skin samples and reduces in the latter phase of the disease whereas GR1+ cells rise with disease progression probably due to the migratory feedback loop with the T cells. CD4+ and CD8+ T cells are highest on Day 4 in spleen samples and slightly decrease with disease progression whereas the percentage of γδ T cells strongly rises. Overall there is no difference in the percentage of immune cell subpopulations between the

two mouse strains. For immune cells isolated from skin the trend is the same except for CD4+ T cells which extremely rise on Day 16 of the disease. Nevertheless, there is no difference observable in skin immune cell subpopulations between B6 and B6-mt^{FVB} mice.

Next, the focus was set on the gut. The gut epithelium is one of the most important interfaces between host and environment. It absorbs nutrients but also keeps pathogens from entering the body. Therefore, the permeability of the intestinal barrier is from great importance. Tight junction proteins are crucial players in maintaining the barrier integrity[243,251] and have already shown to play a role in disease development of many autoimmune diseases such as IBD or Multiple sclerosis[242,252–255]. Therefore, the expression and stability of tight junction proteins in healthy and diseased gut of B6 and B6-mt^{FVB} mice were checked to see whether the mitochondrial mutation has a direct impact on the gut permeability.

For stability I repeated the experiment from Bardenbacher *et al*.[244] where I checked whether Claudin-2 could be degraded by IFNγ. It was shown before that tight junction protein expression can be altered by inflammatory cytokines up to breakdown of the intestinal barrier[244,256,257]. In the Western blot results in Figure 11 the results from Bardenbacher *et al*. [244] could be amplified for IFNγ treated organoids generated from wild type mice. Nevertheless, the results for organoids generated from conplastic mice are not clear enough to conclude anything from this. Right now, it looks like Claudin-2 proteins of conplastic mice are more stable towards IFNγ treatment than Claudin-2 proteins from wildtype mice. As both mouse strains produce Claudin-2 and even the expression pattern is not significantly different although slightly less in small intestine of B6-mt^{FVB} mice. It was shown in rats that Claudin-2 is nitrated by oxidative stress up to degradation[258]. As due to the mitochondrial mutation the ROS levels are higher in different cell types in B6-mt^{FVB} mice (as seen in dissertation of Paul Schilf, University of Lübeck, 2017[259], maybe the Claudin-2 proteins are nitrated and thereby protected from degradation by IFNγ.

Nevertheless, the expression patterns of all tested tight junction proteins do not differ between the mouse strains neither in healthy nor in disease state (Figure 12 + Figure 13). Although, the expression pattern is slightly less in B6-mt^{FVB} small intestine and colon in healthy state and slightly up in disease state. Zeissig *et al.* showed that the expression of Claudin-2, -5 and -8 is decreased in active Crohn's disease[253] , but for active EBA it seems to be not the case. Therefore, one can infer that the expression of tight junction proteins and consequently the permeability of the intestinal barrier is not affected by the induction of EBA.

On the other hand, I checked the influence of the mitochondrial mutation on the immune system of the B6-mt^{FVB} mice. Schilf *et al*. already showed that the conplastic mice have less IL-4 and IL-17 producing CD4+ T cells relative to B6 mice[223].

As a first step focus was set on the cytokine and hormone production in the gut of B6 and B6-mt^{FVB} mice. For hormones the expression of GLP-1 was checked, which was already shown to play a role in diabetes type II and psoriasis[260–262]. GLP-1 is a hormone with anti-inflammatory properties such as decreased cytokine production and inhibition of NF-κB activation[260–262]. In active disease state of EBA the expression of the hormone GLP-1 is significantly reduced in both mouse lines (Figure 14). It was shown before, that during the induction of passive EBA IgG deposits can be found in membranes of all organs of the gastrointestinal tract and inflammation occurs not only in the skin but also in the gut[210]. Therefore, the decrease of GLP1 is probably due to the gut inflammation. And as the expression of GLP-1 in tissue of B6-mt^{FVB} mice does not differ from B6 mice, GLP-1 might not play a role in the milder disease outcome of B6-mt^{FVB} mice at least in the gut.

Additionally, it was shown before that dysbiosis of the intestinal microbiome, which often co-exists in inflamed guts, leads to decrease of the expression of GLP-1 receptor[263,264]. Interestingly, the expression for the GLP-1 receptor is staying on a comparable level for B6-mt^{FVB} mice and even increasing for B6 mice. The increased expression of the receptor in B6 might be a kind of immune response as receptor binding can inhibit NF-κB activation and B6 mice suffer from severe disease development.

Checking the expression of different cytokines, it is demonstrated in Figure 15 that in healthy condition B6-mt^{FVB} mice express slightly less cytokines both pro-inflammatory (Il-1β, TNFα) and anti-inflammatory (IL-10). It was shown in several studies as well as by Schilf *et al*. in this specific model that mitochondria influence the cytokine production[223,265,266]. Looking at the expression pattern in the disease state the results for B6 mice are as expected. Interestingly, for B6-mt^{FVB} mice the expression patterns for the pro-inflammatory cytokines are not as high as for B6 but the expression for the anti-inflammatory cytokine IL-10 is increased. This pattern might be explained by the earlier starting remission of the EBA disease compared to B6 mice.

In summary, I could show that B6-mt^{FVB} mice have less γδ T cells in the epidermis of the back skin which are important for disease progression. Nevertheless, the percentage of the immune cell subpopulations is not impacted by the mitochondrial mutation. On the other hand, I could show that mutation in the *mt-Atp8* gene has no influence on the expression of tight junction proteins nor on the expression of pro- and anti-inflammatory cytokines in the intestine, although there is a trend of slightly decreased expression in the conplastic mice.

4.2 The microbiome is crucial for disease development and influenced by the mitochondrial genome

The microbiome is known to be a driver of health and disease and thus play a role in autoimmune diseases. It was shown before that higher richness and diversity of the skin microbiome prior to immunization alleviates EBA disease progression[280]. To further investigate the role of the microbiome in terms of EBA the induction of the disease was performed in a germ-free facility and compared the disease development of germ-free housed mice to conventional housed mice in parallel. The comparison of germ-free and conventional housed B6 mice during EBA treatment showed clear result. It could be revealed that germ-free mice developed significantly milder disease compared to conventional housed mice even on day 7 and seem to recover already on day 14 whereas conventional housed mice are still on their peak of disease. This clearly indicates the role of the microbiome in disease development. The same phenomenon was shown in the psoriasis mouse model under germ-free conditions[281,282].

It is known that the immune system needs the microbiome for a proper development[283–286]. Therefore, I checked via flow cytometry whether there are differences in the immune cell subpopulation between germ-free and conventional housed mice suffering from EBA. No difference could be detected in cell percentage, neither in blood, spleen nor skin samples, suggesting at least no impaired production of immune cells in germ-free mice.

To take a closer look at the microbiome and its contributing mechanics metabolomics of liver tissue of B6 and B6-mt^{FVB} mouse strains were performed. It was shown before that mice with different genetic backgrounds possess a diverse metabolome[287]. Additionally, it was proven that changes in the gut microbiome of mice directly impact the liver metabolome[288] and that in disease changed metabolomes often co-exist with dysfunctional mitochondria[289,290]. I can see the same pattern when comparing the metabolome data which shows significant metabolites for each of the two mouse strains (Figure 18 + 19) indicating that the mutation in the *mt-Atp8* gene influences the metabolome of the liver. Metabolic changes in the liver have direct consequences for other organs, as they also use liver originated metabolites[291]. This might be an answer to the different response to induced EBA.

Bacterial species are known to have the potential for both beneficial and detrimental effects on the host depending on their environment. In phylogenic analysis of the shotgun metagenomics data two genera were significant abundant*:* *Bifidobacteria* in B6 an *Bacteroides* in B6-mt^{FVB} mice. *Bifidobacteria* are often present in probiotics used to prevent gastrointestinal disorders[292] as a disturbed composition of Bifidobacteria has been described in different diseases such as coeliac

disease[293], IBD[294] and atopy[295,296]. The mostly commensal genus *Bacteroides* can possess detrimental effects when entering the body elsewhere than the gut[297,298]. On the other hand, *Bacteroides* species produce capsular polysaccharides A (PSA), which contribute to the homeostasis, development and stimulation of the immune system[298,299]. PSA is also able to activate the production of anti-inflammatory IL-10[300], which expression levels were also slightly higher in intestine of B6-mt^{FVB} mice. Additionally, Bifidobacteria species are producers of SCFAs acetate and propionate[298], which anti-inflammatory potential is already shown before[301]. In conclusion, the significantly more abundant Bacteroides species in B6-mt^{FVB} mice might contribute to the milder disease progression in EBA.

In further analyses such as indicator species and differential abundant gene families more bacterial species of interest were identified. These were *Duncaniella sp. C9 (muris)*[246]*, Alistipes indistinctus*[224] and *Lactobacillus reuteri*[247]. *Duncaniella sp. C9 (muris*) belongs to the family *Muribaculaceae* (formerly known as *Bacteroidales S24-7*[246]). This family was already identified among the indicator species in the 16S rRNA analysis of stool by Hirose *et al*.[224] and expansion of *D. muris* is associated with improvement of intestinal health and colitis protection in mice[302,303]. Furthermore, Hirose *et al*. also identified bacteria from the genus *Alistipes* as indicator for B6-mt^{FVB} mice[224]. This overlaps with the identified indicator species *Alistipes indistinctus* in the shotgun metagenomics data. The genus *Alistipes* is associated with health as well as diseases[304]. In liver cirrhosis a decrease in abundance of *A. indistinctus* correlates with disease decompensation[304,305]. On the other hand, an increase of *A. indistinctus* is correlated with systolic blood pressure[304,306]. Nevertheless, due to its identification in several independent studies, this species remains of great interest. Additionally, *Lactobacillus reuteri* was identified as it is associated with significant different abundant gene families in the shotgun data. *L. reuteri* is also known for beneficial and pathogenic effects in different diseases. In the mouse model experimental autoimmune encephalitis as well as for necrotizing enterocolitis *L. reuteri* significantly reduces the disease severity[247,307,308]. Other studies showed effects promoting autoimmunity triggered by *L. reuteri*, e.g. in an inducible lupus model via imiquimod[309,310]. So, whether these species are friends or foes in terms of EBA severity needs to be investigated.

Unfortunately, in the shotgun metagenomics data I could not see the difference in beta diversity nor in the Bacteroides/Firmicutes ratio between B6 and B6-mt^{FVB} mice as it was shown before by Hirose *et al*.[224]. Nevertheless, the more detailed analysis of the shotgun metagenomics revealed differential abundant pathways between the two mouse strains. Although SCFA related pathways do not cluster apart from each other, there are several other pathway groups just like pathways involved in biotin biosynthesis, fatty acid metabolism and methionine biosynthesis related pathways. Biotin biosynthesis, the most significant different abundant pathway, was already shown to play a role in immune responses as biotin deficiency triggers inflammatory responses in CD4+ T cells in form of

pro-inflammatory cytokine production, enhanced differentiation towards Th1 and Th17 cells as well as activation of the mTOR signaling pathway[311].

Another interesting field are the methionine biosynthesis related pathways which are more abundant in B6 mice. Checking targeted metabolomics data from Paul Schilf (unpublished data) it shows that methionine concentration is significantly increased in liver of B6-mt^{FVB} mice compared to B6 mice. Additionally, several of the identified metabolites found in B6-mt^{FVB} mice are present in methionine metabolism and methionine salvage pathway (also seen in metabolomics data from cecum content, Supplemental Table 2), whereas there is only one metabolite found in B6 mice which is identified with methionine pathways. It was shown before that methionine itself can function as an antioxidant that decreases ROS[312]. Although no difference in ROS production in liver mitochondria could be yet detected[223], the mitochondrial mutation might still impact the mitochondrial ROS production in B6-mt^{FVB} mice and thus mediated the microbiome towards methionine production as a counteraction. Furthermore, Liu *et al.* showed that methionine supplementation downregulates genes related to immune responses in the intestine during sleep deprivation[312]. Same might be the case for EBA in B6-mt^{FVB} mice as it was already shown for an atopic dermatitis model that Seleno-L-methionine supplementation significantly decreases lesion formation and cellular inflammatory parameters[313]. Further impacts of methionine in terms of EBA development and the mutation in the *mt-Atp8* gene need to be investigated.

To sum this up I aimed to investigate if the microbiome plays a role in disease development and could show that the presence of microbes leads to a much more severe disease development of EBA than the absence, while the percentage of immune cell subpopulations in spleen, skin and blood samples does not differ between conventional and germ-free housed mice. Furthermore, I could show that the mitochondrial mutation impacts the microbiome in the presence of indicator species, abundant pathways and expressed gene families. Further investigation is needed about the specific role of the identified metabolites, bacterial species and pathways in terms of EBA.

4.3 Candidate microbial metabolites of conplastic mice possess anti-inflammatory potential

Bacterial metabolites can have great impact on the immune system of the host. I identified five metabolites (Spermidine, D-Ribose, D-Glucosamine, N-acetyl-D-Glucosamine, Oxalate) that are already known for their mediating effects and are also associated with the identified bacterial genus *Alistipes*.

Spermidine belongs to the polyamines. Polyamines are already known to play an important role in tissue regeneration, cell growth, proliferation, genomic stabilization, controlling apoptosis, inducing autophagy and possess antioxidative properties[314–318]. Spermidine in particular is associated with

beneficial health effects in terms of preventing post-menopausal osteoporosis[319], protection from cardiac aging[320], obesity prevention and improvement of glucose tolerance[321], improvement of function and generation of memory T cells[314,322] and suppression of proinflammatory cytokine secretion[314,320,323]. Thus, this metabolite was of great interest to also play a role in EBA. In *in vitro* experiments I could prove the anti-inflammatory effects as it reduces ATP and NO production in RAW 264.7 cell macrophages in the presence of LPS and a dose effect on TNFα production. Furthermore, I could show that in intestinal organoids Spermidine is keeping up expression levels of tight junction protein ZO-1 under IFNγ treatment indicating a barrier strengthening effect of this metabolite. On the other hand, I could also see a cytotoxic effect of high Spermidine concentrations *in vitro* and in the mouse model even before the induction of EBA, probably due to the autophagy activation of the metabolite. Low, not cytotoxic concentrations of Spermidine had no effect on our EBA mouse model. In conclusion, I could see anti-inflammatory effects of Spermidine in vitro but the optimal number of doses, concentration, and the route of supplementation needs to be further explored.

The next metabolites I was interested in are the amino sugars N-acetyl-D-Glucosamine and D-Glucosamine. The latter was already proven for prevention of osteoarthritis[324], expending lifespan by inducing mitochondrial biogenesis and lowering blood glucose levels[325], and reducing the production of NO and proinflammatory cytokines as well as inhibiting inflammation in the intestinal mucosa in an experimental model of IBD[326]. N-acetyl-D-Glucosamine inhibits proinflammatory cytokine production as well as Th1 and Th17 cell responses in an (MOG)-induced EAE mouse model[327]. Testing both amino sugars *in vitro* I could show the anti-inflammatory effects in terms of reduced ATP and NO production in RAW 264.7 cell macrophages exposed to LPS. Furthermore, I could also verify the suppressing effect of N-acetyl-D-Glucosamine in the expression of IL-8 and TNFα production in cells stimulated with LPS. *In vivo* N-acetyl-D-Glucosamine showed slightly alleviating effects in male B6 mice during EBA. As N-acetyl-D-Glucosamine modulates the synthase of hyaluronic acid in keratinocytes and fibroblasts, which is necessary for maintaining skin elasticity and hydration[328–330], further investigations in form of concentration titration or route of application needs to be performed.

The last metabolite under investigation was the sugar D-Ribose. D-Ribose is of particular interest because supplementation with D-Ribose leads to improvement of cellular processes and mitochondrial function by increasing the production of ATP[331]. As the mitochondrial mutation influences its function in B6-mt^{FVB} mice, it might also favor commensal bacterial species that synthesize D-Ribose to counteract the consequences. Furthermore, D-Ribose was also shown to play a role in several diseases such as cardiovascular diseases[332] and chronic fatigue syndrome[333]. Interestingly, presence of D-Ribose decreases ATP-production in RAW 264.7 cell macrophages

stimulated with LPS. Moreover, the production of NO and TNFα is reduced in the presence of D-Ribose under LPS stimulation, suggesting further anti-inflammatory effects of the metabolite. Another finding supporting this role is the strengthening barrier effect in organoids treated with IFNγ. D-Ribose enhances the expression of the tight junction proteins Occludin and especially ZO-1, which leads to a reduced gut permeability and therefore a reduced inflammatory potential in B6-mt^{FVB} mice. If this metabolite also plays a role in the development and severity of EBA needs to be tested.

In conclusion, I identified promising candidate metabolites and could prove their anti-inflammatory potential *in vitro* in terms of cytokine, ATP and NO production as well as their influence on tight junction protein expression in intestinal organoids in an inflammatory setting. If all metabolites also play a role in alleviating EBA disease severity in B6-mt^{FVB} mice needs to be further investigated. Nevertheless, N-acetyl-D-Glucosamine already showed a promising trend.

4.4 Conclusion

In conclusion, this study gave new insights in the complex relations between the mitochondrial genome, the immune system and the microbiome. I could show that mice with a mutation in the *mt-Atp8* gene have less γδ T cells in the epidermis of the back skin, which are important for the disease progression in EBA. Other immune related functions such as expression of tight junction proteins or cytokines in the gut do not seem to be infected by the mutation in the *mt-Atp8* gene. More important is the microbiome itself. I could show that conventional housed mice develop much milder disease symptoms in EBA than conventional housed mice. Digging deeper in this topic, I could show that B6-mt^{FVB} mice have a distinct microbiome and metabolome compared to B6 mice. The metabolome of the B6-mt^{FVB} mice contains significantly different abundant metabolites which possess anti-inflammatory potential shown *in vitro* and *in vivo* for N-acetyl-D-Glucosamine. Thus, the mitochondrial genome influences the microbiome and the metabolites. Furthermore, I could intensify that the microbiome plays a major role in disease development in EBA. And that the mitochondrial mutation in the *mt-Atp8* gene favors bacterial metabolites with anti-inflammatory potential. Now research is one step closer to disentangle the mechanisms in Bullous pemphigoid diseases, especially EBA, and has new promising candidate species and metabolites to test for therapy approaches.

4.5 Outlook

The results above lead to further questions and more ideas what to do. One of the future projects needs to be uncover the relationship of the mutation in the *mt-Atp8* gene and the number of γδ T cells in the epidermis. Do the mitochondria directly influence the negative selection process in the thymus or the maturation in the skin? Or are the cells overactivated in B6-mt^{FVB} mice and decline

faster? To uncover the last question one can check the amount of γδ T cells in the skin of juvenile up to aged mice and see whether the difference in the back skin between B6 and B6-mt^{FVB} mice is increasing with age. And of course, cell culture experiments with immature γδ T cells and mitochondrial peptides.

I already could show that the presence of the microbiome has a big impact on disease severity in EBA. To uncover the role of the mitochondrial mutation alone the experimental EBA needs be induced in germ-free B6 and B6-mt^{FVB} mice. Furthermore, fecal microbiome transplantation experiments in gnotobiotic mice can tell whether the mitigating effect in EBA depends on the microbiome and whether this effect is transferable.

Further project in terms of therapy approaches need more EBA experiments to test not only the effects D-Glucosamine and D-Ribose on disease severity, but also to titrate the concentrations and application times and routes of Spermidine and N-acetyl-D-Glucosamine. Application routes can be next to the already performed i.p. injection, gavage or topical.

On the other hand, also the role of the identified bacteria species needs to be examined. Interesting would be the effects of bacterial supernatants on intestinal organoids and in immune cell culture such as RAW 264.7 cell macrophages. Parameters can be the same as for the metabolites, namely ATP, NO and cytokine production as well as the effects on the expression of tight junction proteins. Next step would be a co-culture with intestinal organoids and last but not least a the effect of the bacteria strains in a gnotobiotic mouse model during EBA development.

Another direction for further projects can also focus on the role of methionine and its corresponding pathways in terms of EBA. Tests on immune cell metabolism in response to methionine supplementation or metabolites triggering the identified methionine related pathways may be of interest.

5 References

(1) Kramer, P.; Bressan, P. Our (Mother's) Mitochondria and Our Mind. *Perspect. Psychol. Sci.* **2018**, *13* (1), 88–100. https://doi.org/10.1177/1745691617718356.

(2) Siekevitz, P. Powerhouse of the Cell. *Sci. Am.* **1957**, *197*, 131–144. https://doi.org/10.1038/scientificamerican0757-131.

(3) Schmidt-Rohr, K. Oxygen Is the High-Energy Molecule Powering Complex Multicellular Life: Fundamental Corrections to Traditional Bioenergetics. *ACS Omega* **2020**, *5* (5), 2221–2233. https://doi.org/10.1021/acsomega.9b03352.

(4) Donald Voet. *Fundamentals of Biochemistry*; Wiley, 2006.

(5) Neupert, W. Protein Import into Mitochondria. **1997**, 57.

(6) Huang, H. The Role of Oxidative Damage in Mitochondria during Aging: A Review. *Front. Biosci.* **2004**, *9* (1–3), 1100. https://doi.org/10.2741/1298.

(7) Li, X.; Fang, P.; Mai, J.; Choi, E. T.; Wang, H.; Yang, X. Targeting Mitochondrial Reactive Oxygen Species as Novel Therapy for Inflammatory Diseases and Cancers. *J. Hematol. Oncol.J Hematol Oncol* **2013**, *6* (1), 19. https://doi.org/10.1186/1756-8722-6-19.

(8) Hajnóczky, G.; Csordás, G.; Das, S.; Garcia-Perez, C.; Saotome, M.; Sinha Roy, S.; Yi, M. Mitochondrial Calcium Signalling and Cell Death: Approaches for Assessing the Role of Mitochondrial Ca2+ Uptake in Apoptosis. *Cell Calcium* **2006**, *40* (5), 553–560. https://doi.org/10.1016/j.ceca.2006.08.016.

(9) Klinge, C. M. Estrogenic Control of Mitochondrial Function and Biogenesis. *J. Cell. Biochem.* **2008**, *105* (6), 1342–1351. https://doi.org/10.1002/jcb.21936.

(10) Álvarez-Delgado, C.; Mendoza-Rodríguez, C. A.; Picazo, O.; Cerbón, M. Different Expression of α and β Mitochondrial Estrogen Receptors in the Aging Rat Brain: Interaction with Respiratory Complex V. *Exp. Gerontol.* **2010**, *45* (7), 580–585. https://doi.org/10.1016/j.exger.2010.01.015.

(11) Pavón, N.; Martínez-Abundis, E.; Hernández, L.; Gallardo-Pérez, J. C.; Alvarez-Delgado, C.; Cerbón, M.; Pérez-Torres, I.; Aranda, A.; Chávez, E. Sexual Hormones: Effects on Cardiac and Mitochondrial Activity after Ischemia–Reperfusion in Adult Rats. Gender Difference. *J. Steroid Biochem. Mol. Biol.* **2012**, *132* (1), 135–146. https://doi.org/10.1016/j.jsbmb.2012.05.003.

(12) McBride, H. M.; Neuspiel, M.; Wasiak, S. Mitochondria: More Than Just a Powerhouse. *Curr. Biol.* **2006**, *16* (14), R551–R560. https://doi.org/10.1016/j.cub.2006.06.054.

(13) Green, D. R. Apoptotic Pathways: The Roads to Ruin. *Cell* **1998**, *94* (6), 695–698. https://doi.org/10.1016/S0092-8674(00)81728-6.

(14) Green, D. R.; Reed, J. C. Mitochondria and Apoptosis. *Science* **1998**, *281* (5381), 1309–1312. https://doi.org/10.1126/science.281.5381.1309.

(15) Oh-Hama, T. Evolutionary Consideration on 5-Aminolevulinate Synthase in Nature. *Orig. Life Evol. Biosph.* **1997**, *27* (4), 405–412. https://doi.org/10.1023/A:1006583601341.

(16) Rossier, M. F. T Channels and Steroid Biosynthesis: In Search of a Link with Mitochondria. *Cell Calcium* **2006**, *40* (2), 155–164. https://doi.org/10.1016/j.ceca.2006.04.020.

(17) Cserép, C.; Pósfai, B.; Lénárt, N.; Fekete, R.; László, Z. I.; Lele, Z.; Orsolits, B.; Molnár, G.; Heindl, S.; Schwarcz, A. D.; Ujvári, K.; Környei, Z.; Tóth, K.; Szabadits, E.; Sperlágh, B.; Baranyi, M.; Csiba, L.; Hortobágyi, T.; Maglóczky, Z.; Martinecz, B.; Szabó, G.; Erdélyi, F.; Szipőcs, R.; Tamkun, M. M.; Gesierich, B.; Duering, M.; Katona, I.; Liesz, A.; Tamás, G.; Dénes, Á. Microglia Monitor and Protect Neuronal Function through Specialized Somatic Purinergic Junctions. *Science* **2020**. https://doi.org/10.1126/science.aax6752.

(18) Naffah de Souza Breda, C.; Davanzo, G. G.; Basso, P. J.; Saraiva Câmara, N. O.; Moraes-Vieira, P. M. M. Mitochondria as Central Hub of the Immune System. *Redox Biol.* **2019**, *26*, 101255. https://doi.org/10.1016/j.redox.2019.101255.

(19) Weinberg, S. E.; Sena, L. A.; Chandel, N. S. Mitochondria in the Regulation of Innate and Adaptive Immunity. *Immunity* **2015**, *42* (3), 406–417. https://doi.org/10.1016/j.immuni.2015.02.002.

(20) Bengsch, B.; Johnson, A. L.; Kurachi, M.; Odorizzi, P. M.; Pauken, K. E.; Attanasio, J.; Stelekati, E.; McLane, L. M.; Paley, M. A.; Delgoffe, G. M.; Wherry, E. J. Bioenergetic Insufficiencies Due to Metabolic Alterations Regulated by the Inhibitory Receptor PD-1 Are an Early Driver of CD8+ T Cell Exhaustion. *Immunity* **2016**, *45* (2), 358–373. https://doi.org/10.1016/j.immuni.2016.07.008.
(21) O'Neill, L. A. J.; Kishton, R. J.; Rathmell, J. A Guide to Immunometabolism for Immunologists. *Nat. Rev. Immunol.* **2016**, *16* (9), 553–565. https://doi.org/10.1038/nri.2016.70.
(22) Andersson, G. E.; Karlberg, O.; Canbäck, B.; Kurland, C. G. On the Origin of Mitochondria: A Genomics Perspective. *Philos. Trans. R. Soc. Lond. B. Biol. Sci.* **2003**, *358* (1429), 165–179. https://doi.org/10.1098/rstb.2002.1193.
(23) Chan, D. C. Mitochondria: Dynamic Organelles in Disease, Aging, and Development. *Cell* **2006**, *125* (7), 1241–1252. https://doi.org/10.1016/j.cell.2006.06.010.
(24) Anderson, S.; Bankier, A. T.; Barrell, B. G.; de Bruijn, M. H. L.; Coulson, A. R.; Drouin, J.; Eperon, I. C.; Nierlich, D. P.; Roe, B. A.; Sanger, F.; Schreier, P. H.; Smith, A. J. H.; Staden, R.; Young, I. G. Sequence and Organization of the Human Mitochondrial Genome. *Nature* **1981**, *290* (5806), 457–465. https://doi.org/10.1038/290457a0.
(25) Bibb, M. J.; Van Etten, R. A.; Wright, C. T.; Walberg, M. W.; Clayton, D. A. Sequence and Gene Organization of Mouse Mitochondrial DNA. *Cell* **1981**, *26* (2, Part 2), 167–180. https://doi.org/10.1016/0092-8674(81)90300-7.
(26) Wiesner, R. J.; Rüegg, J. C.; Morano, I. Counting Target Molecules by Exponential Polymerase Chain Reaction: Copy Number of Mitochondrial DNA in Rat Tissues. *Biochem. Biophys. Res. Commun.* **1992**, *183* (2), 553–559. https://doi.org/10.1016/0006-291X(92)90517-O.
(27) Falkenberg, M. Mitochondrial DNA Replication in Mammalian Cells: Overview of the Pathway. *Essays Biochem.* **2018**, *62* (3), 287–296. https://doi.org/10.1042/EBC20170100.
(28) Pfeiffer, R. F.; Wszolek, Z. K.; Ebadi, M. *Parkinson's Disease, Second Edition*; CRC Press, 2012.
(29) Seo, A. Y.; Joseph, A.-M.; Dutta, D.; Hwang, J. C. Y.; Aris, J. P.; Leeuwenburgh, C. New Insights into the Role of Mitochondria in Aging: Mitochondrial Dynamics and More. *J. Cell Sci.* **2010**, *123* (15), 2533–2542. https://doi.org/10.1242/jcs.070490.
(30) Sanchis-Gomar, F.; Garcia-Gimenez, J. L.; Gomez-Cabrera, M. C.; Pallardo, F. V. Mitochondrial Biogenesis in Health and Disease. Molecular and Therapeutic Approaches. *Curr. Pharm. Des.* **2014**, *20* (35), 5619–5633. https://doi.org/10.2174/1381612820666140306095106.
(31) Sutovsky, P.; Moreno, R. D.; Ramalho-Santos, J.; Dominko, T.; Simerly, C.; Schatten, G. Ubiquitin Tag for Sperm Mitochondria. *Nature* **1999**, *402* (6760), 371–372. https://doi.org/10.1038/46466.
(32) Luo, S.; Valencia, C. A.; Zhang, J.; Lee, N.-C.; Slone, J.; Gui, B.; Wang, X.; Li, Z.; Dell, S.; Brown, J.; Chen, S. M.; Chien, Y.-H.; Hwu, W.-L.; Fan, P.-C.; Wong, L.-J.; Atwal, P. S.; Huang, T. Biparental Inheritance of Mitochondrial DNA in Humans. *Proc. Natl. Acad. Sci.* **2018**, *115* (51), 13039–13044. https://doi.org/10.1073/pnas.1810946115.
(33) McWilliams, T. G.; Suomalainen, A. Mitochondrial DNA Can Be Inherited from Fathers, Not Just Mothers. *Nature* **2019**, *565* (7739), 296–297. https://doi.org/10.1038/d41586-019-00093-1.
(34) Kaplan, B. J.; Rucklidge, J. J.; Romijn, A.; McLeod, K. The Emerging Field of Nutritional Mental Health: Inflammation, the Microbiome, Oxidative Stress, and Mitochondrial Function. *Clin. Psychol. Sci.* **2015**, *3* (6), 964–980. https://doi.org/10.1177/2167702614555413.
(35) Gardner, A.; Boles, R. G. Is a "Mitochondrial Psychiatry" in the Future? A Review. *Curr. Psychiatry Rev. 1* (3), 255–271.
(36) Dorn, G. W.; Vega, R. B.; Kelly, D. P. Mitochondrial Biogenesis and Dynamics in the Developing and Diseased Heart. *Genes Dev.* **2015**, *29* (19), 1981–1991. https://doi.org/10.1101/gad.269894.115.
(37) Lesnefsky, E. J.; Moghaddas, S.; Tandler, B.; Kerner, J.; Hoppel, C. L. Mitochondrial Dysfunction in Cardiac Disease: Ischemia–Reperfusion, Aging, and Heart Failure. *J. Mol. Cell. Cardiol.* **2001**, *33* (6), 1065–1089. https://doi.org/10.1006/jmcc.2001.1378.

(38) Correia, S. C.; Perry, G.; Moreira, P. I. Mitochondrial Traffic Jams in Alzheimer's Disease - Pinpointing the Roadblocks. *Biochim. Biophys. Acta BBA - Mol. Basis Dis.* **2016**, *1862* (10), 1909–1917. https://doi.org/10.1016/j.bbadis.2016.07.010.
(39) Exner, N.; Lutz, A. K.; Haass, C.; Winklhofer, K. F. Mitochondrial Dysfunction in Parkinson's Disease: Molecular Mechanisms and Pathophysiological Consequences. *EMBO J.* **2012**, *31* (14), 3038–3062. https://doi.org/10.1038/emboj.2012.170.
(40) Martinez-Vicente, M. Neuronal Mitophagy in Neurodegenerative Diseases. *Front. Mol. Neurosci.* **2017**, *10*.
(41) Ceylan, M. F.; Sener, S.; Bayraktar, A. C.; Kavutcu, M. Changes in Oxidative Stress and Cellular Immunity Serum Markers in Attention-Deficit/Hyperactivity Disorder. *Psychiatry Clin. Neurosci.* **2012**, *66* (3), 220–226. https://doi.org/10.1111/j.1440-1819.2012.02330.x.
(42) Griffiths, K. K.; Levy, R. J. Evidence of Mitochondrial Dysfunction in Autism: Biochemical Links, Genetic-Based Associations, and Non-Energy-Related Mechanisms. *Oxid. Med. Cell. Longev.* **2017**, *2017*, e4314025. https://doi.org/10.1155/2017/4314025.
(43) Frye, R. E.; Rossignol, D. A. Mitochondrial Dysfunction Can Connect the Diverse Medical Symptoms Associated With Autism Spectrum Disorders. *Pediatr. Res.* **2011**, *69* (8), 41–47. https://doi.org/10.1203/PDR.0b013e318212f16b.
(44) Andreazza, A. C.; Kauer-Sant'Anna, M.; Frey, B. N.; Bond, D. J.; Kapczinski, F.; Young, L. T.; Yatham, L. N. Oxidative Stress Markers in Bipolar Disorder: A Meta-Analysis. *J. Affect. Disord.* **2008**, *111* (2), 135–144. https://doi.org/10.1016/j.jad.2008.04.013.
(45) Deheshi, S.; Pasqualotto, B. A.; Rintoul, G. L. Mitochondrial Trafficking in Neuropsychiatric Diseases. *Neurobiol. Dis.* **2013**, *51*, 66–71. https://doi.org/10.1016/j.nbd.2012.06.015.
(46) Dietrich-Muszalska, A.; Malinowska, J.; Olas, B.; Głowacki, R.; Bald, E.; Wachowicz, B.; Rabe-Jabłońska, J. The Oxidative Stress May Be Induced by the Elevated Homocysteine in Schizophrenic Patients. *Neurochem. Res.* **2012**, *37* (5), 1057–1062. https://doi.org/10.1007/s11064-012-0707-3.
(47) Boesch, P.; Weber-Lotfi, F.; Ibrahim, N.; Tarasenko, V.; Cosset, A.; Paulus, F.; Lightowlers, R. N.; Dietrich, A. DNA Repair in Organelles: Pathways, Organization, Regulation, Relevance in Disease and Aging. *Biochim. Biophys. Acta* **2011**, *1813* (1), 186–200. https://doi.org/10.1016/j.bbamcr.2010.10.002.
(48) Youle, R. J.; Bliek, A. M. van der. Mitochondrial Fission, Fusion, and Stress. *Science* **2012**. https://doi.org/10.1126/science.1219855.
(49) Lei, Y.; Wang, K.; Deng, L.; Chen, Y.; Nice, E. C.; Huang, C. Redox Regulation of Inflammation: Old Elements, a New Story. *Med. Res. Rev.* **2015**, *35* (2), 306–340. https://doi.org/10.1002/med.21330.
(50) Grimm, A.; Eckert, A. Brain Aging and Neurodegeneration: From a Mitochondrial Point of View. *J. Neurochem.* **2017**, *143* (4), 418–431. https://doi.org/10.1111/jnc.14037.
(51) Gehrke, N.; Mertens, C.; Zillinger, T.; Wenzel, J.; Bald, T.; Zahn, S.; Tüting, T.; Hartmann, G.; Barchet, W. Oxidative Damage of DNA Confers Resistance to Cytosolic Nuclease TREX1 Degradation and Potentiates STING-Dependent Immune Sensing. *Immunity* **2013**, *39* (3), 482–495. https://doi.org/10.1016/j.immuni.2013.08.004.
(52) Kim, J.; Gupta, R.; Blanco, L. P.; Yang, S.; Shteinfer-Kuzmine, A.; Wang, K.; Zhu, J.; Yoon, H. E.; Wang, X.; Kerkhofs, M.; Kang, H.; Brown, A. L.; Park, S.-J.; Xu, X.; Zandee van Rilland, E.; Kim, M. K.; Cohen, J. I.; Kaplan, M. J.; Shoshan-Barmatz, V.; Chung, J. H. VDAC Oligomers Form Mitochondrial Pores to Release MtDNA Fragments and Promote Lupus-like Disease. *Science* **2019**, *366* (6472), 1531–1536. https://doi.org/10.1126/science.aav4011.
(53) West, A. P.; Shadel, G. S. Mitochondrial DNA in Innate Immune Responses and Inflammatory Pathology. *Nat. Rev. Immunol.* **2017**, *17* (6), 363–375. https://doi.org/10.1038/nri.2017.21.
(54) Luca, F. D.; Shoenfeld, Y. The Microbiome in Autoimmune Diseases. *Clin. Exp. Immunol.* **2019**, *195* (1), 74–85. https://doi.org/10.1111/cei.13158.
(55) Passos, M. do C. F.; Moraes-Filho, J. P. Intestinal Microbiota in Digestive Diseases. *Arq. Gastroenterol.* **2017**, *54*, 255–262. https://doi.org/10.1590/S0004-2803.201700000-31.

(56) Quigley, E. M. M. Gut Bacteria in Health and Disease. *Gastroenterol. Hepatol.* **2013**, *9* (9), 560–569.
(57) Robles-Alonso, V.; Guarner, F. [Progress in the knowledge of the intestinal human microbiota]. *Nutr. Hosp.* **2013**, *28* (3), 553–557. https://doi.org/10.3305/nh.2013.28.3.6601.
(58) Jethwani, P.; Grover, K. Gut Microbiota in Health and Diseases – A Review. *Int. J. Curr. Microbiol. Appl. Sci.* **2019**, *8* (08), 1586–1599. https://doi.org/10.20546/ijcmas.2019.808.187.
(59) Gomaa, E. Z. Human Gut Microbiota/Microbiome in Health and Diseases: A Review. *Antonie Van Leeuwenhoek* **2020**, *113* (12), 2019–2040. https://doi.org/10.1007/s10482-020-01474-7.
(60) Arrieta, M.-C.; Stiemsma, L. T.; Amenyogbe, N.; Brown, E. M.; Finlay, B. The Intestinal Microbiome in Early Life: Health and Disease. *Front. Immunol.* **2014**, *5*.
(61) Dominguez-Bello, M. G.; Costello, E. K.; Contreras, M.; Magris, M.; Hidalgo, G.; Fierer, N.; Knight, R. Delivery Mode Shapes the Acquisition and Structure of the Initial Microbiota across Multiple Body Habitats in Newborns. *Proc. Natl. Acad. Sci.* **2010**, *107* (26), 11971–11975. https://doi.org/10.1073/pnas.1002601107.
(62) Nagpal, R.; Tsuji, H.; Takahashi, T.; Nomoto, K.; Kawashima, K.; Nagata, S.; Yamashiro, Y. Ontogenesis of the Gut Microbiota Composition in Healthy, Full-Term, Vaginally Born and Breast-Fed Infants over the First 3 Years of Life: A Quantitative Bird's-Eye View. *Front. Microbiol.* **2017**, *8*, 1388. https://doi.org/10.3389/fmicb.2017.01388.
(63) Belkaid, Y.; Hand, T. Role of the Microbiota in Immunity and Inflammation. *Cell* **2014**, *157* (1), 121–141. https://doi.org/10.1016/j.cell.2014.03.011.
(64) Schanche, M.; Avershina, E.; Dotterud, C.; Øien, T.; Storrø, O.; Johnsen, R.; Rudi, K. High-Resolution Analyses of Overlap in the Microbiota Between Mothers and Their Children. *Curr. Microbiol.* **2015**, *71* (2), 283–290. https://doi.org/10.1007/s00284-015-0843-5.
(65) Fouhy, F.; Watkins, C.; Hill, C. J.; O'Shea, C.-A.; Nagle, B.; Dempsey, E. M.; O'Toole, P. W.; Ross, R. P.; Ryan, C. A.; Stanton, C. Perinatal Factors Affect the Gut Microbiota up to Four Years after Birth. *Nat. Commun.* **2019**, *10* (1), 1517. https://doi.org/10.1038/s41467-019-09252-4.
(66) Hollister, E. B.; Riehle, K.; Luna, R. A.; Weidler, E. M.; Rubio-Gonzales, M.; Mistretta, T.-A.; Raza, S.; Doddapaneni, H. V.; Metcalf, G. A.; Muzny, D. M.; Gibbs, R. A.; Petrosino, J. F.; Shulman, R. J.; Versalovic, J. Structure and Function of the Healthy Pre-Adolescent Pediatric Gut Microbiome. *Microbiome* **2015**, *3*, 36. https://doi.org/10.1186/s40168-015-0101-x.
(67) Agans, R.; Rigsbee, L.; Kenche, H.; Michail, S.; Khamis, H. J.; Paliy, O. Distal Gut Microbiota of Adolescent Children Is Different from That of Adults. *FEMS Microbiol. Ecol.* **2011**, *77* (2), 404–412. https://doi.org/10.1111/j.1574-6941.2011.01120.x.
(68) Reyes, A.; Haynes, M.; Hanson, N.; Angly, F. E.; Heath, A. C.; Rohwer, F.; Gordon, J. I. Viruses in the Faecal Microbiota of Monozygotic Twins and Their Mothers. *Nature* **2010**, *466* (7304), 334–338. https://doi.org/10.1038/nature09199.
(69) Biagi, E.; Rampelli, S.; Turroni, S.; Quercia, S.; Candela, M.; Brigidi, P. The Gut Microbiota of Centenarians: Signatures of Longevity in the Gut Microbiota Profile. *Mech. Ageing Dev.* **2017**, *165* (Pt B), 180–184. https://doi.org/10.1016/j.mad.2016.12.013.
(70) Odamaki, T.; Kato, K.; Sugahara, H.; Hashikura, N.; Takahashi, S.; Xiao, J.-Z.; Abe, F.; Osawa, R. Age-Related Changes in Gut Microbiota Composition from Newborn to Centenarian: A Cross-Sectional Study. *BMC Microbiol.* **2016**, *16*, 90. https://doi.org/10.1186/s12866-016-0708-5.
(71) Schnorr, S. L.; Candela, M.; Rampelli, S.; Centanni, M.; Consolandi, C.; Basaglia, G.; Turroni, S.; Biagi, E.; Peano, C.; Severgnini, M.; Fiori, J.; Gotti, R.; De Bellis, G.; Luiselli, D.; Brigidi, P.; Mabulla, A.; Marlowe, F.; Henry, A. G.; Crittenden, A. N. Gut Microbiome of the Hadza Hunter-Gatherers. *Nat. Commun.* **2014**, *5* (1), 3654. https://doi.org/10.1038/ncomms4654.
(72) Martínez, I.; Stegen, J. C.; Maldonado-Gómez, M. X.; Eren, A. M.; Siba, P. M.; Greenhill, A. R.; Walter, J. The Gut Microbiota of Rural Papua New Guineans: Composition, Diversity Patterns, and Ecological Processes. *Cell Rep.* **2015**, *11* (4), 527–538. https://doi.org/10.1016/j.celrep.2015.03.049.

(73) Zhu, A.; Sunagawa, S.; Mende, D. R.; Bork, P. Inter-Individual Differences in the Gene Content of Human Gut Bacterial Species. *Genome Biol.* **2015**, *16* (1), 82. https://doi.org/10.1186/s13059-015-0646-9.
(74) Chen, C.; Huang, X.; Fang, S.; Yang, H.; He, M.; Zhao, Y.; Huang, L. Contribution of Host Genetics to the Variation of Microbial Composition of Cecum Lumen and Feces in Pigs. *Front. Microbiol.* **2018**, *9*, 2626. https://doi.org/10.3389/fmicb.2018.02626.
(75) Biedermann, L.; Zeitz, J.; Mwinyi, J.; Sutter-Minder, E.; Rehman, A.; Ott, S. J.; Steurer-Stey, C.; Frei, A.; Frei, P.; Scharl, M.; Loessner, M. J.; Vavricka, S. R.; Fried, M.; Schreiber, S.; Schuppler, M.; Rogler, G. Smoking Cessation Induces Profound Changes in the Composition of the Intestinal Microbiota in Humans. *PloS One* **2013**, *8* (3), e59260. https://doi.org/10.1371/journal.pone.0059260.
(76) Biedermann, L.; Brülisauer, K.; Zeitz, J.; Frei, P.; Scharl, M.; Vavricka, S. R.; Fried, M.; Loessner, M. J.; Rogler, G.; Schuppler, M. Smoking Cessation Alters Intestinal Microbiota: Insights from Quantitative Investigations on Human Fecal Samples Using FISH. *Inflamm. Bowel Dis.* **2014**, *20* (9), 1496–1501. https://doi.org/10.1097/MIB.0000000000000129.
(77) Clarke, S. F.; Murphy, E. F.; O'Sullivan, O.; Lucey, A. J.; Humphreys, M.; Hogan, A.; Hayes, P.; O'Reilly, M.; Jeffery, I. B.; Wood-Martin, R.; Kerins, D. M.; Quigley, E.; Ross, R. P.; O'Toole, P. W.; Molloy, M. G.; Falvey, E.; Shanahan, F.; Cotter, P. D. Exercise and Associated Dietary Extremes Impact on Gut Microbial Diversity. *Gut* **2014**, *63* (12), 1913–1920. https://doi.org/10.1136/gutjnl-2013-306541.
(78) Klingensmith, N. J.; Coopersmith, C. M. The Gut as the Motor of Multiple Organ Dysfunction in Critical Illness. *Crit. Care Clin.* **2016**, *32* (2), 203–212. https://doi.org/10.1016/j.ccc.2015.11.004.
(79) Ramnani, P.; Chitarrari, R.; Tuohy, K.; Grant, J.; Hotchkiss, S.; Philp, K.; Campbell, R.; Gill, C.; Rowland, I. In Vitro Fermentation and Prebiotic Potential of Novel Low Molecular Weight Polysaccharides Derived from Agar and Alginate Seaweeds. *Anaerobe* **2012**, *18* (1), 1–6. https://doi.org/10.1016/j.anaerobe.2011.08.003.
(80) Hasan, N.; Yang, H. Factors Affecting the Composition of the Gut Microbiota, and Its Modulation. *PeerJ* **2019**, *7*, e7502. https://doi.org/10.7717/peerj.7502.
(81) Dethlefsen, L.; Relman, D. A. Incomplete Recovery and Individualized Responses of the Human Distal Gut Microbiota to Repeated Antibiotic Perturbation. *Proc. Natl. Acad. Sci. U. S. A.* **2011**, *108 Suppl 1*, 4554–4561. https://doi.org/10.1073/pnas.1000087107.
(82) Hills, R. D.; Pontefract, B. A.; Mishcon, H. R.; Black, C. A.; Sutton, S. C.; Theberge, C. R. Gut Microbiome: Profound Implications for Diet and Disease. *Nutrients* **2019**, *11* (7), 1613. https://doi.org/10.3390/nu11071613.
(83) Forouhi, N. G.; Krauss, R. M.; Taubes, G.; Willett, W. Dietary Fat and Cardiometabolic Health: Evidence, Controversies, and Consensus for Guidance. *BMJ* **2018**, *361*, k2139. https://doi.org/10.1136/bmj.k2139.
(84) David, L. A.; Maurice, C. F.; Carmody, R. N.; Gootenberg, D. B.; Button, J. E.; Wolfe, B. E.; Ling, A. V.; Devlin, A. S.; Varma, Y.; Fischbach, M. A.; Biddinger, S. B.; Dutton, R. J.; Turnbaugh, P. J. Diet Rapidly and Reproducibly Alters the Human Gut Microbiome. *Nature* **2014**, *505* (7484), 559–563. https://doi.org/10.1038/nature12820.
(85) Ray, K. Gut Microbiota: Filling up on Fibre for a Healthy Gut. *Nat. Rev. Gastroenterol. Hepatol.* **2018**, *15* (2), 67. https://doi.org/10.1038/nrgastro.2018.2.
(86) Zhao, L.; Zhang, F.; Ding, X.; Wu, G.; Lam, Y. Y.; Wang, X.; Fu, H.; Xue, X.; Lu, C.; Ma, J.; Yu, L.; Xu, C.; Ren, Z.; Xu, Y.; Xu, S.; Shen, H.; Zhu, X.; Shi, Y.; Shen, Q.; Dong, W.; Liu, R.; Ling, Y.; Zeng, Y.; Wang, X.; Zhang, Q.; Wang, J.; Wang, L.; Wu, Y.; Zeng, B.; Wei, H.; Zhang, M.; Peng, Y.; Zhang, C. Gut Bacteria Selectively Promoted by Dietary Fibers Alleviate Type 2 Diabetes. *Science* **2018**, *359* (6380), 1151–1156. https://doi.org/10.1126/science.aao5774.
(87) Lin, L.; Zhang, J. Role of Intestinal Microbiota and Metabolites on Gut Homeostasis and Human Diseases. *BMC Immunol.* **2017**, *18* (1), 2. https://doi.org/10.1186/s12865-016-0187-3.
(88) Thursby, E.; Juge, N. Introduction to the Human Gut Microbiota. *Biochem. J.* **2017**, *474* (11), 1823–1836. https://doi.org/10.1042/BCJ20160510.

(89) Bron, P. A.; Kleerebezem, M.; Brummer, R.-J.; Cani, P. D.; Mercenier, A.; MacDonald, T. T.; Garcia-Ródenas, C. L.; Wells, J. M. Can Probiotics Modulate Human Disease by Impacting Intestinal Barrier Function? *Br. J. Nutr.* **2017**, *117* (1), 93–107. https://doi.org/10.1017/S0007114516004037.
(90) Singh, R. K.; Chang, H.-W.; Yan, D.; Lee, K. M.; Ucmak, D.; Wong, K.; Abrouk, M.; Farahnik, B.; Nakamura, M.; Zhu, T. H.; Bhutani, T.; Liao, W. Influence of Diet on the Gut Microbiome and Implications for Human Health. *J. Transl. Med.* **2017**, *15* (1), 73. https://doi.org/10.1186/s12967-017-1175-y.
(91) Louis, P.; Flint, H. J. Formation of Propionate and Butyrate by the Human Colonic Microbiota. *Environ. Microbiol.* **2017**, *19* (1), 29–41. https://doi.org/10.1111/1462-2920.13589.
(92) Allen, J. M.; Mailing, L. J.; Niemiro, G. M.; Moore, R.; Cook, M. D.; White, B. A.; Holscher, H. D.; Woods, J. A. Exercise Alters Gut Microbiota Composition and Function in Lean and Obese Humans. *Med. Sci. Sports Exerc.* **2018**, *50* (4), 747–757. https://doi.org/10.1249/MSS.0000000000001495.
(93) Trompette, A.; Gollwitzer, E. S.; Yadava, K.; Sichelstiel, A. K.; Sprenger, N.; Ngom-Bru, C.; Blanchard, C.; Junt, T.; Nicod, L. P.; Harris, N. L.; Marsland, B. J. Gut Microbiota Metabolism of Dietary Fiber Influences Allergic Airway Disease and Hematopoiesis. *Nat. Med.* **2014**, *20* (2), 159–166. https://doi.org/10.1038/nm.3444.
(94) Sampson, T. R.; Mazmanian, S. K. Control of Brain Development, Function, and Behavior by the Microbiome. *Cell Host Microbe* **2015**, *17* (5), 565–576. https://doi.org/10.1016/j.chom.2015.04.011.
(95) Morrison, D. J.; Preston, T. Formation of Short Chain Fatty Acids by the Gut Microbiota and Their Impact on Human Metabolism. *Gut Microbes* **2016**, *7* (3), 189–200. https://doi.org/10.1080/19490976.2015.1134082.
(96) Bindels, L. B.; Porporato, P.; Dewulf, E. M.; Verrax, J.; Neyrinck, A. M.; Martin, J. C.; Scott, K. P.; Buc Calderon, P.; Feron, O.; Muccioli, G. G.; Sonveaux, P.; Cani, P. D.; Delzenne, N. M. Gut Microbiota-Derived Propionate Reduces Cancer Cell Proliferation in the Liver. *Br. J. Cancer* **2012**, *107* (8), 1337–1344. https://doi.org/10.1038/bjc.2012.409.
(97) Mohajeri, M. H.; La Fata, G.; Steinert, R. E.; Weber, P. Relationship between the Gut Microbiome and Brain Function. *Nutr. Rev.* **2018**, *76* (7), 481–496. https://doi.org/10.1093/nutrit/nuy009.
(98) Wei, W.; Sun, W.; Yu, S.; Yang, Y.; Ai, L. Butyrate Production from High-Fiber Diet Protects against Lymphoma Tumor. *Leuk. Lymphoma* **2016**, *57* (10), 2401–2408. https://doi.org/10.3109/10428194.2016.1144879.
(99) Perry, R. J.; Peng, L.; Barry, N. A.; Cline, G. W.; Zhang, D.; Cardone, R. L.; Petersen, K. F.; Kibbey, R. G.; Goodman, A. L.; Shulman, G. I. Acetate Mediates a Microbiome-Brain-β-Cell Axis to Promote Metabolic Syndrome. *Nature* **2016**, *534* (7606), 213–217. https://doi.org/10.1038/nature18309.
(100) LeBlanc, J. G.; Milani, C.; de Giori, G. S.; Sesma, F.; van Sinderen, D.; Ventura, M. Bacteria as Vitamin Suppliers to Their Host: A Gut Microbiota Perspective. *Curr. Opin. Biotechnol.* **2013**, *24* (2), 160–168. https://doi.org/10.1016/j.copbio.2012.08.005.
(101) Abdollahi-Roodsaz, S.; Abramson, S. B.; Scher, J. U. The Metabolic Role of the Gut Microbiota in Health and Rheumatic Disease: Mechanisms and Interventions. *Nat. Rev. Rheumatol.* **2016**, *12* (8), 446–455. https://doi.org/10.1038/nrrheum.2016.68.
(102) Forsythe, P.; Sudo, N.; Dinan, T.; Taylor, V. H.; Bienenstock, J. Mood and Gut Feelings. *Brain. Behav. Immun.* **2010**, *24* (1), 9–16. https://doi.org/10.1016/j.bbi.2009.05.058.
(103) Rhee, S. H.; Pothoulakis, C.; Mayer, E. A. Principles and Clinical Implications of the Brain-Gut-Enteric Microbiota Axis. *Nat. Rev. Gastroenterol. Hepatol.* **2009**, *6* (5), 306–314. https://doi.org/10.1038/nrgastro.2009.35.
(104) Chen, X.; Eslamfam, S.; Fang, L.; Qiao, S.; Ma, X. Maintenance of Gastrointestinal Glucose Homeostasis by the Gut-Brain Axis. *Curr. Protein Pept. Sci.* **2017**, *18* (6), 541–547. https://doi.org/10.2174/1389203717666160627083604.

(105) Soty, M.; Gautier-Stein, A.; Rajas, F.; Mithieux, G. Gut-Brain Glucose Signaling in Energy Homeostasis. *Cell Metab.* **2017**, *25* (6), 1231–1242. https://doi.org/10.1016/j.cmet.2017.04.032.
(106) Mills, S.; Stanton, C.; Lane, J. A.; Smith, G. J.; Ross, R. P. Precision Nutrition and the Microbiome, Part I: Current State of the Science. *Nutrients* **2019**, *11* (4), E923. https://doi.org/10.3390/nu11040923.
(107) Karczewski, J.; Troost, F. J.; Konings, I.; Dekker, J.; Kleerebezem, M.; Brummer, R.-J. M.; Wells, J. M. Regulation of Human Epithelial Tight Junction Proteins by Lactobacillus Plantarum in Vivo and Protective Effects on the Epithelial Barrier. *Am. J. Physiol. Gastrointest. Liver Physiol.* **2010**, *298* (6), G851-859. https://doi.org/10.1152/ajpgi.00327.2009.
(108) Koren, O.; Goodrich, J. K.; Cullender, T. C.; Spor, A.; Laitinen, K.; Kling Bäckhed, H.; Gonzalez, A.; Werner, J. J.; Angenent, L. T.; Knight, R.; Bäckhed, F.; Isolauri, E.; Salminen, S.; Ley, R. E. Host Remodeling of the Gut Microbiome and Metabolic Changes during Pregnancy. *Cell* **2012**, *150* (3), 470–480. https://doi.org/10.1016/j.cell.2012.07.008.
(109) PrabhuDas, M.; Adkins, B.; Gans, H.; King, C.; Levy, O.; Ramilo, O.; Siegrist, C.-A. Challenges in Infant Immunity: Implications for Responses to Infection and Vaccines. *Nat. Immunol.* **2011**, *12* (3), 189–194. https://doi.org/10.1038/ni0311-189.
(110) Siegrist, C. A. Neonatal and Early Life Vaccinology. *Vaccine* **2001**, *19* (25–26), 3331–3346. https://doi.org/10.1016/s0264-410x(01)00028-7.
(111) An, D.; Oh, S. F.; Olszak, T.; Neves, J. F.; Avci, F. Y.; Erturk-Hasdemir, D.; Lu, X.; Zeissig, S.; Blumberg, R. S.; Kasper, D. L. Sphingolipids from a Symbiotic Microbe Regulate Homeostasis of Host Intestinal Natural Killer T Cells. *Cell* **2014**, *156* (1), 123–133. https://doi.org/10.1016/j.cell.2013.11.042.
(112) Olszak, T.; An, D.; Zeissig, S.; Vera, M. P.; Richter, J.; Franke, A.; Glickman, J. N.; Siebert, R.; Baron, R. M.; Kasper, D. L.; Blumberg, R. S. Microbial Exposure During Early Life Has Persistent Effects on Natural Killer T Cell Function. *Science* **2012**. https://doi.org/10.1126/science.1219328.
(113) Valentini, M.; Piermattei, A.; Di Sante, G.; Migliara, G.; Delogu, G.; Ria, F. Immunomodulation by Gut Microbiota: Role of Toll-Like Receptor Expressed by T Cells. *J. Immunol. Res.* **2014**, *2014*, 586939. https://doi.org/10.1155/2014/586939.
(114) Iebba, V.; Totino, V.; Gagliardi, A.; Santangelo, F.; Cacciotti, F.; Trancassini, M.; Mancini, C.; Cicerone, C.; Corazziari, E.; Pantanella, F.; Schippa, S. Eubiosis and Dysbiosis: The Two Sides of the Microbiota. *New Microbiol.* **2016**, *39* (1), 1–12.
(115) Guven-Maiorov, E.; Tsai, C.-J.; Ma, B.; Nussinov, R. Prediction of Host-Pathogen Interactions for Helicobacter Pylori by Interface Mimicry and Implications to Gastric Cancer. *J. Mol. Biol.* **2017**, *429* (24), 3925–3941. https://doi.org/10.1016/j.jmb.2017.10.023.
(116) Kollmann, T. R.; Levy, O.; Montgomery, R. R.; Goriely, S. Innate Immune Function by Toll-like Receptors: Distinct Responses in Newborns and the Elderly. *Immunity* **2012**, *37* (5), 771–783. https://doi.org/10.1016/j.immuni.2012.10.014.
(117) Belkaid, Y.; Segre, J. A. Dialogue between Skin Microbiota and Immunity. *Science* **2014**. https://doi.org/10.1126/science.1260144.
(118) Ghoshal, U. C.; Shukla, R.; Ghoshal, U.; Gwee, K.-A.; Ng, S. C.; Quigley, E. M. M. The Gut Microbiota and Irritable Bowel Syndrome: Friend or Foe? *Int. J. Inflamm.* **2012**, *2012*, 151085. https://doi.org/10.1155/2012/151085.
(119) Lane, E. R.; Zisman, T. L.; Suskind, D. L. The Microbiota in Inflammatory Bowel Disease: Current and Therapeutic Insights. *J. Inflamm. Res.* **2017**, *10*, 63–73. https://doi.org/10.2147/JIR.S116088.
(120) Nishino, K.; Nishida, A.; Inoue, R.; Kawada, Y.; Ohno, M.; Sakai, S.; Inatomi, O.; Bamba, S.; Sugimoto, M.; Kawahara, M.; Naito, Y.; Andoh, A. Analysis of Endoscopic Brush Samples Identified Mucosa-Associated Dysbiosis in Inflammatory Bowel Disease. *J. Gastroenterol.* **2018**, *53* (1), 95–106. https://doi.org/10.1007/s00535-017-1384-4.

(121) Muscogiuri, G.; Balercia, G.; Barrea, L.; Cignarelli, A.; Giorgino, F.; Holst, J. J.; Laudisio, D.; Orio, F.; Tirabassi, G.; Colao, A. Gut: A Key Player in the Pathogenesis of Type 2 Diabetes? *Crit. Rev. Food Sci. Nutr.* **2018**, *58* (8), 1294–1309. https://doi.org/10.1080/10408398.2016.1252712.
(122) Qin, J.; Li, Y.; Cai, Z.; Li, S.; Zhu, J.; Zhang, F.; Liang, S.; Zhang, W.; Guan, Y.; Shen, D.; Peng, Y.; Zhang, D.; Jie, Z.; Wu, W.; Qin, Y.; Xue, W.; Li, J.; Han, L.; Lu, D.; Wu, P.; Dai, Y.; Sun, X.; Li, Z.; Tang, A.; Zhong, S.; Li, X.; Chen, W.; Xu, R.; Wang, M.; Feng, Q.; Gong, M.; Yu, J.; Zhang, Y.; Zhang, M.; Hansen, T.; Sanchez, G.; Raes, J.; Falony, G.; Okuda, S.; Almeida, M.; LeChatelier, E.; Renault, P.; Pons, N.; Batto, J.-M.; Zhang, Z.; Chen, H.; Yang, R.; Zheng, W.; Li, S.; Yang, H.; Wang, J.; Ehrlich, S. D.; Nielsen, R.; Pedersen, O.; Kristiansen, K.; Wang, J. A Metagenome-Wide Association Study of Gut Microbiota in Type 2 Diabetes. *Nature* **2012**, *490* (7418), 55–60. https://doi.org/10.1038/nature11450.
(123) Karlsson, F.; Tremaroli, V.; Nielsen, J.; Bäckhed, F. Assessing the Human Gut Microbiota in Metabolic Diseases. *Diabetes* **2013**, *62* (10), 3341–3349. https://doi.org/10.2337/db13-0844.
(124) Jie, Z.; Xia, H.; Zhong, S.-L.; Feng, Q.; Li, S.; Liang, S.; Zhong, H.; Liu, Z.; Gao, Y.; Zhao, H.; Zhang, D.; Su, Z.; Fang, Z.; Lan, Z.; Li, J.; Xiao, L.; Li, J.; Li, R.; Li, X.; Li, F.; Ren, H.; Huang, Y.; Peng, Y.; Li, G.; Wen, B.; Dong, B.; Chen, J.-Y.; Geng, Q.-S.; Zhang, Z.-W.; Yang, H.; Wang, J.; Wang, J.; Zhang, X.; Madsen, L.; Brix, S.; Ning, G.; Xu, X.; Liu, X.; Hou, Y.; Jia, H.; He, K.; Kristiansen, K. The Gut Microbiome in Atherosclerotic Cardiovascular Disease. *Nat. Commun.* **2017**, *8* (1), 845. https://doi.org/10.1038/s41467-017-00900-1.
(125) Stokholm, J.; Blaser, M. J.; Thorsen, J.; Rasmussen, M. A.; Waage, J.; Vinding, R. K.; Schoos, A.-M. M.; Kunøe, A.; Fink, N. R.; Chawes, B. L.; Bønnelykke, K.; Brejnrod, A. D.; Mortensen, M. S.; Al-Soud, W. A.; Sørensen, S. J.; Bisgaard, H. Maturation of the Gut Microbiome and Risk of Asthma in Childhood. *Nat. Commun.* **2018**, *9* (1), 141. https://doi.org/10.1038/s41467-017-02573-2.
(126) Vuitton, D. A.; Dalphin, J.-C. From Farming to Engineering: The Microbiota and Allergic Diseases. *Engineering* **2017**, *3* (1), 98–109. https://doi.org/10.1016/J.ENG.2017.01.019.
(127) Bunyavanich, S.; Shen, N.; Grishin, A.; Wood, R.; Burks, W.; Dawson, P.; Jones, S. M.; Leung, D. Y. M.; Sampson, H.; Sicherer, S.; Clemente, J. C. Early-Life Gut Microbiome Composition and Milk Allergy Resolution. *J. Allergy Clin. Immunol.* **2016**, *138* (4), 1122–1130. https://doi.org/10.1016/j.jaci.2016.03.041.
(128) Sanford, J. A.; Gallo, R. L. Functions of the Skin Microbiota in Health and Disease. *Semin. Immunol.* **2013**, *25* (5), 370–377. https://doi.org/10.1016/j.smim.2013.09.005.
(129) Rosenfeld, C. S. Microbiome Disturbances and Autism Spectrum Disorders. *Drug Metab. Dispos. Biol. Fate Chem.* **2015**, *43* (10), 1557–1571. https://doi.org/10.1124/dmd.115.063826.
(130) Leung, C.; Rivera, L.; Furness, J. B.; Angus, P. W. The Role of the Gut Microbiota in NAFLD. *Nat. Rev. Gastroenterol. Hepatol.* **2016**, *13* (7), 412–425. https://doi.org/10.1038/nrgastro.2016.85.
(131) Andoh, A.; Nishida, A.; Takahashi, K.; Inatomi, O.; Imaeda, H.; Bamba, S.; Kito, K.; Sugimoto, M.; Kobayashi, T. Comparison of the Gut Microbial Community between Obese and Lean Peoples Using 16S Gene Sequencing in a Japanese Population. *J. Clin. Biochem. Nutr.* **2016**, *59* (1), 65–70. https://doi.org/10.3164/jcbn.15-152.
(132) Estruch; E, R.; J, S.-S.; Mi, C.; D, C.; F, A.; E, G.-G.; V, R.-G.; M, F.; J, L.; Rm, L.-R.; L, S.-M.; X, P.; J, B.; Ma, M.; Jv, S.; Ja, M.; M, F.; A, G.; Ma, H.; Ma, M.-G. Primary Prevention of Cardiovascular Disease with a Mediterranean Diet Supplemented with Extra-Virgin Olive Oil or Nuts. *N. Engl. J. Med.* **2018**, *378* (25). https://doi.org/10.1056/NEJMoa1800389.
(133) Conlan, S.; Mijares, L. A.; NISC Comparative Sequencing Program; Becker, J.; Blakesley, R. W.; Bouffard, G. G.; Brooks, S.; Coleman, H.; Gupta, J.; Gurson, N.; Park, M.; Schmidt, B.; Thomas, P. J.; Otto, M.; Kong, H. H.; Murray, P. R.; Segre, J. A. Staphylococcus Epidermidis Pan-Genome Sequence Analysis Reveals Diversity of Skin Commensal and Hospital Infection-Associated Isolates. *Genome Biol.* **2012**, *13* (7), R64. https://doi.org/10.1186/gb-2012-13-7-r64.
(134) Iwase, T.; Uehara, Y.; Shinji, H.; Tajima, A.; Seo, H.; Takada, K.; Agata, T.; Mizunoe, Y. Staphylococcus Epidermidis Esp Inhibits Staphylococcus Aureus Biofilm Formation and Nasal Colonization. *Nature* **2010**, *465* (7296), 346–349. https://doi.org/10.1038/nature09074.

(135) Diep, B. A.; Gill, S. R.; Chang, R. F.; Phan, T. H.; Chen, J. H.; Davidson, M. G.; Lin, F.; Lin, J.; Carleton, H. A.; Mongodin, E. F.; Sensabaugh, G. F.; Perdreau-Remington, F. Complete Genome Sequence of USA300, an Epidemic Clone of Community-Acquired Meticillin-Resistant Staphylococcus Aureus. *Lancet Lond. Engl.* **2006**, *367* (9512), 731–739. https://doi.org/10.1016/S0140-6736(06)68231-7.
(136) Lai, Y.; Di Nardo, A.; Nakatsuji, T.; Leichtle, A.; Yang, Y.; Cogen, A. L.; Wu, Z.-R.; Hooper, L. V.; Schmidt, R. R.; von Aulock, S.; Radek, K. A.; Huang, C.-M.; Ryan, A. F.; Gallo, R. L. Commensal Bacteria Regulate Toll-like Receptor 3-Dependent Inflammation after Skin Injury. *Nat. Med.* **2009**, *15* (12), 1377–1382. https://doi.org/10.1038/nm.2062.
(137) Harte, A. L.; Varma, M. C.; Tripathi, G.; McGee, K. C.; Al-Daghri, N. M.; Al-Attas, O. S.; Sabico, S.; O'Hare, J. P.; Ceriello, A.; Saravanan, P.; Kumar, S.; McTernan, P. G. High Fat Intake Leads to Acute Postprandial Exposure to Circulating Endotoxin in Type 2 Diabetic Subjects. *Diabetes Care* **2012**, *35* (2), 375–382. https://doi.org/10.2337/dc11-1593.
(138) Gallo, R. L.; Hooper, L. V. Epithelial Antimicrobial Defence of the Skin and Intestine. *Nat. Rev. Immunol.* **2012**, *12* (7), 503–516. https://doi.org/10.1038/nri3228.
(139) Naik, S.; Bouladoux, N.; Wilhelm, C.; Molloy, M. J.; Salcedo, R.; Kastenmuller, W.; Deming, C.; Quinones, M.; Koo, L.; Conlan, S.; Spencer, S.; Hall, J. A.; Dzutsev, A.; Kong, H.; Campbell, D. J.; Trinchieri, G.; Segre, J. A.; Belkaid, Y. Compartmentalized Control of Skin Immunity by Resident Commensals. *Science* **2012**, *337* (6098), 1115–1119. https://doi.org/10.1126/science.1225152.
(140) Clemente, J. C.; Ursell, L. K.; Parfrey, L. W.; Knight, R. The Impact of the Gut Microbiota on Human Health: An Integrative View. *Cell* **2012**, *148* (6), 1258–1270. https://doi.org/10.1016/j.cell.2012.01.035.
(141) Sims, J. E.; Smith, D. E. The IL-1 Family: Regulators of Immunity. *Nat. Rev. Immunol.* **2010**, *10* (2), 89–102. https://doi.org/10.1038/nri2691.
(142) Zheng, Y.; Danilenko, D. M.; Valdez, P.; Kasman, I.; Eastham-Anderson, J.; Wu, J.; Ouyang, W. Interleukin-22, a T(H)17 Cytokine, Mediates IL-23-Induced Dermal Inflammation and Acanthosis. *Nature* **2007**, *445* (7128), 648–651. https://doi.org/10.1038/nature05505.
(143) Lai, Y.; Li, D.; Li, C.; Muehleisen, B.; Radek, K. A.; Park, H. J.; Jiang, Z.; Li, Z.; Lei, H.; Quan, Y.; Zhang, T.; Wu, Y.; Kotol, P.; Morizane, S.; Hata, T. R.; Iwatsuki, K.; Tang, C.; Gallo, R. L. The Antimicrobial Protein REG3A Regulates Keratinocyte Proliferation and Differentiation after Skin Injury. *Immunity* **2012**, *37* (1), 74–84. https://doi.org/10.1016/j.immuni.2012.04.010.
(144) Gaykema, R. P. A.; Goehler, L. E.; Lyte, M. Brain Response to Cecal Infection with Campylobacter Jejuni: Analysis with Fos Immunohistochemistry. *Brain. Behav. Immun.* **2004**, *18* (3), 238–245. https://doi.org/10.1016/j.bbi.2003.08.002.
(145) Schwarcz, R.; Bruno, J. P.; Muchowski, P. J.; Wu, H.-Q. Kynurenines in the Mammalian Brain: When Physiology Meets Pathology. *Nat. Rev. Neurosci.* **2012**, *13* (7), 465–477. https://doi.org/10.1038/nrn3257.
(146) Jiang, C.; Li, G.; Huang, P.; Liu, Z.; Zhao, B. The Gut Microbiota and Alzheimer's Disease. *J. Alzheimers Dis. JAD* **2017**, *58* (1), 1–15. https://doi.org/10.3233/JAD-161141.
(147) Lv, G.; Cheng, N.; Wang, H. The Gut Microbiota, Tumorigenesis, and Liver Diseases. *Engineering* **2017**, *3* (1), 110–114. https://doi.org/10.1016/J.ENG.2017.01.017.
(148) Baliou, S.; Adamaki, M.; Spandidos, D. A.; Kyriakopoulos, A. M.; Christodoulou, I.; Zoumpourlis, V. The Microbiome, Its Molecular Mechanisms and Its Potential as a Therapeutic Strategy against Colorectal Carcinogenesis (Review). *World Acad. Sci. J.* **2019**, *1* (1), 3–19. https://doi.org/10.3892/wasj.2018.6.
(149) Grivennikov, S. I.; Wang, K.; Mucida, D.; Stewart, C. A.; Schnabl, B.; Jauch, D.; Taniguchi, K.; Yu, G.-Y.; Osterreicher, C. H.; Hung, K. E.; Datz, C.; Feng, Y.; Fearon, E. R.; Oukka, M.; Tessarollo, L.; Coppola, V.; Yarovinsky, F.; Cheroutre, H.; Eckmann, L.; Trinchieri, G.; Karin, M. Adenoma-Linked Barrier Defects and Microbial Products Drive IL-23/IL-17-Mediated Tumour Growth. *Nature* **2012**, *491* (7423), 254–258. https://doi.org/10.1038/nature11465.
(150) Otto, M. Staphylococcus Epidermidis--the "accidental" Pathogen. *Nat. Rev. Microbiol.* **2009**, *7* (8), 555–567. https://doi.org/10.1038/nrmicro2182.

(151) Raman, M.; Ambalam, P.; Kondepudi, K. K.; Pithva, S.; Kothari, C.; Patel, A. T.; Purama, R. K.; Dave, J. M.; Vyas, B. R. M. Potential of Probiotics, Prebiotics and Synbiotics for Management of Colorectal Cancer. *Gut Microbes* **2013**, *4* (3), 181–192. https://doi.org/10.4161/gmic.23919.
(152) Kristensen, N. B.; Bryrup, T.; Allin, K. H.; Nielsen, T.; Hansen, T. H.; Pedersen, O. Alterations in Fecal Microbiota Composition by Probiotic Supplementation in Healthy Adults: A Systematic Review of Randomized Controlled Trials. *Genome Med.* **2016**, *8* (1), 52. https://doi.org/10.1186/s13073-016-0300-5.
(153) La Fata, G.; Weber, P.; Mohajeri, M. H. Probiotics and the Gut Immune System: Indirect Regulation. *Probiotics Antimicrob. Proteins* **2018**, *10* (1), 11–21. https://doi.org/10.1007/s12602-017-9322-6.
(154) Ambalam, P.; Raman, M.; Purama, R. K.; Doble, M. Probiotics, Prebiotics and Colorectal Cancer Prevention. *Best Pract. Res. Clin. Gastroenterol.* **2016**, *30* (1), 119–131. https://doi.org/10.1016/j.bpg.2016.02.009.
(155) Ikram, S.; Hassan, N.; Raffat, M. A.; Mirza, S.; Akram, Z. Systematic Review and Meta-Analysis of Double-Blind, Placebo-Controlled, Randomized Clinical Trials Using Probiotics in Chronic Periodontitis. *J. Investig. Clin. Dent.* **2018**, *9* (3), e12338. https://doi.org/10.1111/jicd.12338.
(156) Hendijani, F.; Akbari, V. Probiotic Supplementation for Management of Cardiovascular Risk Factors in Adults with Type II Diabetes: A Systematic Review and Meta-Analysis. *Clin. Nutr.* **2018**. https://doi.org/10.1016/j.clnu.2017.02.015.
(157) McKean, J.; Naug, H.; Nikbakht, E.; Amiet, B.; Colson, N. Probiotics and Subclinical Psychological Symptoms in Healthy Participants: A Systematic Review and Meta-Analysis. *J. Altern. Complement. Med. N. Y. N* **2017**, *23* (4), 249–258. https://doi.org/10.1089/acm.2016.0023.
(158) Ohland, C. L.; Kish, L.; Bell, H.; Thiesen, A.; Hotte, N.; Pankiv, E.; Madsen, K. L. Effects of Lactobacillus Helveticus on Murine Behavior Are Dependent on Diet and Genotype and Correlate with Alterations in the Gut Microbiome. *Psychoneuroendocrinology* **2013**, *38* (9), 1738–1747. https://doi.org/10.1016/j.psyneuen.2013.02.008.
(159) Hsieh, M. H. The Microbiome and Probiotics in Childhood. *Semin. Reprod. Med.* **2014**, *32* (1), 23–27. https://doi.org/10.1055/s-0033-1361819.
(160) Flint, H. J.; Duncan, S. H.; Louis, P. The Impact of Nutrition on Intestinal Bacterial Communities. *Curr. Opin. Microbiol.* **2017**, *38*, 59–65. https://doi.org/10.1016/j.mib.2017.04.005.
(161) Simpson, H. L.; Campbell, B. J. Review Article: Dietary Fibre–Microbiota Interactions. *Aliment. Pharmacol. Ther.* **2015**, *42* (2), 158–179. https://doi.org/10.1111/apt.13248.
(162) Khoruts, A.; Sadowsky, M. J. Understanding the Mechanisms of Faecal Microbiota Transplantation. *Nat. Rev. Gastroenterol. Hepatol.* **2016**, *13* (9), 508–516. https://doi.org/10.1038/nrgastro.2016.98.
(163) Holvoet, T.; Joossens, M.; Wang, J.; Boelens, J.; Verhasselt, B.; Laukens, D.; van Vlierberghe, H.; Hindryckx, P.; De Vos, M.; De Looze, D.; Raes, J. Assessment of Faecal Microbial Transfer in Irritable Bowel Syndrome with Severe Bloating. *Gut* **2017**, *66* (5), 980–982. https://doi.org/10.1136/gutjnl-2016-312513.
(164) Johnsen, P. H.; Hilpüsch, F.; Cavanagh, J. P.; Leikanger, I. S.; Kolstad, C.; Valle, P. C.; Goll, R. Faecal Microbiota Transplantation versus Placebo for Moderate-to-Severe Irritable Bowel Syndrome: A Double-Blind, Randomised, Placebo-Controlled, Parallel-Group, Single-Centre Trial. *Lancet Gastroenterol. Hepatol.* **2018**, *3* (1), 17–24. https://doi.org/10.1016/S2468-1253(17)30338-2.
(165) Aroniadis, O. C.; Brandt, L. J.; Oneto, C.; Feuerstadt, P.; Sherman, A.; Wolkoff, A. W.; Kassam, Z.; Sadovsky, R. G.; Elliott, R. J.; Budree, S.; Kim, M.; Keller, M. J. Faecal Microbiota Transplantation for Diarrhoea-Predominant Irritable Bowel Syndrome: A Double-Blind, Randomised, Placebo-Controlled Trial. *Lancet Gastroenterol. Hepatol.* **2019**, *4* (9), 675–685. https://doi.org/10.1016/S2468-1253(19)30198-0.
(166) van Nood, E.; Vrieze, A.; Nieuwdorp, M.; Fuentes, S.; Zoetendal, E. G.; de Vos, W. M.; Visser, C. E.; Kuijper, E. J.; Bartelsman, J. F. W. M.; Tijssen, J. G. P.; Speelman, P.; Dijkgraaf, M. G. W.;

Keller, J. J. Duodenal Infusion of Donor Feces for Recurrent Clostridium Difficile. *N. Engl. J. Med.* **2013**, *368* (5), 407–415. https://doi.org/10.1056/NEJMoa1205037.
(167) Moayyedi, P.; Surette, M. G.; Kim, P. T.; Libertucci, J.; Wolfe, M.; Onischi, C.; Armstrong, D.; Marshall, J. K.; Kassam, Z.; Reinisch, W.; Lee, C. H. Fecal Microbiota Transplantation Induces Remission in Patients With Active Ulcerative Colitis in a Randomized Controlled Trial. *Gastroenterology* **2015**, *149* (1), 102-109.e6. https://doi.org/10.1053/j.gastro.2015.04.001.
(168) Hansen, J. J.; Sartor, R. B. Therapeutic Manipulation of the Microbiome in IBD: Current Results and Future Approaches. *Curr. Treat. Options Gastroenterol.* **2015**, *13* (1), 105–120. https://doi.org/10.1007/s11938-014-0042-7.
(169) Kump, P. K.; Gröchenig, H.-P.; Lackner, S.; Trajanoski, S.; Reicht, G.; Hoffmann, K. M.; Deutschmann, A.; Wenzl, H. H.; Petritsch, W.; Krejs, G. J.; Gorkiewicz, G.; Högenauer, C. Alteration of Intestinal Dysbiosis by Fecal Microbiota Transplantation Does Not Induce Remission in Patients with Chronic Active Ulcerative Colitis. *Inflamm. Bowel Dis.* **2013**, *19* (10), 2155–2165. https://doi.org/10.1097/MIB.0b013e31829ea325.
(170) Harsch, I. A.; Konturek, P. C. Adhesion Ileus after Fecal Microbiota Transplantation in Long-Standing Radiation Colitis. *Case Rep. Gastrointest. Med.* **2019**, *2019*, 2543808. https://doi.org/10.1155/2019/2543808.
(171) Koren, O. Moody Microbes: Do Microbes Influence Our Behavior? *Eur. Neuropsychopharmacol.* **2017**, *27*, S478. https://doi.org/10.1016/j.euroneuro.2016.09.561.
(172) Hashimoto, T.; Perlot, T.; Rehman, A.; Trichereau, J.; Ishiguro, H.; Paolino, M.; Sigl, V.; Hanada, T.; Hanada, R.; Lipinski, S.; Wild, B.; Camargo, S. M. R.; Singer, D.; Richter, A.; Kuba, K.; Fukamizu, A.; Schreiber, S.; Clevers, H.; Verrey, F.; Rosenstiel, P.; Penninger, J. M. ACE2 Links Amino Acid Malnutrition to Microbial Ecology and Intestinal Inflammation. *Nature* **2012**, *487* (7408), 477–481. https://doi.org/10.1038/nature11228.
(173) Turnbaugh, P. J.; Ley, R. E.; Mahowald, M. A.; Magrini, V.; Mardis, E. R.; Gordon, J. I. An Obesity-Associated Gut Microbiome with Increased Capacity for Energy Harvest. *Nature* **2006**, *444* (7122), 1027–1031. https://doi.org/10.1038/nature05414.
(174) Kelly, J. R.; Borre, Y.; O' Brien, C.; Patterson, E.; El Aidy, S.; Deane, J.; Kennedy, P. J.; Beers, S.; Scott, K.; Moloney, G.; Hoban, A. E.; Scott, L.; Fitzgerald, P.; Ross, P.; Stanton, C.; Clarke, G.; Cryan, J. F.; Dinan, T. G. Transferring the Blues: Depression-Associated Gut Microbiota Induces Neurobehavioural Changes in the Rat. *J. Psychiatr. Res.* **2016**, *82*, 109–118. https://doi.org/10.1016/j.jpsychires.2016.07.019.
(175) Sulakvelidze, A.; Alavidze, Z.; MorrisJr, J. G. Bacteriophage Therapy. *Antimicrob. Agents Chemother.* **2001**. https://doi.org/10.1128/AAC.45.3.649-659.2001.
(176) Scarpellini, E.; Ianiro, G.; Attili, F.; Bassanelli, C.; De Santis, A.; Gasbarrini, A. The Human Gut Microbiota and Virome: Potential Therapeutic Implications. *Dig. Liver Dis. Off. J. Ital. Soc. Gastroenterol. Ital. Assoc. Study Liver* **2015**, *47* (12), 1007–1012. https://doi.org/10.1016/j.dld.2015.07.008.
(177) Parracho, H. M.; Burrowes, B. H.; Enright, M. C.; McConville, M. L.; Harper, D. R. The Role of Regulated Clinical Trials in the Development of Bacteriophage Therapeutics. *J. Mol. Genet. Med. Int. J. Biomed. Res.* **2012**, *6*, 279–286. https://doi.org/10.4172/1747-0862.1000050.
(178) Olbrich, M.; Künstner, A.; Witte, M.; Busch, H.; Fähnrich, A. Genetics and Omics Analysis of Autoimmune Skin Blistering Diseases. *Front. Immunol.* **2019**, *10*, 2327. https://doi.org/10.3389/fimmu.2019.02327.
(179) Schmidt, E.; Zillikens, D. Pemphigoid Diseases. *Lancet Lond. Engl.* **2013**, *381* (9863), 320–332. https://doi.org/10.1016/S0140-6736(12)61140-4.
(180) Jordon, R. E.; Beutner, E. H.; Witebsky, E.; Blumental, G.; Hale, W. L.; Lever, W. F. Basement Zone Antibodies in Bullous Pemphigoid. *JAMA* **1967**, *200* (9), 751–756.
(181) Shirakata, Y.; Amagai, M.; Hanakawa, Y.; Nishikawa, T.; Hashimoto, K. Lack of Mucosal Involvement in Pemphigus Foliaceus May Be Due to Low Expression of Desmoglein 1. *J. Invest. Dermatol.* **1998**, *110* (1), 76–78. https://doi.org/10.1046/j.1523-1747.1998.00085.x.

(182) Jamora, M. J. J.; Jiao, D.; Bystryn, J.-C. Antibodies to Desmoglein 1 and 3, and the Clinical Phenotype of Pemphigus Vulgaris. *J. Am. Acad. Dermatol.* **2003**, *48* (6), 976–977. https://doi.org/10.1067/mjd.2003.438.
(183) Meyer, N.; Misery, L. Geoepidemiologic Considerations of Auto-Immune Pemphigus. *Autoimmun. Rev.* **2010**, *9* (5), A379-382. https://doi.org/10.1016/j.autrev.2009.10.009.
(184) Nishie, W. Update on the Pathogenesis of Bullous Pemphigoid: An Autoantibody-Mediated Blistering Disease Targeting Collagen XVII. *J. Dermatol. Sci.* **2014**, *73* (3), 179–186. https://doi.org/10.1016/j.jdermsci.2013.12.001.
(185) Horváth, B.; Niedermeier, A.; Podstawa, E.; Müller, R.; Hunzelmann, N.; Kárpáti, S.; Hertl, M. IgA Autoantibodies in the Pemphigoids and Linear IgA Bullous Dermatosis. *Exp. Dermatol.* **2010**, *19* (7), 648–653. https://doi.org/10.1111/j.1600-0625.2010.01080.x.
(186) Christophoridis, S.; Büdinger, L.; Borradori, L.; Hunziker, T.; Merk, H. F.; Hertl, M. IgG, IgA and IgE Autoantibodies against the Ectodomain of BP180 in Patients with Bullous and Cicatricial Pemphigoid and Linear IgA Bullous Dermatosis. *Br. J. Dermatol.* **2000**, *143* (2), 349–355. https://doi.org/10.1046/j.1365-2133.2000.03661.x.
(187) Joly, P.; Roujeau, J.-C.; Benichou, J.; Picard, C.; Dreno, B.; Delaporte, E.; Vaillant, L.; D'Incan, M.; Plantin, P.; Bedane, C.; Young, P.; Bernard, P. A Comparison of Oral and Topical Corticosteroids in Patients with Bullous Pemphigoid. *N. Engl. J. Med.* **2002**, *346* (5), 321–327. https://doi.org/10.1056/NEJMoa011592.
(188) Joly, P.; Roujeau, J.-C.; Benichou, J.; Delaporte, E.; D'Incan, M.; Dreno, B.; Bedane, C.; Sparsa, A.; Gorin, I.; Picard, C.; Tancrede-Bohin, E.; Sassolas, B.; Lok, C.; Guillaume, J.-C.; Doutre, M.-S.; Richard, M.-A.; Caux, F.; Prost, C.; Plantin, P.; Chosidow, O.; Pauwels, C.; Maillard, H.; Saiag, P.; Descamps, V.; Chevrant-Breton, J.; Dereure, O.; Hellot, M.-F.; Esteve, E.; Bernard, P. A Comparison of Two Regimens of Topical Corticosteroids in the Treatment of Patients with Bullous Pemphigoid: A Multicenter Randomized Study. *J. Invest. Dermatol.* **2009**, *129* (7), 1681–1687. https://doi.org/10.1038/jid.2008.412.
(189) Kasperkiewicz, M.; Schmidt, E. Current Treatment of Autoimmune Blistering Diseases. *Curr. Drug Discov. Technol.* **2009**, *6* (4), 270–280. https://doi.org/10.2174/157016309789869065.
(190) Thomas, I.; Khorenian, S.; Arbesfeld, D. M. Treatment of Generalized Bullous Pemphigoid with Oral Tetracycline. *J. Am. Acad. Dermatol.* **1993**, *28* (1), 74–77. https://doi.org/10.1016/0190-9622(93)70013-J.
(191) Berk, M. A.; Lorincz, A. L. The Treatment of Bullous Pemphigoid With Tetracycline and Niacinamide: A Preliminary Report. *Arch. Dermatol.* **1986**, *122* (6), 670–674. https://doi.org/10.1001/archderm.1986.01660180076019.
(192) Czernik, A.; Toosi, S.; Bystryn, J.-C.; Grando, S. A. Intravenous Immunoglobulin in the Treatment of Autoimmune Bullous Dermatoses: An Update. *Autoimmunity* **2012**, *45* (1), 111–118. https://doi.org/10.3109/08916934.2011.606452.
(193) Kasperkiewicz, M.; Shimanovich, I.; Ludwig, R. J.; Rose, C.; Zillikens, D.; Schmidt, E. Rituximab for Treatment-Refractory Pemphigus and Pemphigoid: A Case Series of 17 Patients. *J. Am. Acad. Dermatol.* **2011**, *65* (3), 552–558. https://doi.org/10.1016/j.jaad.2010.07.032.
(194) Vorobyev, A.; Ludwig, R. J.; Schmidt, E. Clinical Features and Diagnosis of Epidermolysis Bullosa Acquisita. *Expert Rev. Clin. Immunol.* **2017**, *13* (2), 157–169. https://doi.org/10.1080/1744666X.2016.1221343.
(195) Woodley, D. T.; Chen, M.; Kim, G. *Epidermolysis bullosa acquisita - UpToDate*. UpToDate. https://www.uptodate.com/contents/epidermolysis-bullosa-acquisita#H306466519 (accessed 2021-12-10).
(196) Sakai, L. Y.; Keene, D. R.; Morris, N. P.; Burgeson, R. E. Type VII Collagen Is a Major Structural Component of Anchoring Fibrils. *J. Cell Biol.* **1986**, *103* (4), 1577–1586. https://doi.org/10.1083/jcb.103.4.1577.
(197) Burgeson, R. E. Type VII Collagen, Anchoring Fibrils, and Epidermolysis Bullosa. *J. Invest. Dermatol.* **1993**, *101* (3), 252–255. https://doi.org/10.1111/1523-1747.ep12365129.

(198) Woodley, D. T.; Briggaman, R. A.; O'Keefe, E. J.; Inman, A. O.; Queen, L. L.; Gammon, W. R. Identification of the Skin Basement-Membrane Autoantigen in Epidermolysis Bullosa Acquisita. *N. Engl. J. Med.* **1984**, *310* (16), 1007–1013. https://doi.org/10.1056/NEJM198404193101602.
(199) Lapiere, J. C.; Woodley, D. T.; Parente, M. G.; Iwasaki, T.; Wynn, K. C.; Christiano, A. M.; Uitto, J. Epitope Mapping of Type VII Collagen. Identification of Discrete Peptide Sequences Recognized by Sera from Patients with Acquired Epidermolysis Bullosa. *J. Clin. Invest.* **1993**, *92* (4), 1831–1839. https://doi.org/10.1172/JCI116774.
(200) Gammon, W. R.; Briggaman, R. A. Epidermolysis Bullosa Acquisita and Bullous Systemic Lupus Erythematosus. Diseases of Autoimmunity to Type VII Collagen. *Dermatol. Clin.* **1993**, *11* (3), 535–547.
(201) Jones, D. A.; Hunt, S. W.; Prisayanh, P. S.; Briggaman, R. A.; Gammon, W. R. Immunodominant Autoepitopes of Type VII Collagen Are Short, Paired Peptide Sequences within the Fibronectin Type III Homology Region of the Noncollagenous (NC1) Domain. *J. Invest. Dermatol.* **1995**, *104* (2), 231–235. https://doi.org/10.1111/1523-1747.ep12612780.
(202) Yaoita, H.; Briggaman, R. A.; Lawley, T. J.; Provost, T. T.; Katz, S. I. Epidermolysis Bullosa Acquisita: Ultrastructural and Immunological Studies. *J. Invest. Dermatol.* **1981**, *76* (4), 288–292. https://doi.org/10.1111/1523-1747.ep12526124.
(203) Kim, J. H.; Kim, Y. H.; Kim, S.; Noh, E. B.; Kim, S.-E.; Vorobyev, A.; Schmidt, E.; Zillikens, D.; Kim, S.-C. Serum Levels of Anti-Type VII Collagen Antibodies Detected by Enzyme-Linked Immunosorbent Assay in Patients with Epidermolysis Bullosa Acquisita Are Correlated with the Severity of Skin Lesions. *J. Eur. Acad. Dermatol. Venereol. JEADV* **2013**, *27* (2), e224-230. https://doi.org/10.1111/j.1468-3083.2012.04617.x.
(204) Chen, M.; Kim, G. H.; Prakash, L.; Woodley, D. T. Epidermolysis Bullosa Acquisita: Autoimmunity to Anchoring Fibril Collagen. *Autoimmunity* **2012**, *45* (1), 91–101. https://doi.org/10.3109/08916934.2011.606450.
(205) Ray, T. L.; Levine, J. B.; Weiss, W.; Ward, P. A. Epidermolysis Bullosa Acquisita and Inflammatory Bowel Disease. *J. Am. Acad. Dermatol.* **1982**, *6* (2), 242–252. https://doi.org/10.1016/s0190-9622(82)70017-9.
(206) Gupta, R.; Woodley, D. T.; Chen, M. Epidermolysis Bullosa Acquisita. *Clin. Dermatol.* **2012**, *30* (1), 60–69. https://doi.org/10.1016/j.clindermatol.2011.03.011.
(207) Gammon, W. R.; Heise, E. R.; Burke, W. A.; Fine, J. D.; Woodley, D. T.; Briggaman, R. A. Increased Frequency of HLA-DR2 in Patients with Autoantibodies to Epidermolysis Bullosa Acquisita Antigen: Evidence That the Expression of Autoimmunity to Type VII Collagen Is HLA Class II Allele Associated. *J. Invest. Dermatol.* **1988**, *91* (3), 228–232. https://doi.org/10.1111/1523-1747.ep12470317.
(208) Roenigk, H. H.; Ryan, J. G.; Bergfeld, W. F. Epidermolysis Bullosa Acquisita. Report of Three Cases and Review of All Published Cases. *Arch. Dermatol.* **1971**, *103* (1), 1–10. https://doi.org/10.1001/archderm.103.1.1.
(209) Chen, M.; O'Toole, E. A.; Sanghavi, J.; Mahmud, N.; Kelleher, D.; Weir, D.; Fairley, J. A.; Woodley, D. T. The Epidermolysis Bullosa Acquisita Antigen (Type VII Collagen) Is Present in Human Colon and Patients with Crohn's Disease Have Autoantibodies to Type VII Collagen. *J. Invest. Dermatol.* **2002**, *118* (6), 1059–1064. https://doi.org/10.1046/j.1523-1747.2002.01772.x.
(210) Ishii, N.; Recke, A.; Mihai, S.; Hirose, M.; Hashimoto, T.; Zillikens, D.; Ludwig, R. J. Autoantibody-Induced Intestinal Inflammation and Weight Loss in Experimental Epidermolysis Bullosa Acquisita. *J. Pathol.* **2011**, *224* (2), 234–244. https://doi.org/10.1002/path.2857.
(211) Licarete, E.; Ganz, S.; Recknagel, M. J.; Di Zenzo, G.; Hashimoto, T.; Hertl, M.; Zambruno, G.; Hundorfean, G.; Mudter, J.; Neurath, M. F.; Bruckner-Tuderman, L.; Sitaru, C. Prevalence of Collagen VII-Specific Autoantibodies in Patients with Autoimmune and Inflammatory Diseases. *BMC Immunol.* **2012**, *13*, 16. https://doi.org/10.1186/1471-2172-13-16.

(212) Kirtschig, G.; Murrell, D.; Wojnarowska, F.; Khumalo, N. Interventions for Mucous Membrane Pemphigoid and Epidermolysis Bullosa Acquisita. *Cochrane Database Syst. Rev.* **2003**, No. 1, CD004056. https://doi.org/10.1002/14651858.CD004056.
(213) Woodley, D. T.; Chang, C.; Saadat, P.; Ram, R.; Liu, Z.; Chen, M. Evidence That Anti-Type VII Collagen Antibodies Are Pathogenic and Responsible for the Clinical, Histological, and Immunological Features of Epidermolysis Bullosa Acquisita. *J. Invest. Dermatol.* **2005**, *124* (5), 958–964. https://doi.org/10.1111/j.0022-202X.2005.23702.x.
(214) Sitaru, C.; Mihai, S.; Otto, C.; Chiriac, M. T.; Hausser, I.; Dotterweich, B.; Saito, H.; Rose, C.; Ishiko, A.; Zillikens, D. Induction of Dermal-Epidermal Separation in Mice by Passive Transfer of Antibodies Specific to Type VII Collagen. *J. Clin. Invest.* **2005**, *115* (4), 870–878. https://doi.org/10.1172/JCI21386.
(215) Woodley, D. T.; Ram, R.; Doostan, A.; Bandyopadhyay, P.; Huang, Y.; Remington, J.; Hou, Y.; Keene, D. R.; Liu, Z.; Chen, M. Induction of Epidermolysis Bullosa Acquisita in Mice by Passive Transfer of Autoantibodies from Patients. *J. Invest. Dermatol.* **2006**, *126* (6), 1323–1330. https://doi.org/10.1038/sj.jid.5700254.
(216) Yu, X.; Gimsa, U.; Wester-Rosenlöf, L.; Kanitz, E.; Otten, W.; Kunz, M.; Ibrahim, S. M. Dissecting the Effects of MtDNA Variations on Complex Traits Using Mouse Conplastic Strains. *Genome Res.* **2009**, *19* (1), 159–165. https://doi.org/10.1101/gr.078865.108.
(217) Eipel, C.; Hildebrandt, A.; Scholz, B.; Schyschka, L.; Minor, T.; Kreikemeyer, B.; Ibrahim, S. M.; Vollmar, B. Mutation of Mitochondrial ATP8 Gene Improves Hepatic Energy Status in a Murine Model of Acute Endotoxemic Liver Failure. *Life Sci.* **2011**, *88* (7), 343–349. https://doi.org/10.1016/j.lfs.2010.12.011.
(218) Schröder, T.; Kucharczyk, D.; Bär, F.; Pagel, R.; Derer, S.; Jendrek, S. T.; Sünderhauf, A.; Brethack, A.-K.; Hirose, M.; Möller, S.; Künstner, A.; Bischof, J.; Weyers, I.; Heeren, J.; Koczan, D.; Schmid, S. M.; Divanovic, S.; Giles, D. A.; Adamski, J.; Fellermann, K.; Lehnert, H.; Köhl, J.; Ibrahim, S.; Sina, C. Mitochondrial Gene Polymorphisms Alter Hepatic Cellular Energy Metabolism and Aggravate Diet-Induced Non-Alcoholic Steatohepatitis. *Mol. Metab.* **2016**, *5* (4), 283–295. https://doi.org/10.1016/j.molmet.2016.01.010.
(219) Weiss, H.; Wester-Rosenloef, L.; Koch, C.; Koch, F.; Baltrusch, S.; Tiedge, M.; Ibrahim, S. The Mitochondrial Atp8 Mutation Induces Mitochondrial ROS Generation, Secretory Dysfunction, and β-Cell Mass Adaptation in Conplastic B6-MtFVB Mice. *Endocrinology* **2012**, *153* (10), 4666–4676. https://doi.org/10.1210/en.2012-1296.
(220) Gimsa, U.; Kanitz, E.; Otten, W.; Ibrahim, S. M. Behavior and Stress Reactivity in Mouse Strains with Mitochondrial DNA Variations. *Ann. N. Y. Acad. Sci.* **2009**, *1153*, 131–138. https://doi.org/10.1111/j.1749-6632.2008.03960.x.
(221) Scheffler, K.; Krohn, M.; Dunkelmann, T.; Stenzel, J.; Miroux, B.; Ibrahim, S.; von Bohlen und Halbach, O.; Heinze, H.-J.; Walker, L. C.; Gsponer, J. A.; Pahnke, J. Mitochondrial DNA Polymorphisms Specifically Modify Cerebral β-Amyloid Proteostasis. *Acta Neuropathol. (Berl.)* **2012**, *124* (2), 199–208. https://doi.org/10.1007/s00401-012-0980-x.
(222) Hirose, M.; Schilf, P.; Benoit, S.; Eming, R.; Gläser, R.; Homey, B.; Kunz, M.; Nebel, A.; Peitsch, W. K.; Pföhler, C.; Sárdy, M.; Schreiber, S.; Zillikens, D.; Schmidt, E.; Ibrahim, S. M.; German AIBD Genetic Study Group. Polymorphisms in the Mitochondrially Encoded ATP Synthase 8 Gene Are Associated with Susceptibility to Bullous Pemphigoid in the German Population. *Exp. Dermatol.* **2015**, *24* (9), 715–717. https://doi.org/10.1111/exd.12732.
(223) Schilf, P.; Künstner, A.; Olbrich, M.; Waschina, S.; Fuchs, B.; Galuska, C. E.; Braun, A.; Neuschütz, K.; Seutter, M.; Bieber, K.; Hellberg, L.; Sina, C.; Laskay, T.; Rupp, J.; Ludwig, R. J.; Zillikens, D.; Busch, H.; Sadik, C. D.; Hirose, M.; Ibrahim, S. M. A Mitochondrial Polymorphism Alters Immune Cell Metabolism and Protects Mice from Skin Inflammation. *Int. J. Mol. Sci.* **2021**, *22* (3), 1006. https://doi.org/10.3390/ijms22031006.
(224) Hirose, M.; Künstner, A.; Schilf, P.; Sünderhauf, A.; Rupp, J.; Jöhren, O.; Schwaninger, M.; Sina, C.; Baines, J. F.; Ibrahim, S. M. Mitochondrial Gene Polymorphism Is Associated with Gut

Microbial Communities in Mice. *Sci. Rep.* **2017**, *7* (1), 15293. https://doi.org/10.1038/s41598-017-15377-7.
(225) Tong, L.; Wang, Y.; Wang, Z.; Liu, W.; Sun, S.; Li, L.; Su, D.; Zhang, L. Propionate Ameliorates Dextran Sodium Sulfate-Induced Colitis by Improving Intestinal Barrier Function and Reducing Inflammation and Oxidative Stress. *Front. Pharmacol.* **2016**, *7*.
(226) Ciarlo, E.; Heinonen, T.; Herderschee, J.; Fenwick, C.; Mombelli, M.; Le Roy, D.; Roger, T. Impact of the Microbial Derived Short Chain Fatty Acid Propionate on Host Susceptibility to Bacterial and Fungal Infections in Vivo. *Sci. Rep.* **2016**, *6* (1), 37944. https://doi.org/10.1038/srep37944.
(227) den Besten, G.; Bleeker, A.; Gerding, A.; van Eunen, K.; Havinga, R.; van Dijk, T. H.; Oosterveer, M. H.; Jonker, J. W.; Groen, A. K.; Reijngoud, D.-J.; Bakker, B. M. Short-Chain Fatty Acids Protect Against High-Fat Diet–Induced Obesity via a PPARγ-Dependent Switch From Lipogenesis to Fat Oxidation. *Diabetes* **2015**, *64* (7), 2398–2408. https://doi.org/10.2337/db14-1213.
(228) Koo, S.; Chowdhury, I. H.; Szczesny, B.; Wan, X.; Garg, N. J. Macrophages Promote Oxidative Metabolism To Drive Nitric Oxide Generation in Response to Trypanosoma Cruzi. *Infect. Immun.* **2016**, *84* (12), 3527–3541. https://doi.org/10.1128/IAI.00809-16.
(229) Sato, T.; Vries, R. G.; Snippert, H. J.; van de Wetering, M.; Barker, N.; Stange, D. E.; van Es, J. H.; Abo, A.; Kujala, P.; Peters, P. J.; Clevers, H. Single Lgr5 Stem Cells Build Crypt-Villus Structures in Vitro without a Mesenchymal Niche. *Nature* **2009**, *459* (7244), 262–265. https://doi.org/10.1038/nature07935.
(230) Uritskiy, G. V.; DiRuggiero, J.; Taylor, J. MetaWRAP—a Flexible Pipeline for Genome-Resolved Metagenomic Data Analysis. *Microbiome* **2018**, *6* (1), 158. https://doi.org/10.1186/s40168-018-0541-1.
(231) Milanese, A.; Mende, D. R.; Paoli, L.; Salazar, G.; Ruscheweyh, H.-J.; Cuenca, M.; Hingamp, P.; Alves, R.; Costea, P. I.; Coelho, L. P.; Schmidt, T. S. B.; Almeida, A.; Mitchell, A. L.; Finn, R. D.; Huerta-Cepas, J.; Bork, P.; Zeller, G.; Sunagawa, S. Microbial Abundance, Activity and Population Genomic Profiling with MOTUs2. *Nat. Commun.* **2019**, *10* (1), 1014. https://doi.org/10.1038/s41467-019-08844-4.
(232) Menzel, P.; Ng, K. L.; Krogh, A. Fast and Sensitive Taxonomic Classification for Metagenomics with Kaiju. *Nat. Commun.* **2016**, *7* (1), 11257. https://doi.org/10.1038/ncomms11257.
(233) Wood, D. E.; Lu, J.; Langmead, B. Improved Metagenomic Analysis with Kraken 2. *Genome Biol.* **2019**, *20* (1), 257. https://doi.org/10.1186/s13059-019-1891-0.
(234) Lu, J.; Breitwieser, F. P.; Thielen, P.; Salzberg, S. L. Bracken: Estimating Species Abundance in Metagenomics Data. *PeerJ Comput. Sci.* **2017**, *3*, e104. https://doi.org/10.7717/peerj-cs.104.
(235) Ondov, B. D.; Bergman, N. H.; Phillippy, A. M. Interactive Metagenomic Visualization in a Web Browser. *BMC Bioinformatics* **2011**, *12* (1), 385. https://doi.org/10.1186/1471-2105-12-385.
(236) Franzosa, E. A.; McIver, L. J.; Rahnavard, G.; Thompson, L. R.; Schirmer, M.; Weingart, G.; Lipson, K. S.; Knight, R.; Caporaso, J. G.; Segata, N.; Huttenhower, C. Species-Level Functional Profiling of Metagenomes and Metatranscriptomes. *Nat. Methods* **2018**, *15* (11), 962–968. https://doi.org/10.1038/s41592-018-0176-y.
(237) Mallick, H.; Rahnavard, A.; McIver, L. J.; Ma, S.; Zhang, Y.; Nguyen, L. H.; Tickle, T. L.; Weingart, G.; Ren, B.; Schwager, E. H.; Chatterjee, S.; Thompson, K. N.; Wilkinson, J. E.; Subramanian, A.; Lu, Y.; Waldron, L.; Paulson, J. N.; Franzosa, E. A.; Bravo, H. C.; Huttenhower, C. Multivariable Association Discovery in Population-Scale Meta-Omics Studies. *PLOS Comput. Biol.* **2021**, *17* (11), e1009442. https://doi.org/10.1371/journal.pcbi.1009442.
(238) Tenenbaum, D.; Volkening, J.; Maintainer, B. package. *KEGGREST: Client-side REST access to the Kyoto Encyclopedia of Genes and Genomes (KEGG). R package version 1.36.2.* KEGGREST. https://bioconductor.org/packages/devel/bioc/vignettes/KEGGREST/inst/doc/KEGGREST-vignette.html (accessed 2022-06-16).
(239) Ritchie, M. E.; Phipson, B.; Wu, D.; Hu, Y.; Law, C. W.; Shi, W.; Smyth, G. K. Limma Powers Differential Expression Analyses for RNA-Sequencing and Microarray Studies. *Nucleic Acids Res.* **2015**, *43* (7), e47. https://doi.org/10.1093/nar/gkv007.

(240) Picart-Armada, S.; Fernández-Albert, F.; Vinaixa, M.; Rodríguez, M. A.; Aivio, S.; Stracker, T. H.; Yanes, O.; Perera-Lluna, A. Null Diffusion-Based Enrichment for Metabolomics Data. *PLOS ONE* **2017**, *12* (12), e0189012. https://doi.org/10.1371/journal.pone.0189012.
(241) Picart-Armada, S.; Fernández-Albert, F.; Vinaixa, M.; Yanes, O.; Perera-Lluna, A. FELLA: An R Package to Enrich Metabolomics Data. *BMC Bioinformatics* **2018**, *19* (1), 538. https://doi.org/10.1186/s12859-018-2487-5.
(242) Lerner, A.; Matthias, T. Changes in Intestinal Tight Junction Permeability Associated with Industrial Food Additives Explain the Rising Incidence of Autoimmune Disease. *Autoimmun. Rev.* **2015**, *14* (6), 479–489. https://doi.org/10.1016/j.autrev.2015.01.009.
(243) González-Mariscal, L.; Betanzos, A.; Nava, P.; Jaramillo, B. E. Tight Junction Proteins. *Prog. Biophys. Mol. Biol.* **2003**, *81* (1), 1–44. https://doi.org/10.1016/S0079-6107(02)00037-8.
(244) Bardenbacher, M.; Ruder, B.; Britzen-Laurent, N.; Schmid, B.; Waldner, M.; Naschberger, E.; Scharl, M.; Müller, W.; Günther, C.; Becker, C.; Stürzl, M.; Tripal, P. Permeability Analyses and Three Dimensional Imaging of Interferon Gamma-Induced Barrier Disintegration in Intestinal Organoids. *Stem Cell Res.* **2019**, *35*, 101383. https://doi.org/10.1016/j.scr.2019.101383.
(245) Marshall, A. S.; Silva, J. R.; Bannerman, C. A.; Gilron, I.; Ghasemlou, N. Skin-Resident Γδ T Cells Exhibit Site-Specific Morphology and Activation States. *J. Immunol. Res.* **2019**, *2019*, e9020234. https://doi.org/10.1155/2019/9020234.
(246) Lagkouvardos, I.; Lesker, T. R.; Hitch, T. C. A.; Gálvez, E. J. C.; Smit, N.; Neuhaus, K.; Wang, J.; Baines, J. F.; Abt, B.; Stecher, B.; Overmann, J.; Strowig, T.; Clavel, T. Sequence and Cultivation Study of Muribaculaceae Reveals Novel Species, Host Preference, and Functional Potential of This yet Undescribed Family. *Microbiome* **2019**, *7* (1), 28. https://doi.org/10.1186/s40168-019-0637-2.
(247) Liu, Y.; Alookaran, J. J.; Rhoads, J. M. Probiotics in Autoimmune and Inflammatory Disorders. *Nutrients* **2018**, *10* (10), 1537. https://doi.org/10.3390/nu10101537.
(248) Dosch, M.; Gerber, J.; Jebbawi, F.; Beldi, G. Mechanisms of ATP Release by Inflammatory Cells. *Int. J. Mol. Sci.* **2018**, *19* (4), 1222. https://doi.org/10.3390/ijms19041222.
(249) Kumar, P.; Nagarajan, A.; Uchil, P. D. Analysis of Cell Viability by the Lactate Dehydrogenase Assay. *Cold Spring Harb. Protoc.* **2018**, *2018* (6). https://doi.org/10.1101/pdb.prot095497.
(250) Palmieri, E. M.; McGinity, C.; Wink, D. A.; McVicar, D. W. Nitric Oxide in Macrophage Immunometabolism: Hiding in Plain Sight. *Metabolites* **2020**, *10* (11), 429. https://doi.org/10.3390/metabo10110429.
(251) Yano, T.; Kanoh, H.; Tamura, A.; Tsukita, S. Apical Cytoskeletons and Junctional Complexes as a Combined System in Epithelial Cell Sheets. *Ann. N. Y. Acad. Sci.* **2017**, *1405* (1), 32–43. https://doi.org/10.1111/nyas.13432.
(252) Fasano, A.; Shea-Donohue, T. Mechanisms of Disease: The Role of Intestinal Barrier Function in the Pathogenesis of Gastrointestinal Autoimmune Diseases. *Nat. Clin. Pract. Gastroenterol. Hepatol.* **2005**, *2* (9), 416–422. https://doi.org/10.1038/ncpgasthep0259.
(253) Zeissig, S.; Bürgel, N.; Günzel, D.; Richter, J.; Mankertz, J.; Wahnschaffe, U.; Kroesen, A. J.; Zeitz, M.; Fromm, M.; Schulzke, J.-D. Changes in Expression and Distribution of Claudin 2, 5 and 8 Lead to Discontinuous Tight Junctions and Barrier Dysfunction in Active Crohn's Disease. *Gut* **2007**, *56* (1), 61–72. https://doi.org/10.1136/gut.2006.094375.
(254) Förster, C.; Kahles, T.; Kietz, S.; Drenckhahn, D. Dexamethasone Induces the Expression of Metalloproteinase Inhibitor TIMP-1 in the Murine Cerebral Vascular Endothelial Cell Line CEND. *J. Physiol.* **2007**, *580* (Pt.3), 937–949. https://doi.org/10.1113/jphysiol.2007.129007.
(255) Förster, C. Tight Junctions and the Modulation of Barrier Function in Disease. *Histochem. Cell Biol.* **2008**, *130* (1), 55–70. https://doi.org/10.1007/s00418-008-0424-9.
(256) Mankertz, J.; Tavalali, S.; Schmitz, H.; Mankertz, A.; Riecken, E. O.; Fromm, M.; Schulzke, J. D. Expression from the Human Occludin Promoter Is Affected by Tumor Necrosis Factor Alpha and Interferon Gamma. *J. Cell Sci.* **2000**, *113* (11), 2085–2090. https://doi.org/10.1242/jcs.113.11.2085.

(257) Bruewer, M.; Luegering, A.; Kucharzik, T.; Parkos, C. A.; Madara, J. L.; Hopkins, A. M.; Nusrat, A. Proinflammatory Cytokines Disrupt Epithelial Barrier Function by Apoptosis-Independent Mechanisms. *J. Immunol.* **2003**, *171* (11), 6164–6172. https://doi.org/10.4049/jimmunol.171.11.6164.
(258) Molina-Jijón, E.; Rodríguez-Muñoz, R.; Namorado, M. del C.; Pedraza-Chaverri, J.; Reyes, J. L. Oxidative Stress Induces Claudin-2 Nitration in Experimental Type 1 Diabetic Nephropathy. *Free Radic. Biol. Med.* **2014**, *72*, 162–175. https://doi.org/10.1016/j.freeradbiomed.2014.03.040.
(259) Schilf, P. Interplay of MtDNA, Metabolism and Microbiota in the Pathogenesis of AIBD. Monographie, Universität zu Lübeck, Lübeck, 2017.
(260) Al-Badri, M. R.; Azar, S. T. Effect of Glucagon-like Peptide-1 Receptor Agonists in Patients with Psoriasis. *Ther. Adv. Endocrinol. Metab.* **2014**, *5* (2), 34–38. https://doi.org/10.1177/2042018814543483.
(261) Hogan, A. E.; Tobin, A. M.; Ahern, T.; Corrigan, M. A.; Gaoatswe, G.; Jackson, R.; O'Reilly, V.; Lynch, L.; Doherty, D. G.; Moynagh, P. N.; Kirby, B.; O'Connell, J.; O'Shea, D. Glucagon-like Peptide-1 (GLP-1) and the Regulation of Human Invariant Natural Killer T Cells: Lessons from Obesity, Diabetes and Psoriasis. *Diabetologia* **2011**, *54* (11), 2745–2754. https://doi.org/10.1007/s00125-011-2232-3.
(262) Buysschaert, M.; Tennstedt, D.; Preumont, V. Improvement of Psoriasis during Exenatide Treatment in a Patient with Diabetes. *Diabetes Metab.* **2012**, *38* (1), 86–88. https://doi.org/10.1016/j.diabet.2011.11.004.
(263) Yamane, S.; Inagaki, N. Regulation of Glucagon-like Peptide-1 Sensitivity by Gut Microbiota Dysbiosis. *J. Diabetes Investig.* **2018**, *9* (2), 262–264. https://doi.org/10.1111/jdi.12762.
(264) Sazgarnejad, S.; Yazdanpanah, N.; Rezaei, N. Anti-Inflammatory Effects of GLP-1 in Patients with COVID-19. *Expert Rev. Anti Infect. Ther.* **2022**, *20* (3), 373–381. https://doi.org/10.1080/14787210.2021.1964955.
(265) Monlun, M.; Hyernard, C.; Blanco, P.; Lartigue, L.; Faustin, B. Mitochondria as Molecular Platforms Integrating Multiple Innate Immune Signalings. *J. Mol. Biol.* **2017**, *429* (1), 1–13. https://doi.org/10.1016/j.jmb.2016.10.028.
(266) Bulua, A. C.; Simon, A.; Maddipati, R.; Pelletier, M.; Park, H.; Kim, K.-Y.; Sack, M. N.; Kastner, D. L.; Siegel, R. M. Mitochondrial Reactive Oxygen Species Promote Production of Proinflammatory Cytokines and Are Elevated in TNFR1-Associated Periodic Syndrome (TRAPS). *J. Exp. Med.* **2011**, *208* (3), 519–533. https://doi.org/10.1084/jem.20102049.
(267) Jameson, J. M.; Sharp, L. L.; Witherden, D. A.; Havran, W. L. Regulation of Skin Cell Homeostasis by Gamma Delta T Cells. *Front. Biosci. J. Virtual Libr.* **2004**, *9*, 2640–2651. https://doi.org/10.2741/1423.
(268) Sumaria, N.; Roediger, B.; Ng, L. G.; Qin, J.; Pinto, R.; Cavanagh, L. L.; Shklovskaya, E.; Fazekas de St. Groth, B.; Triccas, J. A.; Weninger, W. Cutaneous Immunosurveillance by Self-Renewing Dermal Γδ T Cells. *J. Exp. Med.* **2011**, *208* (3), 505–518. https://doi.org/10.1084/jem.20101824.
(269) Jameson, J.; Ugarte, K.; Chen, N.; Yachi, P.; Fuchs, E.; Boismenu, R.; Havran, W. L. A Role for Skin Γδ T Cells in Wound Repair. *Science* **2002**, *296* (5568), 747–749. https://doi.org/10.1126/science.1069639.
(270) Mills, R. E.; Taylor, K. R.; Podshivalova, K.; McKay, D. B.; Jameson, J. M. Defects in Skin Γδ T Cell Function Contribute to Delayed Wound Repair in Rapamycin-Treated Mice. *J. Immunol.* **2008**, *181* (6), 3974–3983. https://doi.org/10.4049/jimmunol.181.6.3974.
(271) Roberts, N. A.; White, A. J.; Jenkinson, W. E.; Turchinovich, G.; Nakamura, K.; Withers, D. R.; McConnell, F. M.; Desanti, G. E.; Benezech, C.; Parnell, S. M.; Cunningham, A. F.; Paolino, M.; Penninger, J. M.; Simon, A. K.; Nitta, T.; Ohigashi, I.; Takahama, Y.; Caamano, J. H.; Hayday, A. C.; Lane, P. J. L.; Jenkinson, E. J.; Anderson, G. Rank Signaling Links the Development of Invariant Γδ T Cell Progenitors and Aire+ Medullary Epithelium. *Immunity* **2012**, *36* (3–2), 427–437. https://doi.org/10.1016/j.immuni.2012.01.016.
(272) MacLeod, A. S.; Havran, W. L. Functions of Skin-Resident Γδ T Cells. *Cell. Mol. Life Sci. CMLS* **2011**, *68* (14), 2399–2408. https://doi.org/10.1007/s00018-011-0702-x.

(273) Schwacha, M. G.; Rani, M.; Zhang, Q.; Nunez-Cantu, O.; Cap, A. P. Mitochondrial Damage-Associated Molecular Patterns Activate Γδ T-Cells. *Innate Immun.* **2014**, *20* (3), 261–268. https://doi.org/10.1177/1753425913488969.
(274) Németh, T.; Mócsai, A. The Role of Neutrophils in Autoimmune Diseases. *Immunol. Lett.* **2012**, *143* (1), 9–19. https://doi.org/10.1016/j.imlet.2012.01.013.
(275) Sitaru, C.; Schmidt, E.; Petermann, S.; Munteanu, L. S.; Bröcker, E.-B.; Zillikens, D. Autoantibodies to Bullous Pemphigoid Antigen 180 Induce Dermal-Epidermal Separation in Cryosections of Human Skin. *J. Invest. Dermatol.* **2002**, *118* (4), 664–671. https://doi.org/10.1046/j.1523-1747.2002.01720.x.
(276) Liu, Z.; Giudice, G. J.; Zhou, X.; Swartz, S. J.; Troy, J. L.; Fairley, J. A.; Till, G. O.; Diaz, L. A. A Major Role for Neutrophils in Experimental Bullous Pemphigoid. *J. Clin. Invest.* **1997**, *100* (5), 1256–1263. https://doi.org/10.1172/JCI119639.
(277) Ludwig, R. J.; Vanhoorelbeke, K.; Leypoldt, F.; Kaya, Z.; Bieber, K.; McLachlan, S. M.; Komorowski, L.; Luo, J.; Cabral-Marques, O.; Hammers, C. M.; Lindstrom, J. M.; Lamprecht, P.; Fischer, A.; Riemekasten, G.; Tersteeg, C.; Sondermann, P.; Rapoport, B.; Wandinger, K.-P.; Probst, C.; El Beidaq, A.; Schmidt, E.; Verkman, A.; Manz, R. A.; Nimmerjahn, F. Mechanisms of Autoantibody-Induced Pathology. *Front. Immunol.* **2017**, *8*.
(278) Chiriac, M. T.; Roesler, J.; Sindrilaru, A.; Scharffetter-Kochanek, K.; Zillikens, D.; Sitaru, C. NADPH Oxidase Is Required for Neutrophil-Dependent Autoantibody-Induced Tissue Damage. *J. Pathol.* **2007**, *212* (1), 56–65. https://doi.org/10.1002/path.2157.
(279) Bieber, K.; Witte, M.; Sun, S.; Hundt, J. E.; Kalies, K.; Dräger, S.; Kasprick, A.; Twelkmeyer, T.; Manz, R. A.; König, P.; Köhl, J.; Zillikens, D.; Ludwig, R. J. T Cells Mediate Autoantibody-Induced Cutaneous Inflammation and Blistering in Epidermolysis Bullosa Acquisita. *Sci. Rep.* **2016**, *6* (1), 38357. https://doi.org/10.1038/srep38357.
(280) Ellebrecht, C. T.; Srinivas, G.; Bieber, K.; Banczyk, D.; Kalies, K.; Künzel, S.; Hammers, C. M.; Baines, J. F.; Zillikens, D.; Ludwig, R. J.; Westermann, J. Skin Microbiota-Associated Inflammation Precedes Autoantibody Induced Tissue Damage in Experimental Epidermolysis Bullosa Acquisita. *J. Autoimmun.* **2016**, *68*, 14–22. https://doi.org/10.1016/j.jaut.2015.08.007.
(281) Zákostelská, Z.; Málková, J.; Klimešová, K.; Rossmann, P.; Hornová, M.; Novosádová, I.; Stehlíková, Z.; Kostovčík, M.; Hudcovic, T.; Štepánková, R.; Jůzlová, K.; Hercogová, J.; Tlaskalová-Hogenová, H.; Kverka, M. Intestinal Microbiota Promotes Psoriasis-Like Skin Inflammation by Enhancing Th17 Response. *PLOS ONE* **2016**, *11* (7), e0159539. https://doi.org/10.1371/journal.pone.0159539.
(282) Stehlikova, Z.; Kostovcikova, K.; Kverka, M.; Rossmann, P.; Dvorak, J.; Novosadova, I.; Kostovcik, M.; Coufal, S.; Srutkova, D.; Prochazkova, P.; Hudcovic, T.; Kozakova, H.; Stepankova, R.; Rob, F.; Juzlova, K.; Hercogova, J.; Tlaskalova-Hogenova, H.; Jiraskova Zakostelska, Z. Crucial Role of Microbiota in Experimental Psoriasis Revealed by a Gnotobiotic Mouse Model. *Front. Microbiol.* **2019**, *10*.
(283) Cebra, J. J.; Periwal, S. B.; Lee, G.; Lee, F.; Shroff, K. E. Development and Maintenance of the Gut-Associated Lymphoid Tissue (GALT): The Roles of Enteric Bacteria and Viruses. *Dev. Immunol.* **1998**, *6* (1–2), 13–18. https://doi.org/10.1155/1998/68382.
(284) Jiang, H.-Q.; Thurnheer, M. C.; Zuercher, A. W.; Boiko, N. V.; Bos, N. A.; Cebra, J. J. Interactions of Commensal Gut Microbes with Subsets of B- and T-Cells in the Murine Host. *Vaccine* **2004**, *22* (7), 805–811. https://doi.org/10.1016/j.vaccine.2003.11.022.
(285) Östman, S.; Rask, C.; Wold, A. E.; Hultkrantz, S.; Telemo, E. Impaired Regulatory T Cell Function in Germ-Free Mice. *Eur. J. Immunol.* **2006**, *36* (9), 2336–2346. https://doi.org/10.1002/eji.200535244.
(286) Cebra, J. J.; Jiang, H.-Q.; Boiko, N.; Tlaskalova-Hogenova, H. The Role of Mucosal Microbiota in the Development, Maintenance, and Pathologies of the Mucosal Immune System. *Mucosal Immunol.* **2005**, 335–368. https://doi.org/10.1016/B978-012491543-5/50022-X.

(287) Ahn, I.-S.; Yoon, J.; Diamante, G.; Cohn, P.; Jang, C.; Yang, X. Disparate Metabolomic Responses to Fructose Consumption between Different Mouse Strains and the Role of Gut Microbiota. *Metabolites* **2021**, *11* (6), 342. https://doi.org/10.3390/metabo11060342.
(288) Kieffer, D. A.; Piccolo, B. D.; Marco, M. L.; Kim, E. B.; Goodson, M. L.; Keenan, M. J.; Dunn, T. N.; Knudsen, K. E. B.; Martin, R. J.; Adams, S. H. Mice Fed a High-Fat Diet Supplemented with Resistant Starch Display Marked Shifts in the Liver Metabolome Concurrent with Altered Gut Bacteria. *J. Nutr.* **2016**, *146* (12), 2476–2490. https://doi.org/10.3945/jn.116.238931.
(289) Zhang, Z.; Chen, X.; Cui, B. Modulation of the Fecal Microbiome and Metabolome by Resistant Dextrin Ameliorates Hepatic Steatosis and Mitochondrial Abnormalities in Mice. *Food Funct.* **2021**, *12* (10), 4504–4518. https://doi.org/10.1039/D1FO00249J.
(290) Esterhuizen, K.; van der Westhuizen, F. H.; Louw, R. Metabolomics of Mitochondrial Disease. *Mitochondrion* **2017**, *35*, 97–110. https://doi.org/10.1016/j.mito.2017.05.012.
(291) Raja, G.; Gupta, H.; Gebru, Y. A.; Youn, G. S.; Choi, Y. R.; Kim, H. S.; Yoon, S. J.; Kim, D. J.; Kim, T.-J.; Suk, K. T. Recent Advances of Microbiome-Associated Metabolomics Profiling in Liver Disease: Principles, Mechanisms, and Applications. *Int. J. Mol. Sci.* **2021**, *22* (3), 1160. https://doi.org/10.3390/ijms22031160.
(292) Tojo, R.; Suárez, A.; Clemente, M. G.; de los Reyes-Gavilán, C. G.; Margolles, A.; Gueimonde, M.; Ruas-Madiedo, P. Intestinal Microbiota in Health and Disease: Role of Bifidobacteria in Gut Homeostasis. *World J. Gastroenterol. WJG* **2014**, *20* (41), 15163–15176. https://doi.org/10.3748/wjg.v20.i41.15163.
(293) Collado, M. C.; Donat, E.; Ribes-Koninckx, C.; Calabuig, M.; Sanz, Y. Imbalances in Faecal and Duodenal Bifidobacterium Species Composition in Active and Non-Active Coeliac Disease. *BMC Microbiol.* **2008**, *8*, 232. https://doi.org/10.1186/1471-2180-8-232.
(294) Mylonaki, M.; Rayment, N. B.; Rampton, D. S.; Hudspith, B. N.; Brostoff, J. Molecular Characterization of Rectal Mucosa-Associated Bacterial Flora in Inflammatory Bowel Disease. *Inflamm. Bowel Dis.* **2005**, *11* (5), 481–487. https://doi.org/10.1097/01.mib.0000159663.62651.4f.
(295) Kalliomäki, M.; Kirjavainen, P.; Eerola, E.; Kero, P.; Salminen, S.; Isolauri, E. Distinct Patterns of Neonatal Gut Microflora in Infants in Whom Atopy Was and Was Not Developing. *J. Allergy Clin. Immunol.* **2001**, *107* (1), 129–134. https://doi.org/10.1067/mai.2001.111237.
(296) He, F.; Ouwehand, A. C.; Isolauri, E.; Hashimoto, H.; Benno, Y.; Salminen, S. Comparison of Mucosal Adhesion and Species Identification of Bifidobacteria Isolated from Healthy and Allergic Infants. *FEMS Immunol. Med. Microbiol.* **2001**, *30* (1), 43–47. https://doi.org/10.1111/j.1574-695X.2001.tb01548.x.
(297) Murphy, E. C.; Mörgelin, M.; Cooney, J. C.; Frick, I.-M. 2011. Interaction of Bacteroides Fragilis and Bacteroides Thetaiotaomicron with the Kallikrein–Kinin System. *Microbiology 157* (7), 2094–2105. https://doi.org/10.1099/mic.0.046862-0.
(298) Zafar, H.; Saier, M. H. Gut Bacteroides Species in Health and Disease. *Gut Microbes* **2021**, *13* (1), 1848158. https://doi.org/10.1080/19490976.2020.1848158.
(299) Troy, E. B.; Kasper, D. L. Beneficial Effects of Bacteroides Fragilis Polysaccharides on the Immune System. *Front. Biosci. Landmark Ed.* **2010**, *15* (1), 25–34. https://doi.org/10.2741/3603.
(300) Cohen-Poradosu, R.; McLoughlin, R. M.; Lee, J. C.; Kasper, D. L. Bacteroides Fragilis-Stimulated Interleukin-10 Contains Expanding Disease. *J. Infect. Dis.* **2011**, *204* (3), 363–371. https://doi.org/10.1093/infdis/jir277.
(301) Vinolo, M. A. R.; Rodrigues, H. G.; Nachbar, R. T.; Curi, R. Regulation of Inflammation by Short Chain Fatty Acids. *Nutrients* **2011**, *3* (10), 858–876. https://doi.org/10.3390/nu3100858.
(302) Angoa-Pérez, M.; Zagorac, B.; Francescutti, D. M.; Winters, A. D.; Greenberg, J. M.; Ahmad, M. M.; Manning, S. D.; Gulbransen, B. D.; Theis, K. R.; Kuhn, D. M. Effects of a High Fat Diet on Gut Microbiome Dysbiosis in a Mouse Model of Gulf War Illness. *Sci. Rep.* **2020**, *10* (1), 9529. https://doi.org/10.1038/s41598-020-66833-w.

(303) Chang, C.-S.; Liao, Y.-C.; Huang, C.-T.; Lin, C.-M.; Cheung, C. H. Y.; Ruan, J.-W.; Yu, W.-H.; Tsai, Y.-T.; Lin, I.-J.; Huang, C.-H.; Liou, J.-S.; Chou, Y.-H.; Chien, H.-J.; Chuang, H.-L.; Juan, H.-F.; Huang, H.-C.; Chan, H.-L.; Liao, Y.-C.; Tang, S.-C.; Su, Y.-W.; Tan, T.-H.; Bäumler, A. J.; Kao, C.-Y. Identification of a Gut Microbiota Member That Ameliorates DSS-Induced Colitis in Intestinal Barrier Enhanced Dusp6-Deficient Mice. *Cell Rep.* **2021**, *37* (8), 110016. https://doi.org/10.1016/j.celrep.2021.110016.

(304) Parker, B. J.; Wearsch, P. A.; Veloo, A. C. M.; Rodriguez-Palacios, A. The Genus Alistipes: Gut Bacteria With Emerging Implications to Inflammation, Cancer, and Mental Health. *Front. Immunol.* **2020**, *11*.

(305) Shao, L.; Ling, Z.; Chen, D.; Liu, Y.; Yang, F.; Li, L. Disorganized Gut Microbiome Contributed to Liver Cirrhosis Progression: A Meta-Omics-Based Study. *Front. Microbiol.* **2018**, *9*, 3166. https://doi.org/10.3389/fmicb.2018.03166.

(306) Kim, S.; Goel, R.; Kumar, A.; Qi, Y.; Lobaton, G.; Hosaka, K.; Mohammed, M.; Handberg, E. M.; Richards, E. M.; Pepine, C. J.; Raizada, M. K. Imbalance of Gut Microbiome and Intestinal Epithelial Barrier Dysfunction in Patients with High Blood Pressure. *Clin. Sci.* **2018**, *132* (6), 701–718. https://doi.org/10.1042/CS20180087.

(307) He, B.; Hoang, T. K.; Tian, X.; Taylor, C. M.; Blanchard, E.; Luo, M.; Bhattacharjee, M. B.; Freeborn, J.; Park, S.; Couturier, J.; Lindsey, J. W.; Tran, D. Q.; Rhoads, J. M.; Liu, Y. Lactobacillus Reuteri Reduces the Severity of Experimental Autoimmune Encephalomyelitis in Mice by Modulating Gut Microbiota. *Front. Immunol.* **2019**, *10*.

(308) Liu, Y.; Fatheree, N. Y.; Dingle, B. M.; Tran, D. Q.; Rhoads, J. M. Lactobacillus Reuteri DSM 17938 Changes the Frequency of Foxp3+ Regulatory T Cells in the Intestine and Mesenteric Lymph Node in Experimental Necrotizing Enterocolitis. *PLOS ONE* **2013**, *8* (2), e56547. https://doi.org/10.1371/journal.pone.0056547.

(309) Dehner, C.; Fine, R.; Kriegel, M. A. The Microbiome in Systemic Autoimmune Disease – Mechanistic Insights from Recent Studies. *Curr. Opin. Rheumatol.* **2019**, *31* (2), 201–207. https://doi.org/10.1097/BOR.0000000000000574.

(310) Zegarra-Ruiz, D. F.; El Beidaq, A.; Iñiguez, A. J.; Lubrano Di Ricco, M.; Manfredo Vieira, S.; Ruff, W. E.; Mubiru, D.; Fine, R. L.; Sterpka, J.; Greiling, T. M.; Dehner, C.; Kriegel, M. A. A Diet-Sensitive Commensal Lactobacillus Strain Mediates TLR7-Dependent Systemic Autoimmunity. *Cell Host Microbe* **2019**, *25* (1), 113-127.e6. https://doi.org/10.1016/j.chom.2018.11.009.

(311) Elahi, A.; Sabui, S.; Narasappa, N. N.; Agrawal, S.; Lambrecht, N. W.; Agrawal, A.; Said, H. M. Biotin Deficiency Induces Th1- and Th17-Mediated Proinflammatory Responses in Human CD4+ T Lymphocytes via Activation of the MTOR Signaling Pathway. *J. Immunol. Baltim. Md 1950* **2018**, *200* (8), 2563–2570. https://doi.org/10.4049/jimmunol.1701200.

(312) Liu, X.; Ma, Y.; Yu, Y.; Zhang, W.; Shi, J.; Zhang, X.; Dai, M.; Wang, Y.; Zhang, H.; Zhang, J.; Shen, J.; Zhang, F.; Song, M.; Wang, J. Gut Microbial Methionine Impacts Circadian Clock Gene Expression and Reactive Oxygen Species Level in Host Gastrointestinal Tract. *Protein Cell* **2022**, pwac021. https://doi.org/10.1093/procel/pwac021.

(313) Arakawa, T.; Sugiyama, T.; Matsuura, H.; Okuno, T.; Ogino, H.; Sakazaki, F.; Ueno, H. Effects of Supplementary Seleno-L-Methionine on Atopic Dermatitis-Like Skin Lesions in Mice. *Biol. Pharm. Bull.* **2018**, *41* (9), 1456–1462. https://doi.org/10.1248/bpb.b18-00349.

(314) Madeo, F.; Eisenberg, T.; Pietrocola, F.; Kroemer, G. Spermidine in Health and Disease. *Science* **2018**, *359* (6374), eaan2788. https://doi.org/10.1126/science.aan2788.

(315) Pegg, A. E. Functions of Polyamines in Mammals. *J. Biol. Chem.* **2016**, *291* (29), 14904–14912. https://doi.org/10.1074/jbc.R116.731661.

(316) Igarashi, K.; Kashiwagi, K. Modulation of Cellular Function by Polyamines. *Int. J. Biochem. Cell Biol.* **2010**, *42* (1), 39–51. https://doi.org/10.1016/j.biocel.2009.07.009.

(317) Bardócz, S.; Duguid, T. J.; Brown, D. S.; Grant, G.; Pusztai, A.; White, A.; Ralph, A. The Importance of Dietary Polyamines in Cell Regeneration and Growth. *Br. J. Nutr.* **1995**, *73* (6), 819–828. https://doi.org/10.1079/bjn19950087.

(318) Eisenberg, T.; Knauer, H.; Schauer, A.; Büttner, S.; Ruckenstuhl, C.; Carmona-Gutierrez, D.; Ring, J.; Schroeder, S.; Magnes, C.; Antonacci, L.; Fussi, H.; Deszcz, L.; Hartl, R.; Schraml, E.; Criollo, A.; Megalou, E.; Weiskopf, D.; Laun, P.; Heeren, G.; Breitenbach, M.; Grubeck-Loebenstein, B.; Herker, E.; Fahrenkrog, B.; Fröhlich, K.-U.; Sinner, F.; Tavernarakis, N.; Minois, N.; Kroemer, G.; Madeo, F. Induction of Autophagy by Spermidine Promotes Longevity. *Nat. Cell Biol.* **2009**, *11* (11), 1305–1314. https://doi.org/10.1038/ncb1975.

(319) Yamamoto, T.; Hinoi, E.; Fujita, H.; Iezaki, T.; Takahata, Y.; Takamori, M.; Yoneda, Y. The Natural Polyamines Spermidine and Spermine Prevent Bone Loss through Preferential Disruption of Osteoclastic Activation in Ovariectomized Mice. *Br. J. Pharmacol.* **2012**, *166* (3), 1084–1096. https://doi.org/10.1111/j.1476-5381.2012.01856.x.

(320) Eisenberg, T.; Abdellatif, M.; Schroeder, S.; Primessnig, U.; Stekovic, S.; Pendl, T.; Harger, A.; Schipke, J.; Zimmermann, A.; Schmidt, A.; Tong, M.; Ruckenstuhl, C.; Dammbrueck, C.; Gross, A. S.; Herbst, V.; Magnes, C.; Trausinger, G.; Narath, S.; Meinitzer, A.; Hu, Z.; Kirsch, A.; Eller, K.; Carmona-Gutierrez, D.; Büttner, S.; Pietrocola, F.; Knittelfelder, O.; Schrepfer, E.; Rockenfeller, P.; Simonini, C.; Rahn, A.; Horsch, M.; Moreth, K.; Beckers, J.; Fuchs, H.; Gailus-Durner, V.; Neff, F.; Janik, D.; Rathkolb, B.; Rozman, J.; de Angelis, M. H.; Moustafa, T.; Haemmerle, G.; Mayr, M.; Willeit, P.; von Frieling-Salewsky, M.; Pieske, B.; Scorrano, L.; Pieber, T.; Pechlaner, R.; Willeit, J.; Sigrist, S. J.; Linke, W. A.; Mühlfeld, C.; Sadoshima, J.; Dengjel, J.; Kiechl, S.; Kroemer, G.; Sedej, S.; Madeo, F. Cardioprotection and Lifespan Extension by the Natural Polyamine Spermidine. *Nat. Med.* **2016**, *22* (12), 1428–1438. https://doi.org/10.1038/nm.4222.

(321) Sadasivan, S. K.; Vasamsetti, B.; Singh, J.; Marikunte, V. V.; Oommen, A. M.; Jagannath, M. R.; Pralhada Rao, R. Exogenous Administration of Spermine Improves Glucose Utilization and Decreases Bodyweight in Mice. *Eur. J. Pharmacol.* **2014**, *729*, 94–99. https://doi.org/10.1016/j.ejphar.2014.01.073.

(322) Puleston, D. J.; Simon, A. K. New Roles for Autophagy and Spermidine in T Cells. *Microb. Cell Graz Austria* **2015**, *2* (3), 91–93. https://doi.org/10.15698/mic2015.03.195.

(323) Kibe, R.; Kurihara, S.; Sakai, Y.; Suzuki, H.; Ooga, T.; Sawaki, E.; Muramatsu, K.; Nakamura, A.; Yamashita, A.; Kitada, Y.; Kakeyama, M.; Benno, Y.; Matsumoto, M. Upregulation of Colonic Luminal Polyamines Produced by Intestinal Microbiota Delays Senescence in Mice. *Sci. Rep.* **2014**, *4*, 4548. https://doi.org/10.1038/srep04548.

(324) McAlindon, T. E.; LaValley, M. P.; Gulin, J. P.; Felson, D. T. Glucosamine and Chondroitin for Treatment of Osteoarthritis: A Systematic Quality Assessment and Meta-Analysis. *JAMA* **2000**, *283* (11), 1469–1475. https://doi.org/10.1001/jama.283.11.1469.

(325) Weimer, S.; Priebs, J.; Kuhlow, D.; Groth, M.; Priebe, S.; Mansfeld, J.; Merry, T. L.; Dubuis, S.; Laube, B.; Pfeiffer, A. F.; Schulz, T. J.; Guthke, R.; Platzer, M.; Zamboni, N.; Zarse, K.; Ristow, M. D-Glucosamine Supplementation Extends Life Span of Nematodes and of Ageing Mice. *Nat. Commun.* **2014**, *5* (1), 3563. https://doi.org/10.1038/ncomms4563.

(326) Azuma, K.; Osaki, T.; Kurozumi, S.; Kiyose, M.; Tsuka, T.; Murahata, Y.; Imagawa, T.; Itoh, N.; Minami, S.; Sato, K.; Okamoto, Y. Anti-Inflammatory Effects of Orally Administered Glucosamine Oligomer in an Experimental Model of Inflammatory Bowel Disease. *Carbohydr. Polym.* **2015**, *115*, 448–456. https://doi.org/10.1016/j.carbpol.2014.09.012.

(327) Grigorian, A.; Araujo, L.; Naidu, N. N.; Place, D. J.; Choudhury, B.; Demetriou, M. N-Acetylglucosamine Inhibits T-Helper 1 (Th1)/T-Helper 17 (Th17) Cell Responses and Treats Experimental Autoimmune Encephalomyelitis. *J. Biol. Chem.* **2011**, *286* (46), 40133–40141. https://doi.org/10.1074/jbc.M111.277814.

(328) Marto, J.; Sangalli, C.; Capra, P.; Perugini, P.; Ascenso, A.; Gonçalves, L.; Ribeiro, H. Development and Characterization of New and Scalable Topical Formulations Containing N-Acetyl-d-Glucosamine-Loaded Solid Lipid Nanoparticles. *Drug Dev. Ind. Pharm.* **2017**, *43* (11), 1792–1800. https://doi.org/10.1080/03639045.2017.1339083.

(329) Sayo, T.; Sakai, S.; Inoue, S. Synergistic Effect of N-Acetylglucosamine and Retinoids on Hyaluronan Production in Human Keratinocytes. *Skin Pharmacol. Physiol.* **2004**, *17* (2), 77–83. https://doi.org/10.1159/000076017.

(330) Tu, C.-X.; Zhang, R.-X.; Zhang, X.-J.; Huang, T. Exogenous N-Acetylglucosamine Increases Hyaluronan Production in Cultured Human Dermal Fibroblasts. *Arch. Dermatol. Res.* **2009**, *301* (7), 549–551. https://doi.org/10.1007/s00403-009-0932-z.
(331) Mahoney, D. E.; Hiebert, J. B.; Thimmesch, A.; Pierce, J. T.; Vacek, J. L.; Clancy, R. L.; Sauer, A. J.; Pierce, J. D. Understanding D-Ribose and Mitochondrial Function. *Adv. Biosci. Clin. Med.* **2018**, *6* (1), 1–5. https://doi.org/10.7575/aiac.abcmed.v.6n.1p.1.
(332) Shecterle, L. M.; Terry, K. R.; St. Cyr, J. A. Potential Clinical Benefits of D-Ribose in Ischemic Cardiovascular Disease. *Cureus* **2018**, *10* (3), e2291. https://doi.org/10.7759/cureus.2291.
(333) Jones, K.; Probst, Y. Role of Dietary Modification in Alleviating Chronic Fatigue Syndrome Symptoms: A Systematic Review. *Aust. N. Z. J. Public Health* **2017**, *41* (4), 338–344. https://doi.org/10.1111/1753-6405.12670.

6 Appendix

6.1 Supplemental Figures and Tables

6.1.1 Supplemental Figures

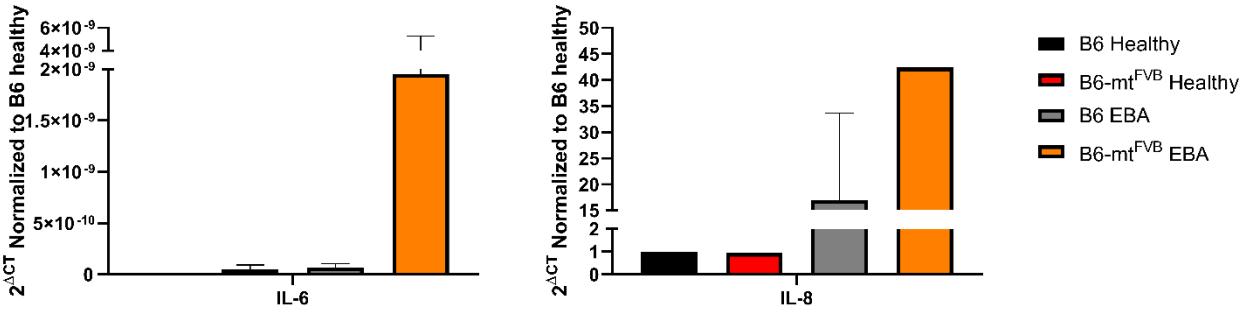

Supplemental Figure 1: Cytokine expression of IL-6 and IL-8 in small intestine of healthy and diseased B6 and B6-mt^{FVB} mice. Healthy B6 mice are shown in black, diseased mice are shown in grey. Healthy B6-mt^{FVB} mice are shown in red, diseased mice are shown in orange. Error bars indicate standard deviation to the mean. (n = 3)

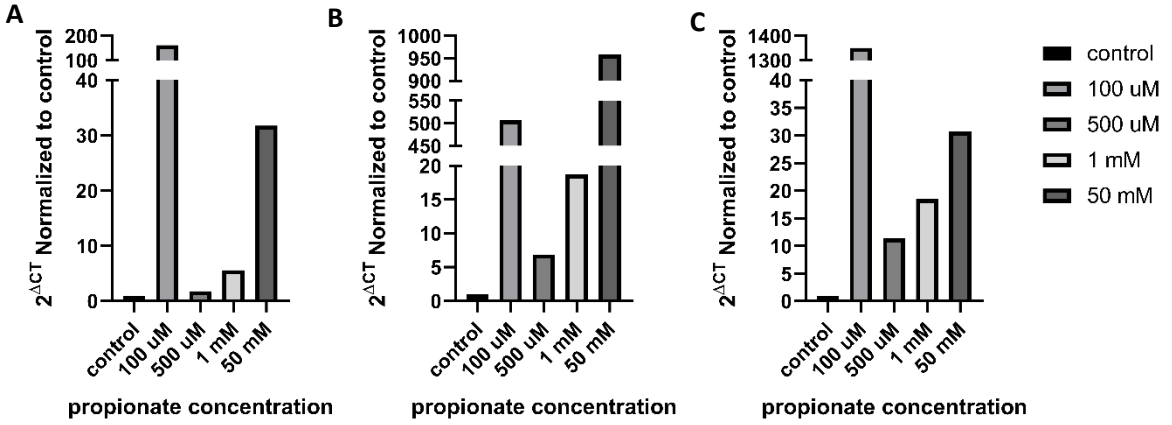

Supplemental Figure 2: Expression of IL-8, TNFα and GLP1 upon stimulation with propionate. Shown are the expression patterns of A) IL-8, B) TNFα and C) GLP-1. On the x-axis different propionate concentrations are shown with control equals no propionate.

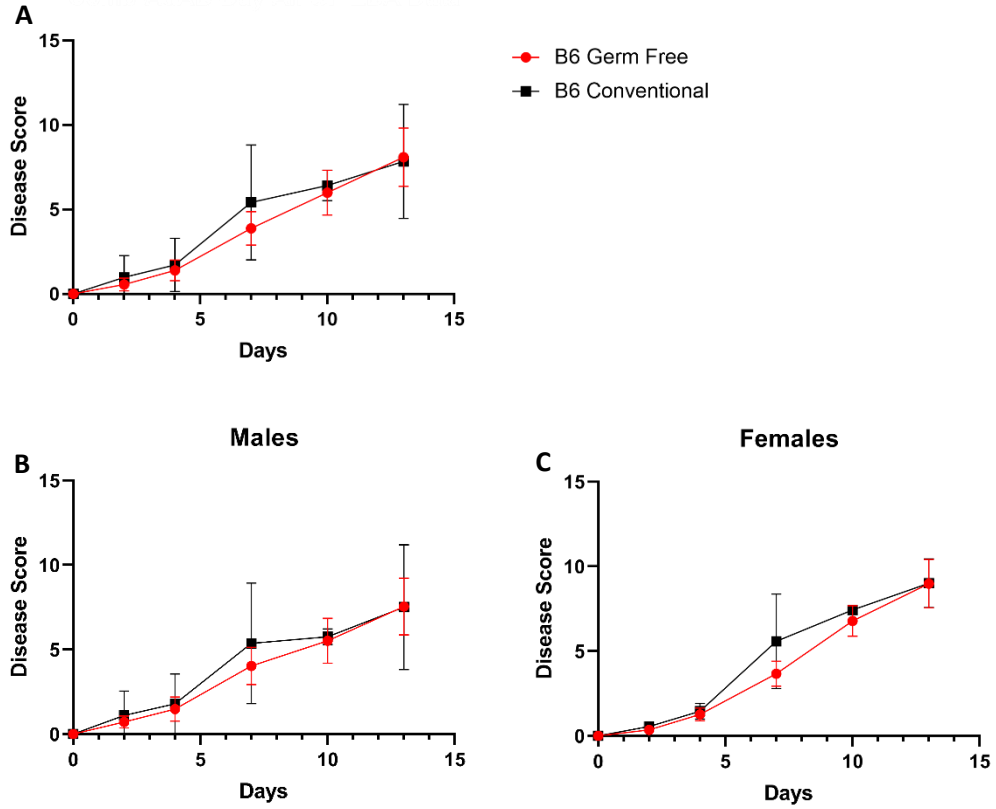

Supplemental Figure 3: EBA in germ-free versus conventional housed B6J mice. Mice were injected with 3 mg total IgG on days 0, 2 and 4 and weighed and scored under anesthesia. Shown are the results from both sexes together (A), males (B) and females (C). Error bars indicate standard deviation to the mean. (Conventional housed mice: males n = 17, females n = 5; germ-free housed mice: males n = 21, females n = 13)

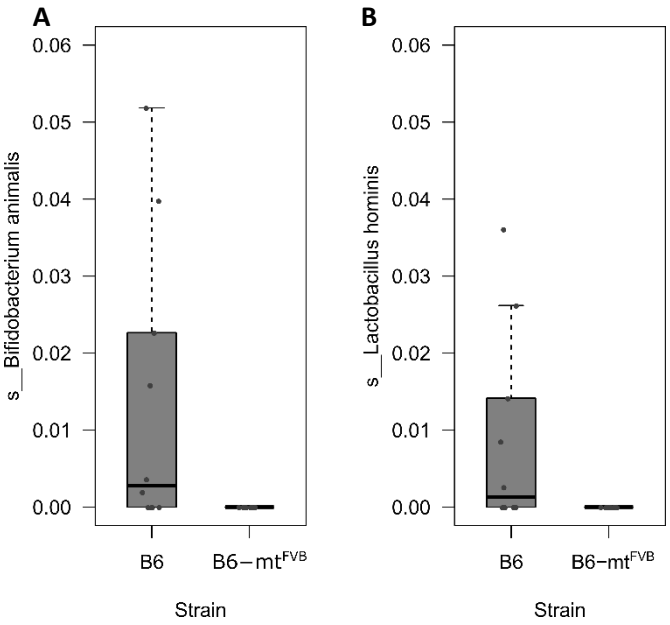

Supplemental Figure 4: Abundance pattern of significantly different abundant species in cecum content of B6 and B6-mt^{FVB} mice ($p < 0.05$). A) Bifidobaterium animalis, B) Lactobacillus hominis.

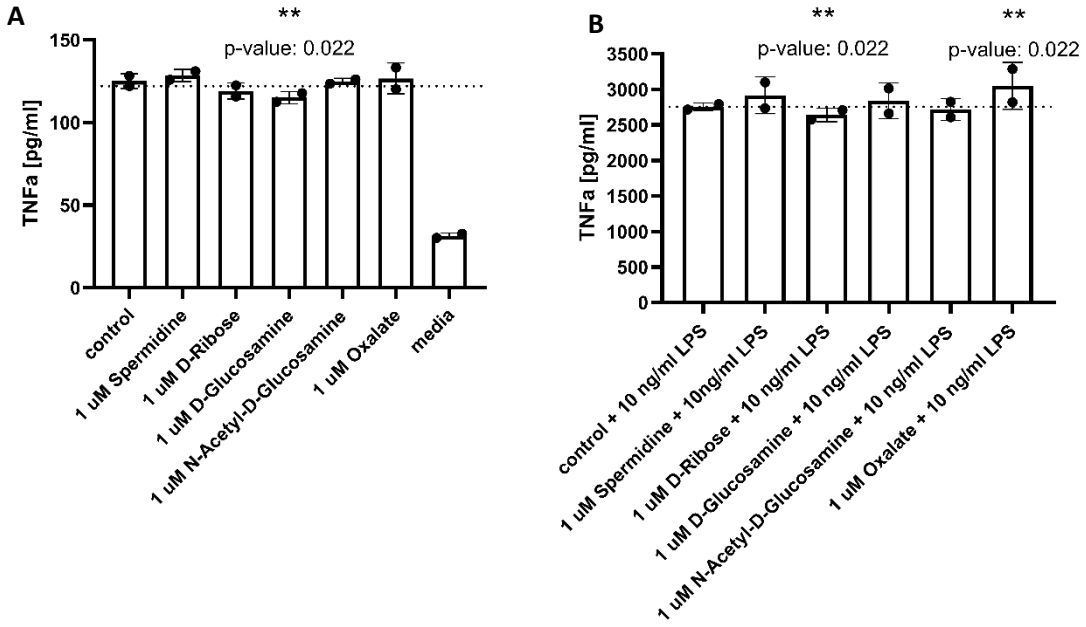

*Supplemental Figure 5: TNFα production of metabolite and LPS treated RAW 264.7 cell macrophages. The macrophages were treated with 1 µM of the respective metabolite A) and together with 10 ng/ml LPS B) over night and the supernatants were used for the TNFα ELISA. Error bars indicate standard deviation to the mean. (Mann-Whitney test, **p = 0.022, n = 2 in triplicates).*

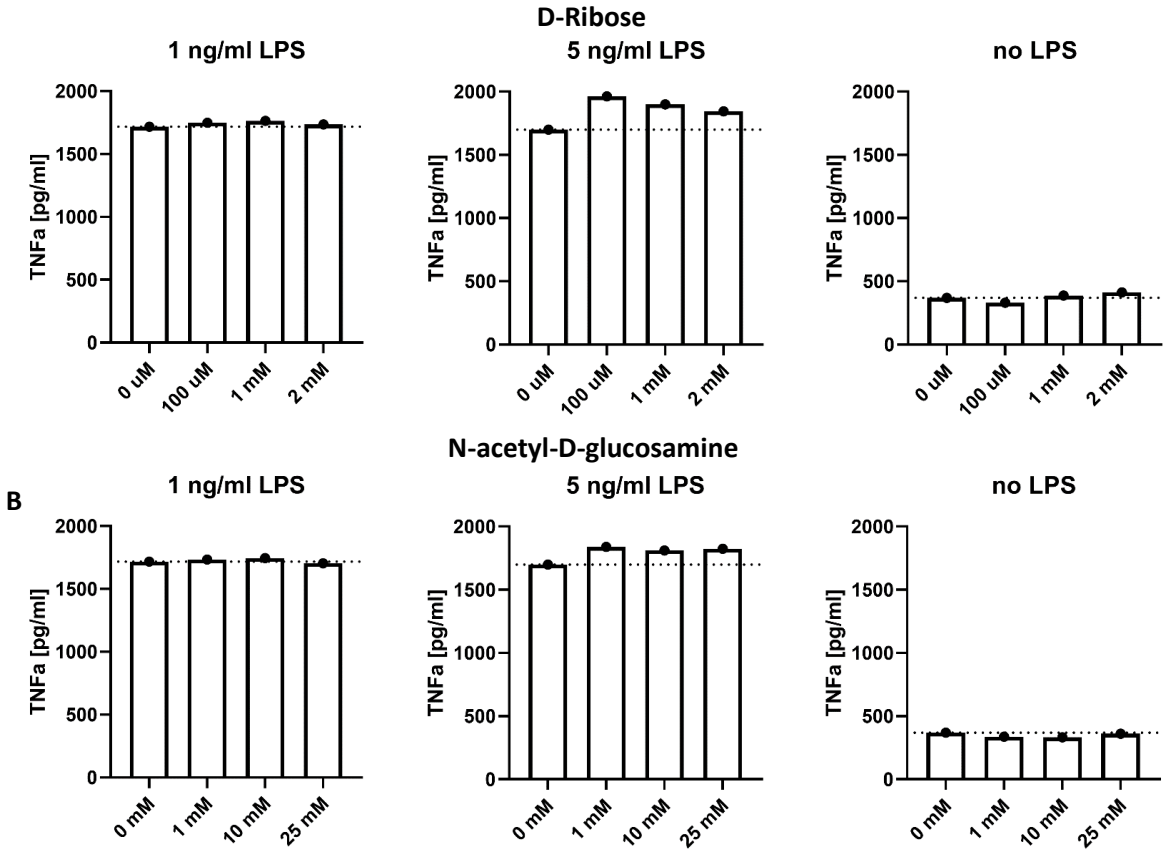

Supplemental Figure 6: TNFa production upon stimulation with different metabolite and LPS concentrations. The macrophages were treated with different concentrations of A) D-Ribose and B) N-acetyl-D-Glucosamine, together with 0 ng/ml, 1 ng/ml and 5 ng/ml LPS overnight. The supernatants were used for the TNFα ELISA.

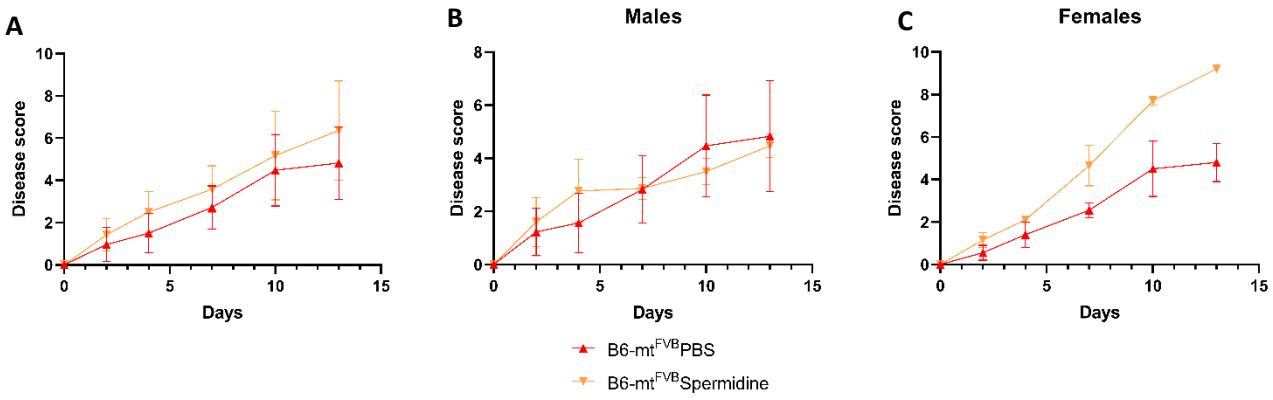

Supplemental Figure 7: EBA disease score in B6-mt^{FVB} mice during Spermidine treatment. A) shows the results of both sexes combined (5 mice per group), B) shows the results for males (3 mice per group) and C) for females (2 mice per group). Mice treated with Spermidine are displayed in orange, control mice treated with PBS are displayed in red. Mice were treated with 5 mg/kg spermidine or PBS as a control on day 0, 2 and 4. Error bars indicate standard deviation to the mean. (Mann-Whitney test, n = 2)

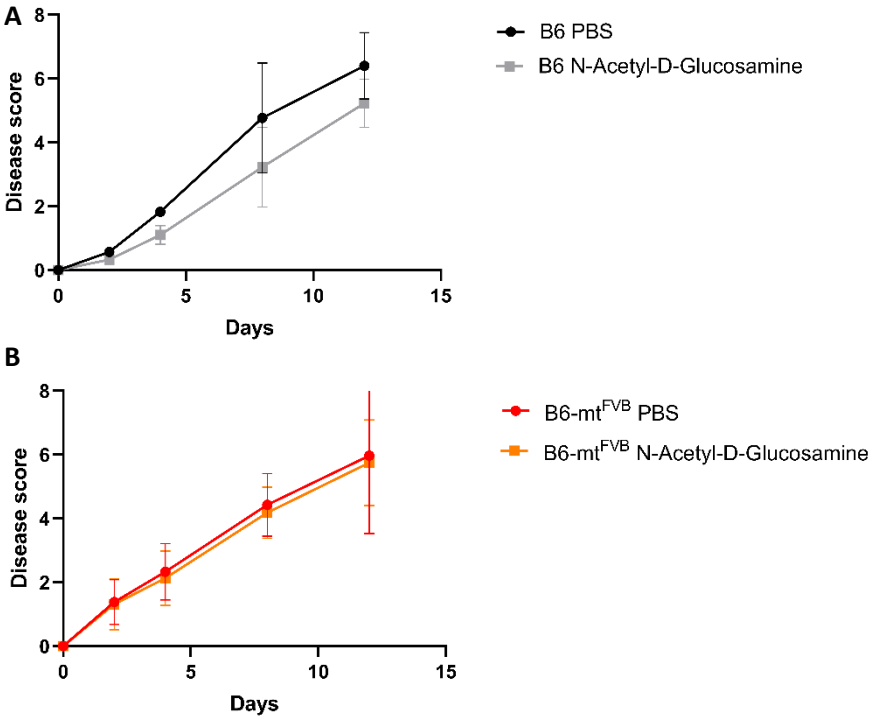

Supplemental Figure 8: EBA disease development during N-acetyl-D-glucosamine (NAG) treatment in B6 females and B6-mt^{FVB} males. A) shows disease development in female B6 (black: control, grey: NAG; n = 3); B) shows disease development in male B6-mt^{FVB} mice (red: control, n = 7; orange: NAG, n = 6). Mice were injected daily with NAG or PBS starting 1 week before onset of disease. Error bars indicate standard deviation to the mean.

6.1.2 Supplemental Tables

Supplemental Table 1: Significantly different abundant metabolites enriched in liver tissue of B6 and B6-mt^{FVB} mice. KEGG database was used for entries. (Limma, n = 4).

KEGG.id	Entry.type	KEGG.name	p.score	Enriched in
mmu04142	pathway	Lysosome - Mus musculus (mouse)	0.008889	B6-mt^{FVB}
mmu05231	pathway	Choline metabolism in cancer - Mus musculus (...	0.00439	B6-mt^{FVB}
M00133	module	Polyamine biosynthesis, arginine => agmatine ...	0.008489	B6-mt^{FVB}
M00368	module	Ethylene biosynthesis, methionine => ethylene	0.00519	B6-mt^{FVB}
2.4.1.90	enzyme	N-acetyllactosamine synthase	0.00369	B6-mt^{FVB}
2.4.2.1	enzyme	purine-nucleoside phosphorylase	0.008689	B6-mt^{FVB}
2.4.2.28	enzyme	S-methyl-5'-thioadenosine phosphorylase	0.00349	B6-mt^{FVB}
2.5.1.16	enzyme	spermidine synthase	0.00449	B6-mt^{FVB}
2.5.1.22	enzyme	spermine synthase	0.00439	B6-mt^{FVB}
2.7.1.59	enzyme	N-acetylglucosamine kinase	0.00179	B6-mt^{FVB}
3.1.1.5	enzyme	lysophospholipase	0.00049	B6-mt^{FVB}
3.1.22.1	enzyme	deoxyribonuclease II	0.008889	B6-mt^{FVB}
3.1.4.2	enzyme	glycerophosphocholine phosphodiesterase	0.00029	B6-mt^{FVB}
3.1.4.45	enzyme	N-acetylglucosamine-1-phosphodiester alpha-N-...	9E-05	B6-mt^{FVB}
3.10.1.1	enzyme	N-sulfoglucosamine sulfohydrolase	0.006889	B6-mt^{FVB}
3.2.1.14	enzyme	chitinase	0.00319	B6-mt^{FVB}
3.2.1.169	enzyme	protein O-GlcNAcase	0.00169	B6-mt^{FVB}
3.2.1.50	enzyme	alpha-N-acetylglucosaminidase	0.00019	B6-mt^{FVB}
3.2.1.52	enzyme	beta-N-acetylhexosaminidase	0.00259	B6-mt^{FVB}
3.3.2.2	enzyme	lysoplasmalogenase	0.00349	B6-mt^{FVB}
3.4.14.9	enzyme	tripeptidyl-peptidase I	0.008889	B6-mt^{FVB}
3.4.23.34	enzyme	cathepsin E	0.008889	B6-mt^{FVB}
5.1.3.8	enzyme	N-acylglucosamine 2-epimerase	0.00279	B6-mt^{FVB}
5.3.1.23	enzyme	S-methyl-5-thioribose-1-phosphate isomerase	0.008889	B6-mt^{FVB}
5.4.2.3	enzyme	phosphoacetylglucosamine mutase	0.008689	B6-mt^{FVB}
R00022	reaction	chitobiose N-acetylglucosaminohydrolase	0.00169	B6-mt^{FVB}
R00178	reaction	S-adenosyl-L-methionine carboxy-lyase [S-aden...	0.00439	B6-mt^{FVB}
R00179	reaction	S-adenosyl-L-methionine methylthioadenosine-l...	0.00199	B6-mt^{FVB}
R00273	reaction	oxalate:oxygen oxidoreductase	0.00429	B6-mt^{FVB}
R00466	reaction	Glyoxylate:oxygen oxidoreductase	0.008689	B6-mt^{FVB}
R00522	reaction	Oxalate carboxy-lyase	0.005989	B6-mt^{FVB}
R00631	reaction	aldehyde:NAD+ oxidoreductase	0.00509	B6-mt^{FVB}
R00646	reaction	Ascorbate + Oxygen + H2O <=> Threonate + Oxal...	0.00149	B6-mt^{FVB}
R00997	reaction	1-aminocyclopropane-1-carboxylate aminohydrol...	0.005889	B6-mt^{FVB}
R01030	reaction	sn-Glycero-3-phosphocholine glycerophosphohyd...	0.00359	B6-mt^{FVB}
R01200	reaction	N-Acetyl-D-Glucosamine amidohydrolase	0.00159	B6-mt^{FVB}
R01201	reaction	ATP:N-acetyl-D-Glucosamine 6-phosphotransfera...	0.00189	B6-mt^{FVB}
R01204	reaction	Acetyl-CoA:D-Glucosamine N-acetyltransferase	0.00169	B6-mt^{FVB}
R01206	reaction	[1,4-(N-Acetyl-beta-D-glucosaminyl)]n glycano...	0.00309	B6-mt^{FVB}
R01207	reaction	N-acetyl-D-Glucosamine 2-epimerase	0.00269	B6-mt^{FVB}
R01401	reaction	methylthioadenosine methylthioribohydrolase	0.00129	B6-mt^{FVB}
R01402	reaction	S-methyl-5'-thioadenosine:phosphate S-methyl-...	0.00239	B6-mt^{FVB}

R01470	reaction	sn-Glycero-3-phosphoethanolamine glycerophosp...	0.00039	B6-mt^{FVB}
R01558	reaction	oxalate:CoA ligase (AMP-forming)	0.005689	B6-mt^{FVB}
R01559	reaction	Succinyl-CoA:oxalate CoA-transferase	0.007989	B6-mt^{FVB}
R01561	reaction	adenosine:phosphate alpha-D-ribosyltransferas...	0.006389	B6-mt^{FVB}
R01676	reaction	Guanine aminohydrolase	0.008789	B6-mt^{FVB}
R01920	reaction	S-adenosylmethioninamine:putrescine 3-aminopr...	0.00249	B6-mt^{FVB}
R01966	reaction	beta-D-glucosaminide glucosaminohydrolase	0.007589	B6-mt^{FVB}
R02053	reaction	phosphatidylethanolamine 2-acylhydrolase	0.00359	B6-mt^{FVB}
R02054	reaction	phosphatidylethanolamine 1-acylhydrolase	0.00409	B6-mt^{FVB}
R02141	reaction	Xanthine + H2O <=> 5-Ureido-4-imidazole carbo...	0.006189	B6-mt^{FVB}
R02143	reaction	Xanthosine ribohydrolase	0.00089	B6-mt^{FVB}
R02297	reaction	Xanthosine:orthophosphate ribosyltransferase	0.00069	B6-mt^{FVB}
R02333	reaction	Chitin amidohydrolase	0.008189	B6-mt^{FVB}
R02334	reaction	[1,4-(N-Acetyl-beta-D-glucosaminyl)]n glycano...	0.00509	B6-mt^{FVB}
R02705	reaction	ATP:N-acyl-D-mannosamine 6-phosphotransferase	0.007389	B6-mt^{FVB}
R02719	reaction	xanthosine 5'-phosphate phosphohydrolase	0.00099	B6-mt^{FVB}
R02720	reaction	XTP pyrophosphohydrolase	0.005989	B6-mt^{FVB}
R02745	reaction	1-(1-alkenyl)-sn-glycero-3-phosphocholine ald...	0.00409	B6-mt^{FVB}
R02746	reaction	1-Acyl-sn-glycero-3-phosphocholine acylhydrol...	0.008289	B6-mt^{FVB}
R02869	reaction	S-adenosylmethioninamine:spermidine 3-aminopr...	0.00399	B6-mt^{FVB}
R03072	reaction	S-Adenosyl-L-methionine:nocardicin-E 3-amino-...	0.005789	B6-mt^{FVB}
R03073	reaction	nocardicin-A epimerase	0.008589	B6-mt^{FVB}
R03415	reaction	1-(1-alkenyl)-sn-glycero-3-phosphoethanolamin...	0.00119	B6-mt^{FVB}
R03416	reaction	1-Acyl-sn-glycero-3-phosphoethanolamine aldeh...	0.00179	B6-mt^{FVB}
R03417	reaction	L-2-Lysophosphatidylethanolamine aldehydohydr...	0.00169	B6-mt^{FVB}
R03733	reaction	L-Threonate:NAD+ 3-oxidoreductase	0.00369	B6-mt^{FVB}
R04143	reaction	ATP:S5-methyl-5-thio-D-ribose 1-phosphotransf...	0.006689	B6-mt^{FVB}
R04420	reaction	5-methylthio-5-deoxy-D-ribose-1-phosphate ket...	0.008689	B6-mt^{FVB}
R04480	reaction	Acyl-CoA:1-acyl-sn-glycero-3-phosphoethanolam...	0.00449	B6-mt^{FVB}
R04864	reaction	2-Acyl-sn-glycero-3-phosphoethanolamine O-acy...	0.006389	B6-mt^{FVB}
R05199	reaction	protein-N(pi)-phosphohistidine:N-acetyl-D-glu...	0.00259	B6-mt^{FVB}
R05332	reaction	Acetyl-CoA:D-Glucosamine-1-phosphate N-acetyl...	0.006989	B6-mt^{FVB}
R05963	reaction	H2O + Globoside <=> N-Acetyl-D-galactosamine ...	0.00369	B6-mt^{FVB}
R06004	reaction	GM2 + H2O <=> GM3 + N-Acetyl-D-galactosamine	0.00369	B6-mt^{FVB}
R07392	reaction	S-methyl-5-thio-D-ribulose-1-phosphate hydro-...	0.008889	B6-mt^{FVB}
R07809	reaction	G13074 + H2O <=> G01391 + N-Acetyl-D-glucosam...	0.00049	B6-mt^{FVB}
R07810	reaction	G13073 + H2O <=> G01391 + N-Acetyl-D-glucosam...	0.00259	B6-mt^{FVB}
R07816	reaction	G13038 + H2O <=> G13039 + N-Acetyl-D-glucosam...	0.00039	B6-mt^{FVB}
R07917	reaction	S-adenosyl-L-methionine:xanthosine N7-methylt...	0.00169	B6-mt^{FVB}
R07918	reaction	7-methylxanthosine ribohydrolase	0.00429	B6-mt^{FVB}
R08193	reaction	N-Acetyl-D-Glucosamine 1-phosphate 1,6-phosph...	0.008489	B6-mt^{FVB}
R08359	reaction	S-adenosylmethioninamine:cadaverine 3-aminopr...	0.005789	B6-mt^{FVB}
R08940	reaction	acyl-[acyl-carrier protein]:S-adenosyl-L-meth...	0.00249	B6-mt^{FVB}

R08968	reaction	ATP:N-acetyl-D-Glucosamine 1-phosphotransfera...	0.00179	B6-mt^{FVB}
R09072	reaction	S-adenosyl-L-methionine:1,2-diacyl-sn-glycero...	0.00199	B6-mt^{FVB}
R09073	reaction	S-adenosylmethionine:diacylglycerylhomoserine...	0.00329	B6-mt^{FVB}
R09076	reaction	spermidine:oxygen oxidoreductase (spermidine-...	0.008189	B6-mt^{FVB}
R09323	reaction	G13057 + H2O <=> N-Acetyl-D-Glucosamine + G13...	0.00049	B6-mt^{FVB}
R09660	reaction	S-methyl-5'-thioadenosine amidohydrolase	0.00189	B6-mt^{FVB}
R09668	reaction	S-methyl-5'-thioinosine:phosphate S-methyl-5-...	0.00559	B6-mt^{FVB}
R09942	reaction	N,N'-diacetylchitobiose:phosphate N-acetyl-D-...	0.00269	B6-mt^{FVB}
R10831	reaction	G00711 + H2O <=> G10008 + N-Acetyl-D-glucosam...	0.00049	B6-mt^{FVB}
R10881	reaction	S-adenosyl-L-methionine:nocardicin-G 3-amino-...	0.00489	B6-mt^{FVB}
R10882	reaction	Nocardicin-C,NADPH:oxygen oxidoreductase	0.008789	B6-mt^{FVB}
R10883	reaction	nocardicin-C epimerase	0.008589	B6-mt^{FVB}
R10903	reaction	Nocardicin G <=> Nocardicin E	0.008089	B6-mt^{FVB}
R11317	reaction	G05477 + H2O <=> G10920 + N-Acetyl-D-glucosam...	0.00049	B6-mt^{FVB}
R11617	reaction	oxamate amidohydrolase	0.00489	B6-mt^{FVB}
C00071	compound	Aldehyde	0.006889	B6-mt^{FVB}
C00093	compound	sn-Glycerol 3-phosphate	0.006589	B6-mt^{FVB}
C00121	compound	D-Ribose	0.008889	B6-mt^{FVB}
C00140	compound	N-Acetyl-D-Glucosamine	0.00049	B6-mt^{FVB}
C00162	compound	Fatty acid	0.006489	B6-mt^{FVB}
C00170	compound	5'-Methylthioadenosine	0.00029	B6-mt^{FVB}
C00209	compound	Oxalate	0.00439	B6-mt^{FVB}
C00315	compound	Spermidine	0.007989	B6-mt^{FVB}
C00329	compound	D-Glucosamine	0.00479	B6-mt^{FVB}
C00357	compound	N-Acetyl-D-Glucosamine 6-phosphate	0.006189	B6-mt^{FVB}
C00385	compound	Xanthine	0.00409	B6-mt^{FVB}
C00461	compound	Chitin	0.00529	B6-mt^{FVB}
C00645	compound	N-Acetyl-D-mannosamine	0.00509	B6-mt^{FVB}
C00655	compound	Xanthosine 5'-phosphate	0.00429	B6-mt^{FVB}
C00670	compound	sn-Glycero-3-phosphocholine	0.006489	B6-mt^{FVB}
C00700	compound	XTP	0.006789	B6-mt^{FVB}
C00734	compound	Chitosan	0.008889	B6-mt^{FVB}
C00750	compound	Spermine	0.006989	B6-mt^{FVB}
C00927	compound	Isonocardicin A	0.006389	B6-mt^{FVB}
C01137	compound	S-Adenosylmethioninamine	0.00499	B6-mt^{FVB}
C01233	compound	sn-Glycero-3-phosphoethanolamine	0.00079	B6-mt^{FVB}
C01234	compound	1-Aminocyclopropane-1-carboxylate	0.00409	B6-mt^{FVB}
C01620	compound	Threonate	0.00149	B6-mt^{FVB}
C01672	compound	Cadaverine	0.007989	B6-mt^{FVB}
C01674	compound	Chitobiose	0.00359	B6-mt^{FVB}
C01739	compound	Nocardicin E	0.007189	B6-mt^{FVB}
C01762	compound	Xanthosine	0.00069	B6-mt^{FVB}
C01941	compound	Nocardicin A	0.008589	B6-mt^{FVB}
C03064	compound	3-Dehydro-L-threonate	0.00369	B6-mt^{FVB}

C03089	compound	5-Methylthio-D-ribose	0.00349	B6-mt^{FVB}
C04132	compound	N-Acetyl-D-Glucosamine 6-sulfate	0.00259	B6-mt^{FVB}
C04188	compound	S-Methyl-5-thio-D-ribose 1-phosphate	0.006689	B6-mt^{FVB}
C04438	compound	1-Acyl-sn-glycero-3-phosphoethanolamine	0.00149	B6-mt^{FVB}
C04501	compound	N-Acetyl-alpha-D-Glucosamine 1-phosphate	0.00539	B6-mt^{FVB}
C04517	compound	1-(1-Alkenyl)-sn-glycero-3-phosphocholine	0.006889	B6-mt^{FVB}
C04582	compound	S-Methyl-5-thio-D-ribulose 1-phosphate	0.008689	B6-mt^{FVB}
C04635	compound	1-(1-Alkenyl)-sn-glycero-3-phosphoethanolamin...	0.005789	B6-mt^{FVB}
C05515	compound	5-Ureido-4-imidazole carboxylate	0.008389	B6-mt^{FVB}
C05973	compound	2-Acyl-sn-glycero-3-phosphoethanolamine	0.00149	B6-mt^{FVB}
C06023	compound	D-Glucosaminide	0.007889	B6-mt^{FVB}
C06156	compound	alpha-D-Glucosamine 1-phosphate	0.007889	B6-mt^{FVB}
C16352	compound	7-Methylxanthosine	0.00179	B6-mt^{FVB}
C16565	compound	Aminopropylcadaverine	0.007789	B6-mt^{FVB}
C17351	compound	Nocardicin C	0.008589	B6-mt^{FVB}
C17352	compound	Isonocardicin C	0.007089	B6-mt^{FVB}
C17355	compound	Nocardicin G	0.008289	B6-mt^{FVB}
C18049	compound	N-Acyl-L-homoserine lactone	0.00249	B6-mt^{FVB}
C18168	compound	Diacylglycerylhomoserine	0.00199	B6-mt^{FVB}
C18169	compound	Diacylglyceryl-N,N,N-trimethylhomoserine	0.00329	B6-mt^{FVB}
C19787	compound	5'-S-Methyl-5'-thioinosine	0.00309	B6-mt^{FVB}
mmu04630	pathway	JAK-STAT signaling pathway - Mus musculus (mo...	0.011189	B6
mmu04977	pathway	Vitamin digestion and absorption - Mus muscul...	0.009689	B6
M00119	module	Pantothenate biosynthesis, valine/L-aspartate...	0.009689	B6
1.13.11.19	enzyme	cysteamine dioxygenase	0.008889	B6
1.13.11.34	enzyme	arachidonate 5-lipoxygenase	0.00359	B6
1.14.14.94	enzyme	leukotriene-B4 20-monooxygenase	0.010389	B6
1.14.16.4	enzyme	tryptophan 5-monooxygenase	0.00209	B6
1.2.3.1	enzyme	aldehyde oxidase	0.00459	B6
1.4.3.5	enzyme	pyridoxal 5'-phosphate synthase	0.009989	B6
2.1.1.1	enzyme	nicotinamide N-methyltransferase	0.011689	B6
2.5.1.151	enzyme	alkylcobalamin dealkylase	0.009689	B6
3.3.2.6	enzyme	leukotriene-A4 hydrolase	0.00099	B6
3.4.19.13	enzyme	glutathione gamma-glutamate hydrolase	0.007989	B6
3.4.19.14	enzyme	leukotriene-C4 hydrolase	0.006489	B6
3.5.1.92	enzyme	pantetheine hydrolase	0.007489	B6
3.5.4.3	enzyme	guanine deaminase	0.00539	B6
4.1.1.11	enzyme	aspartate 1-decarboxylase	0.007389	B6
4.1.1.15	enzyme	glutamate decarboxylase	0.008289	B6
4.1.1.28	enzyme	aromatic-L-amino-acid decarboxylase	0.010889	B6
4.1.1.29	enzyme	sulfinoalanine decarboxylase	0.007789	B6
4.4.1.20	enzyme	leukotriene-C4 synthase	0.00029	B6
R00021	reaction	L-glutamate:ferredoxin oxidoreductase (transa...	0.00359	B6
R00093	reaction	L-glutamate:NAD+ oxidoreductase (transaminati...	0.00349	B6
R00114	reaction	L-glutamate:NADP+ oxidoreductase (transaminat...	0.00359	B6
R00173	reaction	pyridoxal-5'-phosphate phosphohydrolase	0.00389	B6
R00174	reaction	ATP:pyridoxal 5'-phosphotransferase	0.00379	B6

R00253	reaction	L-Glutamate:ammonia ligase (ADP-forming)	0.00319	B6
R00256	reaction	L-glutamine amidohydrolase	0.00309	B6
R00257	reaction	Deamido-NAD+:L-glutamine amido-ligase (AMP-fo...	0.00539	B6
R00277	reaction	pyridoxamine-5'-phosphate:oxygen oxidoreducta...	0.011489	B6
R00494	reaction	glutathione gamma-glutamylaminopeptidase	0.008289	B6
R00527	reaction	S-Formylglutathione hydrolase	0.010289	B6
R00573	reaction	UTP:L-glutamine amido-ligase (ADP-forming)	0.008089	B6
R00575	reaction	HCO3-:L-glutamine amido-ligase (ADP-forming, ...	0.012989	B6
R00576	reaction	L-Glutamine:pyruvate aminotransferase	0.009189	B6
R00578	reaction	L-aspartate:L-glutamine amido-ligase (AMP-for...	0.008589	B6
R00579	reaction	glutamine racemase	0.011089	B6
R00768	reaction	L-glutamine:D-fructose-6-phosphate isomerase ...	0.011989	B6
R00801	reaction	sucrose glucohydrolase	0.006089	B6
R00803	reaction	sucrose:phosphate alpha-D-glucosyltransferase	0.00309	B6
R00805	reaction	sucrose-6F-phosphate phosphohydrolase	0.006589	B6
R00806	reaction	UDP-glucose:D-fructose 2-alpha-D-glucosyltran...	0.00309	B6
R00807	reaction	Sucrose:(acceptor) 3-oxidoreductase	0.006489	B6
R00811	reaction	protein-Npi-phospho-L-histidine:sugar phospho...	0.006989	B6
R01021	reaction	ATP:choline phosphotransferase	0.009589	B6
R01072	reaction	5-phosphoribosylamine:diphosphate phospho-alp...	0.008989	B6
R01103	reaction	Raffinose galactohydrolase	0.00539	B6
R01269	reaction	S-Adenosyl-L-methionine:nicotinamide N-methyl...	0.007189	B6
R01580	reaction	Pyridoxamine-5'-phosphate:2-oxoglutarate amin...	0.012989	B6
R01595	reaction	Arachidonate:oxygen 5-oxidoreductase	0.00369	B6
R01676	reaction	Guanine aminohydrolase	0.00529	B6
R01681	reaction	hypotaurine:NAD+ oxidoreductase	0.00419	B6
R01682	reaction	3-Sulfo-L-alanine carboxy-lyase (taurine-form...	0.00339	B6
R01684	reaction	taurine:2-oxoglutarate aminotransferase	0.00449	B6
R01685	reaction	taurine:ferricytochrome-c oxidoreductase (dea...	0.005889	B6
R01686	reaction	L-arginine:taurine amidinotransferase	0.011789	B6
R01687	reaction	(5-L-glutamyl)-peptide:taurine 5-glutamyltran...	0.010189	B6
R01707	reaction	pyridoxal:NAD+ 4-oxidoreductase	0.00509	B6
R01708	reaction	Pyridoxine:NADP+ 4-oxidoreductase	0.00539	B6
R01709	reaction	pyridoxal:oxygen 4-oxidoreductase	0.00279	B6
R01710	reaction	pyridoxamine:oxygen oxidoreductase (deaminati...	0.00349	B6
R01711	reaction	pyridoxine:oxygen oxidoreductase (deaminating...	0.00399	B6
R01712	reaction	pyridoxamine:pyruvate aminotransferase	0.00299	B6
R01713	reaction	Pyridoxamine:oxaloacetate aminotransferase	0.00329	B6
R01768	reaction	hypoxanthine:NAD+ oxidoreductase	0.005689	B6
R01769	reaction	Hypoxanthine:oxygen oxidoreductase	0.00479	B6
R01814	reaction	L-Tryptophan,tetrahydrobiopterin:oxygen oxido...	0.00259	B6
R01823	reaction	Sucrose:1,4-alpha-D-glucan 4-alpha-D-glucosyl...	0.007089	B6
R01917	reaction	gamma-L-glutamyl-L-cysteinyl-glycine:spermidi...	0.010089	B6
R01918	reaction	gamma-L-glutamyl-L-cysteinyl-glycine:spermidi...	0.009589	B6
R02037	reaction	S-Adenosyl-L-methionine:ethanolamine-phosphat...	0.010689	B6
R02103	reaction	xanthine:NAD+ oxidoreductase	0.005889	B6

R02107	reaction	Xanthine:oxygen oxidoreductase	0.00489	B6
R02120	reaction	Sucrose:1,6-alpha-D-glucan 6-alpha-D-glucosyl...	0.009289	B6
R02141	reaction	Xanthine + H2O <=> 5-Ureido-4-imidazole carbo...	0.006089	B6
R02142	reaction	XMP:pyrophosphate phosphoribosyltransferase	0.006189	B6
R02143	reaction	Xanthosine ribohydrolase	0.008889	B6
R02297	reaction	Xanthosine:orthophosphate ribosyltransferase	0.009089	B6
R02411	reaction	1-alpha-D-Galactosyl-myo-inositol:sucrose 6-a...	0.012989	B6
R02467	reaction	Cysteamine:oxygen oxidoreductase	0.008889	B6
R02473	reaction	(R)-Pantoate:beta-alanine ligase (AMP-forming...	0.006089	B6
R02474	reaction	Pantothenate amidohydrolase	0.006189	B6
R02493	reaction	ATP:pyridoxal 5'-phosphotransferase	0.007489	B6
R02494	reaction	pyridoxamine-5'-phosphate phosphohydrolase	0.007889	B6
R02530	reaction	(R)-S-Lactoylglutathione methylglyoxal-lyase ...	0.008589	B6
R02576	reaction	Phenylacetyl-CoA:L-glutamine alpha-N-phenylac...	0.012189	B6
R02700	reaction	5-Hydroxy-L-tryptophan:2-oxoglutarate aminotr...	0.005689	B6
R02701	reaction	5-Hydroxy-L-tryptophan decarboxy-lyase	0.00249	B6
R02702	reaction	5-hydroxy-L-tryptophan:oxygen 2,3-dioxygenase...	0.006089	B6
R02797	reaction	Taurocholate amidohydrolase	0.009289	B6
R02895	reaction	D-Proline + L-Glutamine <=> Linatine	0.009089	B6
R02973	reaction	(R)-pantetheine amidohydrolase	0.007189	B6
R02992	reaction	4-pyridoxolactone lactonohydrolase	0.009289	B6
R03018	reaction	ATP:pantothenate 4'-phosphotransferase	0.006089	B6
R03057	reaction	(7E,9E,11Z,14Z)-(5S,6S)-5,6-Epoxyicosa-7,9,11...	0.00039	B6
R03058	reaction	arachidonate:oxygen 5-oxidoreductase	0.00039	B6
R03059	reaction	(7E,9E,11Z,14Z)-(5S,6S)-5,6-Epoxyicosa-7,9,11...	9E-05	B6
R03652	reaction	L-Glutamine:tRNA(Gln) ligase (AMP-forming)	0.013089	B6
R03720	reaction	Choloyl-CoA:glycine N-choloyltransferase	0.009589	B6
R03785	reaction	ATP:taurocyamine N-phosphotransferase	0.009089	B6
R03866	reaction	(6Z,8E,10E,14Z)-(5S,12R)-5,12-dihydroxyicosa-...	0.007889	B6
R03905	reaction	Glu-tRNA(Gln):L-glutamine amido-ligase(ADP-fo...	0.012789	B6
R03927	reaction	Pantothenate + 2 Reduced acceptor <=> Pantoth...	0.006389	B6
R03977	reaction	chenodeoxycholoyltaurine amidohydrolase	0.008489	B6
R04085	reaction	Aldehyde:oxygen oxidoreductase	0.007489	B6
R04194	reaction	Sucrose:2,1-beta-D-fructan 1-beta-D-fructosyl...	0.00559	B6
R04212	reaction	Asp-tRNA(Asn):L-glutamine amido-ligase (ADP-f...	0.011789	B6
R04734	reaction	4a-hydroxytetrahydrobiopterin hydro-lyase	0.012789	B6
R05140	reaction	sucrose:2,6-beta-D-fructan 6-beta-D-fructosyl...	0.009289	B6
R05320	reaction	Taurine, 2-oxoglutarate:O2 oxidoreductase (su...	0.006089	B6
R05652	reaction	taurine:pyruvate aminotransferase	0.00459	B6
R05815	reaction	cobyrinate:L-glutamine amido-ligase (ADP-form...	0.013689	B6
R05839	reaction	pyridoxamine:2-oxoglutarate aminotransferase	0.00559	B6
R06868	reaction	S-Adenosyl-L-methionine:methylethanolamine ph...	0.007089	B6
R06869	reaction	S-Adenosyl-L-methionine:phosphodimethylethano...	0.00419	B6
R06871	reaction	Phosphocholine phosphohydrolase	0.009989	B6
R06982	reaction	S-(hydroxymethyl)glutathione formaldehyde-lya...	0.008989	B6
R07034	reaction	Glutathione: 5-HPETE oxidoreductase	0.007089	B6

R07213	reaction	L-tryptophan,tetrahydrobiopterin:oxygen oxido...	0.00559	B6
R07456	reaction	D-ribulose 5-phosphate,D-glyceraldehyde 3-pho...	0.006989	B6
R07965	reaction	7-methylxanthine:oxygen oxidoreductase (demet...	0.00539	B6
R07966	reaction	7-methylxanthine:oxygen oxidoreductase (demet...	0.00529	B6
R07967	reaction	3-methylxanthine:oxygen oxidoreductase (N3-de...	0.00529	B6
R07968	reaction	3-methylxanthine:oxygen oxidoreductase (N3-de...	0.00519	B6
R07969	reaction	1-methylxanthine:oxygen oxidoreductase (N1-de...	0.007289	B6
R07970	reaction	1-methylxanthine:oxygen oxidoreductase (N1-de...	0.007189	B6
R08351	reaction	glutathione:glutathionylaminopropylcadaverine...	0.013189	B6
R08353	reaction	glutathione:glutathionylspermine ligase (ADP-...	0.013589	B6
R08355	reaction	glutathione:glutathionylaminopropylcadaverine...	0.013489	B6
R08408	reaction	Aldehyde:oxygen oxidoreductase	0.00209	B6
R08678	reaction	S-sulfanylglutathione:oxygen oxidoreductase	0.013289	B6
R08745	reaction	3alpha,7alpha-dihydroxy-5beta-cholanoyl-CoA:t...	0.009489	B6
R08874	reaction	N-acetylphosphinothricin amidohydrolase	0.008989	B6
R08876	reaction	N-acetylbialaphos amidohydrolase	0.00309	B6
R08938	reaction	acetyl-CoA:phosphinothricin N-acetyltransfera...	0.008889	B6
R09875	reaction	leukotriene-C4 hydrolase	0.006289	B6
R10784	reaction	(2->6)-beta-D-fructanan 6-(beta-D-fructosyl)-...	0.009289	B6
R11309	reaction	Dextran <=> Isomaltose	0.009389	B6
R11311	reaction	Levan <=> Levanbiose	0.009289	B6
R11481	reaction	Bialaphos <=> L-Phosphinothricin	0.00299	B6
C00018	compound	Pyridoxal phosphate	0.012089	B6
C00051	compound	Glutathione	0.00129	B6
C00064	compound	L-Glutamine	0.00309	B6
C00089	compound	Sucrose	0.00319	B6
C00245	compound	Taurine	0.00209	B6
C00250	compound	Pyridoxal	0.00069	B6
C00268	compound	Dihydrobiopterin	0.012889	B6
C00372	compound	Dextran	0.009289	B6
C00385	compound	Xanthine	0.00289	B6
C00519	compound	Hypotaurine	0.008689	B6
C00534	compound	Pyridoxamine	0.00499	B6
C00588	compound	Choline phosphate	0.007289	B6
C00643	compound	5-Hydroxy-L-tryptophan	0.00269	B6
C00647	compound	Pyridoxamine phosphate	0.010089	B6
C00831	compound	Pantetheine	0.011689	B6
C00847	compound	4-Pyridoxate	0.008389	B6
C00864	compound	Pantothenate	0.00239	B6
C00909	compound	Leukotriene A4	0.00019	B6
C00971	compound	4-Pyridoxolactone	0.006989	B6
C01210	compound	N-Methylethanolamine phosphate	0.007389	B6
C01678	compound	Cysteamine	0.008889	B6
C01725	compound	Levanbiose	0.009289	B6
C01762	compound	Xanthosine	0.010889	B6
C01959	compound	Taurocyamine	0.010989	B6
C02165	compound	Leukotriene B4	0.006489	B6

C02166	compound	Leukotriene C4	0.00289	B6
C02282	compound	Glutaminyl-tRNA	0.012989	B6
C02591	compound	Sucrose 6'-phosphate	0.007089	B6
C02918	compound	1-Methylnicotinamide	0.00559	B6
C03149	compound	N-Phosphotaurocyamine	0.009089	B6
C03193	compound	(5-L-Glutamyl)-peptide	0.010189	B6
C03323	compound	(2,1-beta-D-Fructosyl)n	0.00559	B6
C03451	compound	(R)-S-Lactoylglutathione	0.011589	B6
C03492	compound	D-4'-Phosphopantothenate	0.012489	B6
C04148	compound	Phenylacetylglutamine	0.012189	B6
C04650	compound	L-Phosphinothricin	0.006289	B6
C04805	compound	5(S)-HETE	0.007189	B6
C04853	compound	20-OH-Leukotriene B4	0.007889	B6
C05122	compound	Taurocholate	0.011989	B6
C05356	compound	5(S)-HPETE	0.006589	B6
C05465	compound	Taurochenodeoxycholate	0.011889	B6
C05515	compound	5-Ureido-4-imidazole carboxylate	0.012589	B6
C05646	compound	5-Hydroxyindolepyruvate	0.005689	B6
C05648	compound	5-Hydroxy-N-formylkynurenine	0.008289	B6
C05731	compound	3-Ketosucrose	0.006489	B6
C05842	compound	N1-Methyl-2-pyridone-5-carboxamide	0.00209	B6
C05843	compound	N1-Methyl-4-pyridone-5-carboxamide	0.007489	B6
C05844	compound	5-L-Glutamyl-taurine	0.010189	B6
C05939	compound	Linatine	0.009089	B6
C05944	compound	Pantothenol	0.006389	B6
C06215	compound	Levan	0.009189	B6
C06457	compound	Bialaphos	0.00299	B6
C06735	compound	Aminoacetaldehyde	0.006089	B6
C13482	compound	Phosphodimethylethanolamine	0.00419	B6
C14180	compound	S-(Hydroxymethyl)glutathione	0.012789	B6
C15522	compound	4a-Hydroxytetrahydrobiopterin	0.010389	B6
C16566	compound	Glutathionylaminopropylcadaverine	0.013689	B6
C16688	compound	Sucrose 6-phosphate	0.007689	B6
C17951	compound	N-Acetylbialaphos	0.00489	B6
C17952	compound	N-Acetylphosphinothricin	0.008689	B6

Supplemental Table 2: Significantly different abundant metabolites enriched in cecum content of B6 and B6-mt^{FVB} mice. KEGG database was used for entries. (Limma, n = 3).

KEGG ID	Type	KEGG name	*p*-value (Limma)	Enriched in
mmu00270	pathway	Cysteine and methionine metabolism - Mus musc...	0.010339	B6-mt^{FVB}
mmu00330	pathway	Arginine and proline metabolism - Mus musculu...	0.00411	B6-mt^{FVB}
M00134	module	Polyamine biosynthesis, arginine => ornithine...	0.007659	B6-mt^{FVB}
1.14.18.2	enzyme	CMP-N-acetylneuraminate monooxygenase	0.011959	B6-mt^{FVB}
1.2.1.32	enzyme	aminomuconate-semialdehyde dehydrogenase	0.00547	B6-mt^{FVB}
2.1.1.22	enzyme	carnosine N-methyltransferase	0.00418	B6-mt^{FVB}
2.1.4.1	enzyme	glycine amidinotransferase	0.010219	B6-mt^{FVB}
3.1.3.29	enzyme	N-acylneuraminate-9-phosphatase	0.005669	B6-mt^{FVB}
3.4.13.18	enzyme	cytosol nonspecific dipeptidase	0.00525	B6-mt^{FVB}
4.1.3.3	enzyme	N-acetylneuraminate lyase	0.005949	B6-mt^{FVB}
R00199	reaction	ATP:pyruvate,water phosphotransferase	0.011449	B6-mt^{FVB}
R00200	reaction	ATP:pyruvate 2-O-phosphotransferase	0.010889	B6-mt^{FVB}
R00396	reaction	L-alanine:NAD+ oxidoreductase (deaminating)	0.008059	B6-mt^{FVB}
R00554	reaction	ATP:L-arginine Nomega-phosphotransferase	0.010439	B6-mt^{FVB}
R00559	reaction	L-Arginine:oxygen 2-oxidoreductase (decarboxy...	0.00527	B6-mt^{FVB}
R00562	reaction	N2-(D-1-carboxyethyl)-L-arginine:NAD+ oxidore...	0.00016	B6-mt^{FVB}
R00563	reaction	N2-(D-1,3-dicarboxypropyl)-L-arginine:NADP+ o...	0.010379	B6-mt^{FVB}
R00679	reaction	L-tryptophan:oxygen 2-oxidoreductase (decarbo...	0.00058	B6-mt^{FVB}
R00832	reaction	succinyl-CoA:L-arginine N2-succinyltransferas...	0.00021	B6-mt^{FVB}
R00999	reaction	O-Succinyl-L-homoserine succinate-lyase (deam...	0.0006	B6-mt^{FVB}
R01117	reaction	CTP:N-acetylneuraminate cytidylyltransferase	0.0041	B6-mt^{FVB}
R01164	reaction	L-histidine:beta-alanine ligase (ADP-forming)	0.00082	B6-mt^{FVB}
R01166	reaction	Nalpha-(beta-alanyl)-L-histidine hydrolase	0.00058	B6-mt^{FVB}
R01288	reaction	O4-succinyl-L-homoserine:hydrogen sulfide S-(...	0.00108	B6-mt^{FVB}
R01295	reaction	benzoate,[reduced NADPH---hemoprotein reducta...	0.00089	B6-mt^{FVB}
R01419	reaction	Benzaldehyde:NAD+ oxidoreductase	0.006419	B6-mt^{FVB}
R01420	reaction	benzaldehyde:NADP+ oxidoreductase	0.007589	B6-mt^{FVB}
R01422	reaction	benzoate:CoA ligase (AMP-forming)	0.008089	B6-mt^{FVB}
R01423	reaction	5'-Benzoylphosphoadenosine benzoylhydrolase	0.007119	B6-mt^{FVB}
R01424	reaction	N-Benzoylglycine amidohydrolase	0.006819	B6-mt^{FVB}

R01426	reaction	Benzoate + Acetate + NADH + H+ <=> trans-Cinn...	0.006539	B6-mt^{FVB}
R01777	reaction	Succinyl-CoA:L-homoserine O-succinyltransfera...	0.00073	B6-mt^{FVB}
R01803	reaction	N-acetylneuraminate,ferrocytochrome-b5:oxygen...	0.007089	B6-mt^{FVB}
R01804	reaction	phosphoenolpyruvate:N-acetyl-D-mannosamine C-...	0.00551	B6-mt^{FVB}
R01805	reaction	N-Acetylneuraminate 9-phosphate phosphohydrol...	0.00535	B6-mt^{FVB}
R01811	reaction	N-Acetylneuraminate pyruvate-lyase (N-acetyl-...	0.005699	B6-mt^{FVB}
R01937	reaction	2-Oxoadipate + Ammonia + NAD+ <=> 2-Aminomuco...	0.00047	B6-mt^{FVB}
R01938	reaction	2-Oxoadipate + Ammonia + NADP+ <=> 2-Aminomuc...	0.00074	B6-mt^{FVB}
R01989	reaction	L-Arginine:4-aminobutanoate amidinotransferas...	0.00033	B6-mt^{FVB}
R01990	reaction	4-Guanidinobutanoate amidinohydrolase	0.00048	B6-mt^{FVB}
R02025	reaction	L-methionine:oxidized-thioredoxin S-oxidoredu...	0.0014	B6-mt^{FVB}
R02144	reaction	S-adenosyl-L-methionine:carnosine N-methyltra...	0.00469	B6-mt^{FVB}
R02262	reaction	L-Fuculose-1-phosphate lactaldehyde-lyase	0.00221	B6-mt^{FVB}
R02931	reaction	S-Adenosyl-L-methionine:isoflavone 4-O'-methy...	0.00284	B6-mt^{FVB}
R03096	reaction	Indole-3-acetamide amidohydrolase	0.00045	B6-mt^{FVB}
R03163	reaction	L-fucose aldose-ketose-isomerase	0.012059	B6-mt^{FVB}
R03177	reaction	4-Guanidinobutanal:NAD+ 1-oxidoreductase	0.00537	B6-mt^{FVB}
R03178	reaction	2-oxo-5-Guanidinopentanoate carboxy-lyase	0.010189	B6-mt^{FVB}
R03180	reaction	4-Guanidinobutanamide amidohydrolase	0.00524	B6-mt^{FVB}
R03210	reaction	6-Carboxyhexanoyl-CoA:L-alanine C-carboxyhexa...	0.00076	B6-mt^{FVB}
R03231	reaction	S-Adenosyl-L-methionine:8-amino-7-oxononanoat...	0.011219	B6-mt^{FVB}
R03241	reaction	ATP:L-fuculose 1-phosphotransferase	0.007569	B6-mt^{FVB}
R03260	reaction	O-Succinyl-L-homoserine succinate-lyase (addi...	0.0014	B6-mt^{FVB}
R03887	reaction	2-aminomuconate aminohydrolase	0.00497	B6-mt^{FVB}
R03889	reaction	2-Aminomuconate semialdehyde:NAD+ 6-oxidoredu...	0.005709	B6-mt^{FVB}
R04018	reaction	Acylneuraminyl hydrolase	0.006279	B6-mt^{FVB}
R04020	reaction	Indole-3-acetamide hydro-lyase	0.00065	B6-mt^{FVB}
R04189	reaction	N2-succinyl-L-arginine iminohydrolase (decarb...	0.00182	B6-mt^{FVB}
R04217	reaction	N2-succinyl-L-ornithine:2-oxoglutarate 5-amin...	0.010799	B6-mt^{FVB}
R04435	reaction	phosphoenolpyruvate:N-acetyl-D-mannosamine-6-...	0.011749	B6-mt^{FVB}
R04691	reaction	Stylopine + S-Adenosyl-L-methionine <=> (S)-	0.011399	B6-mt^{FVB}

		c...		
R04699	reaction	protopine,[reduced NADPH---hemoprotein reduct...	0.005679	B6-mt^{FVB}
R04700	reaction	(S)-cis-N-Methylstylopine,[reduced NADPH---he...	0.00546	B6-mt^{FVB}
R04701	reaction	6-Hydroxyprotopine <=> Dihydrosanguinarine + ...	0.010659	B6-mt^{FVB}
R04916	reaction	5-(2'-Formylethyl)-4,6-dihydroxypicolinate + ...	0.00083	B6-mt^{FVB}
R04917	reaction	5-(2'-Formylethyl)-4,6-dihydroxypicolinate + ...	0.00165	B6-mt^{FVB}
R04918	reaction	5-(2'-Formylethyl)-4,6-dihydroxypicolinate + ...	0.011129	B6-mt^{FVB}
R04946	reaction	O4-succinyl-L-homoserine:L-selenocysteine Se-...	0.011319	B6-mt^{FVB}
R05621	reaction	Benzoate + NADH + H+ + Oxygen <=> (1R,6S)-1,6...	0.006249	B6-mt^{FVB}
R05622	reaction	Benzoate + NADPH + H+ + Oxygen <=> (1R,6S)-1,...	0.007389	B6-mt^{FVB}
R06793	reaction	2-hydroxy-2,3-dihydrogenistein hydro-lyase (g...	0.010889	B6-mt^{FVB}
R07514	reaction	6-hydroxypseudooxynicotinemonooxygenase	0.007739	B6-mt^{FVB}
R08197	reaction	L-arginine:pyruvate aminotransferase	0.012109	B6-mt^{FVB}
R08630	reaction	trihomomethionine:2-oxo-acid aminotransferase	0.0003	B6-mt^{FVB}
R08638	reaction	tetrahomomethionine:2-oxo-acid aminotransfera...	0.00037	B6-mt^{FVB}
R08672	reaction	trihomomethionine,[NADPH---hemoprotein reduct...	0.00528	B6-mt^{FVB}
R08673	reaction	tetrahomomethionine,[NADPH---hemoprotein redu...	0.00497	B6-mt^{FVB}
R08838	reaction	benzoate,NADPH:oxygen oxidoreductase (2-hydro...	0.007729	B6-mt^{FVB}
R09088	reaction	Benzoate + Pyruvate <=> Pyruvophenone + CO2	0.010459	B6-mt^{FVB}
R09471	reaction	6-Hydroxypseudooxynicotine + 2 H2O <=> 6-Hydr...	0.00178	B6-mt^{FVB}
R09834	reaction	UDP-2,4-bis(acetamido)-2,4,6-trideoxy-beta-L-...	0.007599	B6-mt^{FVB}
R09841	reaction	phosphoenolpyruvate:2,4-bis(acetylamino)-2,4,...	0.00502	B6-mt^{FVB}
R09843	reaction	CTP:pseudaminate cytidylyltransferase	0.011709	B6-mt^{FVB}
R10124	reaction	pimeloyl-[acyl-carrier protein]:L-alanine C-p...	0.006089	B6-mt^{FVB}
R10699	reaction	L-lysine:8-amino-7-oxononanoate aminotransfer...	0.006639	B6-mt^{FVB}
R10917	reaction	L-dihydroanticapsin:NAD+ oxidoreductase	0.006439	B6-mt^{FVB}
R11049	reaction	5-(N-Methyl-4,5-dihydro-1H-pyrrol-2-yl)pyridi...	0.006449	B6-mt^{FVB}
R11064	reaction	L-alanine:L-anticapsin ligase (ADP-forming)	0.00551	B6-mt^{FVB}

R11604	reaction	L-arginine:oxygen oxidoreductase (deaminating...	0.011819	B6-mt^{FVB}
C00001	compound	H2O	0.011289	B6-mt^{FVB}
C00014	compound	Ammonia	0.011339	B6-mt^{FVB}
C00062	compound	L-Arginine	0.005979	B6-mt^{FVB}
C00074	compound	Phosphoenolpyruvate	0.011939	B6-mt^{FVB}
C00091	compound	Succinyl-CoA	0.011209	B6-mt^{FVB}
C00111	compound	Glycerone phosphate	0.011579	B6-mt^{FVB}
C00151	compound	L-Amino acid	0.006179	B6-mt^{FVB}
C00161	compound	2-Oxo acid	0.007669	B6-mt^{FVB}
C00180	compound	Benzoate	0.00165	B6-mt^{FVB}
C00270	compound	N-Acetylneuraminate	0.00093	B6-mt^{FVB}
C00342	compound	Thioredoxin	0.007199	B6-mt^{FVB}
C00343	compound	Thioredoxin disulfide	0.007119	B6-mt^{FVB}
C00386	compound	Carnosine	0.00078	B6-mt^{FVB}
C00424	compound	(S)-Lactaldehyde	0.007959	B6-mt^{FVB}
C00645	compound	N-Acetyl-D-mannosamine	0.010659	B6-mt^{FVB}
C00814	compound	Biochanin A	0.00284	B6-mt^{FVB}
C01035	compound	4-Guanidinobutanoate	0.00033	B6-mt^{FVB}
C01037	compound	7,8-Diaminononanoate	0.011149	B6-mt^{FVB}
C01092	compound	8-Amino-7-oxononanoate	0.00098	B6-mt^{FVB}
C01099	compound	L-Fuculose 1-phosphate	0.00241	B6-mt^{FVB}
C01118	compound	O-Succinyl-L-homoserine	0.00093	B6-mt^{FVB}
C01262	compound	beta-Alanyl-N(pi)-methyl-L-histidine	0.010759	B6-mt^{FVB}
C01297	compound	6-Hydroxypseudooxynicotine	0.00212	B6-mt^{FVB}
C01682	compound	Nopaline	0.010339	B6-mt^{FVB}
C01721	compound	L-Fuculose	0.007429	B6-mt^{FVB}
C02220	compound	2-Aminomuconate	0.00047	B6-mt^{FVB}
C02291	compound	L-Cystathionine	0.011309	B6-mt^{FVB}
C02647	compound	4-Guanidinobutanal	0.00535	B6-mt^{FVB}
C02693	compound	(Indol-3-yl)acetamide	0.00061	B6-mt^{FVB}
C02938	compound	3-Indoleacetonitrile	0.006009	B6-mt^{FVB}
C02989	compound	L-Methionine S-oxide	0.0014	B6-mt^{FVB}
C03078	compound	4-Guanidinobutanamide	0.00526	B6-mt^{FVB}
C03296	compound	N2-Succinyl-L-arginine	0.00023	B6-mt^{FVB}
C03415	compound	N2-Succinyl-L-ornithine	0.010069	B6-mt^{FVB}
C04137	compound	D-Octopine	0.00033	B6-mt^{FVB}
C04425	compound	S-Adenosyl-4-methylthio-2-oxobutanoate	0.011219	B6-mt^{FVB}
C05189	compound	Protopine	0.00079	B6-mt^{FVB}
C05190	compound	6-Hydroxyprotopine	0.010359	B6-mt^{FVB}
C05654	compound	5-(2'-Formylethyl)-4,6-dihydroxypicolinate	0.010749	B6-mt^{FVB}
C05655	compound	5-(2'-Carboxyethyl)-4,6-dihydroxypicolinate	0.00118	B6-mt^{FVB}
C05945	compound	L-Arginine phosphate	0.010439	B6-mt^{FVB}
C06128	compound	GM4	0.006279	B6-mt^{FVB}
C06163	compound	(S)-cis-N-Methylstylopine	0.010499	B6-mt^{FVB}
C06241	compound	N-Acetylneuraminate 9-phosphate	0.010499	B6-mt^{FVB}
C06321	compound	(1R,6S)-1,6-Dihydroxycyclohexa-2,4-diene-1-	0.006429	B6-mt^{FVB}

		ca...		
C06433	compound	5'-Benzoylphosphoadenosine	0.007119	B6-mt^{FVB}
C06563	compound	Genistein	0.007279	B6-mt^{FVB}
C12631	compound	2-Hydroxy-2,3-dihydrogenistein	0.010479	B6-mt^{FVB}
C17220	compound	2-Oxo-7-methylthioheptanoic acid	0.00547	B6-mt^{FVB}
C17221	compound	Trihomomethionine	0.00023	B6-mt^{FVB}
C17224	compound	2-Oxo-8-methylthiooctanoic acid	0.005869	B6-mt^{FVB}
C17225	compound	Tetrahomomethionine	0.0003	B6-mt^{FVB}
C17246	compound	6-Methylthiohexanaldoxime	0.00528	B6-mt^{FVB}
C17249	compound	7-Methylthioheptanaldoxime	0.00497	B6-mt^{FVB}
C19631	compound	6-Hydroxy-3-succinoylpyridine	0.007389	B6-mt^{FVB}
C19972	compound	2,4-Bis(acetamido)-2,4,6-trideoxy-beta-L-altr...	0.00146	B6-mt^{FVB}
C20082	compound	Pseudaminic acid	0.011069	B6-mt^{FVB}
C20083	compound	CMP-pseudaminic acid	0.011709	B6-mt^{FVB}
C20940	compound	L-Dihydroanticapsin	0.010889	B6-mt^{FVB}
C20941	compound	L-Anticapsin	0.00051	B6-mt^{FVB}
C20942	compound	Bacilysin	0.00551	B6-mt^{FVB}
mmu00770	pathway	Pantothenate and CoA biosynthesis - Mus muscu...	0.00119	B6
mmu04022	pathway	cGMP-PKG signaling pathway - Mus musculus (mo...	0.00159	B6
mmu04024	pathway	cAMP signaling pathway - Mus musculus (mouse)	0.007289	B6
mmu04080	pathway	Neuroactive ligand-receptor interaction - Mus...	0.00269	B6
mmu04261	pathway	Adrenergic signaling in cardiomyocytes - Mus ...	0.00069	B6
mmu04664	pathway	Fc epsilon RI signaling pathway - Mus musculu...	0.00169	B6
mmu04923	pathway	Regulation of lipolysis in adipocytes - Mus m...	0.00029	B6
mmu04924	pathway	Renin secretion - Mus musculus (mouse)	0.00019	B6
mmu05032	pathway	Morphine addiction - Mus musculus (mouse)	0.006989	B6
mmu05034	pathway	Alcoholism - Mus musculus (mouse)	0.008089	B6
mmu05310	pathway	Asthma - Mus musculus (mouse)	0.00309	B6
mmu05410	pathway	Hypertrophic cardiomyopathy (HCM) - Mus muscu...	0.007589	B6
M00037	module	Melatonin biosynthesis, tryptophan => seroton...	9E-05	B6
M00038	module	Tryptophan metabolism, tryptophan => kynureni...	0.008989	B6
M00042	module	Catecholamine biosynthesis, tyrosine => dopam...	0.00039	B6
1.2.1.32	enzyme	aminomuconate-semialdehyde dehydrogenase	0.00199	B6
2.1.1.28	enzyme	phenylethanolamine N-methyltransferase	0.00039	B6
2.1.1.4	enzyme	acetylserotonin O-methyltransferase	0.006289	B6
2.3.1.87	enzyme	aralkylamine N-acetyltransferase	0.00019	B6

2.7.1.20	enzyme	adenosine kinase	0.00449	B6
2.7.1.33	enzyme	pantothenate kinase	0.00019	B6
2.7.11.12	enzyme	cGMP-dependent protein kinase	0.007989	B6
3.2.1.14	enzyme	chitinase	0.006789	B6
3.4.15.1	enzyme	peptidyl-dipeptidase A	0.00019	B6
3.4.19.14	enzyme	leukotriene-C4 hydrolase	0.00299	B6
3.4.21.20	enzyme	cathepsin G	0.010789	B6
3.4.21.4	enzyme	trypsin	0.010389	B6
3.4.21.78	enzyme	granzyme A	0.00269	B6
3.4.22.1	enzyme	cathepsin B	0.00079	B6
3.4.23.15	enzyme	renin	0.00019	B6
4.1.1.105	enzyme	L-tryptophan decarboxylase	0.007189	B6
4.1.1.45	enzyme	aminocarboxymuconate-semialdehyde decarboxyla...	0.006989	B6
4.6.1.2	enzyme	guanylate cyclase	0.009589	B6
6.3.2.51	enzyme	phosphopantothenate---cysteine ligase (ATP)	0.012089	B6
R00045	reaction	3,4-dihydroxy-L-phenylalanine:oxygen oxidored...	0.00529	B6
R00183	reaction	adenosine 5'-monophosphate phosphohydrolase	0.00089	B6
R00185	reaction	ATP:adenosine 5'-phosphotransferase	0.00239	B6
R00192	reaction	S-Adenosyl-L-homocysteine hydrolase	0.00349	B6
R00563	reaction	N2-(D-1,3-dicarboxypropyl)-L-arginine:NADP+ o...	0.00509	B6
R00693	reaction	Acetyl-CoA:L-phenylalanine N-acetyltransferas...	0.00429	B6
R00982	reaction	Anthranilate:CoA ligase (AMP-forming)	0.010489	B6
R00983	reaction	2,3-Dihydroxyindole:oxygen 2,3-oxidoreductase...	0.012089	B6
R00987	reaction	L-Kynurenine hydrolase	0.007189	B6
R00988	reaction	N-Formylanthranilate amidohydrolase	0.010189	B6
R00991	reaction	Anthranilate <=> 2-Formaminobenzoylacetate	0.010389	B6
R01206	reaction	[1,4-(N-Acetyl-beta-D-glucosaminyl)]n glycano...	0.006789	B6
R01245	reaction	Adenosine ribohydrolase	0.009389	B6
R01411	reaction	5-Methylcytosine aminohydrolase	0.010389	B6
R01413	reaction	thymine:acceptor oxidoreductase	0.010089	B6
R01560	reaction	Adenosine aminohydrolase	0.010389	B6
R01561	reaction	adenosine:phosphate alpha-D-ribosyltransferas...	0.008789	B6
R01567	reaction	ATP:thymidine 5'-phosphotransferase	0.005989	B6
R01569	reaction	thymidylate 5'-phosphohydrolase	0.005889	B6
R01570	reaction	thymidine:phosphate deoxy-alpha-D-ribosyltran...	0.006789	B6
R01773	reaction	L-Homoserine:NAD+ oxidoreductase	0.012089	B6
R02078	reaction	L-Tyrosine,L-dopa:oxygen oxidoreductase	0.00519	B6
R02092	reaction	dTDP phosphohydrolase	0.00499	B6

R02094	reaction	ATP:dTMP phosphotransferase	0.00469	B6
R02101	reaction	5,10-Methylenetetrahydrofolate:dUMP C-methylt...	0.010589	B6
R02335	reaction	UDP-N-acetyl-D-glucosamine:chitin 4-beta-N-ac...	0.006789	B6
R02473	reaction	(R)-Pantoate:beta-alanine ligase (AMP-forming...	0.005889	B6
R02474	reaction	Pantothenate amidohydrolase	0.00239	B6
R02533	reaction	S-Adenosyl-L-methionine:phenylethanolamine N-...	0.00219	B6
R02911	reaction	acetyl-CoA:aralkylamine N-acetyltransferase	0.00029	B6
R02919	reaction	4-[(1R)-1-Hydroxy-2-(methylamino)ethyl]-1,2-b...	0.00089	B6
R02920	reaction	S-Adenosyl-L-methionine:catechol O-methyltran...	0.008889	B6
R02971	reaction	ATP:pantothenate 4'-phosphotransferase	0.011189	B6
R02972	reaction	N-((R)-Pantothenoyl)-L-cysteine carboxy-lyase	0.00019	B6
R03018	reaction	ATP:pantothenate 4'-phosphotransferase	0.00099	B6
R03130	reaction	S-Adenosyl-L-homocysteine:N-acetylserotonin O...	0.00019	B6
R03210	reaction	6-Carboxyhexanoyl-CoA:L-alanine C-carboxyhexa...	0.00519	B6
R03269	reaction	N-[(R)-4'-Phosphopantothenoyl]-L-cysteine car...	0.011489	B6
R03889	reaction	2-Aminomuconate semialdehyde:NAD+ 6-oxidoredu...	0.006089	B6
R03916	reaction	(5-glutamyl)-peptide:amino-acid 5-glutamyltra...	0.005989	B6
R03927	reaction	Pantothenate + 2 Reduced acceptor <=> Pantoth...	0.005989	B6
R04230	reaction	(R)-4'-phosphopantothenate:L-cysteine ligase ...	0.011689	B6
R04231	reaction	(R)-4'-phosphopantothenate:L-cysteine ligase	0.011989	B6
R04323	reaction	2-Amino-3-carboxymuconate semialdehyde carbox...	0.008289	B6
R04391	reaction	ATP:pantothenate 4'-phosphotransferase	0.00019	B6
R04903	reaction	5-Hydroxyindoleacetaldehyde:NAD+ oxidoreducta...	0.011189	B6
R04904	reaction	5-hydroxyindoleacetaldehyde:oxygen oxidoreduc...	0.009589	B6
R04905	reaction	S-Adenosyl-L-methionine:N-acetylserotonin O-m...	0.006289	B6
R04906	reaction	5-Hydroxyindoleacetate <=> 5-Hydroxyindoleace...	0.006689	B6
R05055	reaction	Leukotriene D4 + H2O <=> Leukotriene E4 + Gly...	0.00249	B6
R05357	reaction	amidinoproclavaminate amidinohydrolase	0.005889	B6
R05466	reaction	deoxyamidinoproclavaminate,2-oxoglutarate:oxy...	0.006189	B6

R06613	reaction	5,10-methylenetetrahydrofolate,NADPH:dUMP C-m...	0.006189	B6
R06977	reaction	L-2,4-diaminobutyrate:2-oxoglutarate 4-aminot...	0.010689	B6
R07514	reaction	6-hydroxypseudooxynicotinemonooxygenase	0.011789	B6
R08626	reaction	dihomomethionine:2-oxo-acid aminotransferase	0.00069	B6
R08638	reaction	tetrahomomethionine:2-oxo-acid aminotransfera...	0.00039	B6
R08670	reaction	dihomomethionine,[NADPH---hemoprotein reducta...	0.010289	B6
R08673	reaction	tetrahomomethionine,[NADPH---hemoprotein redu...	0.010289	B6
R09079	reaction	carboxyspermidine:NADP+ oxidoreductase	0.006689	B6
R09257	reaction	feruloyl-CoA:putrescine feruloyltransferase	0.00389	B6
R09471	reaction	6-Hydroxypseudooxynicotine + 2 H2O <=> 6-Hydr...	0.005689	B6
R09805	reaction	L-Aspartate-4-semialdehyde:NAD+ oxidoreductas...	0.006189	B6
R09875	reaction	leukotriene-C4 hydrolase	0.00109	B6
R10091	reaction	N2-citryl-N6-acetyl-N6-hydroxy-L-lysine:N6-ac...	0.00549	B6
R10147	reaction	L-aspartate-4-semialdehyde hydro-lyase [addin...	0.011889	B6
R10699	reaction	L-lysine:8-amino-7-oxononanoate aminotransfer...	0.011289	B6
R11022	reaction	2-Aminomuconate semialdehyde <=> Picolinic ac...	0.011189	B6
R11323	reaction	dTTP diphosphohydrolase	0.009689	B6
R12505	reaction	hydrogen sulfide:L-aspartate-4-semialdehyde s...	0.006289	B6
C00079	compound	L-Phenylalanine	0.008789	B6
C00108	compound	Anthranilate	0.006489	B6
C00134	compound	Putrescine	0.007689	B6
C00151	compound	L-Amino acid	0.008589	B6
C00178	compound	Thymine	0.00039	B6
C00212	compound	Adenosine	0.00049	B6
C00364	compound	dTMP	0.00109	B6
C00441	compound	L-Aspartate 4-semialdehyde	0.006089	B6
C00461	compound	Chitin	0.006789	B6
C00788	compound	L-Adrenaline	0.00129	B6
C00822	compound	Dopaquinone	0.00519	B6
C00831	compound	Pantetheine	0.00539	B6
C00864	compound	Pantothenate	0.00029	B6
C00978	compound	N-Acetylserotonin	0.00029	B6
C01092	compound	8-Amino-7-oxononanoate	0.00529	B6
C01187	compound	3-Deoxy-D-manno-octulosonate	0.006489	B6

C01297	compound	6-Hydroxypseudooxynicotine	0.006489	B6
C01674	compound	Chitobiose	0.011289	B6
C01682	compound	Nopaline	0.00499	B6
C02320	compound	R-S-Glutathione	0.00259	B6
C02376	compound	5-Methylcytosine	0.010389	B6
C03519	compound	N-Acetyl-L-phenylalanine	0.00429	B6
C03824	compound	2-Aminomuconate semialdehyde	0.00499	B6
C04079	compound	N-((R)-Pantothenoyl)-L-cysteine	0.00029	B6
C04352	compound	(R)-4'-Phosphopantothenoyl-L-cysteine	0.005789	B6
C04409	compound	2-Amino-3-carboxymuconate semialdehyde	0.007789	B6
C05554	compound	Aerobactin	0.00549	B6
C05588	compound	L-Metanephrine	0.008189	B6
C05634	compound	5-Hydroxyindoleacetaldehyde	0.007889	B6
C05635	compound	5-Hydroxyindoleacetate	9E-05	B6
C05660	compound	5-Methoxyindoleacetate	0.006289	B6
C05729	compound	R-S-Cysteinylglycine	0.006389	B6
C05832	compound	5-Hydroxyindoleacetylglycine	0.006689	B6
C05944	compound	Pantothenol	0.005989	B6
C05951	compound	Leukotriene D4	0.00079	B6
C06657	compound	Guanidinoproclavaminic acid	0.005789	B6
C06658	compound	Proclavaminic acid	0.010989	B6
C10164	compound	Picolinic acid	0.011189	B6
C10497	compound	Feruloylputrescine	0.00389	B6
C17216	compound	2-Oxo-6-methylthiohexanoic acid	0.008689	B6
C17217	compound	Dihomomethionine	0.00079	B6
C17224	compound	2-Oxo-8-methylthiooctanoic acid	0.006989	B6
C17225	compound	Tetrahomomethionine	0.00049	B6
C17245	compound	5-Methylthiopentanaldoxime	0.010289	B6
C17249	compound	7-Methylthioheptanaldoxime	0.010289	B6
C20333	compound	N2-Citryl-N6-acetyl-N6-hydroxy-L-lysine	0.011089	B6

6.2 Materials

Material	**Company**
Acetone	Carl Roth GmbH & Co. KG, Karlsruhe, Germany
Albumin Fraktion V	Carl Roth GmbH & Co. KG, Karlsruhe, Germany
AllPrep DNA/RNA/Protein Mini Kit	Qiagen, Hilden, Germany
Amersham™ Protran® Western blotting membranes, nitrocellulose	GE Healthcare Bio-Sciences AB, Uppsala, Sweden
Amicon® Ultra-15 Centrifugal Filter Units	Merck KGaA, Darmstadt, Germany
Calcium chloride	Carl Roth GmbH & Co. KG, Karlsruhe, Germany
Cell Strainer, 70 µm	Sarstedt, Nümbrecht, Germany
CellTiter-Glo® Luminescent Cell Viability Assay	Promega, Madison, USA
Combitip Adv Biop 10.0 ml 100 pcs	Eppendorf SE, Hamburg, Germany
Corning® Matrigel® Matrix	Corning Inc., Corning, USA
Costar® 24-well Clear TC-treated Multiple Well Plates	Corning Inc., Corning, USA

D-(+)-Glucosamine hydrochloride	Sigma-Aldrich, St. Louis, USA
D(+)-Glucose	Carl Roth GmbH & Co. KG, Karlsruhe, Germany
D-(-)-Ribose	Sigma-Aldrich, St. Louis, USA
Dako Pen	Dako Deutschland GmbH, Hamburg, Germany
DAPI Fluoromount G	Southern Biotech, Birmingham, USA
di-Potassium hydrogen phosphate	Carl Roth GmbH & Co. KG, Karlsruhe, Germany
di-Sodium hydrogen phosphate dihydrate	Merck Millipore, Burlington, USA
Disposable Biopsy Punch	pfm medical AG, Cologne, Germany
DNase I, RNase-free (1 U/µl)	Thermo Fisher Scientific GmbH, Dreieich, Germany
DNeasy® Blood & Tissue Kit	Qiagen, Hilden, Germany
DPBS (1x)	Gibco, Thermo Fisher Scientific GmbH, Dreieich, Germany
Dulbecco's Modified Eagle's Medium – high glucose	Sigma-Aldrich, St. Louis, USA
Dulbecco's Modified Eagle's Medium – low glucose	Sigma-Aldrich, St. Louis, USA
Dulbecco's Modified Eagle's Medium: Nutrient Mixture F-12	Stemcell™ Technologies, Vancouver, Canada
eBioscience™ Fixation/Permeabilization Concentrate	Invitrogen, Waltham, USA
eBioscience™ Fixation/Permeabilization Diluent	Invitrogen, Waltham, USA
eBioscience™ Permeabilization Buffer (10X)	Invitrogen, Waltham, USA
eBioscience™ RBC Lysis Buffer	Invitrogen, Waltham, USA
EDTA	SERVA Electrophoresis GmbH, Heidelberg, Germany
ELISA MAX™ Deluxe Set Mouse TNF-α	BioLegend, San Diego, USA
EMPROVE® ESSENTIAL Ph Eur,BP,JPE,NF,E 338 ortho-Phosphoric acid 85%	Merck Millipore, Burlington, USA
Epredia™ SuperFrost Plus™ Adhesion slides	Thermo Fisher Scientific GmbH, Dreieich, Germany
ExpressPlus™ PAGE Gel	Genscript Biotech Corp, Piscataway Township, USA
FBS Superior	Sigma-Aldrich, St. Louis, USA
FcR Blocking Reagent, mouse	Miltenyi Biotec, Bergisch Gladbach, Germany
20% Galactose Solution	Alpha Teknova, Hollister, USA
GeneRuler 1kb DNA Ladder, ready-to-use	Thermo Fisher Scientific GmbH, Dreieich, Germany
GeneRuler Ultra Low Range DNA Ladder, ready-to-use	Thermo Fisher Scientific GmbH, Dreieich, Germany
Gentle Cell Dissociation Reagent	Stemcell™ Technologies, Vancouver, Canada
Germocid Peracetic Disinfectant Powder	GIMA, Milan, Italy
Glucose Solution (200 g/L)	Gibco, Thermo Fisher Scientific GmbH, Dreieich, Germany
GlutaMAX™	Gibco, Thermo Fisher Scientific GmbH, Dreieich, Germany
Glycerol	Carl Roth GmbH & Co. KG, Karlsruhe, Germany
Glycine	Carl Roth GmbH & Co. KG, Karlsruhe, Germany
Guanidine hydrochloride	Sigma-Aldrich, St. Louis, USA
HBSS (1x)	Gibco, Thermo Fisher Scientific GmbH, Dreieich, Germany
HEPES	Carl Roth GmbH & Co. KG, Karlsruhe, Germany
Hydrochloric acid (2N)	Carl Roth GmbH & Co. KG, Karlsruhe, Germany
Immobilon Western Chemiluminescent HRP Substrate	Merck Millipore, Burlington, USA

innuPREP DOUBLEpure Kit	Analytik Jena, Jena, Germany
innuPREP RNA Mini Kit 2.0	Analytik Jena, Jena, Germany
IntestiCult™ OGM Mouse Basal Medium	Stemcell™ Technologies, Vancouver, Canada
Ketamine hydrochloride	Sigma-Aldrich, Darmstadt, Germany
LE Agarose	Biozym Scientific GmbH, Hessisch Oldendorf, Germany
L-Glutamic acid	Sigma-Aldrich, St. Louis, USA
Lipopolysaccharides from Escherichia coli O111:B4	Sigma-Aldrich, St. Louis, USA
Maxima SYBR Green/ROX qPCR Master Mix	Thermo Fisher Scientific GmbH, Dreieich, Germany
Methanol	Carl Roth GmbH & Co. KG, Karlsruhe, Germany
Microtest Plate 96 Well, F	Sarstedt, Nümbrecht, Germany
Microvette®	Sarstedt, Nümbrecht, Germany
N-Acetyl-D-Glucosamine	Sigma-Aldrich, St. Louis, USA
NextSeq 500/550 High Output Kit v2.5	Illumina, San Diego, USA
N-(1-napthyl) ethylenediamine dihydrochloride	Sigma-Aldrich, St. Louis, USA
Nonfat dried milk powder	AppliChem GmbH, Darmstadt, Germany
NP-40 Alternative	Merck Millipore, Burlington, USA
Nunc™ MicroWell™ 96-Well, Nunclon Delta-Treated, Flat-Bottom Microplate	Thermo Fisher Scientific GmbH, Dreieich, Germany
96 PCR Plate half skirt flat	Sarstedt, Nümbrecht, Germany
PCR SingleCap 8er-SoftStrips 0.2 ml	Biozym Scientific GmbH, Hessisch Oldendorf, Germany
Percoll™	GE Healthcare Bio-Sciences AB, Uppsala, Sweden
Phire™ Hot Start II DNA Polymerase	Thermo Fisher Scientific GmbH, Dreieich, Germany
Phor Agarose	Biozym Scientific GmbH, Hessisch Oldendorf, Germany
Pierce™ BCA Protein Assay Kit	Thermo Fisher Scientific GmbH, Dreieich, Germany
Pierce™ LDH Cytotoxicity Assay Kit	Thermo Fisher Scientific GmbH, Dreieich, Germany
Potassium chloride	Carl Roth GmbH & Co. KG, Karlsruhe, Germany
Potassium dihydrogen phosphate	Carl Roth GmbH & Co. KG, Karlsruhe, Germany
Protease Inhibitor Cocktail Set III, Animal-Free	Merck Millipore, Burlington, USA
Protein G Resin	Genscript Biotech Corp, Piscataway Township, USA
QIAshredder	Qiagen, Hilden, Germany
RevertAid First Strand cDNA Synthesis Kit	Thermo Fisher Scientific GmbH, Dreieich, Germany
RNAlater™	Sigma-Aldrich, St. Louis, USA
RPMI 1640	PAN-Biotech GmbH, Aidenbach, Germany
RPMI Medium 1640	Gibco, Thermo Fisher Scientific GmbH, Dreieich, Germany
SDS Pellets	Carl Roth GmbH & Co. KG, Karlsruhe, Germany
Serological pipette 5 ml	Sarstedt, Nümbrecht, Germany
Serological pipette 10 ml	Sarstedt, Nümbrecht, Germany
Serological pipette 25 ml	Sarstedt, Nümbrecht, Germany
Sodium azide	Sigma-Aldrich, St. Louis, USA
Sodium chloride	Sigma-Aldrich, St. Louis, USA
Sodium deoxycholate	Sigma-Aldrich, St. Louis, USA
Sodium dihydrogen phosphate dihydrate	Merck Millipore, Burlington, USA
Sodium hydroxide	Carl Roth GmbH & Co. KG, Karlsruhe, Germany
Sodium nitrite	Carl Roth GmbH & Co. KG, Karlsruhe, Germany

Sodium oxalate	Sigma-Aldrich, St. Louis, USA
Sodium palmitate	Sigma-Aldrich, St. Louis, USA
Sodium propionate	Sigma-Aldrich, St. Louis, USA
Sodium Pyruvate 100mM	Gibco, Thermo Fisher Scientific GmbH, Dreieich, Germany
Spectra™ Multicolor Broad Range Protein Ladder	Thermo Fisher Scientific GmbH, Dreieich, Germany
Spermidine	Sigma-Aldrich, St. Louis, USA
Sucrose	Sigma-Aldrich, St. Louis, USA
Sulfanilamide	Carl Roth GmbH & Co. KG, Karlsruhe, Germany
TC-Flask T75, Stand., Vent. Cap	Sarstedt, Nümbrecht, Germany
TC Plate 6 Well, Standard, F	Sarstedt, Nümbrecht, Germany
TC Plate 24 Well, Standard, F	Sarstedt, Nümbrecht, Germany
TC Plate 96 Well, Standard, R	Sarstedt, Nümbrecht, Germany
Tissue-Tek Cryomold Intermediate plastic	Sakura Finetek, Torrane, USA
Tissue-Tek O.C.T. Compound	Sakura Finetek, Torrane, USA
Titripur® Sodium hydroxide solution	Merck Millipore, Burlington, USA
Tris	Carl Roth GmbH & Co. KG, Karlsruhe, Germany
Tris-MOPS-SDS Running Buffer Powder	Genscript Biotech Corp, Piscataway Township, USA
Triton™ X-100	Sigma-Aldrich, St. Louis, USA
Trypan Blue Stain (0.4%)	Gibco, Thermo Fisher Scientific GmbH, Dreieich, Germany
Tween® 20	Carl Roth GmbH & Co. KG, Karlsruhe, Germany
UltraPure™ Distilled Water	Invitrogen, Waltham, USA
Xylazine hydrochloride	Sigma-Aldrich, Darmstadt, Germany

Antibody	**Clone**	**Dilution**	**Isotype**	**Company**	**Application**
Biotin anti-mouse CD3ε Antibody	145-2C11	1:100	Armenian Hamster IgG	BioLegend	IHC
Biotin anti-mouse TCR γ/δ Antibody	GL3	1:100	Armenian Hamster IgG	BioLegend	IHC
Streptavidin Protein, DyLight™ 488 conjugate		1:200		Thermo Fisher Scientific	IHC
Streptavidin Protein, DyLight™ 594 conjugate		1:200		Thermo Fisher Scientific	IHC
swine anti-rabbit – FITC conjugated IgG/F(ab)2 antibody		1:200		Southern Biotech	IHC
CD45R (B220) Antibody, anti-mouse, APC	RA3-6B2	1:50	Rat IgG2a, κ	Miltenyi Biotec	FC
APC/Cyanine7 anti-mouse CD3 Antibody	17A2	1:100	Rat IgG2b, κ	BioLegend	FC
FITC anti-mouse CD3 Antibody	17A2	1:100	Rat IgG2b, κ	BioLegend	FC
APC anti-mouse CD4 Antibody	RM4-5	1:100	Rat IgG2a, κ	BioLegend	FC
CD8a Monoclonal	53-6.7	1:100	Rat IgG2a, κ	eBioscience	FC

Antibody, FITC					
FITC anti-mouse/human CD11b Antibody	M1/70	1:100	Rat IgG2b, κ	BioLegend	FC
Brilliant Violet 605™ anti-mouse CD11c Antibody	N418	1:20	Armenian Hamster IgG	BioLegend	FC
PE anti-mouse CD45 Antibody	30-F11	1:100	Rat IgG2b, κ	BioLegend	FC
APC/Cyanine7 anti-mouse F4/80 Antibody	BM8	1:20	Rat IgG2a, κ	BioLegend	FC
TCRγ/δ Antibody, anti-mouse	GL3	1:10	Armenian Hamster IgG	Miltenyi Biotec	FC
APC anti-mouse/human CD207 (Langerin) Antibody	4C7	1:100	Mouse IgG2a, κ	BioLegend	FC
Brilliant Violet 605™ anti-mouse Ly-6C Antibody	HK1.4	1:20	Rat IgG2c, κ	BioLegend	FC
FITC anti-mouse Ly-6G Antibody	1A8	1:200	Rat IgG2a, κ	BioLegend	FC
Zombie Violet™ Fixable Viability Kit		1:1000		BioLegend	FC
β-Actin (13E5) Rabbit mAb #4970	monoclonal	1:1000		Cell signaling technology	WB
Claudin-2 (E1H90) Rabbit mAb	monoclonal	1:1000		Cell signaling technology	WB
Polyclonal Goat Anti-Rabbit Immunoglobulins/HRP	polyclonal	1:4000		Agilent Technologies	WB

Primer name	**Primer sequence**	**Supplier**
β-Actin for	CACTGTCGAGTCGCGTCC	biomers.net GmbH, Ulm, Germany
β-Actin rev	CGCAGCGATATCGTCATCCA	biomers.net GmbH, Ulm, Germany
Claudin-1 for	TCCTTGCTGAACTTGAACA	biomers.net GmbH, Ulm, Germany
Claudin-1 rev	AGCCATCCACTACTTCTG	biomers.net GmbH, Ulm, Germany
Claudin-2 for	TATGTTGGTGCCAGCATTGT	biomers.net GmbH, Ulm, Germany
Claudin-2 rev	TCATGCCCACCACAGAGATA	biomers.net GmbH, Ulm, Germany
Claudin-4 for	TCGTGGGTGCTCTGGGGATGCTTC	biomers.net GmbH, Ulm, Germany
Claudin-4 rev	GCGGATGACGTTGTGAGCGGTC	biomers.net GmbH, Ulm, Germany
Claudin-15 for	GCTTCTTCATGTCAGCCCTG	biomers.net GmbH, Ulm, Germany
Claudin-15 rev	TTCTTGGAGAGATCCATGTTGC	biomers.net GmbH, Ulm, Germany
Occludin for	CCTCCAATGGCAAAGTGAAT	biomers.net GmbH, Ulm, Germany
Occludin rev	CTCCCCACCTGTCGTGTAGT	biomers.net GmbH, Ulm, Germany
ZO-1 for	CCACCTCTGTCCAGCTCTTC	biomers.net GmbH, Ulm, Germany
ZO-1 rev	CACCGGAGTGATGGTTTTCT	biomers.net GmbH, Ulm, Germany
Defα-22-for	AGCAGCCAGGGGAAGAG	biomers.net GmbH, Ulm, Germany
Defα-22-rev	CCTCTATTGCAGCGACGT	biomers.net GmbH, Ulm, Germany

IL-1β for	CTTCCAGGATGAGGACATGA	biomers.net GmbH, Ulm, Germany
IL-1β rev	CACACCAGCAGGTTATCATCATC	biomers.net GmbH, Ulm, Germany
IL-6 for	CTCCCAACAGACCTGTCTATAC	biomers.net GmbH, Ulm, Germany
IL-6 rev	GTGCATCATCGTTGTTCATAC	biomers.net GmbH, Ulm, Germany
IL-8/KC for	TGAGAGTGATTGAGAGTGGACCA	biomers.net GmbH, Ulm, Germany
IL-8/KC rev	TCAGCCCTCTTCAAAAACTTCTCC	biomers.net GmbH, Ulm, Germany
IL-10 for	TCCCTGGGTGAGAAGCTGAAG	biomers.net GmbH, Ulm, Germany
IL-10 rev	CACCTGCTCCACTGCCTTG	biomers.net GmbH, Ulm, Germany
TNFα for	CTGTAGCCCACGTCGTAGC	biomers.net GmbH, Ulm, Germany
TNFα rev	TTGAGATCCATGCCGTTG	biomers.net GmbH, Ulm, Germany
GLP1 for	GGCACATTCACCAGCGACTACA	biomers.net GmbH, Ulm, Germany
GLP1 rev	GCCCTCCAAGTAAGAACTCACATC	biomers.net GmbH, Ulm, Germany
GLP1R for	TCAGAGACGGTGCAGAAATG	biomers.net GmbH, Ulm, Germany
GLP1R rev	CAGCTGACATTCACGAAGGA	biomers.net GmbH, Ulm, Germany
B2M for	GCTATCCAGAAAACCCCTCAA	biomers.net GmbH, Ulm, Germany
B2M rev	CATGTCTCGATCCCAGTAGACGGT	biomers.net GmbH, Ulm, Germany
Beclin for	AATCTAAGGAGTTGCCGTTATAC	biomers.net GmbH, Ulm, Germany
Beclin rev	CCAGTGTCTTCAATCTTGCC	biomers.net GmbH, Ulm, Germany
Lysozym-1 for	GCCAAGGTCTACAATCGTTGTGAGTTG	biomers.net GmbH, Ulm, Germany
Lysozym-1 rev	CAGTCAGCCAGCTTGACACCACG	biomers.net GmbH, Ulm, Germany

6.3 Equipment

Equipment	**Company**
Aesculap Isis rodent shaver li-ion battery	Agntho's AB, Lidingö, Sweden
Allegra® X-15R Centrifuge	Beckman Coulter
Analytical scale ABS/ABJ-BA-def-1019	Kern & Sohn GmbH, Balingen, Germany
Attune™ NxT Flow Cytometer	Thermo Fisher Scientific GmbH, Dreieich, Germany
Bio-photometer plus 8.5 mm	Eppendorf SE, Hamburg, Germany
C100 Touch™ Thermal Cycler	Bio-Rad Laboratories GmbH, Munich, Germany
Centrifuge 5810R	Eppendorf SE, Hamburg, Germany
CFI Plan Apo λ 10x lense	Keyence Deutschland GmbH, Neu-Isenburg, Germany
CFI Plan Apo λ 20x lense	Keyence Deutschland GmbH, Neu-Isenburg, Germany
ChemiDoc Imaging System	Bio-Rad Laboratories GmbH, Munich, Germany
Cryostat CM3050 S	Leica Mikrosysteme Vertrieb GmbH, Wetzlar, Germany
Eppendorf Xplorer®	Eppendorf SE, Hamburg, Germany
Freezer -20˚	Liebherr Hausgeräte GmbH, Ochsenhausen, Germany
Freezer -80˚	Thermo Fisher Scientific GmbH, Dreieich, Germany
Freezer: Comfort NoFrost	Liebherr
Fresco™ 21 Microcentrifuge	Thermo Fisher Scientific GmbH, Dreieich, Germany
Fridge: Comfort	Liebherr
Gelaire Laminarflow Class 100	Gelman Instrument Company
GeneAmp® PCR System 9700	Applied Biosystems
HandyStep S dispenser	BRAND GmbH, Wertheim, Germany
HERAcell incubator	Heraeus Instruments GmbH, Hanau, Germany
Incubator Thermo Scientific BB 15 CO2	Thermo Fisher Scientific GmbH, Dreieich, Germany
Infinite M200 PRO	Tecan Group, Männedorf, Switzerland
Inverted microscope AE2000 Binocular	Motic Deutschland GmbH, Wetzlar, Germany
Keyence microscope BZ-9000E	Keyence Deutschland GmbH, Neu-Isenburg, Germany

Laminar hood	NuAire, Plymouth, Minnesota, USA
Mastercycler ep realplex^2	Eppendorf SE, Hamburg, Germany
Micro centrifuge Micro Star 17R	VWR International GmbH, Darmstadt, Germany
Microtome	Leica Mikrosysteme Vertrieb GmbH, Wetzlar, Germany
Microwave: 700 & Grill	Severin
Mikro 120 Microliter Centrifuge	Hettich, Tuttlingen, Germany
Mini-PROTEAN Tetra System electrophorese chamber	Bio-Rad Laboratories GmbH, Munich, Germany
NanoDrop 2000c spectrophotometer	Thermo Fisher Scientific GmbH, Dreieich, Germany
Neubauer cell counting chamber	Laboroptik GmbH, Friedrichsdorf, Germany
NextSeq 500 System	Illumina, San Diego, USA
pH meter HI208	HANNA instruments, Vöhringen, Germany
Potter-Elvehjem glass homogenizer	Kimble Chase, Rockwood, USA
Power Pac 300	Bio-Rad Laboratories GmbH, Munich, Germany
Power Pac basic	Bio-Rad Laboratories GmbH, Munich, Germany
Precellys 24 Homogenizer	Bertin Instruments, Rockville, USA
Precision balance 440-47N	Kern, Balingen, Germany
QUANTUM ST4 1100 imaging system	Vilber Lourmat Deutschland GmbH, Eberhardzell, Germany
Qubit® Fluorometer	Thermo Fisher Scientific
Refrigerator	Siemens, Munich, Germany
2720 Thermal Cycler	Applied Biosystems, Waltham, USA
Trans-Blot® Turbo™ Transfer System	Bio-Rad Laboratories GmbH, Munich, Germany
Vortex	Vortex-Genie® 2-Scientific Industries Inc., Bohemia, New-York,USA

6.4 Conference contributions

Poster presentations:

1st Frontiers in Microbiome Autumn School, Ebberup, Denmark, October 2019

Conference "New Developments in Immunology, Inflammation and Infection" (NDI_3), Borstel, Germany, November 2019

47th Annual Meeting of the Arbeitsgemeinschaft Dermatologische Forschung (ADF), Berlin (virtual), Germany, March 2021

3rd International Symposium of the RTG1743 Genes, Environment and Inflammation, Kiel (virtual), Germany, May 2021

Oral presentations:

47th Annual Meeting of the Arbeitsgemeinschaft Dermatologische Forschung (ADF), Berlin (virtual), Germany, March 2021

7 Acknowledgements

First of all, I want to thank Prof. Dr. Saleh Ibrahim for giving me the opportunity to conduct my doctoral thesis in his lab. I am beyond grateful for his guidance, his constant faith in me and my capabilities, his optimism regarding my project and for always having an open door.

Special thanks go to Dr. Misa Hirose. Without her knowledge, her endless support, revealing discussions and her ability to always find a solution my project would not have come this far.

Many thanks to Dr. Paul Schilf for always having an advice and his special knowledge of my project. And additionally, I would like to thank the whole Ibrahim lab: Petra Langenstrassen, Miriam Freitag, Stephanie Latif and Agne Garrett for their support in the wet lab and everything bureaucratical.

I am also very grateful for the help and support of the Evolutionary Medicine Group from Max Planck Institute for Evolutionary Biology in Plön, especially Prof. Dr. John Baines for his guidance, Dr. Marie Vallier and Aleksa Cepic for their help with the analysis of the shotgun metagenomics data and Dr. Sven Künzel with his support in coordinating the experiments in the germ-free mouse facility.

I'm much obliged to the Medical Systems Biology group of the Lübeck Institute of experimental Dermatology. Prof. Dr. Hauke Busch for his input in lively discussions and Dr. Axel Künstner and Dr. Michael Olbrich for their help and support regarding the analysis and interpretation of the metabolomics and shotgun metagenomics data.

Many thanks go to Prof. Dr. Christian Sina, Dr. Stefanie Derer and especially Mohab Ragab for our creative brainstorming sessions regarding the B6-mt^{FVB} mouse strain, complement knowledge and teaching the isolation and culturing method of intestinal organoids. Additionally, I am grateful to Prof. Dr. Christian Sadik for providing me access to his lab infrastructure such as TECAN infinite M200 Pro plate reader, Keyence BZ-9000E fluorescence microscope and Trans-Blot Turbo Transfer System. I also want to thank Prof. Dr. Marc Ehlers and Hanna Lunding for providing access and support for the Life technology Attune Nxt acoustic focusing cytometer. Many thanks to the Leibniz Institut für Nutztierbiologie in Dummerstorf for providing the infrastructure to generate the metabolomics data.

Special thanks go to the DFG research training group 1743 Genes, Environment and Inflammation for funding my project and giving me the opportunity to discuss and present my work in front of an interdisciplinary audience as well as providing advanced training options for the development of my scientific and personal career.

Last but not least I want to thank my family and friends for their untired support during my doctoral project. Special thanks to my husband for his constant encouragement and support. Without him I would not have been where I am today.